

## ABSTRACT

Title of Document: TORSIONAL EFFECT ON SOFT STORY FOR LIGHTLY REINFORCED CONCRETE STRUCTURES IN LOW SEISMIC ZONES

Arash Rezavandi, Ph.D., 2015

Directed By: Professor Chung C. Fu, Ph.D., P.E.  
Civil and Environmental Engineering

This study deals with the performance of lightly reinforced concrete moment frames in low seismic zones. The frames under evaluation comprise vertical and/or plan irregularities and were designed for gravity loads only. Nonlinear time history analysis using scaled ground motions and pushover procedure as a supplement method are performed in this study. With the adoption of plastic hinge method, damage levels are addressed according to FEMA 356 definitions. Pivot model is considered for hysteresis behavior. The damage stage and number of formed hinges are classified for the beams and columns. In case of observed plastic hinge with collapse damage level stage, Fast Fourier Transform (FFT) method is applied to investigate the possible reason. Story drift is obtained based on inelastic behavior throughout of all story levels of archetype model inventories. Comparison between models demonstrates that the first story of symmetric plan models may suffer very minor up to moderate damage levels under low seismic intensity. However, the

severity of damages to the asymmetric plan models can be noticeable, specifically for the lower structural models. The result of pushover method shows close to the results of time history analysis only for the vertical irregular frames without plan irregularity. Story drift illustrates that the lower structures suffer some degree of damage levels, especially for unsymmetrical plan models, while the taller models undergo lower drifts. As far as this study alone concerns, lightly reinforced concrete frame buildings may resist seismic events for the taller structures properly, whereas the lower structural models may suffer higher level of damages. The inherent frequency content of applied records affects the models' response more than their vertical and /or plan irregularity formations. Current US seismic design criteria in standard codes may need to be revised for low to moderate seismic zones in terms of vertical irregularity definitions and design criteria.

TORSIONAL EFFECT ON SOFT STORY FOR LIGHTLY REINFORCED  
CONCRETE STRUCTURES IN LOW SEISMIC ZONES

By

Arash Rezavandi

Dissertation submitted to the Faculty of the Graduate School of the  
University of Maryland, College Park, in partial fulfillment  
of the requirements for the degree of  
Doctor of Philosophy  
2015

Advisory Committee:  
Professor Chung C. Fu, Chair/Advisor  
Professor M. Sherif Aggour  
Professor Amade M. Amde  
Professor Sung Lee  
Professor Yunfeng Zhang

© Copyright by  
Arash Rezavandi  
2015

## Acknowledgements

I would like to express sincere appreciation to my advisor Professor Chung.C.Fu for his valuable guidance, advice, and continuous support during this research. He provided many contributions, including editing on this dissertation, suggesting methods to form the objectives, and offering his great recommendations. Appreciation is also extended to members of the dissertation committee, Professors M. Sherif Aggour, Amde M. Amde, Sung Lee, and Yunfeng Zhang for their valuable suggestions and advices.

I would like to thank my parents, who taught me the value of education, for their affection and encouragement throughout my life.

I wish to thank my beloved wife for her continuous support, encouragement, and patience over the past five years. She is a wonderful wife and a true friend. Finally, I would also like to express my deepest love to my daughter. I was not able to devote sufficient time for her while I put in so many hours needed to finish my study.

# Table of Contents

Acknowledgements.....	ii
Table of Contents.....	iii
List of Tables.....	vi
List of Figures and Graphs.....	viii
List of Illustrations.....	xiv
Chapter 1: Introduction.....	1
1.1. Background and Motivation.....	1
1.2. Scope and Organization.....	10
Chapter 2: Literature Review.....	14
2.1. Seismicity in the Eastern and North Eastern America.....	14
2.1.1. Introduction.....	14
2.1.2. Tectonic and Seismicity in the Eastern and North Eastern America..	16
2.2. Soft Story Failure and Irregular Collapse from Past Earthquakes.....	20
2.2.1. Introduction to Soft Story.....	20
2.2.2. Some Example of Soft Story and Irregular Failures in the Past	
Earthquakes.....	26
2.3. Lightly Reinforced Concrete.....	35
2.4. Code Review on Soft Story Irregularity and Torsional Provision.....	39
2.4.1. Code Background and Principle for Irregular Structures.....	39
2.4.2. Summary of US Code Classification for Irregular and Regular Structures	
.....	43
2.5. Previous Research.....	47
2.5.1. Brief Background.....	47
2.5.2. An Overview of Literature Methods and Trends.....	52
2.5.3. Experimental Studies.....	62
2.5.4. Soft Story Studies.....	72
2.5.5. Torsional Studies.....	74
Chapter 3: Linear Static Models, Basic Models of Study.....	79
3.1. Introduction.....	79
3.2. Assumptions and Models as Lightly Reinforced Concrete.....	80
3.2.1. Definition and Geometry of Models.....	81
3.2.2. First Story Height Selection.....	83
3.2.3. Model Tag and Classification.....	84
3.2.4. Determination of Loads and Load Combinations.....	85
3.3. Initial Analysis and Design of Selected Models, Non-Seismic Provisions	86
3.3.1. Wind load versus Static Seismic Load.....	86
3.3.2. Modal Analysis and Selected Models' Periods.....	89
3.4. Results Review for Selected Models.....	92
Chapter 4: Advanced Modeling and Analysis Assumptions.....	107
4.1. Introduction to Current Advanced Modeling Methods.....	107
4.1.1. Introduction to Nonlinear Analysis.....	107
4.1.2. Basic Nonlinear Assumptions for Selected Models.....	109

4.1.3.	Gravity Load Effects .....	110
4.2.	Time History Records Selection .....	112
4.2.1.	Introduction and Background .....	112
4.2.2.	Selected Ground Motion Records .....	120
4.3.	Plastic Hinge Definition and Allocation to the Models .....	127
4.3.1.	Introduction to Lump Plastic Hinge Behavior and Definition .....	127
4.3.2.	Characteristics of the Assigned Plastic Hinges .....	134
4.3.3.	Hysteresis Models for Beams and Columns .....	140
4.4.	Damping Model Development .....	146
4.4.1.	Introduction to Rayleigh Damping Ratio and Assigned Damping to Selected Models .....	146
4.4.2.	Allocated Rayleigh Damping Coefficients to Selected Models .....	151
Chapter 5:	Nonlinear Analysis and Modeling .....	153
5.1.	Nonlinear Dynamic Approach and Current Approaches .....	153
5.1.1.	Introduction .....	153
5.1.2.	Direct-integration Time-history Nonlinear Analysis .....	155
5.1.3.	Analytical Stability Conditions and Output Accuracy .....	159
5.2.	Nonlinear Static Approach on Regular/Irregular Structures .....	162
5.2.1.	Introduction .....	162
5.2.2.	Estimation of the Displacement Demand per FEMA 356 NSA Procedure .....	168
5.2.3.	Analysis Assumptions and Approach .....	171
Chapter 6:	Parametric Study .....	176
6.1.	Evaluation Overview .....	176
6.2.	Hinge Formation Results .....	179
6.2.1.	Overall Hinge Formation Trend .....	189
6.2.2.	Hinge Formation Comparison-Two (2) Story Models .....	190
6.2.3.	Hinge Formation Comparison-Four (4) Story Models .....	192
6.2.4.	Hinge Formation Comparison-Eight Story Models .....	193
6.2.5.	Brief Review of Few Similar Observed Hinge Formation Behaviors in Models .....	195
6.3.	Story Mechanism .....	201
6.4.	Drift Comparison .....	209
Chapter 7:	Summary, Conclusions, and Recommendations .....	225
7.1.	Summary .....	225
7.2.	Overview of the Findings and Conclusion .....	227
7.2.1.	Overview of Important Findings .....	227
7.2.2.	Conclusion .....	230
7.3.	Suggestions for Future Research .....	232
Appendices:	.....	234
Appendix A:	Abbreviations and Acronyms List .....	234
Appendix B:	Software Plastic Hinge Verification .....	236
B.1.	Verification Example for Assigned Beam Yield Moment .....	236
B.2.	Verification Example for Assigned Column Axial Force-Moment Interaction Curve .....	240
Appendix C:	Verification of Software Computed Target Displacement .....	245

Appendix D: Table of Hinge Formation Results for the Selected Models .....	250
Appendix E: Validation of Analysis Procedure through Load-Displacement Response .....	293
Bibliography .....	296

## List of Tables

- Table 3-1: Total wind load for each direction per ASCE 7-05
- Table 3-2: Seismic base shear per UBC 94
- Table 3-3: Models first 3 periods (modes)
- Table 3-4: Typical tie column detail
- Table 3-5a: Required longitudinal reinforcement for beam type B1
- Table 3-5b: Required longitudinal reinforcement for beam type B'1
- Table 3-5c: Required longitudinal reinforcement for beam type B2
- Table 3-5d: Required longitudinal reinforcement for beam type B3
- Table 3-5e: Required longitudinal reinforcement for beam type B4
- Table 4-1: Summary of Properties of Selected Scaled Horizontal Records
- Table 4-2: Summary of Properties of Selected Unscaled Horizontal Record
- Table 4-3: Modeling Parameters and Numerical Acceptance Criteria of RC Beams  
Controlled by Flexure – Nonlinear Procedure
- Table 4-4: Modeling Parameters and Numerical Acceptance Criteria of RC Columns  
Controlled by Flexure – Nonlinear Procedure
- Table 4-5: Viscous Damping Coefficients for Selected Models
- Table 5-1a: NSA results for the symmetric plan models
- Table 5-1b: NSA results for the asymmetric plan models
- Table 6-1: Performance levels
- Table 6-2: Period in the N-S direction
- Table 6-3: Maximum absolute drift ( $d_i$ )
- Table D-1: Number of Hinge Formation for Selected Model 2A12

Table D-2: Number of Hinge Formation for Selected Model 2A15

Table D-3: Number of Hinge Formation for Selected Model 2A18

Table D-4: Number of Hinge Formation for Selected Model 2B12

Table D-5: Number of Hinge Formation for Selected Model 2S15

Table D-6: Number of Hinge Formation for Selected Model 2S18

Table D-7: Number of Hinge Formation for Selected Model 4A12

Table D-8: Number of Hinge Formation for Selected Model 4A15

Table D-9: Number of Hinge Formation for Selected Model 4A18

Table D-10: Number of Hinge Formation for Selected Model 4B12

Table D-11: Number of Hinge Formation for Selected Model 4S15

Table D-12: Number of Hinge Formation for Selected Model 4S18

Table D-13: Number of Hinge Formation for Selected Model 8A12

Table D-14: Number of Hinge Formation for Selected Model 8A15

Table D-15: Number of Hinge Formation for Selected Model 8A18

Table D-16: Number of Hinge Formation for Selected Model 8B12

Table D-17: Number of Hinge Formation for Selected Model 8S15

Table D-18: Number of Hinge Formation for Selected Model 8S18

## List of Figures and Graphs

Figure 2-1: Comparison of the US annualized seismic losses

Figure 2-2: Especial zones and maximum magnitude for the Central, Eastern and North Eastern parts of US

Figure 2-3: Possible moderate to severe seismic design category for New York City

Figure 2-4: Typical Seismic Built-Event-Learn Cycle

Figure 2-5: Soft story mechanism

Figure 2-6: Soft story mechanism and plastic hinge in weak column-strong beam frame

Figure 3-1, Wind and seismic load comparison for the selected models

Figure 3-2, Typical frame elevations for the two stories selected models, E-W direction

Figure 3-3, Typical frame elevations for the four stories selected models, E-W direction

Figure 3-4a, Typical frame elevations for the eight stories selected models, E-W direction

Figure 3-4b, Typical frame elevations for the eight stories selected models, E-W direction

Figure 3-5, Typical frame elevations for the four stories selected models, N-S direction

Figure 3-6, Typical column sections

Figure 3-7, Typical column tie schedule

Figure 3-8a, Roof and floor plans for all frame types B, S, and A, except as noted

Figure 3-8b, First story plan for all frame type A

Figure 3-9a, Typical East-West beam reinforcements

Figure 3-9b, Typical North-South beam reinforcements

Figure 4-1, the code-specified design response spectrum in accordance with Code  
ASCE/SEI 7-05

Figure 4-2, Shear Wave Velocity in the Eastern parts of the US

Figure 4-3, Target response spectrum against the scaled selected ground motions  
spectrum

Figure 4-4a, LPR time series for Fault Normal direction

Figure 4-4b, LPR time series for Fault Parallel direction

Figure 4-5a, WNA time series for Fault Normal direction

Figure 4-5b, WNA time series for Fault Parallel direction

Figure 4-6a, NOR time series for Fault Normal direction

Figure 4-6b, NOR time series for Fault Parallel direction

Figure 4-7a, NAH time series for Fault Normal direction

Figure 4-7b, NAH time series for Fault Parallel direction

Figure 4-8a, Typical backbone curve derives from hysteretic behavior

Figure 4-8b, Typical idealized curve derived from backbone curve- Ductile  
components

Figure 4-9, Idealized curve and threshold points

Figure 4-10, Example of suitable idealized curve for LRC structures under cyclic deformation

Figure 4-11, One story- one span moment frame

Figure 4-12, Example of an experimental and idealized hysteresis behavior of a RC component

Figure 4-13, Typical Pivot hysteresis parameters

Figure 5-1, Example of extended analysis time duration up to damped free vibration

Figure 5-2, Pushover analysis approach: conversion of a system response to equivalent SDOF system

Graph 6-1a, Hinge formation results for selected model 2B12

Graph 6-1b, Hinge formation results for selected model 2S15

Graph 6-1c, Hinge formation results for selected model 2S18

Graph 6-1d, Hinge formation results for selected model 2A12

Graph 6-1e, Hinge formation results for selected model 2A15

Graph 6-1f, Hinge formation results for selected model 2A18

Graph 6-2a, Hinge formation results for selected model 4B12

Graph 6-2b, Hinge formation results for selected model 4S15

Graph 6-2c, Hinge formation results for selected model 4S18

Graph 6-2d, Hinge formation results for selected model 4A12

Graph 6-2e, Hinge formation results for selected model 4A15

Graph 6-2f, Hinge formation results for selected model 4A18

Graph 6-3a, Hinge formation results for selected model 8B12

Graph 6-3b, Hinge formation results for selected model 8S15

Graph 6-3c, Hinge formation results for selected model 8S18

Graph 6-3d, Hinge formation results for selected model 8A12

Graph 6-3e, Hinge formation results for selected model 8A15

Graph 6-3f, Hinge formation results for selected model 8A18

Graph 6-4, Number of maximum drift - classified as group number and plan type

Figure 6-1, Hinges at 2nd level (plan) of model 2A12 under NOR N-S excitation at time 50s; Hinge at 5th level (plan) of model 8A15 under WNA E-W excitation at time 60s

Figure 6-2, Hinges at 1st level (plan) of model 4A18 under NAH N-S excitation at time 35s, overall increase in total of hinges and more severe damage level for hinges at axis 4 around column B4

Figure 6-3, Hinges at axis 1 (elevation) of model 4A12 under NAH E-W excitation at time 26s; Hinges at axis 1 (elevation) of model 8A18 under NAH E-W excitation at time 40s

Figure 6-4, Hinges at axis 2 (elevation) of model 4S18 under NOR N-S excitation at time 55s

Figure 6-5, Damage level under LPR N-S excitation at time 41.0s for axis 1(Elevation view): a) top, story mechanism for model 2A12, b) middle, low damage level for model 2A15, c) bottom, model 2A18 without story mechanism damage level

Figure 6-6, FFT of LPR record in N-S direction and period range for model 2A12

Figure 6-7, FFT of Acceleration response at joint C1 under LPR record in N-S direction for model 2A12

Figure 6-8, Acceleration vs. time for Joint C1 at the first story under LPR record in N-S direction response at joint C1 under LPR record in N-S direction, a) Top: model 2A12, b) Middle: model 2A15, c) Bottom: Model 2A18

Figure 6-9, FFT of Acceleration response at master point of roof level under LPR record in N-S direction for model 2A18

Figure 6-10, Group 1, asymmetric plan models, average drift response for E-W direction (left) and N-S direction (right)

Figure 6-11, Group 1, symmetric plan models, average drift response for E-W direction (left) and N-S direction (right)

Figure 6-12, Group 2, asymmetric plan models, average drift response for E-W direction (left) and N-S direction (right)

Figure 6-13, Group 2, symmetric plan models, average drift response for E-W direction (left) and N-S direction (right)

Figure 6-14, Group 3, asymmetric plan models, average drift response for E-W direction (left) and N-S direction (right)

Figure 6-15, Group 3, symmetric plan models, average drift response for E-W direction (left) and N-S direction (right)

Figure 6-16, Average drift response for models with the first story height equal to twelve feet, E-W direction (top) and N-S direction (bottom)

Figure 6-17, Average drift response for models with the first story height equal to fifteen feet, E-W direction (top) and N-S direction (bottom)

Figure 6-18, Average drift response for models with the first story height equal to eighteen feet, E-W direction (top) and N-S direction (bottom)

Figure B-1: Example of Software Allocated Hinge Parameters-Moment M3

Figure B-2: Example of Software Allocated Hinge Parameters-PM2M3 Type

Figure C-1: Software computed target displacement and related coefficient for model  
2A15 (East-West direction)

Figure C-2: Definition for idealized force-displacement curves for two different post  
yield cases

Figure E-1: Base-shear versus displacement response of model 4B12 for intensified  
LPR and Pushover case

## List of Illustrations

Photo 2-1a: Soft story mechanism and column reinforcement buckling, New Zealand earthquake

Photo 2-1b: Soft story mechanism and column concrete crash, Bhuj India earthquake

Photo 2-2: Columns' damaged due to soft story mechanism, Olive View Medical Center

Photo 2-3: Collapse due to soft story and plan irregularity effect in 2001 India earthquake

Photo 2-4: Architectural condition and collapsed-damaged of The Palace Corvin in 1967 Caracas Venezuela earthquake

Photo 2-5: Soft story damage combine with torsional effect in Taipei

Photo 2-6: Pancake collapse of a RC structure in 1999 Izmit earthquake

Photo 2-7: Total collapse of a RC structure in 1999 Athens earthquake

Photo 2-8: Collapse of a RC structure cause by weak story mechanism and torsional response in Sichuan China earthquake

Photo 2-9: A classic example of soft story failure of RC buildings in L'Aquila earthquake

Photo 2-10: Breakdown of a concrete structure in Mexico City 1985 earthquake, partially because of irregularity

# Chapter 1: Introduction

## **1.1. Background and Motivation**

A review of structural codes and standards in developed and developing countries reveals the constant increase of seismic provisions and restrictions throughout all regions in recent decades. Many zones before were assumed with zero-seismic activity, are now shift to higher seismic level. There are many seismic design requirements that must be applied to even low seismic zones. It behooves many private and public property owners to evaluate their assets and properties against possible damages during earthquake event in the regions where previously known as zero-seismic areas. The needs for more realistic nonlinear dynamic analysis, enhanced guidelines and criteria for structural assessment, and also benchmarking and calibration of current acceptance criteria in seismic analysis (Deierlein 2012) are the common encountered problems in any advanced evaluation of existing buildings against earthquake. Challenges come from many uncertainties in analysis and design procedure for dynamic response of existing structures (Ibid). For instance, cyclic models with strength and stiffness degradation, several different models of deteriorations and failure modes, and non-ductile Reinforced Concrete (RC) systems are few of them (Ibid). The requirements to elaborate better modeling and understanding of performance indices is not new, indeed during the breakthrough of structural performance assessment in 90s the importance of suitable analysis and design in computational approaches were mentioned (White 1996). The most well computational methods for nonlinear dynamic or nonlinear static analysis can hardly be performed for designing of structures. The major purpose is not to provide precise reproduction of the structural response during earthquake, but to reach a reasonable assessment of structure performance (Powell 2004). The first steps in seismic assessment of structures are finding deficiencies and weak points. These deficiencies

may imply to several broad issues, from the applied material and quality of construction to the structural configurations.

One of the configurations, which have been attractive among modern architectural design since early 20th century, is known in architectural technical term as the open floor (Guevara-Perez, 2012). This configuration is one the most possible format of imposing vertical and/or plan irregularities in structures. In fact, the appropriate configuration of the structural system is one of the most important factors for seismic performance evaluation of the buildings. Nonetheless, most of the time, insufficient attention is paid to this aspect in seismic design, particularly in the areas where are known as low seismic zones. Only few of the recent design codes underline the configuration problem (Parducci et al. 2005). Configurations and shapes are the elementary principle formats in seismic evaluations or design process. The shape considerations in the classic earthquake engineering may be divided into absolute dimensions, compactness and symmetry, and regularity (Mezzi and Parducci 2005). The basic configuration parameters, mainly building dimensions, are correlated to the seismic behavior of structures, which are the first applied considerations in structure design standards (Ibid.). One of the most important objectives in seismic design is avoiding the irregular distribution of induced forces. By this, in the best case of an intact seismic design procedure all the structural members involve to the seismic resistance and energy dissipation process (Mezzi and Parducci 2005). Thus, distribution of masses, resistances, stiffness, and eccentricities extremely affect the seismic response, and impose significant limits to the variation of selected structural configuration. Any vertical or plan irregularity may distract and disturb proper seismic force flow in a structural system, specifically if the seismic design regulations have not been followed during design procedure.

While there is a general agreement on severe hazardous side effects of irregularities on structural seismic response, the irregular aspects are very attractive, at least for low- to medium-height buildings. As mentioned before, the regularity principles are often against some visions of the modern architecture, such as the soft first story and/or plan irregularity. The irregularities have been, and still are, widely applied by architects to represent one of the modern architecture elements in design

(Mezzi and Parducci 2005). The open floor aspect may comprise of a taller story (soft story in seismic terminology) which may combine with elimination of some columns on the same floor elevation (lead to torsional problem). Soft first story creates a sense of floating and bright spaces in architectural point of view. The famous architect Le Corbusier was one of the developers and pioneers who applied the idea of soft first story (Fakhouri and Igarashi 2011). Design of many buildings is significantly influenced by either aesthetic or functional considerations that are often against the simplicity and symmetry preference in seismic design. Consequently, the majority of such structures would be categorized as irregular, both in plan and in elevation (De Stefano and Pintucchi 2008). Starting from the first steps of the architectural design, when the morphology of the building is defined up to the final stage of construction, the vertical and plan irregularity situations may be manipulated in the buildings. Since this type of composition can provide attractive and advantageous solutions from the architectural point of view, i.e. both aesthetical and functional, there are numerous typical multi-story RC buildings in the United States (US), where the architectural design often applied irregularities widely.

As pointed out by Haselton et al. (2011), the empirical nature of the design provisions and their development impose a degree of vague to collapse safety and in this specific case, many aspects of current building codes and standards are not clear. This uncertainty increased in low and moderate seismic zones since reliable data and records are rare in these regions. Developments in advanced approaches such as nonlinear dynamic analysis, seismic hazard analysis, and performance-based earthquake engineering are allowing more precise and scientific assessment of structural collapse risk and how it is affected by building code design requirements (Ibid.) for high seismic areas. However, these fields of research are not popular in low and moderate seismic zones, whereas the high seismic zones get more and more attention from local authorities. For instance, the report with the subject: Potentially Hazardous Soft, Weak, or Open Front Story Buildings (City Manager Report 2005) can be considered as a good example for high seismic zone awareness.

Another issue is lack of code definitions for irregularity resulting from the combination of both plan and vertical irregularities. Structural system irregularity

does not exclusively depend on structural properties. The ground motion characteristics and the distortion in structural properties due to variable, such as cracked concrete elements, shall be stipulated (Nafday 2011). Story shear distribution is mostly due to dynamic excitation and response of a structure, which in turn, evidently depend on the relative stiffness of adjacent floor levels. In frame system structures, large changes in story stiffness may occur by changing columns' height or cross section. Similarly, shifting, relocation, or elimination of columns in building plan plays an important role as well. For concrete frame structures, these changes are the foremost effective contributors to the overall seismic response. Actually, plan or elevation irregularity may lead to uneven concentration of deformation, and the damage concentration tends to be more severe and unpredictable when the concrete frame experiences significant inelastic deformation. Therefore, an initial inappropriate structural design without suitable balance of the relative stiffness of adjacent floors, especially for irregular structures, may create a complex reaction along with dangerous and unsafe condition. Indeed, soft story mechanism is one the most observed failure modes of RC structures which mostly happens in the bottom story of the building (Plumier et al. 2005) in many suffered earthquake occurrences.

To enlighten the deficit level in this case, it should be mentioned that the structural irregularity is an extremely complex phenomenon and structural configuration is a very important factor on the seismic behavior response which has been implied directly or indirectly in seismic related codes and standards. Indeed, structural irregularity has been a major concern in the earthquake engineering and structural design over the last several decades. Bearing in mind that code provisions for torsion and elevation irregularities have been derived mostly from elastic studies or from inelastic simplified studies, almost all Codes and Building standards put limitations and penalties for the vertical and planar irregularities, especially in the high seismic zones.

Nevertheless, the ASCE 7-05 and ASCE 7-10, which are the two most dominant and accepted structural loading standards in the US, have not put any strict regulations for the irregular structures in the low to moderate seismic zones. Truly speaking, for some vertical irregularities such as soft story irregularities, there is not

any restriction in the afore-mentioned code for the low to moderate seismic areas (e.g. see table 12.3-2 on ASCE 7-05, types 1a, 1b, and 2), neither they put some exceptions to exempt vertical irregularity provisions for those areas (e.g. see Exceptions 1 & 2 under section 12.3.2.2, ASCE 7-10).

Mid- and low-rise RC frames are very popular building systems in the mid part of the US (Ramamoorthy et al. 2008), and in the Eastern or North Eastern parts they represent a common type of construction. Actually, in most parts of the US, the most prevalent RC building construction is non-ductile frame structure which continues almost to the present (Hamburger and Scawthorn 2005). These types of structures have been constructed with several undesirable seismic configurations. Moehle (2008) listed a top ten non-ductile concrete structures characteristics. These characteristics are categorized based on the commonly associated building collapses. The list particularly shows the problem in reinforced concrete design, mostly common design practice of the older codes (pre-1976 in California), even though he mentioned that they most likely be encountered anywhere in the world. The Moehle's list is (2008):

“A) Column mechanism: Weak-column, strong beam moment frame or similar system prone to story collapse;

B) Other concrete moment frames: Moment frames (other than category A) with typical era details in columns, beams, joints;

C) Captive columns: Shear and axial failure of columns due to partial-height infills;

D) Shear-critical piers: Shear and axial failure of piers in perforated or pier/spandrel wall buildings;

E) Open first story: Weak first story prone to sidesway collapse due to discontinuous concrete or masonry infill in stories above;

F) Discontinuous wall: Columns prone to crushing from overturning of discontinuous concrete or masonry infill wall, as distinct from category E;

G) Severe plan irregularity: Conditions (including some corner buildings) leading to torsional-induced demands;

H) Deformation Compatibility: Gravity system collapse under imposed lateral drifts, including slab-column, beam-column, lift slab, and other framing;

I) Pounding: Collapse caused by pounding of adjacent buildings;

J) Foundation failure: Inadequate foundation conditions, including ground failure, ground settlement.”

It can be seen among his list that items A, E, F, and G are directly related to the vertical and torsional irregularity mechanism. Parenthetically, items B, C, and H can also be triggered or created by torsional and vertical irregularities. NEHRP (2010a) also provides a very similar list to the Moehle’s list, in which 10 categorized seismic deficiencies are listed as deficiency A to J. Among the NEHRP list, Deficiency E through Deficiency J are mentioned as system-level deficiencies, which alone or in combination with the other structural paucities can increase the collapse potential of the whole structures. Four of these major system-level deficiencies are directly related to the vertical and/or plan irregularity problem. In this study, some of these factors associates with irregularities are considered.

Kirac et al. (2011) classified some parameters, which are the most affected soft story irregularity formation in structures. Although without deliberate considering of probable torsional exacerbation influence, their list may add some other overall configuration issues to the problem:

1. Weak story height;
2. Existence of mezzanine floor;
3. Rigidity and distribution of columns, or sometimes shear walls and bracings, in weak story, which increase torsional irregularities;
4. Overhang and cantilever projection in a weak story;
5. Infill wall material properties, specially stiff but brittle materials such as solid masonry bricks;
6. Soil class and site seismic properties;
7. Number of floor in the building;
8. Seismic conditions of site.

Clearly, all the former lists illustrate that the existence of both torsional and vertical irregularities in a structure can lead to significant seismic damage risk. As

mentioned before, most of soft story settings are located at the first or ground story, also due to the drastic plan changes, torsional irregularities frequently detected at the same story. Accordingly, if the first story is damaged or collapsed, the whole building will be destroyed or become at least unusable. In addition, irregularities usually induce uneven response for higher stories. The higher stories may have regular format in plan or elevation by themselves, but induce uneven displacement or force flow from the irregular first story may impose critical structural condition to the higher stories.

In recent decades, seismically damaged or collapsed structures have revealed several common element related deficiencies. Besides the afore-mentioned configuration issues, several other issues can be classified under the lightly reinforced concrete (LRC), which simply means insufficient embedded rebar in the concrete. They are mainly due to a)-inadequate reinforcement details, b)- lack of confinement in beams and especially columns which have been designed per old seismic codes, c)- shear failure due to low aspect ratio of shear span to depth ratio, and d)- inadequate reinforcement for members compression or tension capacity. Adding element deficiencies and lightly reinforcements, the unbalanced layout of structural members in elevation or plan acerbates poor seismic behavior and ultimately can lead buildings to downfall partially or completely. From the previous discussion regarding irregularity issues, combination of these two dangers, i.e. individual structural members with insufficient capacity and skeleton plan and vertical irregularities, may generate a life threaten hazard, which are mostly ignored in low or moderate seismic zones. General practice in these zones for low- to mid-height structures, at least up to the last decades, has been considered as design for gravity loads and sometimes wind loads as lateral loads. In these regions, seismic provisions were applied, if any, for very important structures. Consequently, a moderate seismic event may cause many structural problems and even severe life endangering risk for those structures that “added up” all frame, plan, elevation, and elements vulnerabilities, which all of them are usually unacceptable for high seismic regions.

The problem may get worst in many low to moderate seismic zones such as the Eastern and North Eastern parts of the US. There are vast areas that in the past were assumed to have low seismic area or even with zero hazard danger, but currently seismic standards allocate them to higher level of seismicity. In this regard, the Central part of the US gets more attention. However, particularly speaking, the Eastern and Northern areas of the US, which are usually accepted as low seismic areas, have potential for recurring hazardous earthquakes. Lower attenuation capability of the ground layers, abundance of weak and non-ductile structures, immature seismicity knowledge and practice in these areas, higher population in comparison with the mountain zones (Southern and even the West coast of the US), poor soil condition in many areas, and more uncertainties regarding seismicity show the need for more attention to the seismic hazard and risk assessment in the Eastern and Northern parts of the US. With gradually more stringent requirements for earthquake resistant construction in the standards and jurisdiction codes, a large number of existing structures is now categorized as seismically vulnerable to various degrees in these regions. Incidentally, evaluation of existing structures regarding seismic protection would be a higher priority. The replacement cost of most of these structures and economical side effects are significant (Pardalopoulos et al. 2005), which may clarify the level of importance for this case.

As a consequence, the configurations of the buildings having a "soft first story" and also "asymmetric plan" in terms of mass or stiffness, especially when they amalgamate together, are one of the most recurrences which can be observed both in seismic and non-seismic zones. As mentioned earlier, these configurations are very popular in low seismic zones, as the buildings codes usually have not put strict regulations regarding irregularities for those zones in current standards. While there are several researches with respect to horizontally irregular structures, the studies regarding the behavior of structures with vertical irregularities are small in number (De Stefano and Pintucchi 2008). Besides, most research activities in this field have been almost dealt exclusively with 2D frames extracted from 3D plan-symmetric structures so that torsional effects have not been thoroughly involved (Ibid.). De Stefano and Pintucchi (2008) found the shortcomings of simplified popular one-story

models for plan irregularities. They noticed that in the studies in which more realistic multi-story models have been accomplished, the inelastic response have been acquired more precisely. Depending on the building configuration and the arrangement of structural and even architectural members, the structural irregularity is a mutual combination of irregular distribution of stiffness, strength, and mass within the structure height and plan. However, the number of researches that take into account both of them in one structure and study their side effects as part of the whole response is very rare. Almost all researches consider each irregular vertical or planar effect individually. Furthermore, many times in a building with soft story case the center of strength and center of mass are virtually eccentric. In this situation, the building is expected to translate and rotate in plan, amplifying the drift demands in columns located further distant from the center of strength, which may lead to severe damages.

Basically, the problem has not been taken into adequate consideration in the current professional practice in many low seismic areas. Moreover, as explained before, the majority of design in these regions has been accomplished without any seismic provisions. Deficits attribute to lack of seismic activities in low to moderate zones may lead to underestimate of the effect of several undesirable seismically structural responses. The result can have drastic effect in the retrofitting design of existing buildings. There are wide spread of low- to mid-rise RC structures, which not only are classified as LRC, but also have irregular configurations. These structures have been assumed to be located in low seismic zones. In order to evaluate their response, traditional static analysis may not be sufficient. Their possible dangerous deficiencies require more precise nonlinear analytical methods. While there is a general agreement on low damage level from ground motions in low seismic zones, there is a considerable agreement with respect to the impact of overall ignored structural weaknesses to the safety of non-seismically designed buildings. These ignored weaknesses may lead to concentrate and accentuate damage in some specific parts of gravity load designed RC structures, and consequently may tend to cause significant seismic risk. The more sophisticated analytical and mathematical procedures are essential to reflect their close-to-real behavior during seismic event,

and ultimately provide an estimate of code regulations and effect on the public safety. Throughout the world, there are vast areas in every continent known as low to moderate seismic zones commensurate to the recorded ground activities. Obviously, not all these areas can be covered within the framework of this study. Thus, only the North Eastern part of the US is considered. To the best knowledge of the author, there has not being any specific study accomplished regarding irregularity effects on seismic response of non-seismic resistance designed RC structures in low to moderate seismic zones. Therefore, the development of this study is instigated by the lack of such studies in order to provide an insight primary knowledge regarding damage level of the existing irregular LRC structures in low seismic zones.

## **1.2. Scope and Organization**

This study is anticipated to contribute in two ways to the response of lightly concrete structures located in low seismic zones. First, this work is expected to explore the plan and elevation irregularity effect on the structural behavior during earthquake. Second, the nonlinear analysis will be uses to examine adequacy of current US seismic standard code provisions for this type of structures located in low seismic zones.

The common series of design steps for the performance and correlation estimation process incorporate as: 1) Preparing the mathematical model of buildings and definition of material properties and member sections which also include allocation of live, dead, and wind loads. Typical building dimension selections are part of the first step as well. 2) Next, preliminary and final designs with detailing based on static analysis method, estimation and definition of the mechanical characteristics of structural elements, and formulation of the building models will be completed. The common design and construction practice will be followed to provide the closest possible structural models resembling real buildings. 3) Then, nonlinear dynamic and static (pushover) analyses will be performed based on advanced material behavior definition. Ground motions will be selected and scaled, based on the low seismic zone classification. In order to compare and satisfy corresponding failure

criteria, relevant forces and deformations at the global level will be monitored. In this study, the influence of plan and/or elevation irregularities associated to the first-story-level columns will be composed with the focus of possible soft story formation. Inherent Capacity (IC) of the frames, i.e. the capacity provided by the gravity system alone, which may also be affected by wind load, will be considered as the only seismic resistance system of the studying archetype structures.

It should be mentioned that literally there is a delicate difference between “Weak” and “Soft” story definition although many researchers are used these two words interchangeably to explain one seismically hazard phenomena on technical texts and literatures. “Soft story” and “Weak story” are often mistaken for each other (Guevara-Perez 2012). The soft story is simply defined as a flexible story with difference of stiffness between one story and the rest. On the other hand, the weak story is significant difference of lateral resistance against seismic forces between building’s levels (Ibid.). These vertical irregularities may occur simultaneously, and mostly common at the first story above ground level, although each of them could be happened at any intermediate level as well. In fact, the stiffness irregularity consists “soft story”: “A soft story is one in which the lateral stiffness is less than 70% of that in the story above or less than 80% of the average stiffness of the three stories above” (Kirac et al. 2011). In contrast, the discontinuity in capacity and strength creates weak story: “A weak story is one in which the story strength is less than 80% of that in the story above. The story strength is the total strength of all seismic-resisting elements sharing the story shear for the direction under consideration” (Ibid.). Despite the subtle technical difference, this study is in line with the several accepted codes in the US and the majority of pertinent literatures, “Soft” term is used to describe the vertical irregularities with emphasis on the Soft Story condition.

Chapter two (2) of this study provides an introduction of the seismicity in the Eastern and North Eastern regions of America as the selected low seismic zone. This is followed in section two with a description of the soft story that comprises the irregularity related failures in the past earthquakes. Description of lightly reinforced concrete (LRC) structures is the next part of this chapter. Building codes have

specific provisions regarding irregular structures, which are discussed with emphasis on the US codes. Literature review is the last part of chapter two.

Static analysis and design are described in chapter three (3), along with the applied lightly reinforced concrete design philosophy and principles for the model classifications. Acceptable non-seismic performance, modal analysis, and review of wind load versus static seismic loads are other parts of this chapter. Plans, elevations, sections and assigned reinforcements, which are used as basis for nonlinear analysis, are the last part of chapter three.

Nonlinear seismic methods and analysis assumptions are discussed in chapter four (4). Basic nonlinear assumptions and effect of gravity load encompass the first section. Detailed guidance for the time history record selection is the second section of this chapter. Plastic hinge definition, nonlinear assumptions, and allocation to the structural members based on a rigorous hysteresis method are also part of this chapter. Development of damping ratio is the last part of chapter four, which also includes the selection of proposed coefficients to be assigned to the selected models.

Both nonlinear analysis methods, time history and pushover procedures, are included in chapter five (5). The application of direct-integration time history along with analytical stability condition and output accuracy is contained in the first section. Nonlinear static approach is used as the secondary method in this study. Assumptions, estimate of the target displacement per FEMA 356 (2000) and overall procedure are described in the last part of chapter five.

Parametric study and analysis issues are covered in chapter six (6). First, a general evaluation overview is presented. Next, hinge formations, sequences, and damage levels for all the selected models are discussed. Afterwards, the observed story mechanism is discussed in more detail through the frequency domain study of time history responses for few affected models. Finally, this chapter ends with story drift discussion. Response of the selected models is reviewed in order to realize consequence of irregularities on all stories regarding type of models, first story height, and plan irregularity.

As a final point, summary, conclusions, and recommendations for future research are provided in chapter seven (7).

Acronyms and abbreviations are in appendix A. To verify the software allocated plastic hinges, a sample calculation for the beam and column is presented in appendix B. In order to verify the accuracy of pushover method, the software calculation is compared with numerically computed target displacement in appendix C. The total results of hinge formations for all the models corresponding to the four applied seismic record sets are covered in appendix D. With the general aim of overall software result verification, Appendix E devotes to an example of load-displacement response review for both time history and pushover cases of one selected models.

## Chapter 2: Literature Review

### **2.1. Seismicity in the Eastern and North Eastern America**

#### **2.1.1. Introduction**

In the Central and Eastern United States, which are known as moderate and/or low seismicity zone, seismic evaluation is rarely done and seismic rehabilitation are almost nonexistent (NEHRP 2010a), although in the case of federal buildings, ICSSC RP 6/NISTIR 6762 (Standards of Seismic Safety for Existing Federally Owned and Leased Buildings) requires that the existing federal buildings in the moderate and low seismicity zones to be treated similar to the federal buildings in regions of high seismicity (Ibid.). Compared to the Western seismic activities, the typical seismic hazard characteristics of the Eastern ground motion can be summarized in higher amplitudes at higher frequencies and slower attenuation with distance (NEHRP 2011). The central part of the US adopted seismic code several decades ago due to the severe historic earthquakes of New Madrid (1811-12) and Charleston (1886), which are surprisingly the largest historical documented seismic events in the US. Even with that fact, the Eastern and North Eastern parts of the US have taken on the seismic provisions only few decades ago, for example, Boston was the first Eastern US city which adopted a seismic code in 1973, and New York in 1995 considered its seismic code (Nikolaou et al. 2012). Seismic activity in the Eastern part of the US is not well defined, but the ratio of peak ground acceleration of maximum credible earthquake to maximum expected earthquake could be about 6:1 on the East Coast important facilities (Ellingwood, et al. 2007). In comparison, the same ratio is about 5:4 in the West coast of US. This comparison enlightens possibility of high level of damage in low seismicity zones for seismic vulnerability of an existing concrete building with the non-seismic consideration in design and construction process (Ibid.). FEMA has

published risk analysis in term of annualized losses for the US (FEMA 366 2008). The FEMA’s study has revealed that except California, the amount of annual loss for the Central, Eastern, and North Eastern US can be equal or higher than most part of the US. Figure 2-1 shows a general comparison of the annual earthquake losses from their report.

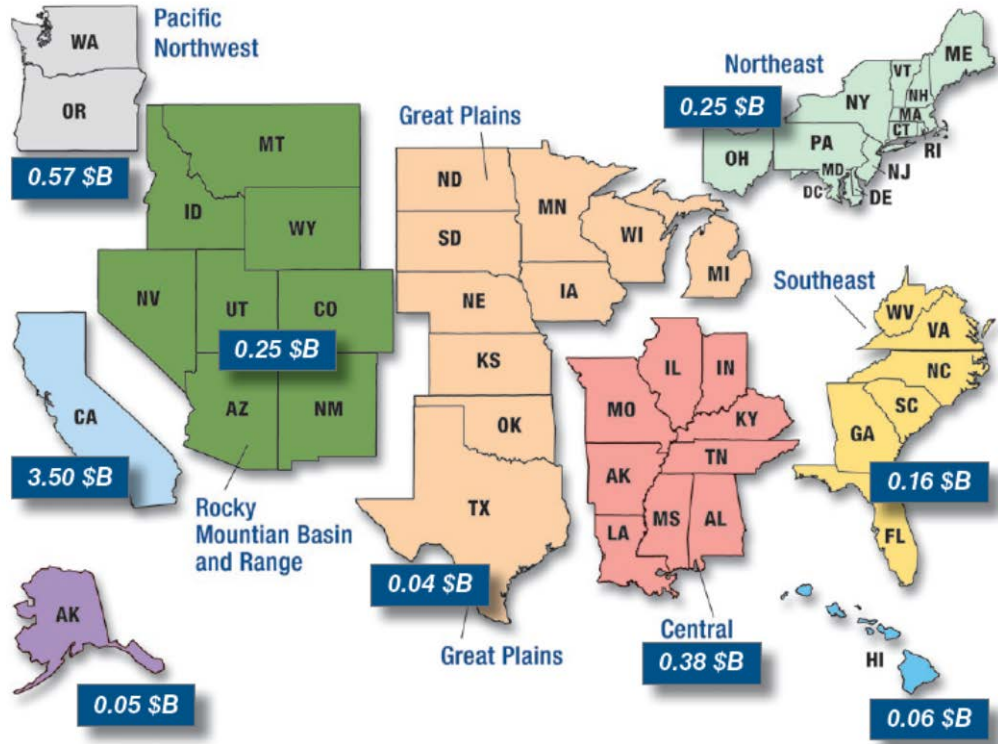


Figure 2-1: Comparison of the US annualized seismic losses (Source: FEMA 366 2008)

The August 2011 earthquake in Virginia was a moderate to low magnitude seismic event in terms of seismic terminology. Nonetheless, total damage was estimated about \$300 million spread over a large area, caused widespread confusion among public and emergency agencies and lack of preparedness among their personnel, and cellphone service and public transportations were disrupted in areas which were closer to the seismic center (Nikolaou 2013). The 2011 seismic event in Virginia acted as a reminder to prove that although infrequent in nature, earthquakes do occur in this part of the US. Post investigation of 23 August 2011 earthquake in

Virginia showed that the asymmetric distribution of the seismic intensity, unique geotechnical form of bed rock, and tectonic of the North-East caused more seismic propagation energy toward Northern and Eastern areas, such as Washington DC and New York (Horton and Williams 2012) and (Nikolaou 2013). US Geological Survey published a comparison between M=5.8 magnitude Virginia earthquake (23 August 2011) and one of similar magnitude and depth seismic events in California (M=6.0, 28 September 2004). The comparison illustrated that the earthquake effect was felt over much larger areas in the Eastern US than the West Coast although the West Coast is known as high seismic active zones (Ibids.). The comparison between 1895 M=6.8 Charleston (Missouri) earthquake and the 1994 M=6.7 Northridge (California) earthquake (Wren 2006) showed the same pattern, i.e. more feeling areas and wider propagation reported toward the North and East of the US in comparison with the West Coast area for two similar magnitude earthquakes. It is worth to note that still considerable uncertainties remain about the nature, source, magnitude, and type of the seismic activity and hazard possibility associated with the Eastern, Central and Northern parts of the US (Horton and Williams 2012).

### **2.1.2. Tectonic and Seismicity in the Eastern and North Eastern America**

The Eastern US has unique geological and tectonic characteristics, such as very hard bedrock, sparse strong motion data or lack of data, and very different overburden soil (Nikolaou et al. 2012). From seismological point of view, the Intra-plate mechanism, i.e. an earthquake along a fault within the stable region of a plate boundary, is the main reason of seismic activity in the most Central part of the US, and the known source of the seismic events in the Eastern and Northern portions of the US. Typically, there are a lot of uncertainties about intra-plate earthquakes. Generally, the specific mechanisms for these earthquakes are poorly understood, and their occurrences are very infrequent. The causative faults in the Central and Eastern US are shallow in term of tectonic, less than 25 km, and possible rupture mechanisms can be explained as shear failure of the brittle rocks due to very old fractures in beneath of the continental crust. In the Western part of the US there are many active faults and probably few unknown faults which are known as major seismic event

makers. On the other hand, in the Eastern part, it is much more difficult to identify active faults, therefore localizing geo-structures (i.e. an identifiable geological structure caused seismic activity) and seismo-tectonic provinces (i.e. a region with a known seismic hazard but without any identifiable active fault) are source of occurring earthquakes. These parameters create a complex semiology wave propagation, since the high frequency bedrock and low frequency deep soft soil impose different and wide range of wave shapes, and also the attenuation of the engaged layers are less in comparison with the mountain zones or the west coast area. In the Central and North Eastern America with low or moderate seismicity, it is difficult to identify and allocate potential seismic sources and regional faults sources have usually been considered as 'areal source zones' (Chandler and Lam 2001). Hence, seismic activity is dispersed over the entire region instead of concentrated at a few fault lines, and large magnitude earthquake events can transmit long period ground motions over very long distances due to the crustal environment of most part of the Central and North Eastern America (Ibid.).

Figure 2-2 shows the location of especial zones with regional maximum magnitude for the Central, Eastern, and North Eastern parts of the US (USGS 2008). Magnitude of 7.0 and more usually demonstrates a considerable potential of seismic event. Clearly, a probable severe seismic hazard event in the Eastern US may create more serious structural damage. The Eastern, North Eastern and some parts of Central US are regions with moderate but highly unpredictable earthquake activity, and most structures do not have sufficient seismic design. Therefore, in these areas structures are exposed to almost a high seismic risk with potentially significant socioeconomic and extremely life threatening effects (Nikolaou 2013). There are other primary issues for the Central, Eastern and North Eastern America that distinguish them from high seismic regions (Hines et al. 2011), such as: lack of recorded strong motions and therefore uncertainty with respect to magnitude (M) and distance (R); and also soil amplification factor is usually greater since the soil performs linearly at the lower intensity seismic action (Ibid.).

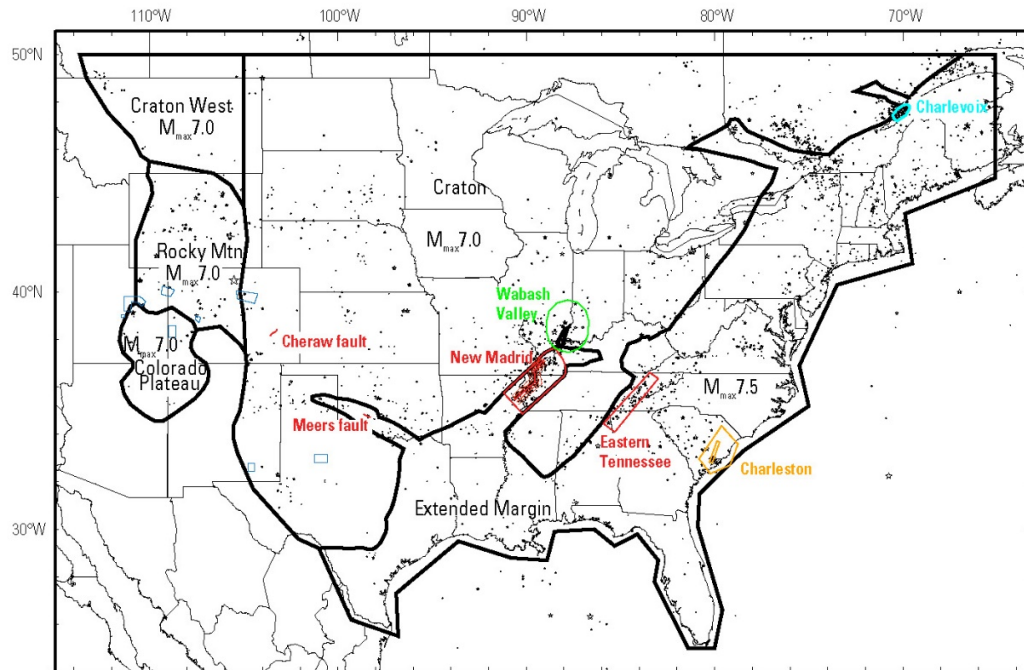


Figure 2-2: Especial zones and maximum magnitude for the Central, Eastern and North Eastern parts of US (Figure from source: USGS 2008)

For the seismic design of the new structures, according to the ASCE 7-05 or ASCE 7-10, the Seismic Design Category (SDC) should be determined which are classified from A to F, (ASCE 7-10). In the Eastern and North Eastern parts of US, depending on the site and facility class, SDCs B, C, and D are the most common hazard categories with some higher and exceptions toward the Central US (Nikolaou et al. 2012).

Unlike the older seismic code provisions, applied seismic loads in the IBC 2000 and ASCE 7-02 and their newer releases have been drastically affected by the site classes. Therefore, difference in site class, i.e. site soil, in low or moderate seismicity regions may change SDC. Consequently, due to site soil classification, many commercial and residential buildings would have a  $0.2g$   $S_{DS}$  or even greater than  $0.33g$  (Nikolaou et al. 2012), which can also be directly referred to United States Geological Survey (USGS) hazard map at:

<http://earthquake.usgs.gov/hazards/products/> (2014). New York City from the North Eastern part of the US is presented to enlighten the previous discussion. The USGS seismic hazard map, origin of the current hazard map for ASCE 7-10 and IBC (2012),

shows  $S_s=0.278g$  and  $S_1=0.072g$  for New York City. Then, assuming a case with Soil Class E and Importance Occupancy Category I to II, and by using USGS Geologic Hazards Science Center application (Figure 2-3), the result would be SDC C, which shows a moderate to severe condition for seismic design (ASCE 7-10 2010). In case of Occupancy Category IV, SDC falls into D classification which interestingly represents a higher level of seismic design category. By the way, it is worth to note that by using ASCE 7-05 seismic provision instead of ASCE 7-10, one might get even higher seismic zone for most part of the North Eastern and Eastern parts of the US (Nikolaou 2013). For instance, again assuming New York City and similar Occupancy Category as above, and by moving from ASCE 7-10 to ASCE 7-05 code, one can see shifting from SDC C to SDC D (Ibid.)

Moreover, the abovementioned results were basically for a seismic hazard with 475 years return periods. From USGS hazard maps, the hazard for the two percent (2%) probability of exceedance in 50 years can be compared with the hazard for 10 percent (10%) probability of exceedance in 50 years. The two percent probability shows 2~4 times higher values than the 10 percent in 50 years exceedance in Central and Eastern parts of the US maps (USGS 2008).

**USGS Design Maps Summary Report**  
**User-Specified Input**

Building Code Reference Document ASCE 7-10 Standard  
 (which utilizes USGS hazard data available in 2008)  
 Site Coordinates 40.73083°N, 73.98667°W  
 Site Soil Classification Site Class E - "Soft Clay Soil"  
 Risk Category I/II/III



**USGS-Provided Output**

$S_s = 0.278 \text{ g}$        $S_{M2} = 0.671 \text{ g}$        $S_{M1} = 0.447 \text{ g}$   
 $S_1 = 0.072 \text{ g}$        $S_{M3} = 0.251 \text{ g}$        $S_{D1} = 0.167 \text{ g}$

For information on how the  $S_s$  and  $S_1$  values above have been calculated from probabilistic (risk-targeted) and deterministic ground motions in the direction of maximum horizontal response, please return to the application and select the "2009 NEHRP" building code reference document.

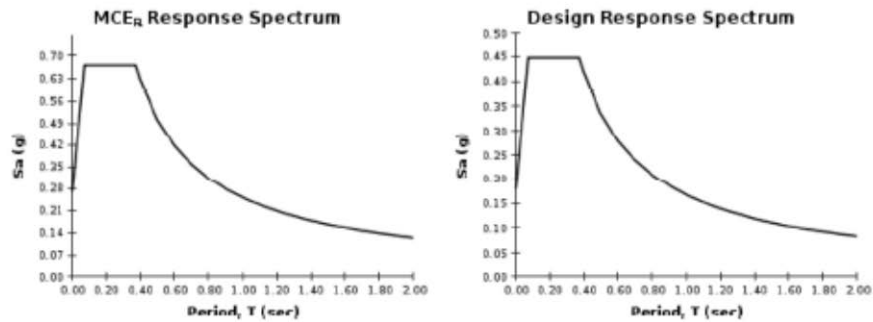


Figure 2-3: Possible moderate to severe seismic design category for New York City

## 2.2. Soft Story Failure and Irregular Collapse from Past

### Earthquakes

#### 2.2.1. Introduction to Soft Story

In essence, seismic design is a comprehensively try and error practice which can be classified as typical Build-Event-Learn circle shown in Figure 2-4 (FEMA P-752 2013). Every single considerable ground shaking event may feed several

important and new information regarding earthquake engineering in general, and structural design in particular. Seismic design and analysis broadly rely on the previous events where the past damages and collapse mechanisms deeply help to clarify the future design procedure.

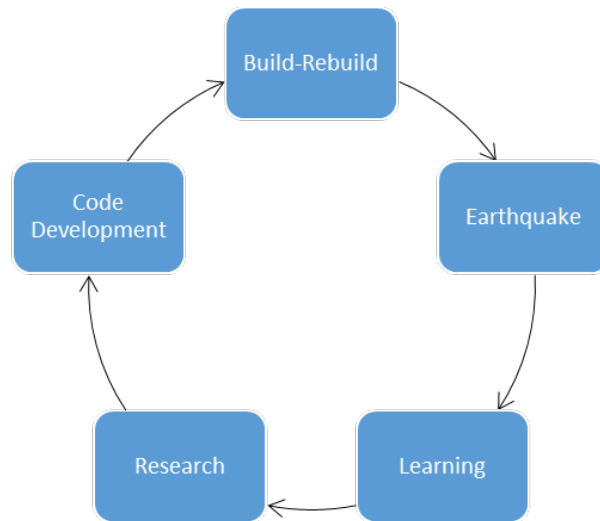


Figure 2-4: Typical Seismic Built-Event-Learn Cycle (FEMA P-752 2013)

From the past events, collapsed and damaged structures are studied. Three components whose failures have often been linked with older reinforced concrete building collapse are (Moehle 2008): Column failure, beam column joint excessively overstressed, and inadequate seismic capacity of flat slab systems. A major priority in any seismic assessment is to examine the strength and deformability of those components, especially for the structures which are not designed to resist earthquake, or do not have enough seismic capacity. Typically, collapse of a reinforced concrete building is caused by failure of the main vertical load bearing components. Basically, a soft story mechanism, which may completely or partially lead to collapse of a structure, is associated to column failure. Column failures can arise from a number of deficiencies. Lack of sufficient shear strength causes shear failure, and consequently loss of vertical load carrying system creates axial failure. Flexural-compression failures are also possible for columns. Widely spaced transverse reinforcement is the major reason of flexural-compression failure, especially for exterior and corner

columns where overturning effects of earthquakes can result in large axial compression. Another main deficiency is bond failures which are related to large flexural bond demands. In addition, inadequate longitudinal reinforcement and lap splices have caused column failure, although it is believed that collapse is seldom linked directly to this type of insufficiencies (Ibid.). Figure 2-5 depicts the soft story mechanism.

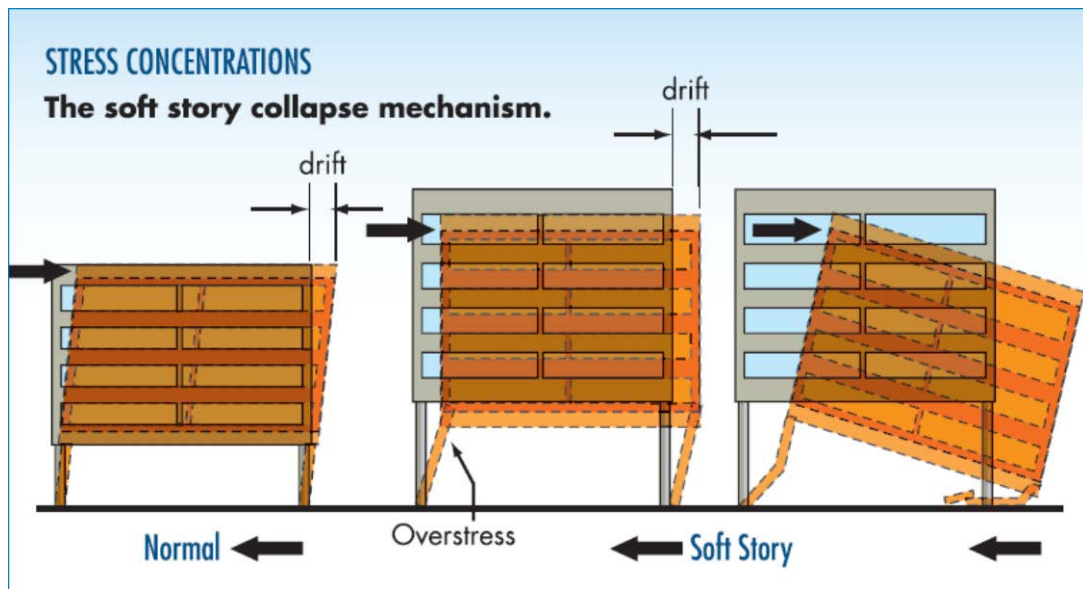


Figure 2-5: Soft story mechanism (Adopted from: Design Guide for Improving Hospital Safety in Earthquakes, Floods, and High Winds: Providing Protection to People and Buildings FEMA 577, June 2007)

Soft (Weak) first stories are usual in multi-story residential buildings in urban areas, in which first story is used for open space, commercial facilities or garage. For example, structural walls, or even columns, may be discontinued in the first story to get more flexible usage space. The first story columns during earthquake must resist a large base shear, inevitably leading to large story drift concentrated in that story (Otani 2004). Usually, reconnaissance reports are published shortly after each moderate to significant earthquake event all around the world, mainly to evaluate damages. One of the commonly reported damages in almost all reconnaissance reports is soft story which is closely related to architectural configuration (Guevara-Perez 2012). Indeed, from a simple structural point of view, soft story building is like

an inverted pendulum where the most drift is concentrated at the soft story level in general and columns in particular. In another word, soft story has substantially less stiffness, or inadequate ductility, or insufficient strength to resist induced displacements and forces during a seismic event. Dooley and Bracci (2001) showed that the probability of a story mechanism in a frame building reduced as the column-to-beam strength ratio increased.

Soft story is directly related to maximum structural drift (Figure 2-5). The determination of maximum drift comprises building displacement during inelastic response phase. As shown in figure 2-5 for regular buildings, the elastic modal shape can approximately determine the inelastic displacement response (Chandler and Lam 2001). However, due to formation of plastic hinges, the elastic modal analysis may not show the possible inelastic displacement of vertical structural elements, such as soft story mechanism. Basically, the plastic hinge rotation capacity corresponds to the ultimate compressive strain of confined concrete ( $\epsilon_{cu}$ ) and the ultimate tensile reinforcement strain ( $\epsilon_{su}$ ). In which,  $\epsilon_{cu}$  is a function of the volumetric ratio of the confinement (tie spacing) and  $\epsilon_{su}$  is associated to stress-strain property of the longitudinal reinforcements (Chandler and Lam 2001).

For soft story mechanism, almost all inelastic deformations take place in a single story, which is often the first story of structure as shown in figure 2-6. The mechanism takes place only if the plastic hinges develop at both ends of vertical element and in opposite bending action (Fardis 2009). The rotation at the ends of the vertical elements ( $\phi_{st}$ ) can be calculated as the roof displacement,  $\delta$ , divided by the height of the soft story,  $H_{st}$ , or:  $\phi_{st} = \delta / H_{st}$ . The rotation ductility ratio in the soft story columns may calculate as  $H_t / H_{st}$  multiple by the global displacement ductility factor,  $\mu_\delta$ . Apparently, considering normal buildings' story height, this ratio would be very high. Therefore, it is very hard to reach a reasonable rotation capacities to meet the required rotation demands in medium or high-rise buildings in which usually  $H_t \gg H_{st}$  (Ibid.) even with a very low ductility demand such as  $\mu_\delta = 2.0$ . Consequently, it is almost unfeasible to seismically design and detail a building to show a controllable sway structural behavior. To prevent soft story mechanism, the vertical elements

should be enforced to stay elastic above the base elevation, and only allow them to enter in the inelastic response after the horizontal elements plastic hinges have been formed.

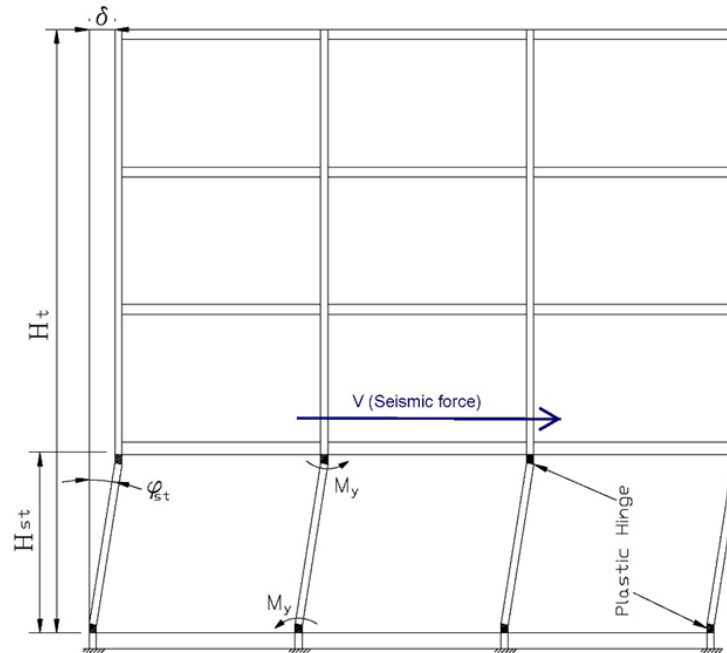


Figure 2-6: Soft story mechanism and plastic hinge in weak column-strong beam frame, Sketch adopted from (Fardis 2009)

Also there are some other concerns with regard to vertical elements, and particularly for concrete columns. Due to the adverse effect of axial compression force, the ductility of vertical elements is less (Fardis 2009). Integrity and stability of the whole structure is very sensitive to columns reactions and behavior. Under any reversible loads, concrete sections start cracking. Cracks are spread rapidly in concrete elements during any moderate to heavy seismic event. Cracks predominantly affect the mechanical and geometrical properties of concrete elements which should be considered as well. Incidentally, strong columns are ultimately promoted frame systems by strict inter-story drift limits, which subsequently may lead to less probable soft story mechanism.

As mentioned above, ductile behavior of columns is a key element for any seismic design, which is more critical for structures with susceptible soft story

behavior and with lightly furnished reinforcement. RC columns in a designed structure without seismic provision may fail in an unexpected non-ductile mode. The brittle behavior of columns is often initiated by buckling of the reinforcement at lower than anticipated load capacity and drifts, followed by column concrete core crush. Photos 2-1a and 2-1b illustrate the soft story mechanism due to the buckling of reinforcement in New Zealand earthquake and concrete crush in India earthquake (Bhuj), respectively. Concrete columns in structures which are located in low to moderate seismic area can be very vulnerable if they fall into any potential soft story category. The problem would be worsened in case of soft story and plan irregularities both occurring in a structure. This type of structure will be studied in following chapters.



Photo 2-1a: Soft story mechanism and column reinforcement buckling, New Zealand earthquake (Photo source: [www.hylandconsultants.com](http://www.hylandconsultants.com))



Photo 2-1b: Soft story mechanism and column concrete crash, Bhuj India earthquake  
(Photo source: [www.nexus.globalquakemodel.org](http://www.nexus.globalquakemodel.org))

### **2.2.2. Some Example of Soft Story and Irregular Failures in the Past Earthquakes**

Almost up to the mid-70s, there was consent among some seismic design researchers that a weak or soft story in the first elevation of a structure could be used as an energy and force absorber system similar to a base isolator system. For example, Fintel and Khan (1969) suggested that a shock-absorbing soft story with a bilinear force-displacement characteristic could be designed to absorb all high intensity seismic forces. Then all stories above this soft story could be designed for wind load only and these stories remain elastic during an earthquake. The impropriety of this type of assumptions was proven after some major structural collapses, such as Olive View Medical Center during the San Fernando earthquake in 1971. In this six story medical facility, the upper stories moved as a unit and lightly damaged. The severe damage occurred due to large change in stiffness and strength across the second floor. There was vertical irregularity in the form of presence of a structural wall above the second floor which was discontinued toward the first floor. Also excess mass in the form of earth fill at the first story created plan irregularity. The

vertical stiffness and strength abruptness plus heavy mass led to an unforeseen ductility demand in the first and second stories. Therefore, the bottom stories, which supported all the other stories, were failed first. Several columns in the ground floor failed due to inadequate lateral confinement of core concrete and longitudinal reinforcements. The building was demolished as a result of excessive damage and deformation. Photo 2-2 shows the facility damaged columns.



Photo 2-2: Columns' damaged due to soft story mechanism, Olive View Medical Center (Adopted from: USGS Photographic Library)

In many of past earthquake events it was found that irregular structures have shown deficient behavior in comparison with regular structural forms in plan and/or in elevation (Bento and Azevedo 2000). Indeed stiffness and/or mass irregularities in elevation and plans usually induce more damages. Stiffness irregularities in elevation are made by a sharp transition in the stiffness of vertical elements such as considerable longer columns in the first story (Ibid.). Likewise, when structures are

designed symmetrically in plan, asymmetries may exist because of the imprecise nature of construction or actual use and even minor architectural alteration. Torsional excitation is a mechanism which always occurs in a seismic response of a structure during earthquake (Sfura et al. 2002). Photo 2-3 shows an apartment complex which was collapsed in January 2001 Bhuj earthquake (India) due to the soft first story condition plus possible effect of plan irregularity (Goel 2003, see: [ceenve.calpoly.edu/faculty-pages/goel/indian\\_eqk/index.htm](http://ceenve.calpoly.edu/faculty-pages/goel/indian_eqk/index.htm)). Similarly, considerable strength balance difference between the first story and the upper stories was the major source for a collapsed building during the Kobe earthquake, Japan 1995. The building was a very new RC structure at the time of the seismic event, with somehow asymmetric plan (Yoshimura 2003).



Photo 2-3: Collapse due to soft story and plan irregularity effect in 2001 India earthquake (Photo and cause source: Goel, R.K, [http://ceenve.calpoly.edu/faculty-pages/goel/indian\\_eqk/index.htm](http://ceenve.calpoly.edu/faculty-pages/goel/indian_eqk/index.htm))

The Palace Corvin in Caracas Venezuela was collapsed (Right wing) and heavily damaged (West wing) during July 1967 moderate Venezuela earthquake with

an approximate 6.5 Richter magnitude. The building was a concrete frame structure with masonry walls throughout the whole stories except the first story of the right wing. Lack of stiff masonry walls in the first story caused the soft story mechanism and ultimately collapse of the whole right wing of the building (Guevara-Perez 2012). Photo 2-4 illustrates the collapsed right wing and damaged west wing.

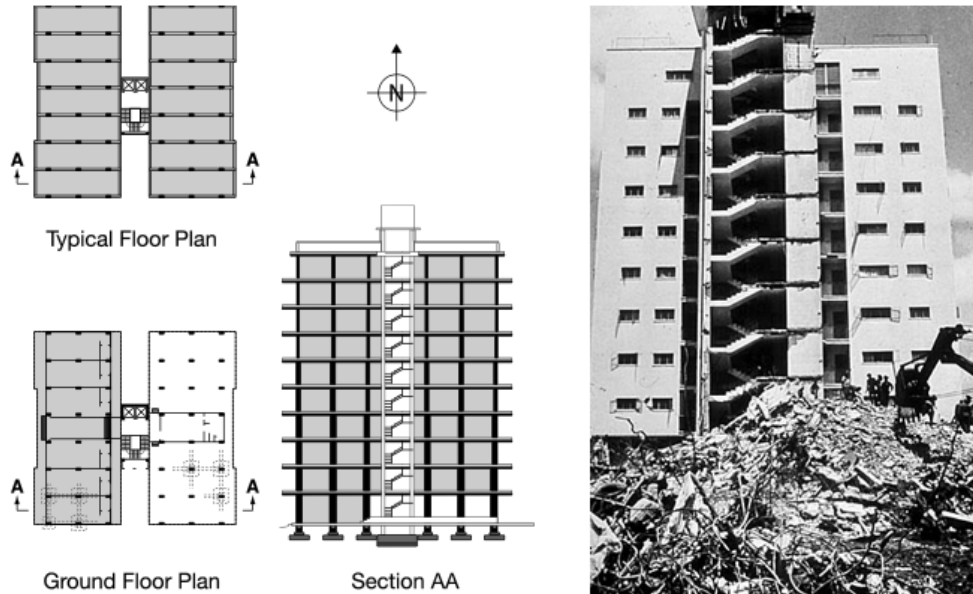


Photo 2-4: Architectural condition and collapsed-damaged of The Palace Corvin in 1967 Caracas Venezuela earthquake (Photo source: Guevara-Perez 2012)

The 921 Chi-Chi earthquake (1999) with  $M_S=7.6$  in Richter scale caused collapse or serious damages to many buildings. Several collapsed structures had a pedestrian corridor and open front at the ground floor (Tsai and Weng 2001) which directly or indirectly related to soft story or combined soft story and torsional effect (Photo 2-5).



Photo 2-5: Soft story damage combine with torsional effect in Taipei (Photo source: [www2.rcep.dpri.kyoto-u.ac.jp/~sato/taiwan/index.html](http://www2.rcep.dpri.kyoto-u.ac.jp/~sato/taiwan/index.html))

Zuccaro et al. (2002) did a vulnerability survey, mostly concentrated on the RC buildings, for the Izmit 1999 earthquake (Turkey) and in the Northern suburbs of Athens (Greece 1999 earthquake). For the Izmit earthquake, they observed that most dominant damages were soft story collapse mechanism in the entire area. The soft story led to pancake collapse due to the strong beam and weak column behavior. This behavior created a very large interstory drift and the torsional deformation of columns and beams due to the plan irregularities intensified the destructions (Photo 2-6). In point of fact, it is reported that at 1999 Izmit earthquake (Turkey) among 1215 heavily damaged buildings 725 damaged were due to the weak story phenomena (Kirac et al. 2011). Moreover, they observed that the long side of some columns was placed in orthogonal direction to comfort usage in the street face of many commercial buildings. As the consequence, lateral rigidity in the direction of street-facing side

was significantly lower than the other direction (Ibid.), and for that reason the destructive effects of soft story was increased because of plan stiffness irregularities.



Photo 2-6: Pancake collapse of a RC structure in 1999 Izmit earthquake (Photo source: USGS photo gallery)

For the Athens earthquake, even though the seismic intensity was not significant with almost  $M_w = 5.9$ , they detected some damages caused or triggered by the irregular condition of the surveyed structures (Zuccaro et al. 2002). The soft or weak story and plan irregularities resulted in many catastrophic total collapse of RC structures (Photo 2-7). Antonopoulos and Anagnostopoulos (2010) cited that in Greece, and from earthquakes in the past three decades, most of the major collapses of buildings, particularly RC structures, belong to soft story mechanism which occurred mostly during moderate scale seismic events.

In March 1977 a moderate to strong earthquake (magnitude: 7.2 Richter) occurred in Bucharest Romania. There was almost a complete collapse of a RC building because of soft and weak ground floor (Chesca et al. 2007). This building consisted of RC columns in the ground floor which was used as commercial area and RC shear walls in the upper stories. The major vulnerabilities of the aforementioned building were due to the concentration of displacement and seismic dissipated energy

in the ground floor, inadequate ductility for RC columns in the ground floor, and insufficient shear capacity in the RC upper shear walls. Besides the vertical irregularity, the building had some torsional irregularities on the upper stories.



Photo 2-7: Total collapse of a RC structure in 1999 Athens earthquake (Photo source: [www.itsak.gr](http://www.itsak.gr))

In recent years, Wilson et al. (2008) and Wibowo et al. (2011) did investigation about damages and collapse risk from earthquake excitation for existing buildings in low and moderate seismicity regions, such as Australia, China, and some part of east southern Asia. They indicated that the unreinforced masonry buildings and soft story structures have the maximum vulnerability risk. In China, they mentioned that many lightly reinforced concrete buildings were significantly damaged with drifts up to 7.5% measured which was much higher than the code recommendation of about 0.5% (Ibid.). Photo 2-8 shows a collapsed RC building in 2008 Sichuan China earthquake ( $M_w = 7.9$ ). The damage mostly caused by weak story mechanism and torsional response of building to the induced ground motion.



Photo 2-8: Collapse of a RC structure cause by weak story mechanism and torsional response in Sichuan China earthquake (Photo source: reidmiddleton.wordpress.com)

In 2009, an earthquake occurred in L'Aquila, Italy, with a 6.3  $M_w$  magnitude. Usually this scale of ground shaking is classified as moderate seismic event. However, the L'Aquila earthquake caused several failures in RC buildings, which were not designed for seismic loads, and many of these failures happened because of the soft story mechanism and/or unsymmetrical plan (Rajeev and Tesfamariam 2012). Photo 2-9 illustrates a building with soft story problem due to heavily infill walls in upper stories in combination with torsional effect due to irregular plan. Several surveys and analyses have been done after 1985 Mexico earthquake. These investigations determined that almost 50% of the structural failures were attributed either directly or indirectly to irregularity of structural form i.e., stiffness/strength or mass distributions (Dutta 2001). Photo 2-10 shows a complete collapse of a concrete structure in 1985 Mexico City earthquake. Non-ductile concrete details, irregular structural form, and possible pounding imposed by the adjacent buildings are some of the major parameters which caused collapse of this building.



Photo 2-9: A classic example of soft story failure of RC buildings in L'Aquila earthquake (Photo source: [www.air-worldwide.com](http://www.air-worldwide.com))



Photo 2-10: Breakdown of a concrete structure in Mexico City 1985 earthquake, partially because of irregularity (Photo source: [www.eeri.com](http://www.eeri.com))

### **2.3. Lightly Reinforced Concrete**

Generally speaking, information regarding collapse of low ductility structures in low to moderate seismic regions is rare (Hines et al. 2011). Recent cognizance of a potential seismic event in low to moderate seismic zones bring up more concerns regarding safety and vulnerability of existing reinforced concrete structures in which seismic provision has not been considered explicitly in the design and detailing procedure of these type of structures (Kunnath et al. 1995a). For the taller buildings and/or for area located in Hurricane risk, lateral forces due to wind loads may have been included in analysis and design procedure. In these areas, although the seismic demand may be less than the lateral capacity of a structure designed to resist against wind loads, it is still important to consider seismic evaluation, as there would be possibility of soft story mechanisms due to the higher mode effects in the structure (Kunnath et al. 1995a).

The inventories of reinforced concrete structures that do not comply with seismic provisions are almost enormous all over the world (Pardalopoulos et al. 2005). Those structures were designed to a variety of earlier design codes and they usually are referred to Lightly Reinforced Concrete (LRC) or “substandard construction” in term of seismic design (Ibid.). There are several common deficiencies among LRC buildings, mostly include: (1) confinement problem due to lack of enough tie or stirrups, (2) overall low reinforcement ratios, (3) inadequate anchorage or lap-splice or development length, (4) insufficient anchorage of transverse reinforcements, (5) low strength or inferior quality of materials, (6) poor layout, (7) improper capacity-design considerations, (8) plan eccentricities which exacerbate torsional response. The previous deficiencies are the most frequently observed problems in LRC structures (Pardalopoulos et al. 2005). Among aforementioned deficiencies, two major problems may affect columns seriously, and as result the whole structure behavior during a seismic event: (1) Columns may be weaker than the adjacent beams, which leading to a soft story mechanism, and (2) discontinuous positive beam flexural reinforcement in the beam to column joint area (Aycardi et al. 1994). These deficiencies can be classified under the improper

capacity design and inadequate anchorage. The latter deficiencies may be observed in many recently designed structures, and consequently, from an earthquake resistance standpoint, turn them to a lightly reinforced concrete structure. Particularly, a brittle soft story collapse mechanism due to inadequate ductility in column sections may occur during a strong or even moderate seismic event. As a result of the insufficient reinforcement, the large displacements arise in the area with vertical or plan irregularities which in turn impose larger story drifts to the structure. The large displacement associates with insufficient or even lack of reinforcement are not necessarily a ductile deformation and create a progressive rapid damage circle. In this condition, maximum building base shear ( $V$ ) is limited to the rotation at the ends of the column ( $\phi_{st}$ ), which is corresponding to the flexural resistance of the first story columns,  $M_y$ , (See Figure 2-6). In case of plastic hinge formation, simply by static analysis one can calculate the maximum base shear ( $V_{max}$ ):

$$V_{max} = \Sigma M_y / H_{st} \quad [2-1]$$

From equation 2-1, it is clear that the maximum base shear in case of a first story mechanism would directly be associated with the flexural capacity at the top and bottom of each column, which is considerably related to the amount of reinforcement and core confinement of concrete. Also, it can be seen that first story height has a reverse effect in the maximum achievable seismic base shear capacity.

As mentioned earlier, column failure is one of the most major problems in the structures with insufficient seismic resistance capacity. The collapse mechanism of lightly reinforced concrete buildings, emphasized column failure, was investigated by Moehle et al. (2006). They used data from laboratory results and then incorporated the failure models in nonlinear dynamic analysis software to evaluate collapse progress. They tested a 3-bay, 3-story structure under seven different ground records. Their model represented a typical office building, similar to the construction in California during 1960s and 1970s, in which beam depth and reinforcement were chosen to create a weak column-strong beam mechanism. They applied pushover method for the analytical section, and noticed that yielding of all first floor columns

longitudinal steel occurred at about 0.8% horizontal drift. A drift of 0.8% on the first floor was believed as the collapse drift. Response of the structure was very sensitive to the ground motions and a vast difference between the results were observed (Ibid.). The capacity and ductility level of a column is a key element to study LRC structures. For the lightly reinforced concrete, the first step of assessment would be the definition of column deficiencies such as flexure-critical, shear-critical, or flexure-shear-critical (Moehle 2008). A flexure-critical means flexure yields before the static shear strength and shear failure does not occur. A shear-critical column means shear failure takes place before flexural yield. A flexure-shear-critical column means the column initially yields in flexure and then cyclic degradation eventually leads to the shear failure. This classification is approximate, due to the fact that both flexure and shear behaviors would be varied with cyclic loading flexure-shear interactions. High compression loads and light transverse reinforcements are two important factors which increase the vulnerability of RC columns to sudden failures when columns are subjected to lateral load (Ibid.).

On the other hand, as long as concrete core confinement is fulfilled by adequate transverse reinforcement, columns with lower amount of longitudinal reinforcement than the code requirements may reach to a higher level of flexural capacity. Priestley and Benzoni (1996) tested two large-scale circular columns, archetype of typical sections for bridge column, with low longitudinal reinforcement ratio, 0.5% and 1%. They applied cyclic inelastic lateral displacements to simulate seismic response, and they mentioned that both columns exhibited good performance and reaction to the applied displacements. For the tested circular sections and spiral transverse reinforcements, they concluded that the concrete component strength might be considered independent from longitudinal reinforcements (Ibid.).

Reinforced concrete structures in low- to medium seismicity zones, such as Eastern part of the United States, historically have been designed only for gravity loads (Aycardi et al. 1994). In these parts of the US, structures usually possess reinforcement details which do not comply with the modern seismic standards. While such structures have not been designed to resist against induced seismic loads, they may still retain an inherent lateral strength capacity. As mentioned before, their

hidden lateral resistance capacity may give them capability to display some degree of withstanding against moderate earthquake events. However, lack of sufficient reinforcements and deficient in member detailing can cause questionable structural performance in case of any moderate to strong seismic event (Aycardi et al. 1994). In fact, most experimental and analytical researches are dedicated on high seismic zone area (Lee and Woo 2002). Most of seismic design portion of standard codes are focused on the higher seismic zones, and coefficients for lower seismic regions are simply assumed as a fraction to higher zones. An investigation showed that such a simple prorated assumption may lead to a considerable higher possible over-strength capacity for structures located on low to moderate seismic zones, namely for low-rise buildings, and for higher dedicated design live load (Lee and Woo 2002), such as many commercial buildings which are essentially designed to carry higher live load. On the other hand, in low-to-moderate seismic areas throughout the US, seismic design and detailing requirements for the weak beam/strong column are slightly considered or completely ignored. Consequently, most RC columns have not been essentially stronger than beams, and special transverse reinforcement detailings have not been applied near potential hinge regions to create enough member ductility (Dooley and Bracci 2001). Thus, those structures are susceptible to soft-story mechanisms during moderate to strong seismic events due to their inadequate column strength at joint regions and poor ductility detailing (Ibid.).

The above studies show that although in low- to moderate seismic zones and for regular buildings the capacity of LRC structures might be sufficient, for some more vulnerable conditions, e.g. soft story mechanism combined with LRC structural system, the possibility of severe damages or even risk of collapse may radically increase.

## **2.4. Code Review on Soft Story Irregularity and Torsional**

### **Provision**

#### **2.4.1. Code Background and Principle for Irregular Structures**

The overall tendency in the design of irregular structures among seismic codes is to use simplified linear or non-linear analysis methods and to perform structural evaluation or design accurately. In order to reach this goal, seismic codes try to incorporate a realistic and explicit way to involve asymmetry and irregularity. The first editions of seismic design codes did not mention about irregular structures, and the issues of vertical irregularity and plan asymmetry have gradually been presented in the design codes. The performance of a structure can considerably be affected by its configuration during a seismic event. In the building code standards, configuration is defined as horizontal and vertical formations. Commonly, most seismic design provisions were derived for regular configuration structures, but almost all occurred earthquakes have shown that those buildings having irregularities, vertically and/or horizontally, have suffered heavier damages in comparison with regular buildings. Poor performance of the irregular structures emanates from several reasons. In a regular structure, the inelastic response and energy dissipation are well distributed throughout the structure. On the other hand, in irregular structures, inelastic behavior can be concentrated due to irregularities and therefore leads to quick failure of structural elements in these areas (FEMA P-750 2009). In addition, irregularities may create unforeseen demands in some structural elements. Furthermore, it should be mentioned that the elastic analysis methods, which are typically performed in the design of regular structures, usually cannot predict the distribution of earthquake demands in an irregular structure. As a result, it may lead to insufficient capacity in the areas related to the irregularity (Ibid.).

The first edition of the Uniform Building Code (UBC) in 1927 adopted the seismic coefficient method for structural design based on the experience from 1925 Santa Barbara earthquake. Those coefficients were varied based on the soil condition between 0.075 and 0.10. The 1935 UBC adopted variations in design seismic force

for three different levels (Otani 2004). Initially, the concept of irregularity was presented in the UBC as a qualitative method to identify potential structural irregular condition, and starting in 1998, UBC quantified configuration parameters, classifications, specific analytical requirements, and penalties for irregular formations (Nafday 2011). Rosenblueth in 1957 and Housner and Outinen in 1958 notified structural engineers to the problem of possible damage caused by the rotational response of irregular plan structures during earthquakes (Rutenberg and Tso, 2004). Nowadays, most seismic standards have enclosed guidelines for torsional provisions (Ibid.).

Severe earthquakes are rare in nature, and occurring at intervals of hundreds up to thousands years. The infrequency of return period of an affecting seismic event conduces to impractical structural design to resist against such rare but severe earthquake without some level of damage. Building seismic standards have implied a specific philosophy to prevent life loss during a catastrophic rare event. The current situation in most codes for seismic design in general, and for reinforced concrete design in particular, are based on emphasis on Life Safety (Fardis 2009). Accordingly, traditional seismic design codes for buildings target is protecting human life by preventing local or global collapse. The safety level is attained by considering a single level of seismic risk. In most present codes, the “design seismic action” for ordinary structures is conventionally chosen as the one having a specific percentage (usually 10%) of probability to be exceeded in a conventional service life of a structure, namely 50 years. This corresponds to a mean return period (475 years in general) for the “design seismic action” (Ibid.), and an about 1.5-times stronger "Maximum Considered Earthquake” (MCE), for which Collapse Prevention should be achieved and a return period of about 2,475 years. US standards, namely IBC (2012) and ASCE 7-10, stipulate the combination of strength and ductility depending on the site seismicity, type of occupancy, and importance of the building (Fardis 2009). According to these factors, “Seismic Design Categories” (SDC) A to F shall be designated. The lowest category is A, in which the 5%-damped elastic spectral acceleration at both  $1_s$  period ( $S_{D1}$ ) and at the short period ( $S_{Ds}$ ), are less than 0.067g and 0.167g, respectively. The next threshold level of  $S_{D1}$  and  $S_{Ds}$  are 0.133g and

0.33g correspondingly, below which the structure is classified as B, or C in case the building classified as an essential or hazardous facility. The next threshold level is 0.2g for  $S_{D1}$  and 0.5g for  $S_{Ds}$ , below which the structure is classified as C or D in case of an essential or hazardous facility. For  $S_{D1}$  above 0.2g and  $S_{Ds}$  higher than 0.5g, the structure is classified as seismic category D. If the value of  $S_1$  for the MCE (Maximum Considered Earthquake) over firm rock goes beyond 0.75g, then the structure shall be categorized as type E, or as type F for essential or hazardous facilities. In case of SDC A, the structure is only required to have a complete tied-together lateral load resisting system, and should be designed for a lateral force equal to 1% of total weight. Under the tent of SDC B, the structure does not need to be designed with special detailing under the ACI 318-08 (2008) seismic design provisions, and “Ordinary Moment Frame” (OMF) would be sufficient. Although OMF system does not need any specific stringent detailing requirements, still there are a few provisions for this type of system. SDC C frame structures are subject to the mild detailing requirements under the ACI 318-08 requirements for “Intermediate Moment Frames” (IMF). Any structure in SDC D, E or F should be detailed to have high ductility which is defined as “Special Moment Frames” (SMF) or walls of “special” ductility per ACI 318-08 seismic provisions (Fardis 2009). As mentioned in the previous sections, in the Eastern or the North Eastern parts of US, a building most probably would fall into SDC B, or SDC C. From ACI 318-08 (or ACI 318-05) and ASCE 7-05 (2005) (or ASCE 7-10, 2010), the RC frame structures within these zones shall have minimum ductility according to the Ordinary Moment Frame (OMF) or higher ductility levels (i.e. IMF or SMF). Nonetheless, there are many structures in the above-mentioned area which have not been designed for any form of acceptable seismic ductility range, and therefore these types of structure are under risk of damage or even life loss. In fact, current reinforced concrete practice in low seismic zones has some distinct non-ductile detailing routine. By refer to the previous sections, widely spaced transverse rebar (stirrups or ties usually are placed in the order of the minimum column dimension) is a common procedure in these areas. Wider transverse rebar distance leads to ineffective concrete confined (Wilson et al. 2008). Moreover, wider ties are less effective to prevent longitudinal reinforcements

from buckling (Wilson et al. 2008). Besides, absence of beam-column joint design, the lower amount of longitudinal reinforcement, and strong beam/weak column condition can be seen almost in every concrete structure. For area with high seismicity, such kind of detailing are extremely restricted and design standards for moderate seismic zones recommend a very low drift capacity for columns with a low level of acceptable seismic detailing (Ibid.).

For retrofitting of existing structures, ASCE 41-06 (2007a) is currently accepted by many jurisdictions. ASCE 41-06 supersedes FEMA 356 (2000) and provides a wider range of performance in comparison to the contemporary conventional design codes. Three major performance levels for structural and non-structural elements for the rehabilitation of the existing buildings are included in ASCE 41-06, although it can be used for the evaluation of new buildings as well. The hazard level, based on different occurrence return periods, combining with the performance levels yields the rehabilitation objective that makes the aforementioned code as a performance-based approach code.

As discussed in the previous sections, the central principle for a good seismic design is to distribute the inelastic deformation throughout the height of structure, preferably in the pre-assumed positions, and with established suitable deformation modes. Formation of flexural plastic hinges at the end of a beam, but not at the column-beam joint, is one of the appropriate conditions. ASCE 7 (e.g. ASCE 7-05, 2005) recognizes this as a desirable goal for seismic performance in requiring the designer to verify that the structure does not have either weak or soft stories and tries to encourage the designer to avoid asymmetric plans. In fact, the seismic design codes try to preclude concentration of inelastic deformations in few members or locations (soft story) by several methods, such as combination of stiff and strong vertical structural spine through height of the structure, imposing plastic hinge locations, controlling the inelastic response mechanism, and by encouraging and directing of the designer to imply a favorable structural layout in terms of symmetry and regularity (Fardis 2009). The regular and irregular structures are basically recognized based on certain strength, mass, setbacks or offsets limitations of one story with respect to adjacent stories, and acquired from analytical and experimental studies, empirical

observation, aftershock field reconnaissance, and engineering judgments (Nafday 2011) which are almost similar in the current seismic codes.

Modern seismic design codes use “capacity design” method in their standard. Indeed, capacity design means strengths of any individual elements related to the load path of inertia forces and the strength of the structural system is governed by the ductile behavior. Although capacity design approach is well known as to be applied during detailed design, the method should basically be started on the layout and sizing in early stage of design process, and simply during conceptual design (Fardis 2009). Continuous load path is a key element in any seismic design and almost all new codes strongly emphasizes on complete load path, e.g. IBC 2012 on clauses 1604.9 and 2304.9.6. Lack or insufficient load path is one major problem in weak or soft story mechanism, and changing stiffness may also lead to severe plan irregularity.

#### **2.4.2. Summary of US Code Classification for Irregular and Regular Structures**

Almost all the US counties and cities adopt building regulations based on the International Building Code (IBC), which in turn adopts most of its own structural regulations, and particularly the seismic provisions, through reference to the ASCE 7 standard (e.g. see IBC 2012). The ASCE seismic requirements are themselves established based on the NEHRP Recommended Seismic Provisions for New Buildings and Other Structures (FEMA P-750 2009). The ASCE 7-10 (2010) and the former one, ASCE 7-05 (2005), have very similar regulations regarding the vertical and horizontal irregularities and almost all definitions in both of them are the same except very minor changes in the newest 2010 version. ASCE 7-05 classifies irregularities under the section 12.3.2., horizontal and vertical irregularities with reference to its tables 12.3-1 and 12.3-2, respectively. Compared to regular structures, those tables place more limitations and prohibitions, higher level of analysis modeling and methods, and more stringent requirements regarding the irregular structures, and many of them are obliged the irregular limitations to the seismic design category B and C. It is worth to note that categories B and C are known as Low and Moderate seismicity zones, respectively.

On Table 12.3-1 of ASCE 7-10 (2010) or 7-05 (2005), Irregularity Type 1a is defined as: “Torsional Irregularity is defined to exist where the maximum story drift, computed including accidental torsion, at one end of the structure transverse to an axis is more than 1.2 times the average of the story drifts at the two ends of the structure. Torsional irregularity requirements in the reference sections apply only to structures in which the diaphragms are rigid or semi-rigid.” Consequently, in case of torsional response and even for the seismic categories B and C, which are part of this study, the designer should imply three-dimensional modeling of structure. Also cracked section consideration for the RC analysis and Amplification of Accidental Torsional Moment are other part of the compulsory analysis and design requirements.

The vertical irregularities are presented on Table 12.3-2 of ASCE 7-05 (2005) and 7-10 (2010), which can be divided into two subcategories, force-distribution irregularity, including 1a thru 3, and the second category can be recognized as load path irregularities which covered Types 4 and 5 on the abovementioned table. The ASCE code places prohibitions for the vertical irregularity types 1a thru 3, and any structure with those types of irregularities shall be analyzed by dynamic approach methods. The latter irregular types cover soft story mechanism. However, ASCE mentions that the required prohibitions are just for seismic categories D thru F and moderate and low zones are exempt from many limitations. In essence, according to the ASCE 7-10 (2010), one can analyze and design any structure having vertical irregularity types 1a thru 3 in seismic zone B or C with the linear static procedure method.

For the irregularity types 4 and 5, which are mostly related to the load path and weak story conditions, ASCE 7 prescribes limitations in total structure height, analysis method, and required more design strength thru design process, which shall be applied as over-strength factor consideration in the seismic load combinations, or application of extra loads for the collector element design. Again, in this part of Table 12.3-2, the penalties for the weak stories are limited to the higher seismic categories. There is not any specific penalty in both ASCE 7-05 (2005) and ASCE 7-10 (2010) for having simultaneous vertical and horizontal irregularities in a structure.

It is worth to repeat that per ASCE 7-10 (2010) classifications, the weak story is designated as: “to exist where the story lateral strength is less than 80% of that in the story above. The story lateral strength is the total lateral strength of all seismic-resisting elements sharing the story shear for the direction under consideration.” The Discontinuity in Lateral Strength–Extreme Weak Story Irregularity is mentioned to have 65% lesser strength instead of 80% for the weak story condition. The soft story is defined as: “to exist where there is a story in which the lateral stiffness is less than 70% of that in the story above or less than 80% of the average stiffness of the three stories above.” and for the stiffness-extreme soft story condition, the 70% and 80% are reduced to 60% and 70% correspondingly.

Accidental eccentricity is used in seismic codes to cover random unexpected irregularities, stiffness and mass, and probable rotational component of the ground motion. Accidental eccentricity shall be applied even for a perfect symmetric plan structure. In fact, impact of architectural ornamentals and elements in structural response, uncertainties in stiffness and masses, uncontrolled location of live loads, and in general unknown factors and conditions may occur independently even for a symmetric plan structural system. ASCE 7-05 (2005) and 7-10 (2010) imply the accidental eccentricity for the semi-rigid or rigid diaphragm conditions, and the applied eccentricity is distance equal to 5% of the dimension of the structure perpendicular to the direction of the applied force. Per ASCE 7-10 (2010), in case where earthquake forces are applied concurrently in two orthogonal directions, the accidental eccentricity may not be implied in both orthogonal directions at the same time. ASCE 41-06 has a very similar approach to ASCE 7-10 (2010) method for the accidental eccentricity. Few most recent nonlinear time history analysis studies bring doubt about effectiveness of accidental eccentricity provisions (e.g. see Stathopoulos and Anagnostopoulos 2010). Results of their accidental eccentricity analysis did not show any considerable reduction or better distribution of ductility demands against analysis without any accidental eccentricity consideration. Moreover, few newly seismic design recommendations have started omitting the accidental torsion on their technical text, for instance CTBUH seismic guide (CTBUH 2008) does not consider any accidental eccentricity for any tall structure analysis method.

ASCE 41-06 (2007a) puts stringent limits on the linear analysis for building with vertical and/or horizontal irregularities which are categorized in four configurations. The intent is to ensure that the response of irregular structure will be nearly elastic during earthquake in case of using linear analysis method. To get the elastic response, ASCE 41-06 implies the demand capacity ratio (DCR) limitations, which is the force due to the gravity and seismic loads to the expected strength of component based on the applicable ASCE 41-06 (2007a) methods accordingly. The required DCR calculation procedures are cumbersome and only use to determine structural regularity. At the end, the DCR results may lead to the rejection of linear analysis and a new structural evaluation based on the nonlinear analysis should be performed. Besides, the ASCE 41-06 (2007a) distinguishes the torsional and vertical irregularities based on strength and the stiffness where linear static analysis is prohibited for any vertical and/or torsional stiffness irregularities. Therefore, ASCE 41-06 (2007a) commentary has suggested that for structures with complex shape and obvious irregular configurations it is perhaps easier to use the nonlinear methods for such structures from the beginning of analysis process.

Nonlinear static analysis in ASCE 41-06 (2007a) has its own limitations regarding the strength ratio and higher mode effects although less restrictive criteria than linear static method was applied there. Some of these limitations, directly or indirectly, are related to the structure irregularities. However, the nonlinear dynamic analysis has no limitations except the some awareness about sensitively to the assumptions and inputs.

Just for a quick comparison, Eurocode 8, 1994, mentioned some simplify rules regarding regularity criteria in elevation, in which the lateral stiffness and mass of the individual stories shall remain constant or reduce gradually without abrupt changes (Bento and Azevedo 2000). If those criteria were not satisfied, there were some penalties in terms of increased seismic forces.

The ACI 318-71 was the first edition of the American Concrete Institute (ACI) which considered some provisions under the A.6.2. section for preventing plastic hinge formation in columns and therefore story mechanism, then the ACI 318-83 introduced more details and restricted provisions, and more developed

requirements were presented in the ACI 318-99 mostly based on recommendations from ACI-ASCE 352-91 joint venture committee report to avoid weak column/strong beam condition (Dooley and Bracci 2001). The objective of current US seismic codes (Material Standards) is to force plastic hinge formation into the beams instead of the columns to prevent soft story mechanism (Fardis 2009). To fulfill the strong column/weak beam criteria, the concept of ACI 318-08 (2008) criteria are basically acquired through equilibrium and static analysis of plastic hinges, and may be defined as:

$$\Sigma M_{nc} \geq \gamma_{Rd} \Sigma M_{nb} \quad [2-2]$$

In which:  $\gamma_{Rd}$  over-strength factor,  $M_{nc}$ , and  $M_{nb}$  denote the moment resistances of columns or beams, respectively.

## **2.5. Previous Research**

In this section, first, a general brief review of seismic studies in the literatures which are partially, directly or indirectly related to irregular response is discussed. Then, an overall study trend among researchers regarding the main objective of this study is presented. An in-depth brief literature review with regard to the experimental tests, soft story mechanism, and torsional response will be recollected, respectively.

### **2.5.1. Brief Background**

Otani (Otani 2004) mentioned that the first scientific investigation about earthquake has been done by Robert Mallet, who studied the physic-mechanical investigation of earthquake wave propagation. His investigation carried out after 1857 Naples (Italy) earthquake. The first equation in seismic design was (Ibid.):

$$a > B/H \quad [2-3]$$

in which  $a$  referred to the maximum ground acceleration (as the ratio to gravitational acceleration),  $B$  is the rigid body width, and  $H$  denotes the height attached on the ground. Obviously, from the first steps of seismic structural design studies, the effect of height and width had been considered in which indirectly can be referred to regularity of a structure. In fact, the development towards modern seismic analysis started in the first decade of 20 century with the two major earthquakes of San Francisco, the USA (1906) and Messina, Italy (1908) (Calvi 2010). The first quantitative seismic design recommendation was introduced after 1908 Messina earthquake in Italy. Per recommendation, the height of building was limited to three stories. Moreover, it was stated that the first story be designed for 1/12 the weight above, and the second and third stories to be designed for 1/8 of the building weight above (Otani 2004). These regulations seemed to cover the effect of irregularities indirectly.

In 1923 Kanto earthquake (in Japan) it was found that the damage to the reinforced concrete buildings was relatively low although there had not been any enforced seismic design code requirements prior to the earthquake. Some of the observed damages to the reinforced concrete structures were: poor reinforcement detailing, short lap splice length, and irregular configuration (Otani 2004). Newmark developed a new direction in seismic design, especially for the reinforced concrete structures. He defined the lateral resistance required for survival of a structure and also considered ductility and plastic mechanism in seismic design criteria. He reported the relation between the maximum response of linearly elastic and elasto-plastic simple system having the same initial periods (Otani 2004). Bertero (Bertero and Bertero, 1995) developed a Conceptual Seismic Code based on structural hinges and displacement method, which established a platform for several performance designed methods and basically the base method for some most important part of nonlinear irregularity investigations.

An important parameter of a good seismic design is structural redundancy. In cast reinforced concrete structures, the system is inherently monolith. Thus, redundancy in RC frame structures is normally achieved by continuity between moment-resisting elements and provision of multiple load paths (Derecho and

Kianoush 2001). Another vital region in dynamic response to induced ground motions is reactions to reversed cycles of deformations in critical elements. The back-and-forth dynamic responses of critical elements tend to concentrate deformation demands in the highly stressed regions of members. The yielding response is the desirable reaction in the potential hinging regions, and experience and observation have shown that properly designed, detailed, and constructed RC buildings can provide enough strength, stiffness, and inelastic deformation capacity against seismic excitation (Derecho and Kianoush 2001). The inelastic deformation capacity of RC members is the important element of RC structures to resist against seismic. Indeed, earthquake-resistant design relies on ductility of members, which means the RC members can tolerate cyclic deformations well beyond the elastic limits without any substantial loss of their load-carrying capacity (Panagiotakos and Fardis 2001) or any sudden brittle failures in the main members.

Bearing in mind that strength deterioration in RC structures is mostly governed by detailing, a poorly detailed member exhibits a very considerable strength drop under cyclic loadings. However, it is shown that even many of normally detailed RC members may exhibit considerable strength deterioration (Dutta 2001). The ductility in reinforced concrete structures depends mostly on: Rate of Loading, Confinement Reinforcement, Shear, and Sectional Ductility. The ductility of a section subjected to flexure or combined flexure and axial load can be defined as the ratio,  $\mu$ , of the ultimate curvature attainable without significant loss of strength,  $\phi_u$ , to the curvature corresponding to first yield of the tension reinforcement,  $\phi_y$ . The parameters which affecting ductility may be categorized as (Ibid.): a) material variables, such as the maximum usable compressive strain in concrete (particularly related to the confinement, and grade of reinforcement); b) geometric variables (including tension and compression reinforcement, and the shape of the section); c) and loading variables (such as the axial load and corresponding shear force).

Although there is a number of complicated equations for curvature calculation, Panagiotakos and Fardis (2001) mentioned that simple semi-empirical expressions:  $\phi_y = 1.7f_y / E_s h$  for beams and  $\phi_y = 2.12f_y / E_s h$  for rectangular columns, overall provide an equally good average fit with only slightly higher scatter in

comparison with more complex formulas (Ibid.). In the former equations,  $h$  represents the depth of member cross section and  $E_s$  indicates the elastic modulus of steel. Simply, the ductile response of a concrete section is highly related to the reinforcement yielding capacity and dimension of a section.

Based on several studies, Priestley (2000) mentioned that a frame building would perform better if it could be proved that plastic hinges would occur in beams rather than in column, which is known as weak beam/strong column mechanism. He pointed out that strength distribution through a structure is more important than the absolute value of the base shear. Per his study, it was mentioned that the story yield drift of reinforced concrete frames can be expressed by (Ibid.):

$$\theta_y = 0.5\varepsilon_y l_b / h_b \quad [2-4]$$

Where  $\theta_y$  is the story yield drift,  $\varepsilon_y = f_y/E_s$ ,  $l_b$  is the beam bay length, and  $h_b$  is the beam depth.

Priestley (Ibid.) also suggested that for the displacement-based analysis and to develop a single-degree-of-freedom model, the effective mass of structure in analysis procedure typically can be considered as 70% of total involving mass. In his study, he came up with some implications of performance-based seismic design and showed some effects such as indecency of design base shear force. He concluded that the required strength is proportional to the square of seismic intensity. His latter conclusion has fundamental important differences between forced-design method and displacement-based design method in low seismicity regions. In fact, the elastic limit of a structure can be approximately estimated by using its geometry alone (Calvi 2010). For instance, by using the yield deformation of the reinforcement ( $\varepsilon_y$ ), pier diameter ( $D$ ), and pier height ( $H$ ) of a circular pier, the secant yield rotation ( $\theta_y$ ) of a bridge can be estimated as (Ibid.):

$$\theta_y = 0.75 \varepsilon_y H/D \quad [2-5]$$

For the pinching in the load-displacement hysteresis loop, since the area under the load-deflection curve is a measure of the energy-dissipation capacity of the member, the pinching in this curve due to sliding shear represents degradation. The degradation occurs not only for the strength, but also for the energy-dissipation capacity of the hinging region as well. Where the longitudinal steel is not adequately restrained by lateral reinforcements, inelastic buckling of the compressive reinforcement, followed by a rapid loss of flexural strength, can take place (Derecho and Kianoush 2001). It should be noted that in high seismic regions local or national codes put stringent regulations regarding nonlinear analysis and the corresponding implication procedures. The 2008 Los Angeles Tall Buildings Structural Design Council (LATBSDC) Guideline states that all structural elements, which demands for any of the time history analysis is within a range that significant strength degradation may anticipate, should be identified and the corresponding effects must be appropriately considered in the analysis (Naeim 2010). Although the similar limitations may seem very harsh for regular structures in the low-to moderate seismic zones, the former effects for nonlinear time history analysis of irregular structures in low-to moderate zone might be dominate. These effects are discussed and applied to the models in Chapter 4.

Overall, study of nonlinear response of irregular building has been established similar to capacity design method. “Capacity design is an approach whereby the designer establishes which elements will yield (and need to be ductile) and those which will not yield (and will be designed with sufficient strength) based on the forces imposed by yielding elements.” (NEHRP 2010b). The well-known (previously mentioned) “strong column/weak beam” is an example of a capacity design method, which is one of the important key elements of the collapse prevention and structural demand control in the irregular structure design method. The major intent of the capacity design can be summarized as preventing inelastic hinging in columns (Ibid.), particularly prior to plastic hinge formations in the beams. That could lead to premature story mechanisms and rapid strength degradation in columns with high axial loads (NEHRP 2010b). The desired hinging sequence in frame structures is related to the strong column/weak beam concept. However, it does not ensure that

plastic hinge mechanism will not take place in columns. As one of the reasons, some experimental results on beam-column specimens have indicated that where bidirectional loading occurs in rectangular RC columns, reduction in the strength of the column due to spalling of concrete cover and bond deterioration along the column longitudinal bars at and near the corner can shift the hinge formation from the beams to columns (Derecho and Kianoush 2001). The current study holds the same reason for two-directional plastic hinge allocation, in which all columns have been assigned with two way plastic hinge moment capacity patterned (refer to Chapter 4).

Rutenberg and Tso (2004) mentioned that the studies on the bidirectional seismic excitation indicated some effects on the response of structures, but it has not been appeared to be substantial. They cited that with the advent of efficient, reliable and user-friendly 3D linear and nonlinear programs the need to extrapolate from unidirectional to bidirectional response may lose its practical importance (Ibid.).

## **2.5.2. An Overview of Literature Methods and Trends**

### **General related RC frame seismic studies**

Kunnath et al. (1995a and 1995b) studied the effect of the Nahanni earthquake, which happened in the North Eastern part of America continent, on reinforced concrete structures. Their investigation concentrated on seismic response of gravity load design structures in the Eastern and Midwestern parts of the US. First, they had designed their models based on the gravity load system only, and then they analyzed frames under four different time history records including Nahanni earthquake. They showed that the structural damages under Nahanni earthquake were minor although they only considered the 2D modeling and symmetric frames on their research.

Marsh and Browning (2002) performed parametric study in order to simulate a variety of typical existing RC buildings. They considered four (4), eight (8), twelve (12), and sixteen (16) stories, 20ft bay, 10ft story height, except for their tall model, 4 ksi concrete strength, modulus of elasticity equal to 4000 ksi, Hognestad compressive stress-strain relationship for concrete with 0.004 ultimate strain, bi-linear model for 60 ksi yield steel, and tri-linear model for the moment curvature behavior with 1%

post yield slope (Marsh and Browning 2002). Their model configurations were 4bay regular frame, tall at 1<sup>st</sup> story, and stepped frame. For the time history analysis, the selected eight (8) different seismic ground motions, such as El Centro and Loma Prieta (California), and Nahanni (Canada), and linearly scaled them. They mentioned that the nonlinear static analysis results may differ from one-half to nearly twice the values from the dynamic analyses, and most differences were noticed in the 12- and 16-story models.

Panagiotakos and Fardis (2001) carried out a state-of-the-art research based on more than 1000 tests to examine and develop common use assumptions for the deformation of RC members at yielding or failure condition, in terms of geometric and mechanical properties of the members. They cited that the yield and the ultimate curvature assumptions based on the plane-section theory provide good average agreement with test results although large scatter was observed. The same theory can be applied to the RC models for the ultimate drift or chord-rotation capacity calculation through the curvatures and plastic hinge concept. Moreover, they mentioned that comparison between semi-empirical models and test results determined good average agreement for the drift or chord-rotation at member yielding although still again with considerable scatter (Ibid.).

In another research, Magliulo et al. (2004) showed the seismic behavior of RC frames with strength irregularities in elevation. The results of nonlinear static analyses on the regular RC frames were compared to the irregular frames. The irregularity was applied by assigning over-strengths either to the beams or to the columns of the regular frames. The comparison was performed in terms of inter-story drifts, maximum rotations at the element ends, and the demand to the capacity in term of plastic rotations (Ibid.). They mentioned that the frames characterized by the over-strength assigned to the beams illustrated irregular behavior. For the beams and columns, they used lumped plasticity at the ends of each element with a tri-linear moment-rotation relationship. Comparison between nonlinear static analyses and nonlinear time history analysis showed inadequacy of nonlinear static analysis results for irregular structures (Ibid.). Although nonlinear static methods are usually more accurate than the conventional methods, nonlinear static methods still require further

refinement in order to provide reliable response of irregular structures in general and particularly for the concrete irregular structures. Even incorporating several methods and different push load patterns have not been improved the dispersing and scattering of the results, e.g. see (Mahdi and Soltan Gharai 2011), (Athanassiadou 2008), and (Erduran 2008) for more discussion regarding this subject.

Zeris et al. (2005) performed parametric study for typical existing irregular RC frames designed according to the previous generations of Greece seismic code. They applied different forms of typical vertical and plan irregularities by imposing the layout of the structural system or infill distributions, including setbacks, discontinuous members, tall ground story, and irregular distribution of perimeter infill. Moreover, they set up regular control buildings as bare frames corresponding to each group of irregular forms. Their analysis method was pushover, and comparison was done by Incremental Dynamic Analysis method using three time history records. The over-strength evaluation, the global ductility capacity, and the available behavior factor were focused on their research. The selected frames were four by three bays in plan, each bay 3.5 or 6.0 meter depending on group classification, five stories with typical story height of 3.0 meter except the tall first story with 5.0 meter height. The applied loads were self-weight, surcharge (1.5 KN/m<sup>2</sup>), live load (2.0 KN/m<sup>2</sup>), and the interior masonry infill as extra surcharge in plan equal to 1.0 KN/m<sup>2</sup> and uniform load due to the exterior wall. The effect of concrete slab reinforcement within the effective width was considered as well. The columns and beams were modeled using two-component lumped plasticity beam column element with degraded hysteretic characteristics. They used average material properties and considered the effect of axial force in the columns. The established parameters for time history analysis were vertical inter-story drift distributions, the magnitude of the inelastic rotational demands in all elements, and the distribution of inelastic energy absorption among beams and columns. Their study about the dynamic behavior showed there were up to 65% variability regarding the mean of the estimated ductility capacity and behavior factor among irregular frames although the static pushover method and nonlinear time history analysis demonstrate reasonable corroboration. In addition, the tall first story structure was the least susceptible to scatter among different earthquakes while the

discontinuous first story column structure was the most susceptible one. The minimum roof drift at failure point using nonlinear dynamic analysis was noticeably less than the obtained amount from static pushover methods. The estimation of expected inelastic performance was observed sensitive to some analysis parameters. The main effective parameters were mentioned specifically as the model type, and the refinement of the failure criteria, particularly the estimation of shear strength in joints and the adequacy of reinforcement anchorage, and also the performance point estimation method. By the way, they cited that the sensitivity evaluation cannot be obtained using static pushover only. Therefore, nonlinear dynamic analysis should perform as an essential tool for the vulnerability assessment of such irregular structures (Ibid.).

Liel et al. (2006) did a research about RC structures based on the four-story moment frame which were designed to be representative of a) pre-1970 non-ductile RC construction and b) modern, ductile RC construction per IBC 2003. The second group of four-story RC moment frame structures was considered as modern code-conforming into three major groups: a) special (SMF), b) intermediate (IMF), and c) ordinary moment frames (OMF). They created several possible collapse scenarios for their study. Based on the nonlinear analyses it showed that the new designed OMF or pre-1970 design structure can be classified as High (refer to damage level) for all considered possible sidesway collapse scenarios. Bearing in mind that OMF is typical RC design and construction structures in the low to medium seismic zones in the US, and considering that their study did not involve any torsional effect, this study again shows likelihood of collapse owing to the soft story mechanism in the Eastern part of the US. By the way, since ASCE 7-05 (2005) edition has released, the OMF concrete structures are allowed to be used only in the Seismic Design Category (SDC) B or A. There are many areas in the Eastern and North Eastern parts of the US which their seismic category are classified as SDC C. Nonetheless RC buildings on those areas need more ductile RC systems, such as IMF system. However, in the past most of RC structures in these areas not only were not designed for OMF or IMF, but also designed only for the gravity and wind loads. It is worth noting that FEMA P695 report states that the OMF systems provide an acceptable level of collapse safety only

for SDC B, but not for SDC C or higher (FEMA P695 2009), which is consistent with the ASCE 7-05 (2005). Therefore, even OMF systems, which have more ductility against seismic than the gravity designed frames, are not able to provide an adequate safety margin for the buildings in the SDC C category.

Ellingwood et al. (2007) studied three and six stories reinforced concrete structures which were designed only for gravity loads as a typical construction in the Central and Eastern parts of the US. The modified Kent and Park model were applied to calculate cover and core concrete properties. Steel properties were characterized through a bilinear steel model with 0.5% strain hardening. The effective width of concrete slab per ACI 318, lumped mass at column-beam joints, and assumed 2% viscous damping for the first two modes were considered as well. Maximum inter-story drift angle was selected as the demand variable (Ibid.). They said that this item gives a better understanding about the overall or local collapse of structural elements. Their analysis showed that for the Central and Eastern parts of the US, the gravity-designed reinforced concrete structures might not be able to resist current design-basis ground motions without suffering severe damage or collapse.

De Stefano and Pintucchi (2008) did a state-of-the-art review paper in both vertical and plan irregularities. Based on their study, in the past, torsional coupling response in irregular building structures were mostly studied by means of simple one-story models. Nevertheless, due to the complexity of multistory asymmetric buildings, such models were used to study of few real cases of asymmetric buildings (Ibid.). Furthermore, they mentioned that besides the complexity of inelastic seismic analysis, there are several different parameters which influencing the response of irregular structures. Thus, complexity of analysis and variety in parameters lead to a lack of general accepted conclusions for irregular structures. From the parametric analysis performed primarily on torsional-stiff and mass-eccentric systems they summarized the main findings as: "...global torsional effects in inelastic structures are similar to the elastic ones, since differences between elastic and inelastic response are more pronounced in the translational part of motion, rather than in the rotational one. However, quantitatively, the change in response depends on the magnitude of inelastic deformations." (Ibid.). It is found that the characteristics of the seismic input

would influence the inelastic torsional response intensely which mostly depends on the frequency content of the input ground motion. Torsional response in the inelastic range may cause either larger or smaller displacements in comparison to the elastic results (De Stefano and Pintucchi 2008). The inelastic response of eccentric multi-story RC frame buildings, three and five-story models, under bi-directional seismic excitation had been mentioned as well. The results showed that frames at the flexible side encountered with increasing of inelastic deformations, while those at the stiff side faced to deformation decrease with respect to their symmetric counterparts (Ibid.). As one of the important pinpoint in De Stefano and Pintucchi (2008) state-of-the-art study, they mentioned that “...up to their study time, for what concerns experimental research, there are only very few studies on vertically irregular buildings, as already noted for plan-asymmetric building structures.”

Per De Stefano and Pintucchi (2008) study, some researchers also focused on five- and nine-story RC frames which were designed according to EC8 provisions for the “low” ductility class. Vertical irregularities due to the differences in either mass, stiffness or strength were investigated separately. Furthermore, the appropriateness of many seismic code criteria regarding detecting vertical irregularities was investigated by several researchers (Ibid.). The actual increase in inelastic demands and seismic performance were compared to their regular counterpart models. Results showed that the specified irregularity criteria by major seismic codes may not be able to recognize the regular or irregular status of a building (Ibid.). Regarding mass irregularity, their finding, i.e. variations in mass do not necessarily result in increase in plastic demands, is consistent with conclusions from other researches, e.g. (Tremblay and Poncet 2005) and (Stathopoulos and Anagnostopoulos 2010). Concerning strength irregularity, it was found that only over-strength of beams would increase plastic demands (De Stefano and Pintucchi 2008). On the other hand, over-strength in columns and variation of the building height may result to negligible effects on the plastic demand. Many code criteria, such as IBC 2012, are basically considered variations of story strength which mainly depends on column strengths. Therefore, per De Stefano and Pintucchi (2008) those codes are unable to calculate the vertical strength irregularities properly.

The sensitivity of vertically irregular RC frame to P- $\Delta$  effect was also investigated (De Stefano and Pintucchi 2008). Comparison between fragility curves with and without P- $\Delta$  effect showed a considerable differences in structural performance. They also mentioned that several papers have dealt with the effectiveness of the modal pushover analysis. By those studies, it was concluded that for taller structures, the modal pushover analysis cannot predict collapse although modal pushover may capture the overall mechanism (Ibid.). Hence, the modal pushover analysis is not appropriate for investigation at near structural collapse situation (Ibid.).

Antonopoulos and Anagnostopoulos (2010) investigated the feasibility of removing the soft story weakness by applying two methods of strengthening for a five-story RC building designed with the old Greek codes, one using steel bracing in ground story bays and another using column jacketing system. They studied a symmetric plan for simplicity, although they declared that their case study was not quite representative of old RC buildings, which regularly are asymmetric in plan, with horizontal and vertical irregularities that lead to a significant torsional response.

Thuat and Ichinose (2004) studied RC wall buildings with vertically irregular configurations by conducting dynamic time history analyses of various seven and eleven-story wall structures with discontinuous wall in the first story. They investigated overall collapse mechanism in their study. In another research, the story strength demands and soft story mechanism for irregular vertical stories with discontinuous columns of RC frames under nonlinear time history analyses were studied by Thuat (2011). He pointed out that the long-span transfer beams, which were located between the omitted columns and governed by gravity load requirement, tended to increase the possibility of column yielding formation at the soft stories. The omitted middle column and its plan irregularity effect in vertical soft story response is considered in the current study.

Haselton et al. (2011) used lumped plasticity beam-column elements and finite joint shear panel springs in their study. Lumped plasticity elements were applied as fiber-type models to capture the strain softening associated with rebar buckling and spalling phenomena. These effects may be critical for simulating

structural collapse in RC frame structures (Ibid.). The beam/column elements were modeled by using a nonlinear hinge with strength and stiffness degrading response. Strength-irregular variations were involved to overdesign of the upper story members to create story strength irregularities in the first and second stories (Ibid.). They showed that in case of strength variation, combined with limiting the story strength irregularities to the maximum values permissible by ASCE 7-02, the benefits of increased strength in the upper stories tend to offset the negative effects of localized damage in the lower stories (Ibid.).

Effect of concrete strength variation on irregularities has also been studied by some scholars. For example, De Stefano and his co-workers (2013) studied the interaction of concrete strength variability with irregularity for a non-seismic design four-story frame RC building. They mentioned that under the medium to high variability of concrete strength ( $f_c$ ), a building can experience both plan and elevation irregular responses during earthquake, even if the structure possess double symmetric geometrically and shows regular in elevation. The strength variability can be made with poor materials, low control during the construction phase, and effect of time and so on. They applied nonlinear time history and also nonlinear static analysis among statistical methods based on the acquired concrete samples for their case study building. They cited that although the pushover method gave conservative results, both nonlinear methods illustrated irregular responses especially for drift and chord rotations (Ibid.).

#### **Several proposed methods on irregularity in literatures**

Ichinose and Umeno (2000) proposed a story- shear-safety-factor method to avoid story collapse in the existing buildings. Fragility Curves, uncertainties, and probabilistic analysis are some of the most popular fields and for different situations in the vertical and plan irregularities studies, e.g. (Ellingwood et al. 2007), (De Stefano and Pintucchi 2008), (Ramamoorthy et al. 2008), (Haselton et al. 2011), (Liel et al. 2011), (El-Howary and Mehanny 2011), and (Rajeev and Tesfamariam 2012) are few of them.

Akita and Kuramoto (2008) proposed a method to consider the effect of higher mode responses in evaluating of the multi-story irregular RC buildings which

are consisting of mixed soft and rigid stories and the story collapse mechanism. Their method was based on the equivalent participation vector acquired per the dominant effect of higher mode. Their method was evaluated the time history responses of the inter-story shear and drift. They applied end spring using the Takeda model to the beams, and the multi spring model to the columns and shear walls. Shear springs with the stiffness degradation due to the shear cracks were set in the center of the columns and shear walls without considering shear yielding action (Ibid.). Viscous damping for the analysis was assumed equal to 5% damping coefficient with respect to the elastic first mode period. As one of their conclusions, it was pointed out that in case of building with soft story mechanism, the mode variation accompanied by the progress of the plasticity was significant and it may not be justified to consider the first mode of vibration only.

Bhatt and Bento (2011) studied FEMA 440 and ATC40 pushover methods and they extended a new method for plan-asymmetric concrete structures with poor ductility. Three real asymmetric plan LRC buildings with three (3), five (5), and eight (8) stories were modeled and studied. The eight- story building had a soft first story. The time history analysis was accomplished in order to verify their extended method for torsional plan structures by comparing of normalized top story displacements (Ibid.).

Varadharajan et al. (2014) proposed a method named Irregularity Index. They considered variation and combination of vertical, mass, and stiffness irregularities for different magnitude and location and examined their methods by nonlinear time history analyses. They stated that when stiffness and strength irregularities were present at the bottom stories, the critical condition occurred. Also, they mentioned that the least impact on the irregularity index emanated from changing in bay width (Ibid.).

#### **New and innovated methods in irregularity rehabilitation**

Miyamoto and Scholl (1996) retrofitted a historical hotel in the North of California by adding viscous dampers to the first story. The first story was the weak story in the non-ductile reinforced concrete structure, which was structurally improved by adding viscous dampers and steel moment frame. Kabeyasawa et al.

(2002) investigated the strengthening of reinforced concrete columns designed per the old building code which are actually lightly reinforced members. They retrofitted eight (8) column specimens with polyester sheets and tested the specimens under constant gravity loads and cyclic lateral loads to maintain axial load capacity of the concrete columns under very large lateral deformation. Per their study result, their method is very effective and can lead to more than 10% inter-story drift without collapse, which in turn may prevent any soft story mechanism in a concrete frame structure. Parducci et al. (2005) and Mezzi and Parducci (2005) used an innovated method to solve soft story problem which are observed very frequent at the first level of the reinforced concrete buildings in Italy. Instead of traditional strengthening the structural elements by popular retrofitting techniques, they studied alternative dissipating system to improve the critical ends of columns by a confinement of the column combined with a set of special mechanical dampers as the primary dissipation system in the structure. They applied rehoplastic concrete and FRP wrapping to confine the column sections and increase the column ductility. The seismic rehabilitation solution was applied for an existing building in Bucharest, Romania, through using combination of fluid viscous dampers and steel jacketing in the ground floor columns and upper stories structural walls by Chesca et al. (2007). The linear dynamic analyses were used for establishing the seismic rehabilitation and for calibrating damping parameters, pushover analysis for the building capacity evaluation, and also the nonlinear dynamic analyses method were performed for verification of the building behavior (Ibid.). Pinarbasi et al. (2007) studied the effect of Isolators, specified per IBC2000, on a hypothetical five-story RC building with a soft ground story through modal and nonlinear time history analyses. They showed that the seismic isolation increased the flexibility of the soft story. Using Fluid Viscous Dampers, the possible use of innovative Smart materials to control of irregular structures, Base Isolation Systems, and Friction Pendulum Dampers are several advanced methods and new approaches in the field of research on torsional and vertical behavior studies (De Stefano and Pintucchi 2008).

Briman and Ribakov (2009) introduced a new retrofitting idea for existing structures with a soft story by replacing the weak columns with seismic isolation

column. Their system is comprised of well-known Friction Pendulum principle to provide seismic isolation for a column as a kinematic system. They did numerical example to show the effectiveness of the seismic isolation column system (Ibid.). To increase capability of reinforced concrete columns, especially to prevent early failure of reinforcement or crushing of concrete, some hi-tech material has been used and developed. For instance, Bournas and Triantafillou (2010) cited that Fiber Reinforced Polymer (FRP), also known as Fiber Reinforced Plastic, have been used in the many lightly and/or poorly reinforced columns. They also mentioned about another method which is called near-surface mounted (NSM) reinforcement. They studied NSM-based flexural strengthening of RC columns under simulated seismic loading (Ibid.). Multiple sliding surface, which was primary developed for seismic retrofitting of bridges, was studied for the soft story frame structure rehabilitation by Fakhouri and Igarashi (2011). The base of method was relied on the multiple-slider bearing on the top of the middle columns and rubber bearing at the top of edge columns. They considered a five-story RC frame with a soft first story for their study. The multiple-slider bearing minimized the seismic damage and protected the soft first story from excessive large ductility demand while the superstructure above the bearings behaved almost in the elastic range (Ibid.). Valente (2013) studied the seismic retrofitting of a gravity load designed concrete structure with irregular plan. The studied structure had been built and tested in the laboratory under dynamic seismic loads before. He used nonlinear time history analysis and nonlinear pushover method for retrofitting assessment of the structure. Also reducing of torsional response by stiffening different structural elements has been part of his research. FRP wrapping of a few columns, RC jacketing of the columns, and combined method had been studied numerically. It has been shown that in comparison with the two other methods, the combined approach improved significantly the overall seismic performance, increased strength and ductility, and better performance had been achieved (Valente 2013).

### **2.5.3. Experimental Studies**

Aycardi et al. (1994) investigated the seismic response and behavior of reinforced columns which were primary designed for dead and live loads only. The

prototype model was built based on a typical frame building common in the Eastern and Central US. They built a one-third scale model, and tested their prototype model on the shaking table testing system (Aycardi et al. 1994). They mentioned that plastic analysis and hysteretic rules developed from experimental test results gave a reasonably good prediction of the inelastic displacement and base shear of the entire model structure. Under their test program, failure in the columns was flexural dominated although it was depended on the level of axial loads. They also mentioned that in their experimental model, the interior columns showed a weak column-strong beam mechanism (Ibid.). By expanding of Aycardi et al. experimental research, Bracci et al. performed more experimental and analytical researches (Bracci et al. 1995a) and (Bracci et al. 1995b). They concluded that gravity load designed reinforced concrete frames may possess an inherent lateral strength capacity to resist minor to moderate earthquakes. However, formation of undesirable side-sway mechanisms may intensify the substantial inter-story deformations (Bracci et al. 1995a). They mentioned that the overall structural response of the model was governed by strong beam-weak column behavior. In other words, the soft story mechanism occurred as the columns cracked and yield before the beams (Ibid.). They also did plastic analysis and pushover analysis by applying the companion component and sub-assembly test results. Both analyses showed first soft story mechanism.

Bracci et al. (1995b) also studied three retrofitting methods for soft story problem, without considering the possible effect of torsional irregularity. Based on their study, a partially prestressed concrete alternative and two masonry retrofit alternatives were analyzed for improving the local and global response performance of RC frame structures designed only for gravity loads which were constructed in low-to-moderate seismic region (Ibid.). The objective of their proposed retrofits was to reconfigure the structural failure mode. Indeed, they tried to prevent a more catastrophic soft story collapse and implied a more ductile beam sidesway mechanism. The prestressed concrete jacketing alternative was applied to the column of the one-third scale model RC frame building. They concluded that the seismic performance of vulnerable soft story system (gravity load design frames) may be efficiently improved by strengthening limited columns (Ibid.).

El-Attar et al. (1997) used the same 3D concrete frame prototype models to extend the previous studies by Bracci et al. on gravity load design reinforced concrete frames which are popular in the Central and Eastern US over the past 60 years. El-Attar et al. cited that comparison with analytical results indicated that the slab contribution to beam flexural strength is a vital step in the assessment of the performance of gravity load design reinforced concrete structures since it had the possible ability to alter the relatively ductile strong column-weak beam mechanism to a more brittle soft-story mechanism (El-Attar et al. 1997). They applied Taft (1952) records to their test model. The records were scaled and set at increasing higher values, and then results controlled and followed by the analytical analyses. They performed the same input records for the nonlinear time history analyses (Ibid.). They studied crack patterns and propagation in the concrete beams and columns. Their study showed that the columns cracks were concentrated at top and bottom of the column height in the first and second stories. In the analytical model, the stiffness degradation, strength deterioration, pinching behavior, and 2% critical damping were adopted. Furthermore, the effect of T-section width was taken for beams (Ibid.).

Lu et al. (1999) did analytical and experimental study about the vertical and plan irregularities separately. Two six-story, three-bay, RC frames had studied. One model had a tall first story (BF1), and the other model had a discontinuous interior column (DCF). Both models were designed according to Eurocode 8. The 1:5.5-scale models were constructed and tested on an earthquake simulator. The main objectives of their investigation were to study the structural effects of these particular irregularities and to check the relevant design code provisions (Lu et al. 1999). They cited that the frame BF1 performed in a reasonably regular manner. For the frame DCF, the response during the moderate earthquakes was strongly influenced by the increased in flexibility which was mentioned at the direction towards the missing column side, combined with the gravitational effects on the suspended beam spans. They mentioned that per their experimental observations, the response of the frame DCF to the strong ground motions was affected by an apparent soft first-story mechanism (Ibid.).

Kusunoki et al. (2001) investigated torsional response of one-span, one-bay, two-story steel structure with different eccentric factors by pseudo-dynamic and shaking table test technique (Kusunoki et al. 2001). The 3D models scaled down to half size of the real structures. They considered both bi-directional and one-directional eccentricities in their studies, and applied earthquake ground acceleration as input motions. They mentioned that torsional response angle increases according to the eccentric factor.

Nonlinear torsional responses of simple one-story, symmetric and asymmetric plans, to bi-directional lateral seismic motions were investigated by Sfura et al. (2002). They investigated both experimental and analytical models to characterize the lateral torsional response for a variety of mass, stiffness, and strength configurations by shaking table test and FE analytical method. They concluded that the torsional motions of the structures are very difficult to be predicted accurately.

Lee and Woo (2002) considered the seismic performance of a three-story RC ordinary moment-resisting frame (OMF) for their study. Their model was not designed to resist against earthquake. They performed experimental study to evaluate the reliability of the available static and dynamic inelastic analysis methods (Ibid.). A 1:5 scale model was constructed according to the Korean non-seismic detailing and they imposed the similitude law to a series of the shaking table motions as Taft N21E component earthquake record. Due to the limitation in the capacity of their shaking table system, they performed a pushover test to observe the ultimate capacity of their model after earthquake simulation tests. They also evaluated their model with nonlinear analyses, considering both analytical and experimental results for their study. They mentioned that the model revealed fairly good resistance to the higher levels of earthquake simulation tests though it was not designed for seismic load. The main mechanisms of resistance against the high level of earthquakes were appeared to be: 1) the high over-strength of components and materials, 2) the elongation of the fundamental period of structure, 3) the minor dissipation of energy by inelastic deformations, and 4) the increase of the damping ratio. The drifts of the model under the tests were reported nearly within the acceptable limit (Lee and Woo 2002). The results of the pushover test indicated that the model structure had the overall

displacement ductility ratio of 2.4 and approximately the over-strength coefficient was 8.7 (Ibid.). They did not apply any plan irregularity for their investigation although the test results of their regular plan building indicated that almost negligible torsional behaviors occurred in their model for both earthquake simulation and pushover tests. The collapse mechanism observed in the final stage of the experiment, i.e. lightly RC frame in low seismicity region, was soft story mechanism in the first story (Ibid.).

Kim and Kabeyasawa (2004) performed shaking table test to examine the torsional response characteristics of a reinforced concrete frame with asymmetric plan. The frame consists of concrete columns and shear wall and five scaled ground excitations were applied to the model in order to study the response of the structure from elastic to inelastic condition. A macro model of the columns was proposed to scrutinize the experimental results, and the analysis results were verified through comparison with the experimental results. They concluded that particularly the inelastic torsional response was slightly larger than the elastic response which might be caused by the large strength eccentricity in the tested model. In line with the former study, Kim et al. (2012) performed another experimental dynamic test to investigate the collapse process of RC structures with light transverse reinforcement, soft stories, and eccentric plans. Each sample consists of a one-third scale model, and was designed per 1970s reinforcement detail practice in Japan with stiffness and strength eccentricity in the first story. A comparison of collapse behaviors with and without strengthening method of super reinforced with flexibility (SRF, polyester belt/sheet material with urethane adhesive) was accomplished and showed the efficiency of their method, despite that the torsional response was more in the inelastic range than in the elastic range. The strengthen method prevented the loss of column axial load capacity, with confining the column core and precluding of cracking progress (Ibid.).

Also in another experimental program and in line with a three-years research program to the aim of improving assessment of older non-seismically designed structures, Mola et al. (2004) tested a real size plan-wise irregular three-story RC frame. The bi-directional pseudo-dynamic was the selected test method, and pushover

analysis was used to compare the results. The frame was a regular structure at elevation, asymmetric plan, two bays, with balcony on one side, and intentionally designed for the gravity loads only. Their analytical model based on FEMA 356 and New Zealand code led to larger rotations, particularly concentrated in the first floor columns, thus resulting to larger displacements and soft story mechanism due to the plan irregularity. They pointed out that for the displacement assessment the experimental results did not show a good agreement with the code results. In fact, the first-story displacements were overestimated. On the other hand, the second-story displacements were underestimated (Ibid.).

The degradation of shear strength and effect on plastic hinge and ductility was experimentally studied by Biskinis et al. (2004). They mentioned that the cyclic degradation of shear resistance is expected to be larger within flexural plastic hinges, and the degradation of shear strength takes place mostly in the RC members that develop flexural plastic hinges prior to their shear resistance (Ibid.).

One of the rare researches regarding simultaneous effect of vertical and planar irregularities has been done by Lee and Ko (2004). They investigated the seismic response of high-rise RC bearing-wall structure systems with three types of irregularity at the bottom stories by using the shaking table test. They built three 1:12 scale seventeen-story RC models according to the similitude law. The upper fifteen stories had a bearing-wall system while the lower two stories had the frame system with different layouts in plan (Ibid.). For the first one, they considered only a moment resistant frame system, and for the second they implied an infilled shear wall in the central frame. The third model had an infilled shear wall in only one of the exterior frames to imply plan irregularity. Then, they applied ground motion excitations. They considered three kinds of global deformations in the lower frame including: shear, overturning, and torsional deformations in terms of angle measurement from the primary condition of the structures. Their test results showed that (Ibid.): 1) The existence of shear wall considerably reduces shear deformation at the lower frame, but had nearly a negligible effect on the reduction of the overturning deformation, base shear, and overturning moment; 2) As they increased the earthquake intensity, they observed that the models with symmetric plan experienced shift of the rotating

axis (rocking behavior) caused by overturning moment. The model with torsional irregularity showed the uni-directional overturning moment orthogonal to the direction of the applied seismic record. Combination of the orthogonal overturning moment and torsional moment were created a complex distribution of axial forces in columns; and 3) the value of torsional stiffness varied depending on the effective mode of vibrations. They cited that a higher mode of vibration induced larger torsional stiffness. Besides, they mentioned that the hysteretic curve and the strength diagram, between base shear and torsion, indicated the dominant mode of vibration. This response may lead to failure of the system (Ibid.).

Sub-structure pseudo dynamic tests for six-story and twelve-story RC buildings with soft first story had been done by Matsumoto et al. (2004). Their model consisted of a bare frame in the first story and shear walls in the upper stories, and the failure mechanism had been investigated (Matsumoto et al. 2004). They applied four (4) earthquake ground motion records in their tests. They mentioned that flexural yielding of the column caused the collapse mechanism in both the six-story and twelve-story frames. The preliminary response analysis of the sub-structure showed good conformant with the test outputs on the shear, drift and axial force of columns at the first story (Ibid.).

Encasing of the lower levels of reinforced concrete column with steel profile to mitigate the soft story problem was investigated by Plumier et al. (2005). They set up a test, and considered low ductility under low seismicity (PGA= 0.2g) loading criteria. They cited that the composite sections in their study significantly increased the ductility, rotation capacity at maximum resistance (Ibid.).

Pinho (2007) mentioned a case study about the dynamic analysis of a four-story and three-bay RC bare frame. The building had been designed and built at the European Laboratory for Structural Assessment (ELSA) in Ispra, Italy. The full-scale model was constructed for pseudo dynamic testing. In addition to gravity loads, the frame was designed for a nominal lateral load of 8% of its weight. The reinforcement details had been considered to show the construction practice of the Southern European countries in the 1950's and 1960's. According to the test results, the bare frame had a soft story at the third floor. The main reason was a drastic change in

strength and stiffness at this level, due to the reduction in both the reinforcement and the section dimensions in the columns between the second and third stories, plus coinciding of the location of lap-splicing. This condition is typical among the buildings designed mainly for gravity-loading and the failure of a story midway up a building has been observed in past earthquakes (Pinho 2007). The structure was modeled in a FE software (Seismosoft). Vertical loads and masses were applied at each beam node and at the beam-column joints, concrete is modeled by a uniaxial constant confinement model and calibrated using testing data. The Menegotto-Pinto steel model with an isotropic hardening constitutive relationship was used to model rebars. The shear strains across the element cross section, warping strains and warping effects were not considered in the model. For the analysis purpose, viscous damping was not considered in any dynamic analysis, since energy dissipation was already included within the nonlinear fiber model formulation of the inelastic frame elements, and non-hysteretic type damping was assumed to be negligible (Pinho 2007). Using time history nonlinear dynamic analysis, the results of experimental tests were close to the analytical results in terms of drift and displacement responses (Pinho 2007). Again, in this study plan irregularity was not part of the experimental procedure.

Thru experimental work, Pantazopoulou and Syntzirma (2010) cited that deformation prediction has more limitations and uncertainties. As an example, they mentioned that “whereas the lateral load strength of a simple structure such as a well detailed cantilever RC column may be quantified with a margin of error within 10% of the actual value, the estimated drift capacity with the available tools today may be as far off as 100% of the actual value, with a generally inestimable and uncertain margin of safety.” They compared a series of reinforced concrete column-specimens under reversed cyclic loads. Their specimens modelled per former RC detailing practices relevant in 1950s to 1970s (Ibid.). The experimental tests showed that all specimens failed in a brittle mode, and flexural shear and anchorage strengths degraded at different rates with increasing displacement. They found discrepancies in the estimated strength of laps and overestimate of rotation at yielding condition. They

also concluded that mostly the deviation in the estimated residual value of shear and lap strengths created the discrepancies between the tests and analytical results (Ibid.).

An experimental field test for soft story study of a five-story precast building has been done by Wibowo et al. (2010) using pushover method basis. They also performed nonlinear analytical study to compare with the experimental results. They found that the tested precast soft story system had sufficient displacement capacity for lower to moderate seismic regions. The same research team did experimental study on four-column specimens (Wibowo et al. 2011). The columns were designed as prototype of the non-ductile reinforced concrete columns to represent old buildings in low-to-moderate seismic regions. The axial load and longitudinal steel reinforcement ratio were the variable parameters, also in their model the provided transverse reinforcements were lower than current common code requirements. They concluded that non-ductile structures may have drift and axial load capacity much higher than code recommendations, which are important for low-to-moderate seismic regions (Ibid.).

Teramoto and his co-workers (2012) studied the soft story failure mechanism for the corner columns of RC structures. They examined a substructure model under the pseudo-dynamic tests to observe damage mechanism of corner columns which may encounter severe varying axial force during strong ground motion excitation. Two major failure modes of soft story were investigated, flexural yielding in the soft story columns and yielding of whole reinforcement of the tension side of a structure due to overturning moment. It has been found that the flexural yielding of corner columns displayed more damages in comparison to the overturning moment effect (Ibid.).

Ghannoum and Moehle, in part of a research program about typical lightly reinforced concrete building in California, and pursued one of the previous investigation by Moehle et al. (2006), did a series of analytical (Ghannoum and Moehle 2012b) and experimental (Ghannoum and Moehle 2012a) studies. The main propose of their study was to calibrate and ensue analytical models on the basis of experimental results. They applied fiber elements to model columns and beams, and Rayleigh damping proportional with the first and second mode of vibration were

considered with 2% ratio of the critical damping ratio along with the experimental results. According to their experimental study, the collapse of frames was the results of columns shear and axial failure with widely spaced transverse reinforcements. Their test also showed that the failure type and rate were influenced by the amount of axial load, stiffness of surrounding framing, and duration and intensity of applied shaking (Ghannoum and Moehle 2012a). They reached a good correlation between analytical models and experimental results (Ghannoum and Moehle 2012b).

Yavari and his co-workers (2013) tested four 1/2.25 scaled RC-frame specimens. Using shaking table, the models tested under few selected scaled peak ground accelerations. Each frame was two-story, two-bay and modeled to represent non-seismic detailing structure under high or moderate axial forces with different joint in terms of confined or unconfined condition. The models were established to create strong beam/weak column mechanism, typical of older construction. They cited that collapse of the models were due to failure of non-ductile RC columns, and collapse under the failure of unconfined beam-column joints was less compare to the former collapse mechanism (Ibid.).

De-la-Colina and his coworkers (2013) performed an experimental research to study the effect of foundation rotation on a two-story RC model. The torsional response under soil-structure interaction during seismic event with linear static behavior was studied (Ibid.). They showed that the torsional response of a regular plan RC structure may increase if soil-structure interaction is considered (Ibid.). The nonlinearity and vertical and/or horizontal irregularity were not accomplished in their experimental study.

As part of a comprehensive research, a full scaled four (4) story wood-frame building has been built at Network for Earthquake Engineering Simulation (NEES) large high performance outdoor shake table facility (Bahmani et al. 2014). Bahmani and his co-workers have been studying torsional response of the wood-frame built model which had soft story deficiency at the ground level. Retrofitting method was also encompassed within their study scope. The objective of their study comprises seismic evaluation of a retrofitted wood structure with Performance-Based Seismic Retrofit procedure (Ibid.). They have been validating their numerical retrofit method

with the experimental data. Their model basically consists of an equivalent SDOF system for simplification. Per their primary result publication, it is mentioned that the level of accuracy of their proposed method is satisfactory (Ibid.).

#### **2.5.4. Soft Story Studies**

Fiber model was used to perform nonlinear dynamic analyses of the soft story (Bento and Azevedo 2000). Also, damage index was used by several researchers to study soft story mechanism (Bento and Azevedo 2000) and (Stathopoulos and Anagnostopoulos 2000). Bento and Azevedo (2000) methodology was based on the vulnerability functions and probabilistic definition of the seismic action to quantify the structural responses. They did nonlinear dynamic analyses, and their model consisted of a linear elastic beam element with nonlinear rotational spring at each end. All nonlinear deformations were concentrated in the two end plastic hinges, whereas the elastic deformations were considered with elastic elements. They did not consider strength degradation with cyclic loads, also the stress-strain curves implemented to model confined or unconfined concrete (Ibid.). They cited that due to the concentration of damage at soft story and excessive inter-story drift, the structures with soft story illustrated less safe behavior. Unlike NEHRP recommendation for effect (NEHRP 2010b) regarding low  $P-\delta$  effect on nonlinear results, they mentioned that  $P-\delta$  is important in nonlinear analysis of structure with soft story condition (Bento and Azevedo 2000).

Tsai and Weng (2001) studied the generalized shape functions which were constructed from the nonlinear static pushover analysis of shear type building systems. Analytical results indicated that soft first-story structures may show a story drift demands significantly greater than the regular buildings with shorter fundamental period. They also mentioned that per results of nonlinear dynamic analysis of a six-story structure, the maximum story drift demand can be reasonably predicted. They cited that to remain in a reasonable range, the story spectral drift which is constructed from the generalized shape functions should be used (Tsai and Weng 2001).

Fardis and Panagiotakos (2001) compared the drift ratio capacity of different reinforced concrete columns. They mentioned that columns of soft story buildings designed for immediate occupancy under the corresponding seismic hazard level may meet marginally the deformation capacity demands at the collapse prevention level. They considered two different first-story heights, 3 and 7.5 meters, to pursue soft story condition. For parametric study, they also imposed several alternative conditions such as column sizes, different  $f'_c$  for the concrete strength, different soil types, and the effect of multistory on performance. They did not investigate the torsional effect on their extensive research and parametric study.

Yoshimura (2003) did the nonlinear dynamic analyses for a model which representing weak-first-story buildings to study the first-story drift demand. He considered the first-story strength and the strength balance along the height as analysis variables, and also he checked some of his results with the pushover analysis. For columns, he considered the flexural nonlinearity by using two springs placed at both ends. The hysteresis behavior of columns was represented by the Takeda model. For walls, flexural and shear nonlinearities were considered. He also applied the 1995 Kobe record and 1940 El Centro records for the time history analysis. For both records, he adjusted the records so that the maximum ground velocity was equal to 0.5m/s based on the Japanese seismic design. Viscous damping relative to the instantaneous stiffness with a ratio of 3% with respect to the fundamental natural frequency was applied. The fundamental natural period of the building was 0.52sec (Ibid.). Pushover analysis was also conducted to compare the dynamic and static analyses. Lateral load distribution was assumed corresponding with the design shear coefficient distribution factor according to Japan's seismic code. He mentioned that the nonlinear static results were similar in trend to the nonlinear dynamic results (Ibid.). As a conclusion, he mentioned that the first-story drift demand is governed not only by the first-story strength but also by the strength of the upper stories and the strength balance between the first story and upper stories. He also pointed out that the second-story strength can affect the first-story results (Yoshimura 2003).

Ramdane et al. (2004) evaluated the seismic capacity through non-linear numerical analyses of typical RC buildings of six (6), ten (10), and fourteen (14)

stories with soft first story. They investigated the response characteristics and method of seismic design improvement for these types of structures. They represented an expression which was derived based on the energy constant law, and they compared results from the numerical analyses to verify the adequacy of their expression. Their models were analyzed with time history method under seven (7) different records. For the first story, they assumed elastic shear and axial springs and Takeda Model for the flexural spring, and the applied damping was proportioned to the instant stiffness of 5% (Ibid.).

Richard et al. (2010) through nonlinear time history analysis showed that for an intermediate reinforced concrete structure (IMF), which was designed for a moderate seismic zone condition, the prominent possible failure modes were soft story mechanism. They pointed out that 32.5% of the ground motions caused the formation of a single story mechanism at the first story (Ibid.).

NEHRP (2010a) suggested a simplified model that could be used to investigate the story stiffness ratio and story shear strength ratio for buildings with vertical irregularities. In their method, the stiffness and strength of each story are concentrated by allocation of single nonlinear shear spring which is selected based on typical values for real buildings.

Hejazi et al. (2011) studied the structural behavior and retrofitting of high-rise RC buildings with soft story through bracing devices for moderate seismic zones. Moreover, they compared the soft story structural response with various type of bracing arrangement.

#### **2.5.5. Torsional Studies**

Paulay (1996) cited that the reference yield displacement for a structural system would be influenced by some properties such as: stiffness of the elastic components and structural geometry, the ultimate relationship between the element ductility capacity and system ductility capacity, and combined properties of both elastic and inelastic response. Considering the degree of torsional restraint, hence, the torsional design forces at ultimate limit state is then based on the location of the center of resistance or center of strength regarding the center of mass (CM). He also

pointed out that the possible degradation of torsional stiffness did not necessarily result in further restriction on the displacement ductility demand of structural system (Paulay 1999).

Plastic hinge idealization was used to study the inelastic seismic torsional response by Stathopoulos and Anagnostopoulos (2000). In their research, shear beam type model, and ten earthquake records in a one-story reinforced concrete building was considered to examine some effects, such as double eccentricities and different type of earthquake motions. They concluded that in their research, motions with different characteristics cause similar post-elastic behavior and bi-axial eccentricities did not show significant different results from single eccentricities condition (Ibid.).

In another study by Dusicka et al. (2000), it is found that strength eccentricity impacts the structural response in torsional inelastic phase. Even structural system with perfect balanced elastically form may show torsional response due to the strength irregularities during inelastic phase. Also, they mentioned that the relationship between element stiffness and element strength depend on the type of lateral resisting system, member dimensions, and element material properties (Dusicka et al. 2000).

Dutta (2001) compared two structural symmetric and asymmetric one-story systems with the same response reduction factor. He discussed that under a specific analytical condition, while the symmetric structure remained elastic, the eccentric structure with the same lateral strength entered the nonlinear range. He mentioned the major reasons would be classified as unsymmetrical yielding behavior, change into a system with large strength eccentricity, and progressive strength deterioration. Further, under bi-directional ground excitation the effect of strength deterioration was more dominant (Ibid.). He also culminated that in structural elements of asymmetric RC buildings consideration of a bilinear hysteresis behavior without strength deterioration may underestimate the torsional ductility demand. Therefore, the strength deterioration characteristics should be considered in the hysteresis behavior of RC structural members in buildings with plan eccentricity (Ibid.).

Fajfar (2002) discussed how to combine two horizontal excitations in nonlinear analysis, mainly nonlinear static analysis in asymmetric structures. He

mentioned that the independent uni-directional static load application in two directions without result combination usually lead to un-conservative results. On the other hand, it is very conservative to consider simultaneous loads from two orthogonal directions to reach a full target displacement and it will lead to a torsional plastic mechanism. For inelastic time history dynamic analysis of torsionally stiff structures, plastic hinges usually occur, but they last only a short time and do not influence the overall structural response (Ibid.). In general, nonlinear time history analysis can be applied in two directions separately and then the results can also be combined with SRSS rule. This rule have been widely applied in elastic analysis methods, and with more dispersion, demonstrates acceptable results in the inelastic range as well.

Per Dimova and Alashki (2003) research, approximate analytical solution proved that even under small accidental eccentricities the symmetric structures may exhibit “irregular behavior”. They mentioned that the accidental torsional effects (regulated in several seismic standard codes) were not able to be properly considered by static application of torsional moments (Ibid.). They did the sensitivity analysis of the response with regard to the uncertainty in the element stiffness. They showed that the response of nominally symmetric plan models increased by a greater amount compared with asymmetric-plan models. Using results from Monte Carlo simulations for estimation of the effects of the uncertainty of the structural stiffness, they introduced a function to show the design eccentricity effect (Ibid.). The ratio ( $p$ ) of the uncoupled translational periods to the torsional natural periods was considered. Their numerical results indicated that the design eccentricity increased to a maximum at  $p \approx 0.9$ , and declined to a minimum amount at  $p \approx 1$ , then, at next stage again increased to a maximum at  $p \approx 1.2$ , and remained nearly constant for  $p \geq 1.2$  (Dimova and Alashki 2003).

Pardalopoulos et al. (2005) did parametric analyses which were carried out to quantify the effect of plan eccentricity with the various mechanisms of resistance. Their frame system was studied by applying the same ground motion records that were used in the actual tests in another study. Several mechanisms studied which were: member effective stiffness, flexure, shear, capacity of anchorages and lap

splices, and joint shear (Ibid.). Response parameters were considered as the time histories of the trajectories of the Center of Mass in the three floors, inter-story drift, floor twist, and also the time history response of demand to supply ratios for the various resistance mechanisms (Ibid.). They examined several parameters such as: eccentricity owing to the large stiffness of column, different span lengths, eccentric beam-column and beam-to-beam connections, and setbacks. RC members were modelled as elastic FEs. Concentrated inelasticity at different specific locations along the member length and beam-column joints as rigid links were also considered. They modelled floor slabs as rigid diaphragms. The first floor columns were considered fixed at the ground level.  $E_c$  (Young's modulus) was calculated by experimental data of samples taken during the construction phase. To reflect the initial RC member cracking, the tangent modulus of elasticity for unconfined concrete was decreased by 15%. The axial-flexural inelastic deformations of columns were considered at the top and the bottom of each column (Pardalopoulos et al. 2005). Axial moment PM hinges was taken into account for the columns. The plastic hinge length is assumed equal to  $0.5d$ , in which  $d$  denotes the depth of the cross-section and provides a good estimate of plastic hinge length (Pardalopoulos et al. 2005). Several similar assumptions are used in the current study as well.

Tremblay and Poncet (2005) studied the influence of mass irregularity on building seismic response. They considered an eight-story concentrically braced steel frame with different setback configurations to get abruptness in plan dimensions and seismic weight along the height of the structure with three different locations of mass discontinuity, 25, 50, and 75% of the building height, together with two ratios of seismic weight, 200 and 300%. Using FEMA recommendations and time history analysis methods, and also considering uncertainties in their numerical work, they cited that the mass irregularities alone did not affect the response of the structure rigorously (Ibid.). Recent studies evidenced that among the mass, stiffness, and strength vertical irregularities, the last one has implied the worst response in terms of negative influence on the nonlinear seismic behavior of the frame structures (Magliulo et al. 2004). The previous conclusion is also mentioned by Thuat and

Ichinose (2004), Dooley and Bracci (2001), and Lu et al. (1999) in which the strength irregularities plays the dominant role in nonlinear structural response.

Kosmopoulos and Fardis (2007) studied inelastic response of four (4) real buildings, three to six stories, with significant plan irregularities, and low engineered seismic resistance. The nonlinear bi-directional inputs were compared to elastic modal analysis results with SRSS combination of the two directional seismic components. They mentioned that static elastic analysis tends to overestimate the inelastic torsional response at the flexible or central part of the torsionally flexible buildings, and underestimate them at their stiff side. Further, the modal response spectrum analysis showed overestimate result for the inelastic torsional effects, at the stiff or central part of the torsionally stiff buildings, while underestimate them at the flexible side (Ibid.). The results of experimental tests on the two-story building were used to verify their analytical procedure. The six story structure was a very irregular structure in both elevation and plan, an *L* shape plan, which was collapsed in the Athens 1999 earthquake. Their third case was a two independent theatre facility buildings act as a unit structure and separated by a seismic joint which had vertical and horizontal irregularities. The lumped inelasticity at end point hinges, bilinear moment rotation, and modified Takeda hysteresis model have been assumed. Elastic stiffness of the elements was taken equal to the secant stiffness at yielding, joints were considered as rigid but with longitudinal rebar slippage possibility. Masses were concentrated at their nearest nodes of the model, 5% Rayleigh type damping with two periods of the elastic 3D model corresponding to the largest horizontal direction modal mass, and  $P-\Delta$  effect through the linearized geometric stiffness matrix of columns were considered as well (Ibid.). In average, their study shows a reasonable difference between analytical models and real structures.

## Chapter 3: Linear Static Models, Basic Models of Study

### 3.1. Introduction

Structures may suffer different types of forces during vibration. These forces are (Karnovsky and Lebed, 2010):

- Distributing forces which are divided into immovable periodical loads, impact forces, moving dynamics loads (such as train loading), and seismic loads. Seismic loads are due to the ground motion which induces ground acceleration and displacement to the structures. These forces depend on the type and amount of the ground motion, mass distribution within the structure, and the elastic and plastic properties of the structure members.
- Restoring forces which are caused by displacement of the structure from a static equilibrium position, and tendency of the system to return to the initial position. They are mainly related to the elastic character of the structure.
- Resisting forces which are basically due to the inelastic resistance such as friction or damping.

Traditionally, in majority of civil engineering disciplines, particularly for structural engineering, dynamic forces and their reactions have been simplified to static forces and reactions. These static loads and reactions many times produce reasonable and conservative results and significantly reduce inelastic and nonlinear behavior and complexity of the dynamic forces, especially for simple structural systems. But they do not always give accurate or correct response. Results of the above-mentioned dynamic forces may show extreme dispersion or even lead to a highly and risky un-conservatism result. In this chapter, several selected archetype building models are introduced to be studied. The models are designed via linear static analysis method where typical dead, wind, and live loads are applied to the

models as static loads per building standard codes criteria. The models will be defined to have elevation and plan irregularities. The effect of plan or elevation irregularities has very limited impact on the general static analysis and design procedure of these types of structures under non-seismic loads. This practice is widely applied and accepted in the low to moderate seismic zones. The irregularity effect has been studied in following chapters.

In this chapter, design and analysis of concrete frame structures are mostly governed by provisions of ACI 318-08 (2008) as the concrete standard code, and ASCE 7-05 (2005) as the applicable building standard for design loads. The required minimum strengths of the reinforcements, concrete elements, beams, columns, and connections plus serviceability requirements and deflection limitations are considered. Computer structural analyses with the applicable load combinations are carried out to determine the required dimensions and strengths of the structural members. Then, the results will be used to create advanced models on the next chapter.

### **3.2. Assumptions and Models as Lightly Reinforced Concrete**

In order to analyze the seismic performance of a Lightly Reinforced Concrete (LRC) structure, the representative archetype frames are statically analyzed and designed to be indicative of a building that might actually be the designs in the past, and the models can be classified as LRC per section 2.3 of this study. Therefore, the archetype design has been done without seismic provision within a moderate or low seismic zone in the current codes. Technically, seismic design provisions, especially in the moderate and high seismic zones, mandate rigorous requirements regarding member size, ductility, details, connections, and capacity. Consequently, seismic members (structural elements which participate in lateral resistance) and even some non-seismic-designed members need to have more energy dissipation capacity which, in turn, are usually achieved by providing more and closer reinforcements. Compared to stringent seismic design requirements and restrictions in the seismic codes, the conventional Dead, Live (including all the live load family such as snow) and Wind

loads very likely lead to a lightly reinforced structure in a common low- to mid-rise residential or office building in a moderate seismic zone area. The seismic criteria may even dictate design requirements of a low- to mid-rise building in low seismic region, which will be discussed later in this chapter.

### **3.2.1. Definition and Geometry of Models**

In this study, moment frames with first story vertical and plan irregularity are considered. The models are two, four and eight stories, divided into three main families, namely BASE models without any irregularity, SYMMETRIC models with the first tall story irregularity, and ASYMMETRIC models with the first story plan irregularity which may or may not have the first story elevation irregularity. The designated abbreviations for each group are identified with letter *B* for Base, *S* for Symmetric and *A* for Asymmetric condition correspondingly. In the North-South direction, each model has three bays, and for the East-West direction two bays are assumed. Three different scenarios are assumed for the first story, normal height (NH), medium height (MH), and extra height (EH). The primary calculations for MH and EH are presented at the next section (3.2.2). To study plan irregularity similar to typical common construction in the US, the central columns are eliminated. Figures 3-2 to 3-5 show the elevations, and figures 3-8a and 3-8b are the typical plans of these models.

Thus, basically for both the static and dynamic nonlinear analyses, there are three major different variables, i.e. number of stories (2, 4, and 8), first story height (NH, MH, and EH) and two different first plan condition, symmetric and asymmetric.

A typical floor height of 12 foot is adopted similar to the study by Ellingwood, et al. (2007), which was originally designed based on the Central and Eastern parts of the US. The span bay of 18 foot in the North-South direction, again similar to the afore-mentioned study, and 20 foot in the East-West direction are allocated to the models to represent a typical plan of low-to mid-rise office or residential building in current practice of the US.

To comply with the previous design methods with respect to structural materials, ASCE 41-06 and its supplement (2007a and 2007b) recommendation is

used. Reinforcing steel has a minimum nominal yield strength of 60.0 ksi per Table 6-1 of ASCE 41-06 supplement No.1 (2007b), and concrete has a minimum specified characteristic strength in compression of 4.0 ksi per Table 6-3 of the ASCE 41-06 (Ibid.), which are also similar to the study by Ellingwood and his coworkers (2007).

The frame elements are basically three dimensional, prismatic, and two-node frame members with six degrees of freedom, three translations and three rotations, at each end (CSI Analysis Reference Manual 2013). These frame elements create the basic bed for nonlinear analysis replicate the effect of axial and biaxial shear deformations, biaxial bending, torsion, and axial forces (Ibid.). The column connections to the base support and to the beams are considered as fix for the static analysis. Beam-column joint effect is considered based on the relative strength of the interacted frame elements, i.e. beams and columns which are ending into the joint. This method is accepted as a relatively accurate technique by both ASCE 41-06 Supplement No. 1 (2007b) and PEER/ATC 72-1 (2010). SAP2000 (2012) software is able to calculate the end effect (offsets in SAP2000 definition) automatically for each element based on the maximum section dimensions of all connected frame elements at a common joint (CSI Analysis Reference Manual 2013). Focus of the current study is on the column behavior. Therefore, solid slab as rigid diaphragm is used at roof and floors with a constant thickness of 5 inches in both linear and nonlinear study. The shell type element is selected for all slab models to represent both in-plane and out-of-plane resistances. The gravity loads are transferred to the beams based on the automatic allocated tributary areas by the software (Ibid.). The slab is designed to have the minimum thickness requirement per common practice design for residential and office buildings. Basically, slab thickness should satisfy both strength and serviceability considerations, and also fire rating obligations. Both former slab criteria are fulfilled within the slab thickness selection, but the fire regulation is not checked in this study. Major concrete beams in the selected models are on the perimeter of structures, and especially under the seismic effect. That means those beams will suffer reverse curvatures, and slab reinforcement interaction with beam can be eliminated for modeling purpose. So the beam sections assumed as rectangular shape by ignoring the T or L action.

### 3.2.2. First Story Height Selection

In seismic design procedure, dissipation of energy through inelastic deformation is one of the major factors. Concrete columns with smaller slenderness ratios disperse substantially more energy prior to column rupture. As a negative side, sturdier and stiffer concrete columns usually are likely to fracture at a lower story drift. The story drift in a frame structure basically depends on the geometry of columns, and therefore stocky concrete columns need relatively larger plastic rotation and local strain at the plastic hinge. To estimate the first story height which may create soft story mechanism in the models, a simple method is established on the column geometry and height selection.

For a beam-column the simplified flexural stiffness ( $k$ ) is given by:

$$k = \frac{12EI}{L^3} \quad [3-1]$$

$L$  is the length (Height here),  $E$  is modulus of elasticity, and  $I$  is moment of inertia of the section.

ASCE 7-05 (2005) in the table 12.3-2 under the type 1a description stipulates that “Stiffness-Soft Story Irregularity is defined to exist where there is a story in which the lateral stiffness is less than 70% of that in the story above or less than 80% of the average stiffness of the three stories above.”. In this study, it is assumed that all stories above the first story have equal height, such that just the first portion of the previous ASCE 7-05 (2005) is considered. Therefore, the stiffness requirement can be simplified as:

$$k_{bot} \geq 0.7 \times k_{top} \quad [3-2]$$

or:

$$\frac{12EI_{bot}}{L_{bot}^3} \geq 0.7 \times \frac{12EI_{top}}{L_{top}^3}$$

The *bot* and *top* subscripts represent the bottom (1<sup>st</sup>) and top (2<sup>nd</sup>) story mechanical or geometrical properties. Considering equal square cross sections for the

first and second stories, and by altering equation 3-3 based on the cross section dimension,  $b$ , the ratio is:

$$\frac{b_{bot}}{b_{top}} \geq 0.915 \times \left(\frac{L_{bot}}{L_{top}}\right)^{0.75} \quad [3-4]$$

Equation 3-4 is derived by considering ASCE 7-05 (2005) requirements for soft story prevention and some basic assumptions of the current study. The first and second stories are assumed to have equal square cross section,  $b_{bot} = b_{top}$ , and the second story height ( $L_{top}$ ) is furnished equal to 12ft. Therefore, to satisfy the soft story restriction on ASCE 7-05, the bottom story height should be approximately less than 13.5 feet per equation 3-4.

By using the same procedure for Stiffness-Extreme Soft Story Irregularity under ASCE 7-05 (2005) table 12.3-2 type 1b description, in which the lateral stiffness is less than 80% of the story above, one can reach equation 3-5:

$$\frac{b_{bot}}{b_{top}} \geq 0.88 \times \left(\frac{L_{bot}}{L_{top}}\right)^{0.75} \quad [3-5]$$

In the Stiffness-Extreme Soft Story Irregularity case, the maximum bottom story height should be approximately 14.23 feet, and more than that may create extreme soft story mechanism in structure.

Hence, in this study the first story normal height (NH), medium height (MH), and extra height (EH) are selected as twelve (12), fifteen (15), and eighteen (18) feet, respectively to cover extreme condition of possible soft story irregularity in the low and moderate seismic zones, which specifically in the past were not part of the design practice consideration and designers attention.

### 3.2.3. Model Tag and Classification

For the sake of brevity, each model is designated with a specific concise name which shows the number of stories, plan condition, and story height throughout of this study. To do this, each model name is labeled with three parts, a digit at first to represent number of story (i.e. 2, 4, or 8), any of letter *A*, *B*, or *S* as for Asymmetric,

Base or Symmetric per section 3-2-1, and then the first story height (12, 15 or 18 feet). For instance, the model 2S15 means two (2) story, symmetric plan (no central column elimination) and fifteen (15) feet height of the first story, and also 8A18 means the eight (8) story model with asymmetric first plan and eighteen (18) feet height of the first story. By this definition, the total number of models is equal to eighteen archetype models.

#### **3.2.4. Determination of Loads and Load Combinations**

For gravity load design, the self-weight of the structural members in addition to a typical 10-psf extra dead load on the floors is considered. 20-psf extra dead load is applied to the roof to cover sloping, isolation, and insulation. The perimeter wall of the structure (cladding) is assumed to have 500-plf weigh on each story edge beams on axes 1, 4, A, and C, and 200-plf on the roof to consider parapet weight for edge beams. The building cladding is considered as non-bearing wall and architectural façade only.

Roof live load, actually snow load, is 30-psf which is a governing live load in several Eastern and North Eastern parts of the US (e.g. see ASCE 7-05 Snow Map). ASCE 7-05 (2005) stipulates the applied floor live load in an office building should be minimum 50-psf. Therefore, except roof, live loads of all stories are 50-psf.

Exposure type “B” is selected to calculate wind load. Per ASCE 7-05 (2005), this type of exposure represents typical residential and commercial terrain in urban and many suburban areas. Wind speed is assumed 90 miles per hour (mph), and both of Importance and Topographical factors are considered equal to one, which are pretty common for residential and office buildings in the Eastern and North Eastern parts of the US. The static linear analysis and structural design were carried out with the SAP2000 computer software (SAP2000 2012). This program can automatically apply wind load to the structure per ASCE code provision. The wind loads are applied separately to both North-South and East-West directions. For each model, the total wind load is summarized in Table 3-1.

For the trial design the load combinations are selected based on the Appendix C of ACI 318-08 (2008) to represent the prevalent design method and load

combinations in the 80s and 90s as ACI 318-99 in SAP2000 (2012) Concrete Design Manual. These types of load combinations are still permitted to be used in strength method per ACI 318-08 (2008), and are presented through the following equations:

$$(i) \quad U = 1.4D + 1.7L \quad [3-6a]$$

$$(ii) \quad U = 0.75 (1.4D + 1.7L + 1.6W) \quad [3-6b]$$

$$(iii) \quad U = 0.9D + 1.6W \quad [3-6c]$$

In which  $U$  represent the required strength, and  $D$ ,  $L$ , and  $W$  stand for Dead, Live, and Wind load respectively.

Table 3-1: Total wind load for each direction per ASCE 7-05

Frame Tag*	Wind Load, East-West (Kips)	Wind Load, North-South (Kips)
2B12, 2A12	13.885	10.285
2S15, 2A15	15.322	11.35
2S18, 2A18	17.117	12.679
4B12, 4A12	37.677	27.909
4S15, 4A15	39.621	29.349
4S18, 4A18	41.897	31.034
8B12, 8A12	96.235	71.285
8S15, 8A15	98.786	73.175
8S18, 8A18	101.653	75.298

\*: Wind load on each direction is based on the Exposure area which is equal for frames with similar height and width.

### **3.3. Initial Analysis and Design of Selected Models, Non-Seismic**

#### **Provisions**

##### **3.3.1. Wind load versus Static Seismic Load**

To have a preliminary view of the seismic load effect, the base shear force for each frame model based on the linear static method, also known as Equivalent Lateral Force procedure, has been calculated. UBC 94 (1994) is the selected seismic code.

This code, now superseded by IBC, showed a low seismic effect for the Eastern and North Eastern parts of the US. Nonetheless, newer accepted standard codes, e.g. IBC (2006) or ASCE 7-05 (2005), may impose higher seismic loads for the above-mentioned part of the US. The effective mass of the frames were considered equal to the applied dead load plus self-weight of each model. For a typical office and residential building, the live load mass participation can be assumed equal to zero per UBC and/or ASCE 7 standards. Moreover, for those types of buildings the Importance Factors are usually equal to one. Time period, seismic code approximate fundamental periods and their limitation, is calculated automatically by the SAP2000 per UBC 94 (1994) code provision. To do this, the lateral resisting system shall be defined in advance. The selected lateral load resisting system is Ordinary Moment resisting Frames (OMF) with  $R_w$  equal to 5.0. Higher value of  $R_w$  usually means lower seismic loads and may be achieved per Table 16-N of UBC 94 by selecting Intermediate or Special Moment Resisting Frame System. However, higher value of  $R_w$  shall comprise more stringent details and member sizes which are, however, irrational and impractical for a low seismic zone area. The buildings assumed located on the Washington DC metropolitan area, so the seismic Zone Factor ( $Z$ ) per Figure 16-2 and Table 16-1 of UBC 94 is equal to the 0.075, i.e. located on the Zone 1 of UBC 94. The site coefficient are assumed to be Type  $S_2$  which is equal to coefficient 1.2 per Table 16-J of UBC 94 (1994), although higher value of  $S_3=1.5$  may be more reasonable for Washington DC metropolitan area. Indeed lower amount of the site coefficient usually lead to lower seismic load and vice versa. Here, somewhat unconservatively, the lower value is picked.

The SAP2000 version 15.2.1 provides Auto Seismic Load library with ability to calculate and apply several pre-code-defined seismic load patterns including UBC 94 (SAP2000 2012). The afore-mentioned coefficients were implied to each model individually with application of SAP2000 built-in UBC 94 code. Table 3-2 shows Seismic Base Shear results.

From Table 3-2, it is clear that for certain conditions, even in a low seismic region, the seismic load may be more dominant than the wind load. Table 3-2 also shows that for all the irregular plan structures (Asymmetric type) the seismic base

shears are more crucial than the Symmetric plan type structures. It is worth to note that as long as the total exposure area of two similar type structures are the same, the wind load for a symmetric and asymmetric plan structure will be equal. Definitely, neglecting the seismic load in low and certainly in moderate seismic zones may cause un-conservative and light structural designs, particularly for irregular buildings. The effect of irregularity on lightly reinforced concrete structures will be more clarified on the next chapters by application of more accurate analysis procedures. The current static calculation is presented to give a preview and basic comparison of seismic load effect for a low seismic zone.

Table 3-2: Seismic base shear per UBC 94\*

Frame Tag**	Seismic Load (Kips)**
2B12 (2A12)	32.927 (40.607)
2S15( 2A15)	31.464 (38.528)
2S18 (2A18)	30.113 (37.407)
4B12 (4A12)	47.002 (56.208)
4S15 (4A15)	46.006 (55.151)
4S18 (4A18)	44.986 (54.201)
8B12 (8A12)	91.093 (101.802)
8S15 (8A15)	91.64 (102.396)
8S18 (8A18)	92.569 (103.257)

\*: The effective seismic mass and the lateral resisting system on both directions are the same. Therefore, the seismic forces of the North-South and East-West directions are equal.

\*\* : The seismic base shear for Asymmetric frames, 2A12 through 8A18, are mentioned on the prentices which have shown higher loads in comparison with S and B model types.

Figure 3-1 shows the wind and seismic load comparison between the symmetric plan model structures with different first story height. The maximum wind loads for each group of models are compared with corresponding seismic loads. The graph shows that for the selected models, the difference between wind and seismic loads are larger for the two story models. For the two story models seismic load is the predominant load. For the eight story structures, the wind load becomes the controlling lateral load. Regardless of the first story height, for the Asymmetric models, which are not shown in the graph, the seismic load shows the highest load value for all selected models.

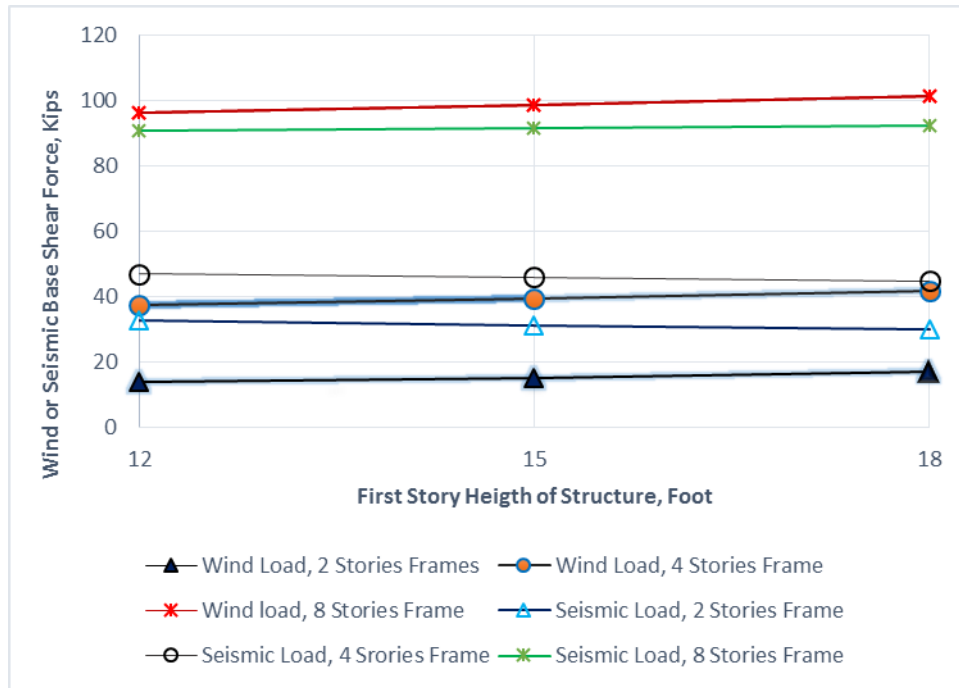


Figure 3-1, Wind and seismic load comparison for the selected models

### 3.3.2. Modal Analysis and Selected Models' Periods

Modal analysis is one of the most informative and important part of seismic analysis. This analysis shall be done to determine the natural modes and periods of a structure. Some useful information regarding overall behavior of a structure may be obtained from modal analysis as well. For certain type of analysis, such as Modal Response Analysis, ASCE 7 (e.g. ACSE 7-05 2005) stipulates that the number of conducted modes for each orthogonal directions of a structure should cover at least 90% of the actual effective mass. Almost for any type of nonlinear seismic analysis, initial modal analysis should be done; particularly when the structural system is classified as irregular, the modal analysis is one of the ground rules in any modern and state-of-the-art seismic codes.

The base of the modal analysis relies on the classic dynamic equation of motion. Equation of motion is decoupled into a set of  $n$  uncoupled equations of motion using the classic normal mode theory of vibration (Elnashai and Di Sarno, 2008). Then, each uncoupled equation of motion denotes an individual SDOF system.

The effective mass and stiffness of each individual SDOF affect the evaluation of eigenvalues in modal analysis of structural systems (Ibid.). According to ASCE 7, the effective mass source is only self-weight of members and applied dead load, and there is no need to put any live load as part of effective mass source. SAP2000 software can provide results of the modal analysis in different ways. Eigenvector Analysis is the selected method for modal analysis of the models, and analysis involves the solution of the generalized classic eigenvalue equation (CSI Analysis Reference Manual 2013):

$$[K - \Omega^2 M] \phi = 0 \quad [3-7]$$

where  $K$  is the stiffness matrix,  $M$  is the diagonal mass matrix,  $\Omega^2$  is the diagonal matrix of eigenvalues, and  $\phi$  is the matrix of corresponding eigenvectors.

From equation 3-7, it is clear that the modal responses are sensitive to the stiffness of structure members. On the other hand, due to inherent nonlinearities in reinforced concrete behavior associated with cracking, the definition of the stiffness of a RC member depends on the load and deformation which are varied. Commentary of ACI 318-08 (2008), chapter 10, allows a simplified but satisfactory method for analysis purpose of vibrations and building periods. To consider the cracked effect for service level per ACI 318-08 Commentary, the concrete modulus of elasticity remains unchanged and un-factored, but the moment of inertia can be considered as:

For columns:  $I_{cr} = I_g$ , and for beams  $I_{cr} = 0.5I_g$  in which  $I_{cr}$  and  $I_g$  stand for the cracked moment inertia and gross moment of inertia of a member respectively. The slab moment of inertia is considered as uncracked, which generally prevents the unnecessary flexibility of the models. Uncracked flat plate is a common assumption for serviceability modeling of concrete slabs, e.g. see (Shin, et al. 2010). In this study, the above-mentioned cracked moment of inertias are used to calculate modes of the selected models. Table 3-3 shows the first three (3) periods (modes) of each model (unit: Second). It is important to mention that since it is not easy to provide columns with a typical specific stiffness or strength, it is not easy to provide structures with

various stiffness or strength eccentricity that have the same natural period (Kusunoki, et al. 2001).

Table 3-3: Models first 3 periods (modes)

<b>8 Stories Selected Models</b>						
<b>Model Name</b>	<b>8A12</b>	<b>8A15</b>	<b>8A18</b>	<b>8B12</b>	<b>8S15</b>	<b>8S18</b>
1 <sup>st</sup> Mode Period (s)	2.77	2.87	2.95	3.06	3.17	3.25
2 <sup>nd</sup> Mode Period (s)	2.68	2.75	2.79	3.01	3.12	3.17
3 <sup>rd</sup> Mode Period (s)	2.41	2.44	2.49	2.84	2.95	3.03
<b>4 Stories Selected Models</b>						
<b>Model Name</b>	<b>4A12</b>	<b>4A15</b>	<b>4A18</b>	<b>4B12</b>	<b>4S15</b>	<b>4S18</b>
1 <sup>st</sup> Mode Period (s)	1.34	1.43	1.54	1.79	1.93	2.16
2 <sup>nd</sup> Mode Period (s)	1.28	1.34	1.41	1.74	1.89	2.11
3 <sup>rd</sup> Mode Period (s)	1.13	1.16	1.21	1.70	1.84	2.07
<b>2 Stories Selected Models</b>						
<b>Model Name</b>	<b>2A12</b>	<b>2A15</b>	<b>2A18</b>	<b>2B12</b>	<b>2S15</b>	<b>2S18</b>
1 <sup>st</sup> Mode Period (s)	1.05	1.34	1.37	1.15	1.30	1.59
2 <sup>nd</sup> Mode Period (s)	0.96	1.23	1.25	1.12	1.28	1.56
3 <sup>rd</sup> Mode Period (s)	0.86	1.10	1.10	1.11	1.27	1.56

From table 3-3, the symmetric type models, *B* and *S* types, demonstrate flexible behavior in comparison with the asymmetric models. The asymmetric models are created by middle row columns elimination, which subsequently lead to the stiffer frames in other spans. The result of modal analyses shows that for the *B* and *S* structures the first and second dominant periods are corresponded to the East-West and North-South direction, respectively, and attributed with translational mode shapes. As it should be expected from a symmetric plan structure, the 3<sup>rd</sup> mode reflects the torsional behavior. The associated participate effective mass ratio was more than 90% for each mode direction and for both of *B* and *S* archetype models. On the other hand, for the typical asymmetric models, i.e., *A* archetype models, the first mode shape was corresponded to the North-South direction and exhibits translational mode shape. The second mode reflected the East-West modal shape form with some degree of torsional behavior on the second mode response. The effect of torsional modal shape on the general translational shape of the second mode was increased from model 2A12 to 8A18. Also almost for all *A* archetype frame models, the

participated effective mass ratio of the all three modes were less than 75% of total effective mass of the structures.

### **3.4. Results Review for Selected Models**

All columns' and beams' dimensions and reinforcement are as shown in figures 3-2 to 3-9, and also in tables 3-4 and 3-5. In the plan and elevation views, all beams are identified with the letter B and three or four digits following the letter B. The first two digits denote the beam height per inch, and one or two other remaining digit/digits show the beam width per inch. For instance, B128 means a concrete beam with 12" height and 8" width. For the frame columns, each section is started with the letter C, then dimensions of square section are indicated, and the last part is the column designated reinforcements. For example, C1616-8#7 means a 16 inches by 16 inches column section with eight (8) number 7 rebar (#7) as the allocated column section reinforcements.

With regarding to the strength and serviceability, the reference standard code requirements in ACI 318-08 (2008) and ASCE 7-05 (2005) are fulfilled in the current design procedure of archetype models. Concrete sections, Reinforcements, and Configurations of the models are selected and designed to be as much similar as possible to the common practice among the structural designers and contractors in the Eastern and North Eastern parts of the US. These types of reinforcement details were also used by several researchers to study LRC prototype frame models, e.g. (Kunnath, et al. 1995a) and (Kunnath, et al. 1995b), or to perform numerical study of LRC models, e.g. (Ellingwood, et al. 2007). As mentioned earlier, during the design process, the regular and common methods among the professional structural engineers were adapted to be followed. Usually the first priority is the safety, and the second goal is the economy of the design whilst the standard code requirements regarding minimum strength and serviceability would be complied. To achieve economy in design and construction, some common practical techniques are accepted among professional structural engineers. An example of these techniques is reduction in number of typical beams and column sections. Another common approach is

application of similar reinforcements in terms of number, length, shape, and type. Also in practice, it is common to lower the required steel as the minimum acceptable, permitted by the code or safety. The above-mentioned techniques are a number of the distinctive common design approaches in the low seismic areas for a typical office or residential structural design. To accommodate with common practice, these techniques are also considered in this study.

Most focuses are on the first story columns. Furthermore, the current trial designs have shown that for the selected archetype frames the load combination involving dead and live loads, equation 3-6a, is almost the prominent governed analysis and design combinations for all frame members.

The ratio of total rebar area to the column gross cross section area is detained to minimum 1%. For the beam sections, the minimum tension reinforcement per chapter 10 of the ACI 318 is:

$$3 \left( \frac{\sqrt{f'_c}}{f_y} \right) \times b_w d \geq 200 b_w d / f_y \quad [3-8]$$

$f'_c$  is equal to 4.0 ksi,  $f_y$  is equal to 60.0 ksi,  $d$  denote the effective beam height in inch, and  $b_w$  stands for the beam width. The basic assumption of this study is LRC structures in low-to-moderate seismic zones, therefore the minimum usual seismic requirements in chapter 21 of ACI 318-08 (2008) which entails at least one rebar at each corner of a beam, regardless of tension or compression action, are not considered for beam design.

All slabs are surrounded by the concrete beams. Slab short and long lengths are 18.0ft and 20.0ft, respectively, which means almost square shape, therefore they are classified as Two Way slab systems per ACI 318 standard code. With five inches typical slab thickness, one layer, two directional #5@10" (center to center) reinforcement is enough to fulfill design criteria per ACI 318 code requirements.

Figures 3-2 to 3-5 illustrate typical frames elevation views for the selected models. For the East-West (E-W) direction the elevation views of all typical models are presented separately. However, due to the overall frame similarity in the North-South (N-S) direction, only the four story frames are illustrated through axes A to C.

The column sections and tie schedule are depicted on figures 3-6 and 3-7 respectively. Table 3-4 shows the typical tie schedule for the columns sections on figure 3-6. As mentioned before, the current tie schedule has not satisfied the seismic requirements of ACI 318-08 (2008) as well.

Table 3-4: Typical tie column detail

S: Tie Spacing Schedule per Inch for Columns (see Figures 3-6 and 3-7), assumed Tie size #4			
Vertical Rebar Size		#7	#9
Column Side Dimension (Inches)	10"	10"	10"
	12"	12"	12"
	14"	14"	14"
	16"	14"	16"
	18"	14"	18"
	24"	14"	18"

Figure 3-8a shows the typical story plan for the symmetric (S) and base (B) models. Roof and story plan in asymmetric models are similar to S and B models in all stories, except for the first story plan which is shown on Figure 3-8b. Figure 3-9a presents typical beam reinforcements for axes A, B, C, and D. Typical beam reinforcements for axes 1, 2, and 3, the North-South direction of the selected models, are shown in Figure 3-9b.

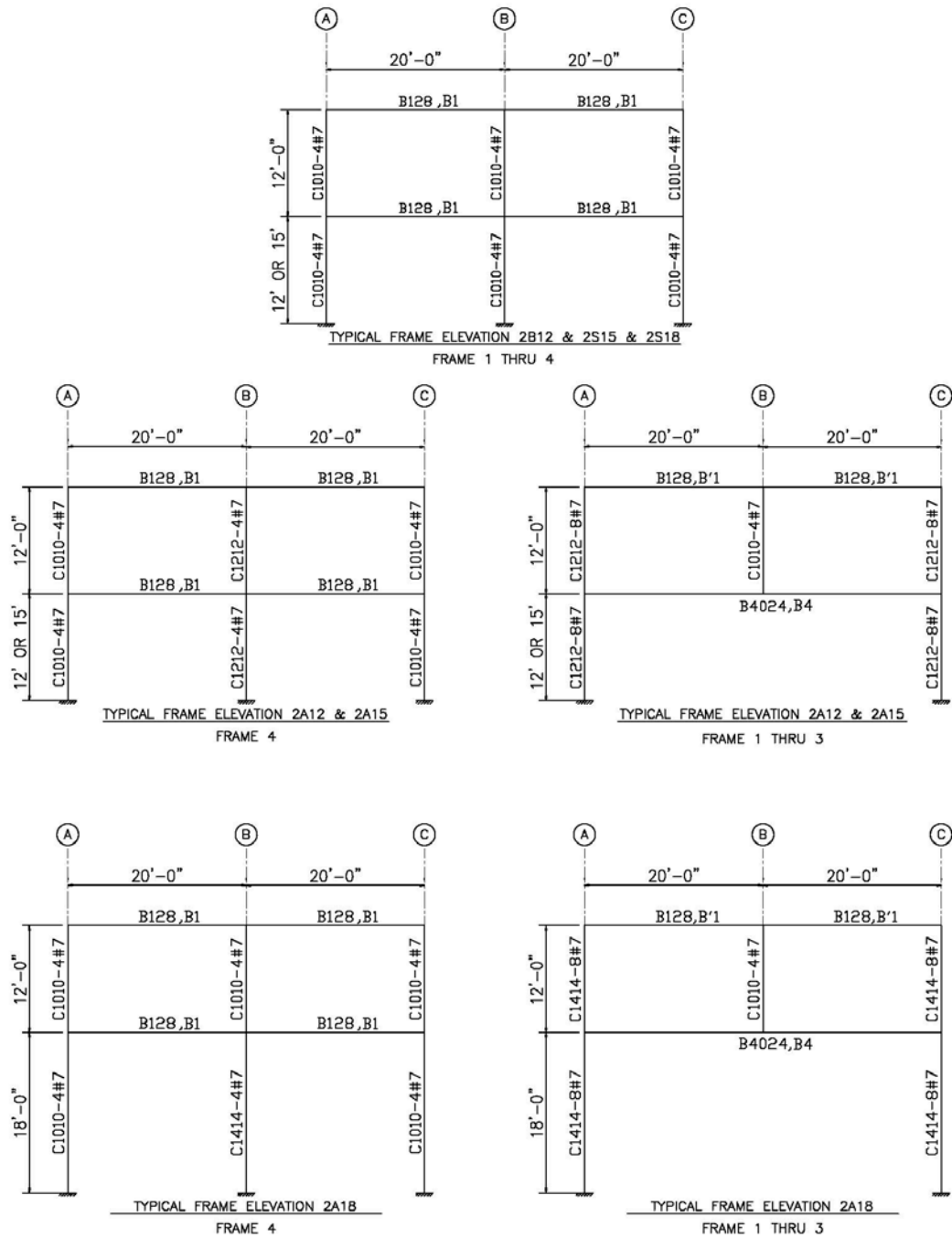


Figure 3-2, Typical frame elevations for the two stories selected models, E-W direction

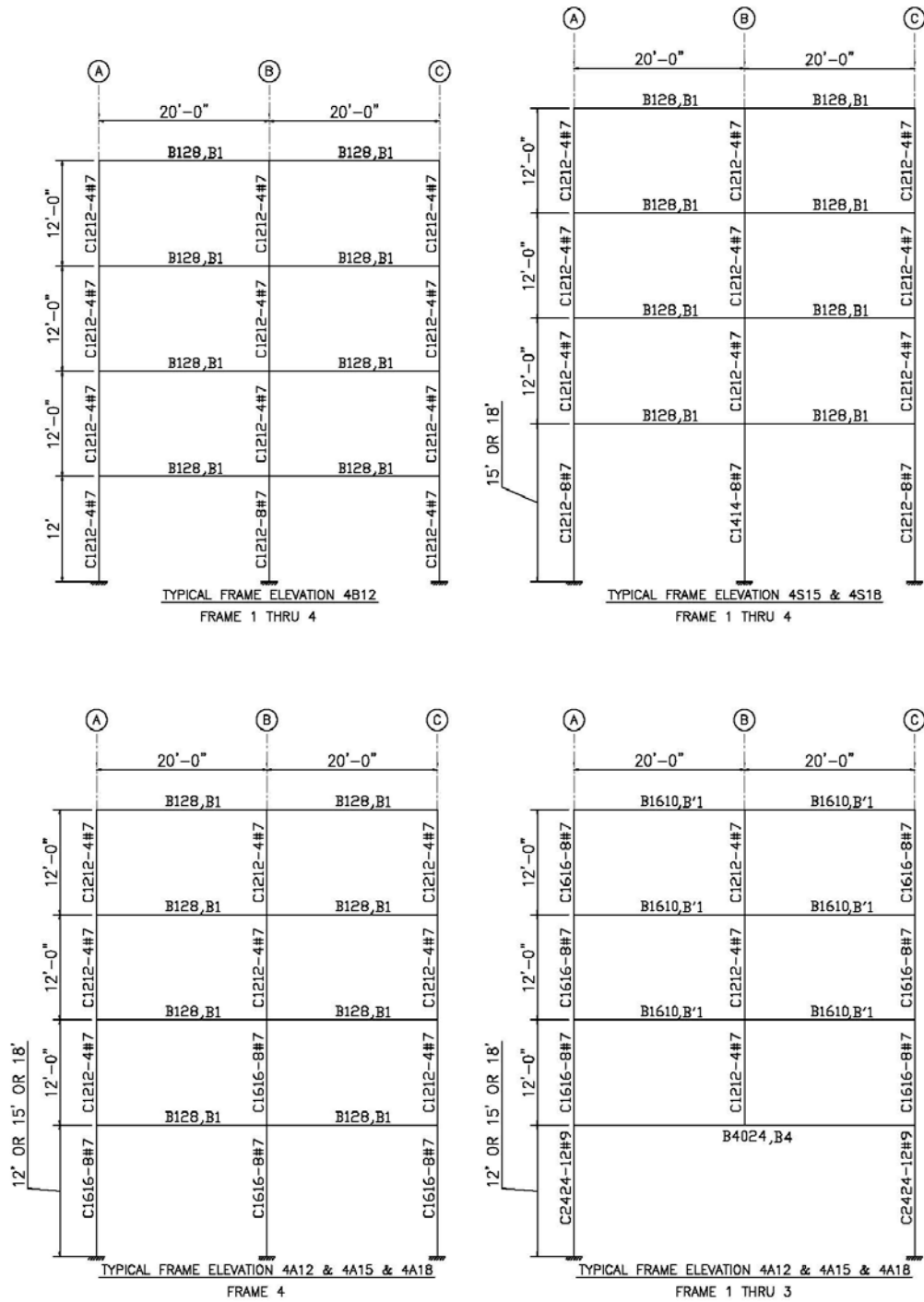


Figure 3-3, Typical frame elevations for the four stories selected models, E-W direction

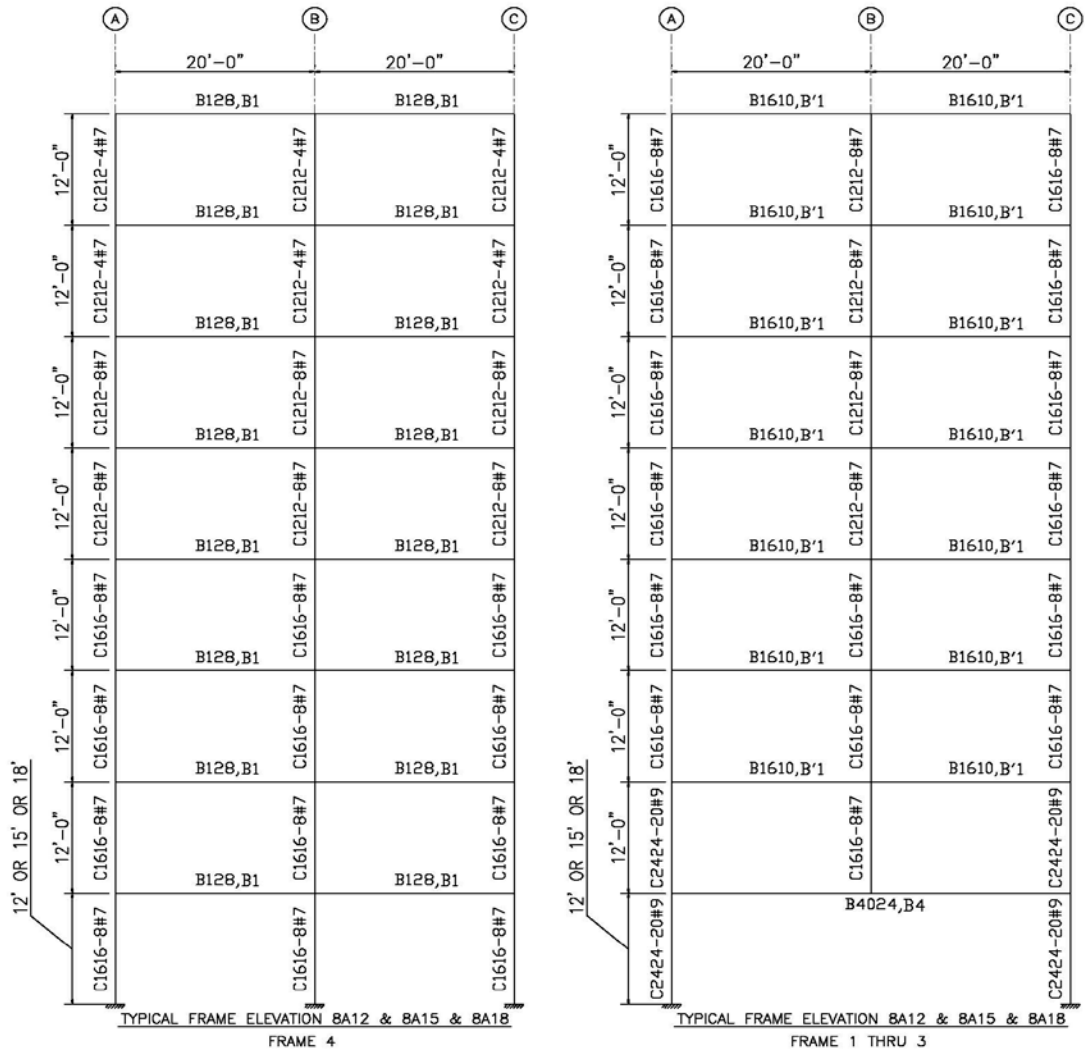


Figure 3-4a, Typical frame elevations for the eight stories selected models, E-W direction

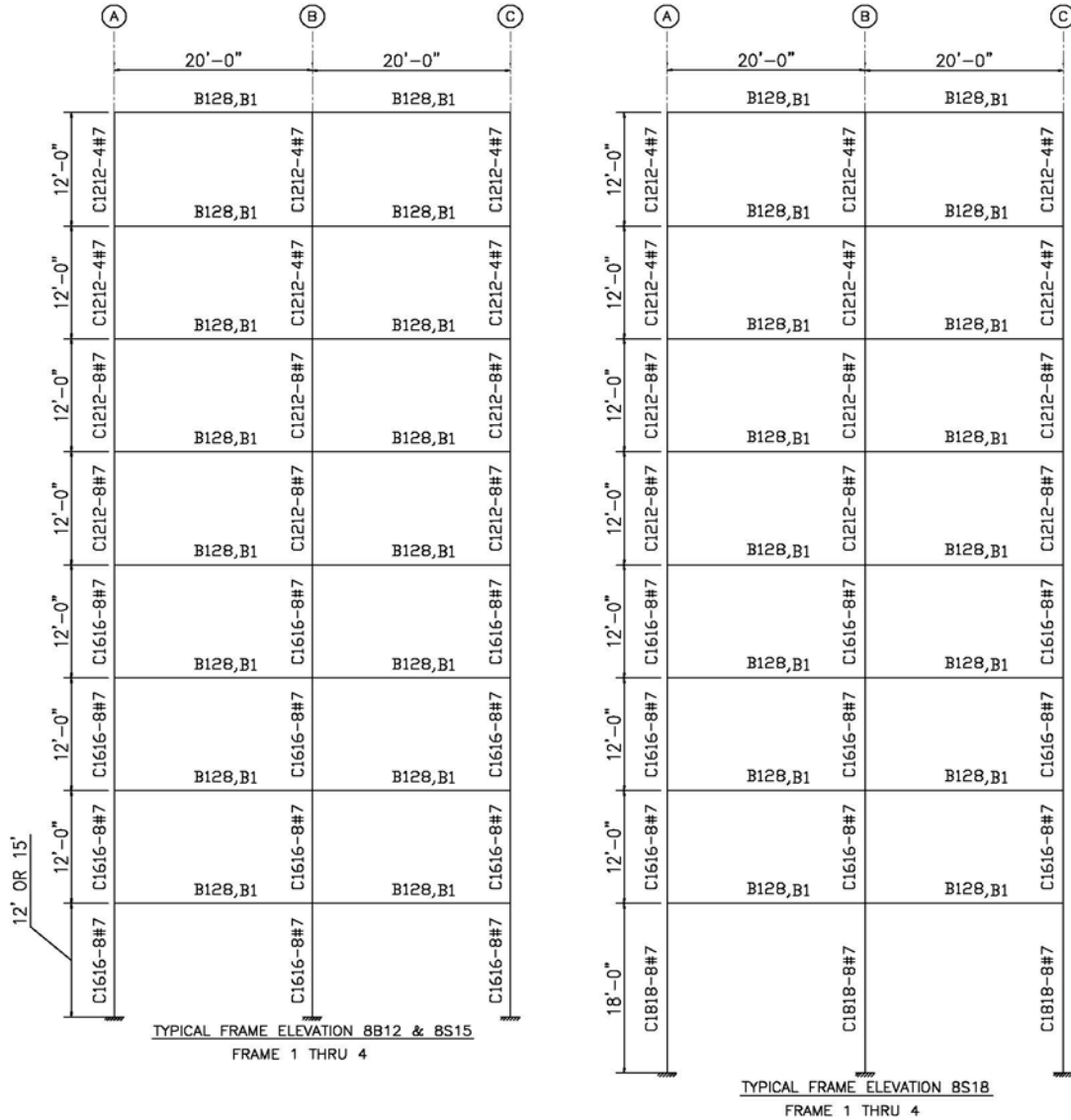


Figure 3-4b, Typical frame elevations for the eight stories selected models, E-W direction

Besides the beams' height and width depending on the elevation, number of stories, type of the models, and beam direction in the plan, each beam may need different reinforcement length and configuration to satisfy the design requirements. To show these differences, each beam has a specific name: B1, B'1, B2, B3, and B4, which are shown on the frame elevations presented in Figures 3-2 through 3-5.

The required reinforcements at top or bottom of each aforesaid typical beam also are illustrated in Figures 3-9a and 3-9b, which are acquired per SAP2000 (2012)

concrete design results and ACI 318 minimum requirements. The detail designed rebar on Figure 3-9a and 3-9b are entitled with the letter  $A_i$  to  $G_i$ , in which  $i = 1, 2, 3, 4$ . Tables 3-5a through 3-5d deliberate the longitudinal top or bottom reinforcements. Thus, for beams B1 to B4, and corresponding to the structural model (A, B, or S), rebar position at top or bottom of the beams, rebar type, i.e.  $A_i$  to  $G_i$ , and probable additional rebar are shown.

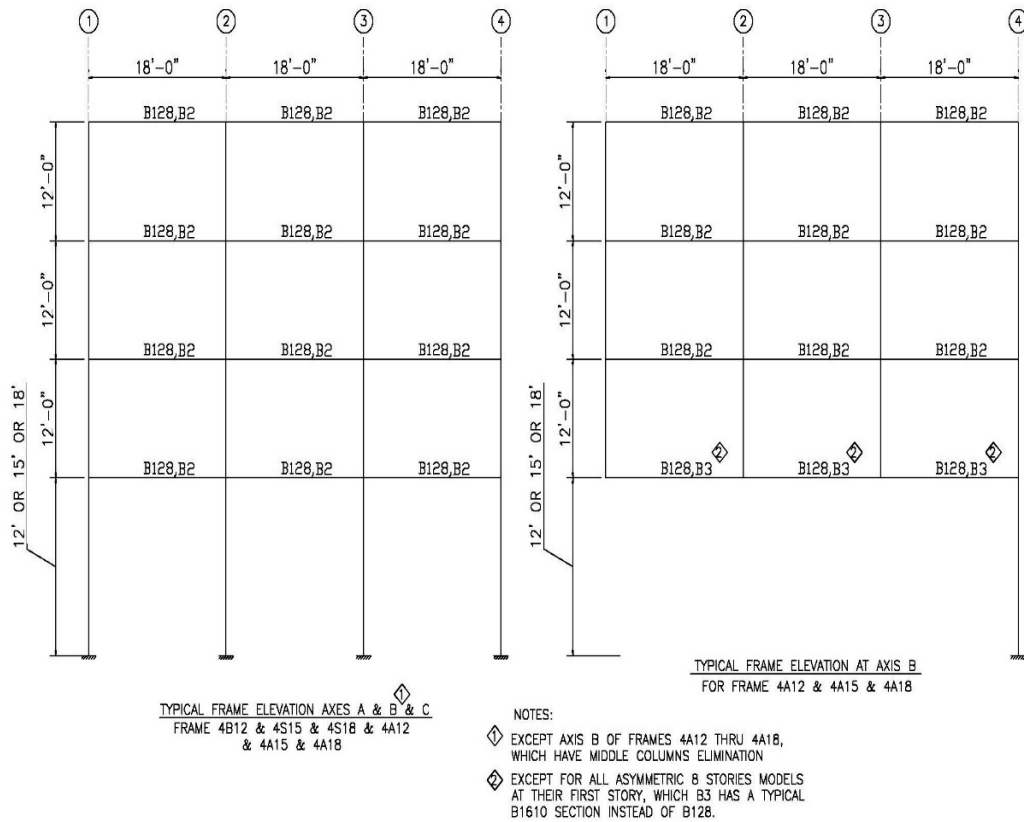


Figure 3-5, Typical frame elevations for the four stories selected models, N-S direction

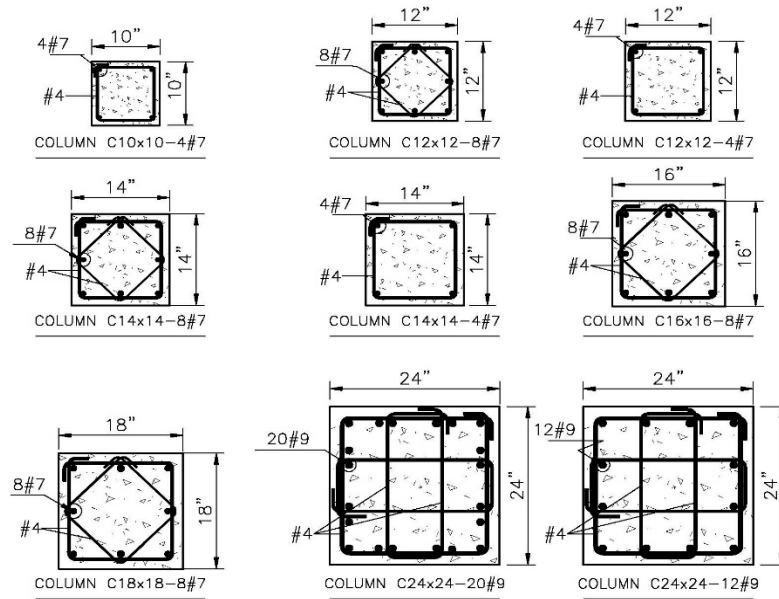


Figure 3-6, Typical column sections

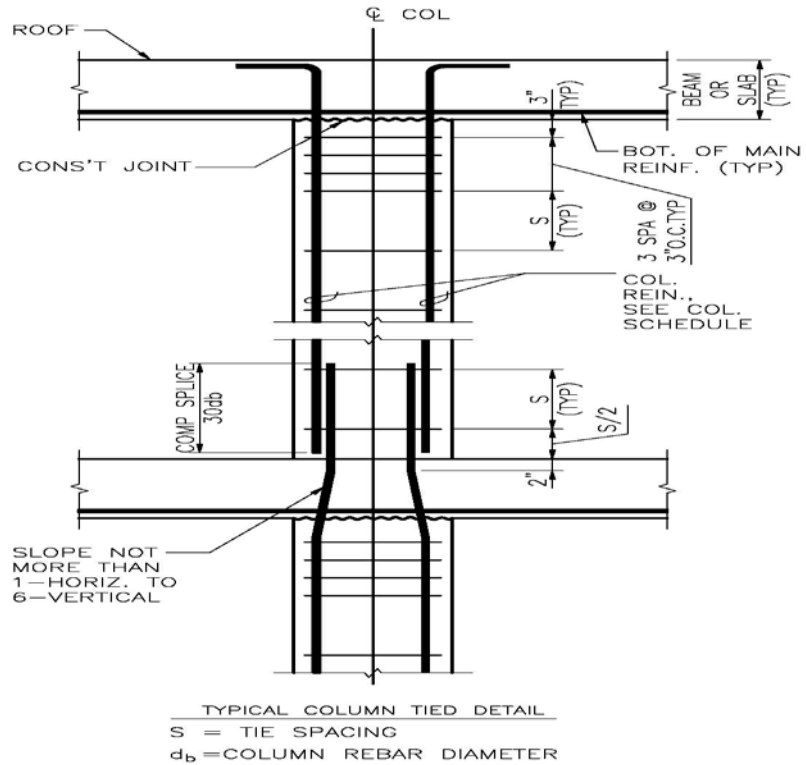


Figure 3-7, Typical column tie schedule

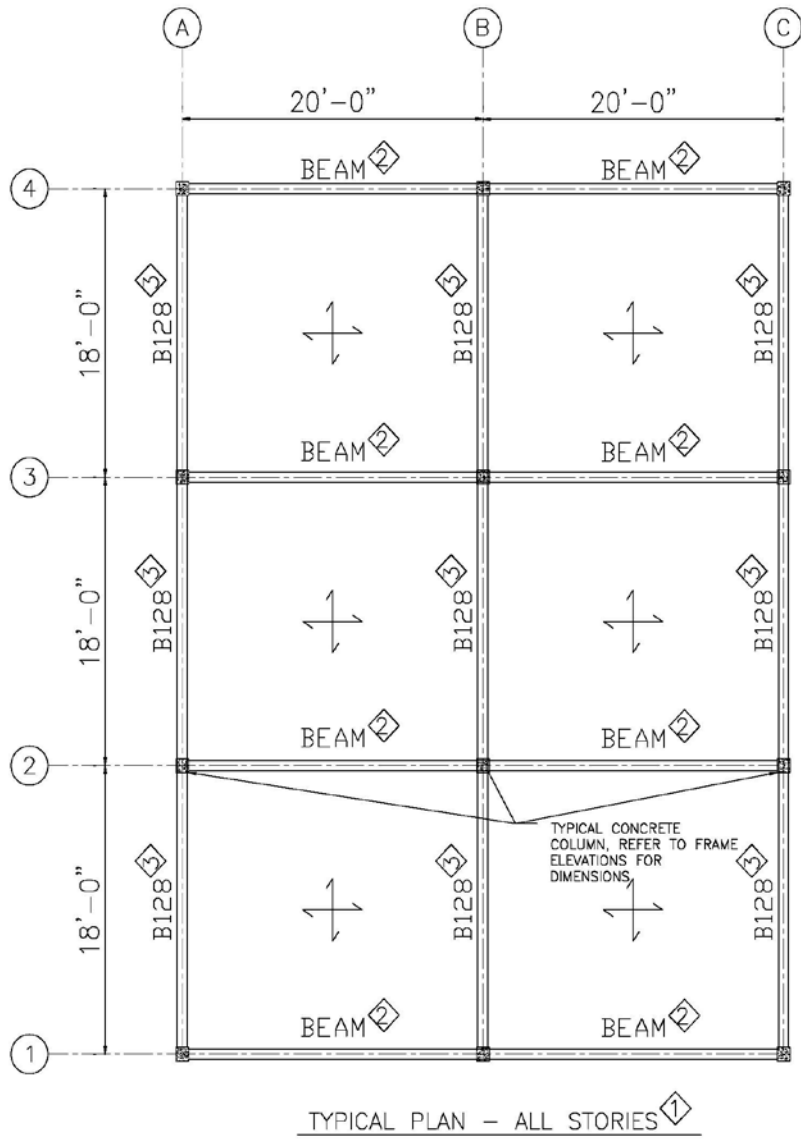
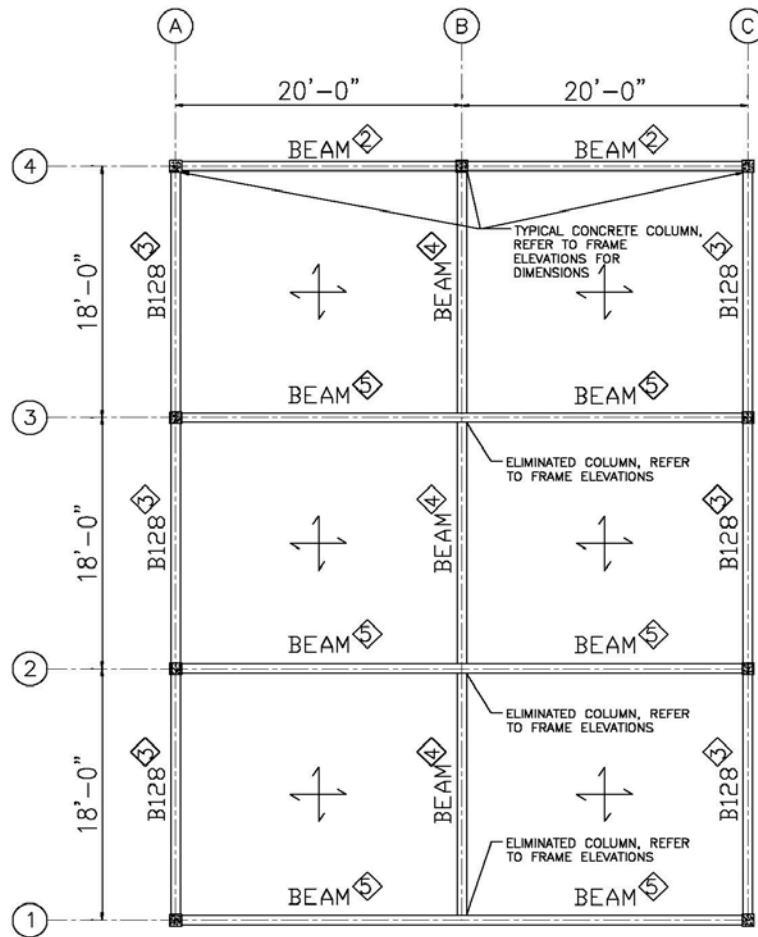


Figure 3-8a, Roof and floor plans for all frames type B, S, and A, except as noted

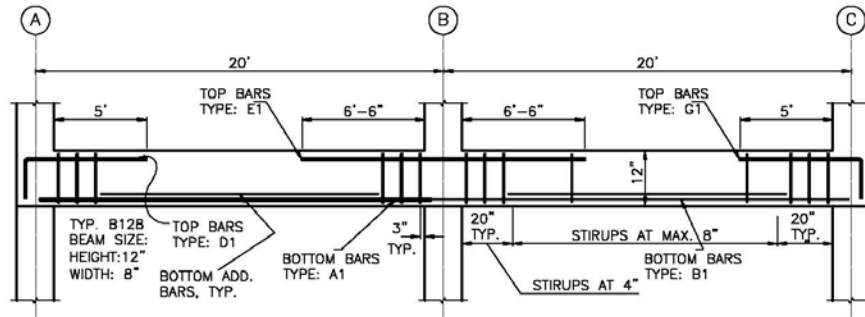


FIRST STORY PLAN FOR ASYMMETRIC (A) TYPE MODELS

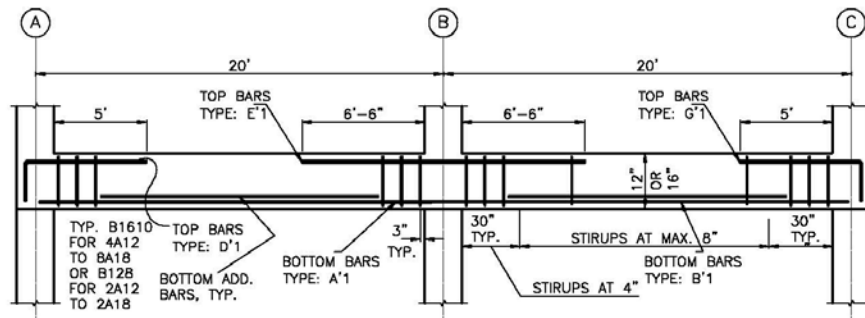
NOTES:

- |  |  |
|--|--|
| <p>① TYPICAL STORY PLAN FOR MODELS B &amp; S &amp; A, EXCEPT THE FIRST FLOOR OF THE ASYMMETRIC PLAN TYPE MODELS</p> <p>② BEAM TYPE: B1, SEE FRAME ELEVATION FOR THE BEAM SECTION AND DIMENSIONS</p> <p>③ B128: BEAM TYPE B2, WITH 12" HEIGHT &amp; 8" WIDTH, TYPICAL FOR ALL BEAMS IN AXES 1, 2, AND 3, EXCEPT FOR THE FIRST FLOOR OF THE ASYMMETRIC PLAN MODELS</p> | <p>④ B1610: BEAM TYPE B3, WITH 16" HEIGHT &amp; 10" WIDTH, TYPICAL FOR 8A12, 8A15, AND 8A18. B128: BEAM TYPE B3, WITH 12" HEIGHT &amp; 8" WIDTH FOR ALL OTHER BEAMS IN AXIS B OF THE FIRST FLOOR OF ASYMMETRIC MODELS</p> <p>⑤ BEAM TYPE: B4, SEE FRAME ELEVATION FOR THE BEAM SECTION AND DIMENSION</p> |
|--|--|

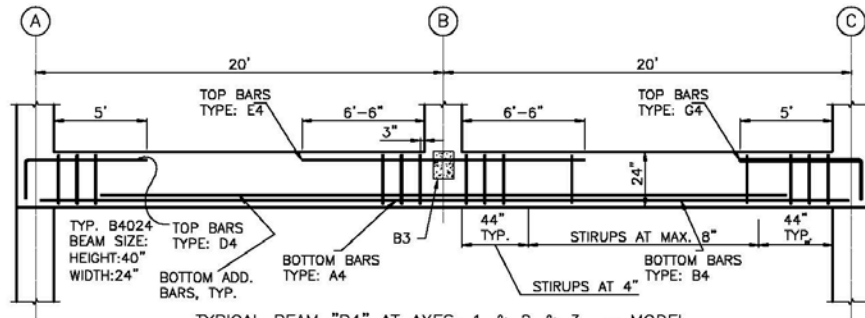
Figure 3-8b, First story plan for all frames type A



TYPICAL BEAM "B1" AT AXES: 1 & 2 & 3 & 4 - MODEL  
 TYPES: B & S, AND AXIS 4 OF A TYPE MODELS  
 SEE BEAM REINFORCEMENT SCHEDULE TABLE



TYPICAL BEAM "B1" AT AXES: 1 & 2 & 3 - MODEL  
 TYPE: A, EXCEPT THE FIRST STORY  
 SEE BEAM REINFORCEMENT SCHEDULE TABLE



TYPICAL BEAM "B4" AT AXES: 1 & 2 & 3 - MODEL  
 TYPE: A, ONLY THE FIRST STORY  
 SEE BEAM REINFORCEMENT SCHEDULE TABLE

Figure 3-9a, Typical East-West beam reinforcements

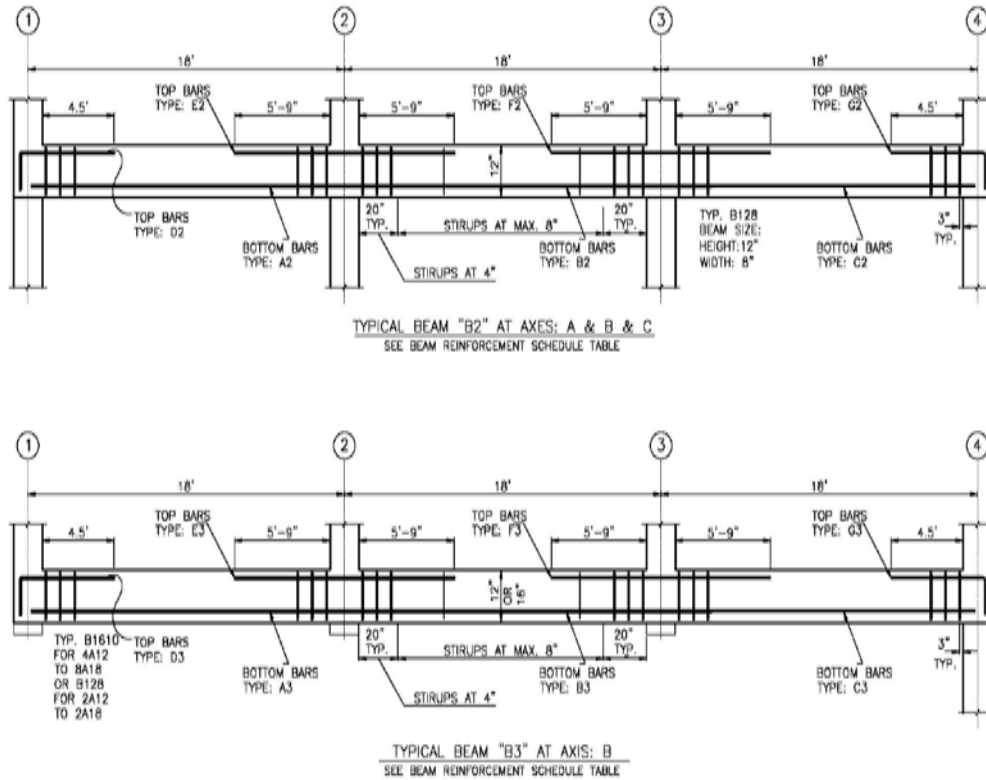


Figure 3-9b, Typical North-South beam reinforcements

Table 3-5a: Required longitudinal reinforcement for beam type B1

Beam B1 Reinforcement Schedule at Axes 1, 2, 3, and 4				
Model Name	Rebar Position	Rebar Name	Designed Reinforcement	Notes
2B12, 2S15, 2S18, 4B12, 4S15, 4S18, and only axis 4 for: 2A12, 2A15, 2A18, 4A12, 4A15, 4A18	TOP	D1 & G1	2#6 + 1#4	
	TOP	E1	2#6	
	BOTTOM	A1 & B1	2#6 + 1#6	1#6 is additional rebar
8B12, 8S15, 8S18, and only axis 4 for: 8A12, 8A15, 8A18	TOP	D1 & G1	4#6 + 1#4	1#4 additional rebar throughout spans
	TOP	E1	3#6 + 2#4	1#4 additional rebar at the specific location, and 1#4 additional rebar throughout spans
	BOTTOM	A1 & B1	2#6 + 1#6	1#6 is additional rebar

Table 3-5b: Required longitudinal reinforcement for beam type B'1

<b>Beam B'1 Reinforcement Schedule at Axes 1, 2, 3, and 4</b>				
Model Name	Rebar Position	Rebar Name	Designed Reinforcement	Notes
2A12, 2A15, 2A18, except axis 4 (see table 3-5a) and the 1 <sup>st</sup> story (see table 3-5e)	TOP	D'1 & G'1	3#6 + 1#4	
	TOP	E'1	3#6	
	BOTTOM	A'1 & B'1	2#6 + 1#6	1#6 is additional rebar
4A12, 4A15, 4A18, except axis 4 (see table 3-5a) and the 1 <sup>st</sup> story (see table 3-5e)	TOP	D'1 & G'1	5#6	
	TOP	E'1	2#6	
	BOTTOM	A'1 & B'1	2#6 + 1#4	
8A12, 8A15, 8A18, except axis 4 (see table 3-5a) and the 1 <sup>st</sup> story (see table 3-5e)	TOP	D'1 & G'1	2#9 + 2#6	
	TOP	E'1	2#6	2#6 throughout the bay
	BOTTOM	A'1 & B'1	3#6 + 1#4	

Table 3-5c: Required longitudinal reinforcement for beam type B2

<b>Beam B2 Reinforcement Schedule at Axes A, B, and C</b>				
Model Name	Rebar Position	Rebar Name	Designed Reinforcement	Notes
2B12, 2S15, 2S18, 4B12, 4S15, 4S18	TOP	D2 & G2	2#6	
	TOP	F2 & E2	2#6 + 1#4	
	BOTTOM	A2 & B2 & C2	2#6	
8B12, 8S15, 8S18	TOP	D2 thru G2	3#6	
	BOTTOM	A2 thru C2	2#6	
2A12, 2A15, 2A18, 4A12, 4A15, 4A18	TOP	D2 & E2	2#6	
	TOP	F2 & G2	3#6	
	BOTTOM	A2 thru C2	2#6	
8A12, 8A15, 8A18	TOP	D2 & E2 & F2	3#6	
	TOP	G2	5#6	
	BOTTOM	A2 & B2	2#6	
	BOTTOM	C2	3#6 + 1#4	

Table 3-5d: Required longitudinal reinforcement for beam type B3

<b>Beam B3 Reinforcement Schedule at Axis B</b>				
Model Name	Rebar Position	Rebar Name	Designed Reinforcement	Notes
2A12, 2A15, 2A18, 4A12, 4A15, 4A18	TOP	D3 & G3	4#6	
	TOP	F3 & E3	2#6	
	BOTTOM	A3 & B3 & C3	3#6	
8A12, 8A15, 8A18	TOP	D3 & E3 & F3	3#6 + 1#4	
	TOP	G3	6#6	
	BOTTOM	A3 & B3	2#6	
	BOTTOM	C3	3#6	

Table 3-5e: Required longitudinal reinforcement for beam type B4

<b>Beam B4 Reinforcement Schedule at Axes 1, 2, 3</b>				
Model Name	Rebar Position	Rebar Name	Designed Reinforcement	Notes
2A12, 2A15, 2A18, only the 1 <sup>st</sup> story	TOP	D4 & G4	3#9	
	TOP	E4	2#6	
	BOTTOM	A4 & B4	4#9 + 4#11	4#11 is additional rebar
4A12, 4A15, 4A18, only the 1 <sup>st</sup> story	TOP	D4 & G4	4#9 + 1#6	
	TOP	E4	2#6	
	BOTTOM	A4 & B4	4#9 + 5#11	5#11 is additional rebar
8A12, 8A15, 8A18, only the 1 <sup>st</sup> story	TOP	D4 & G4	8#9 + 1#6	2#9 throughout the bay
	TOP	E4	2#9	2#9 throughout the bay
	BOTTOM	A4 & B4	5#9 + 9#11	5#11 is additional rebar

## Chapter 4: Advanced Modeling and Analysis Assumptions

### **4.1. Introduction to Current Advanced Modeling Methods**

#### **4.1.1. Introduction to Nonlinear Analysis**

In general, structural response to strong ground motions cannot be precisely predicted. Indeed, large uncertainties and randomness of structural properties, dispersion in material characteristics, and ground motion parameters create ambiguities to any presumed analytical methods. Consequently, excessive sophistication in structural analysis is not warranted (Fajfar 2002). As mentioned in Chapter 2, there are numerous existing buildings which do not comply with the current seismic codes' regulations in low to high seismic zones. For most of these buildings, precluding of structural failure is important and perhaps essential, although some limited damages are usually tolerable. In fact, nonlinear structural analysis has been used for the past 30 years (Chandrasekaran et al., 2010) to evaluate structural safety and capacity of new or existing buildings and bridges. Rapid development of the performance-based seismic design and assessment concept was particularly shown in the last decades. Typical performance-based design basically evaluates seismic demands and consequent damages mostly for existing structures. In this method, damage is usually related to the nonlinear behavior under different level of seismic scenarios. In other words, the concept of performance-based seismic assessment is directly associated to nonlinear analysis procedures (Aydınoglu and Önem 2010). The structural nonlinear analysis methods are classified as: Nonlinear Static Analysis (mostly known as Pushover, NSA), Nonlinear Dynamic Response History Analysis (mostly recalled as Time History Analysis, THA), Incremental Nonlinear Dynamic Analysis (IDA), and Probabilistic Approaches which the latter is fundamentally a different method. So far, the nonlinear dynamic approach (THA) is

considered the most accurate method (Pinho 2007) among researchers. However, the most rational analysis and advancement techniques for practical applications might be the simplified nonlinear static procedures, which can be done by a relatively simpler mathematical model than the THA procedure.

The basic process of inelastic nonlinear static analysis is similar to conventional linear elastic method. Developing an appropriate mathematical model of the structure is the first step, then the model would be subjected to a defined load pattern which represent of the anticipated seismic ground motion (FEMA 440 2005). Unlike most linear cases, different nonlinear static procedures may produce considerably different results for the same structure model and under the same ground motion representation (Ibid.). Except one important factor, the overall structural modeling for any nonlinear dynamic analysis is almost similar to the nonlinear static method. The exception is modeling cyclic behavior of material which is not required for nonlinear static modeling process. It is worthy to note that the uncertainties increase as the structure becomes more nonlinear. Actually, besides attributed hazard uncertainties, such as intensity or duration of a ground motion record, structural behavior and modeling assumptions demonstrate uncertainties as well. These uncertainties are arising from inherent nonlinearity, natural inelastic, and the variability in: (1)- physical characteristics of the structure, such as material properties, geometry, and details; (2)- nonlinear behavior of the structural components and system; (3)- mathematical model of the actual behavior (NEHRP 2010b). The nonlinear analysis for RC structures engenders more concerns. The nonlinear dynamic analysis, such as THA, even brings more difficulties in modeling, which is basically due to inherent RC unique behavior. Reinforcement steel and concrete portion of RC structures compose two different phases, in which concrete itself has its own compound and material complexity. Hence, the response analysis of reinforced concrete under reversal loads is more complicated than the other structural material types. The main reasons come from the force-deformation relation, which varies with the loading history, and other factor is damage spreading along the RC member (Otani 2004). Indeed, stiffness of members is more sensitive to concrete cracking, and columns and joint-panels usually show sensitive post-yield response to applied axial

load (NEHRP 2010b). Thus, any acceptance criteria regarding deformations should be limited to areas with predictable behavior where sudden strength and stiffness degradation does not occur (Ibid.).

#### **4.1.2. Basic Nonlinear Assumptions for Selected Models**

The current study performed the nonlinear time history analysis as the main method and the nonlinear static analysis is considered to provide some supplement information. NSA is performed in order to study overall behavior and to examine the accuracy of pushover method in low to moderate seismic zones for irregular structures. Usually after static analysis, the first step in common nonlinear analysis procedure is to perform a nonlinear pushover analysis of each model to identify general characteristics behavior of the system such as force redistribution, initial yield locating of plastic hinges, and linear behavior limit. Then, nonlinear time history analysis can be accomplished using different sets of ground motions to assess the seismic demand and to observe some responses such as local or overall collapse (Ellingwood et al. 2007). Nonetheless, the complexity of the irregular structures, in plan and elevation, severely decreases the reliability of pushover analysis for this type of structures. While nonlinear archetype models, including the selected models in this study, are anticipated to interrogate some response of the models, they are not able to capture all feasible types of seismic performance (FEMA P695 2009). Essentially, the seismic design and analysis of highly irregular structures are only possible through dynamic analysis methods as stipulated by standard codes such as ASCE 7-10 (2010).

As mentioned in the previous section, nonlinear behavior in frame type models should be limited to clearly define certain members and specific regions (Naeim 2010). Assuming that the selected archetypes are accurately modeled, concentrated hinge models may typically be suitable for simulating nonlinear response of columns and beams in frame systems (FEMA P695 2009). To achieve a suitable analytical model some steps are necessary. First, acceptable and accurate structure model should be defined per code-wise structural design, which has been done earlier in Chapter 3. Then, allocation of appropriate nonlinear behavioral parameters is important, which will be defined in the following sections in this

Chapter. These types of models have some practical advantages, such as straightforward approach to characterizing strength and inelastic deformation, and providing a reasonable in-depth view into the overall superior or poor seismic design criteria of the models. The versatility of lumped plasticity models make them adjustable to show the deterioration associated with rebar buckling and stirrup fracture, which the latter may even lead to loss of confinement (FEMA P695 2009). By proper hinge definition, they can simulate degradation of strength and stiffness, which is crucial in any collapse modeling (Ibid.). Lumped plasticity elements, which are used here, follow ASCE/SEI 41-06 (2007a), Supplement No.1 of ASCE 41-06 (2007b), and the precedent FEMA 356 guideline (2000). The allocated lump plastic hinges will be discussed later in Section 4-3.

For the purpose of 3D modeling of frame type structures and in traditional dynamic frame analysis, masses are usually allocated at the floor levels. Lumped masses at floor levels are also adequate to impose inertial effects in the two horizontal directions plus rotation about the vertical building axis (NEHRP 2010b). Vertical mass effects and vertical ground motion components should be modeled for structures with long-span framing, e.g. arena roofs or long bridges. Indeed, in these types of structures the vertical period of vibration may be excited by the vertical component of earthquake ground motions (NEHRP 2010b) which are not part of the current study. Considering type and span of the selected structures, total mass at each floor level is performed with rigid diaphragm action which connects all slabs together to act as a rigid plane (ref. to Chapter 3). The rigid diaphragm model has several advantages, illustrating benefit of lumped mass systems and decreasing unnecessary DOF of models.

#### **4.1.3. Gravity Load Effects**

There is a major difference between linear and nonlinear analyses regarding the gravity load effect. Nonlinear analyses depend on load path, in which the combined gravity and lateral load affect the results. Also for nonlinear analysis, the superposition rule is not applicable. Consequently, any gravity load effect shall be considered as nonlinear at first, and then they can be devoted to total nonlinear

analysis procedure. The applied gravity load should be equal to the expected gravity load to the structure, which is different from applied factored gravity loads in standard design codes and linear analysis approaches (PEER/ATC 72-1 2010). Considering gravity loads, Dead ( $Q_D$ ) and Live ( $Q_L$ ) loads in this study, the expected dead plus live load combination ( $Q_G$ ) is presented in Equation 4-1 which is adopted from ASCE 41-06, Equation 3-2, (2007a):

$$Q_G = 1.1(Q_D + Q_L) \quad [4-1]$$

As it can be seen in both ASCE 41-06 (2007a) and FEMA 356 (2000), live load has been reduced from the nominal design live load to 0.25 of the original design live load to reflect (PEER/ATC 72-1 2010):

- 1- The lower probability of the nominal design code prescribed live load occurring throughout the whole structure;
- 2- The lower probability of concurring the total nominal live load and seismic event simultaneously.

Usually, the first of these two live load reduction factors is 0.4 and the second reduction live load factor is equal to 0.5. The net live load reduction factor can then be easily calculated as  $0.4 \times 0.5 = 0.2$  (Ibid.). Due to standard code procedure for safety factor margin, the applied factor to nominal live load is increased to 0.25, which should be applied to the nominal live load in Equation 4-1. In current study, Equation 4-1 is performed as nonlinear gravity load in analysis process. Moreover, due to the fact that this study is limited to office and residential buildings, only dead load is used to calculate the seismic mass, which in turn will be applied in the nonlinear analysis as well.

$P-\delta$  effect (individual frame member deflection due to gravity loads) usually does not need to be considered in nonlinear seismic analysis, and has a minor effect on the response of structure (NEHRP 2010b) and (PEER/ATC 72-1 2010). On the other hand,  $P-\Delta$  effect may ultimately lead to a complete failure of lateral resistance system, or impose structural ratcheting (a gradual accumulation of residual deformations under cyclic loading), and dynamic instability (NEHRP 2010b). From a

dynamic point of view, P- $\Delta$  can considerably amplify the displacement response of a structure, in case the displacement demands from induce seismic load are large enough to enter the range of negative stiffness (PEER/ATC 72-1 2010). In order to apply P- $\Delta$  force, total vertical gravity dead loads on the entire structure are applied in the analysis. A pushover analysis is useful for understanding overall sensitivity of a structure to P- $\Delta$ . However, THA analysis is required to capture the structural response and possible instability due to P- $\Delta$ , especially for moment frames which have shown more flexible response than the other type of structural systems (Ibid.). The total dead load of each selected model with applied load factor equal to 1.0 is considered for P- $\Delta$  analysis. The SAP2000 software comprises nonlinear P- $\Delta$  case with ability to adjust the stiffness matrix of structure automatically (as per CSI Analysis Reference Manual 2013). P- $\Delta$  effects may lead to the onset of collapse; therefore, P- $\Delta$  effect for both THA and NSA analysis procedures has been performed in this study.

In summary, each THA or NSA contains two basic nonlinear analyses. The first nonlinear step is P- $\Delta$  effect with dead load factor equal to 1.0. Next, the final P- $\Delta$  state comprises the initial nonlinear condition for the gravity load (in Equation 4-1). Then, the final step of nonlinear gravity combination acts as initial state of any nonlinear seismic consideration, either THA or NSA procedure.

## **4.2. Time History Records Selection**

### **4.2.1. Introduction and Background**

In terms of vibration, each occurred earthquake poses a unique non-periodic wave with a wide range of frequencies resulting from several factors: the ground motion excitation, specific site tectonic, the fault rupture mechanism, and soil (layers) characteristics. Incidentally, the peak magnitude and duration of all seismic waves are different. Thus, earthquake records cannot be expressed in any functional mathematical formats. The same recorded data is statistically impossible to be ever repeated, and each ground motion record has its own inherent frequency content. Almost for all time history analyses, the key ground motion parameters should be

identified properly to reflect the characteristics of a seismic record. These factors are classified as the amplitude, duration, and frequency content of the ground motion record.

Although nonlinear time history analysis is known as the best available method for seismic evaluation of structures, afore-mentioned uncertainties in ground motion selection make this approach complicated. In reality, all seismic records are random in space and time, which are caused by the seismic wave path from the fault-plane source through bedrock, and then pass through the soil layers to reach the base of a structure (Katsanos et al. 2010). Historically, the peak horizontal acceleration is widely used to describe a ground motion, and most ground motion data have been collected as the seismic acceleration records. The explanation is due to the inherent relationship between acceleration with inertial forces (Harris et al. 2013). The first acceleration record sets of strong seismic motions were acquired during the Helena (Montana) earthquake in 1938 Ferndale (California). El Centro earthquake (California) in 1940 is the first recorded seismic event which has been vastly used for time history analysis. Usually an earthquake acceleration signal is quite random with highly non-linear digitized curve in nature, and there is a wide range of high frequency component in almost all records (Otani 2004). Although time history excitation can be practically done by any typical well-known mathematical wave such as sine or cosine functions, the application of real recorded seismic events is widely held for structural analysis approach. The first step to any time history analysis is the record selection, and the most recognized record selection methods are as follows (Katsanos et al. 2010):

- Record selection based on earthquake magnitude (M) and distance (R);
- Based on soil profile;
- Strong motion duration;
- Acceleration to velocity ratio (a/v);
- Record selection based on spectral matching;

The most popular and practical record selection is based on the elastic response spectrum to obtain or generate seismic records that shows similar ground motion characteristics. The elastic response spectrum contains the maximum elastic

response of a SDOF system as a function of the natural frequency and critical damping ratio, and indirectly shows the amplitude, frequency content, and somehow the duration of a seismic event (Harris et al. 2013). For typical structures, the definition and determination of the elastic response spectrum can be done as per ASCE 7 provisions, such as Section 11.4 of ASCE 7-10 (2010). Therefore, the next step would be to compare between compatibility of the selected record with the elastic response spectrum. In case of inadequate compatibility, the selected record should be scaled. Although the scaling method may seem straightforward, the problem emanates from ambiguous methodology. In fact, there is no well-established and clear procedure in the seismic code standards to find, select, and scale seismic time histories (Harris et al. 2013). The basis of most recent accepted scaling method in the US is to establish compatibility between the ground motion elastic response spectrum, create from seismic records, with the code design base elastic response spectrum (ASCE 7-05 2005), (ASCE 41-06 2007a), (IBC 2012), and (PEER/ATC 72-1 2010). It should be noted that although the scaling main approach is very similar for each seismic design code, there are considerable differences between their definitions and methods. For instance, while 2008 edition of Los Angeles Tall Buildings Structural Design Council (LATBSDC) simply refers to section 16.1.3 and Chapter 21 of ASCE 7-05 for selection and scaling of ground motion records, PEER Guidelines dedicates a whole chapter with more detail discussion to specific site classification and earthquake record scaling approach (Naeim 2010). Thus, each standard may show a considerable difference in comparison with the other standards.

Due to the wide range of frequencies and acceleration content within seismic records, ASCE 7-05 (2005) and 7-10 (2010) require that for a time history analysis at least three (3) pair records shall be applied. If the mean value of the responses in the analysis and design process is preferred, at least seven (7) pair ground motion records shall be considered, although some researchers showed that the seven (7) records are conservative and with fewer number of records a reasonable result may be achieved, e.g. see (Reyes and Kalkan 2012). In fact, the required sets of ground motions were placed in the 1980s and early 1990s for seismic isolation design and there is no

technical basis for the current rules, either maximum response for three record sets or mean values for seven record sets (NEHRP 2011).

To select ground motions, PEER Ground Motion database (2013), Beta version (2010b), is used in this study. The PEER website provides an extensive variety of seismic records. Not only recorded ground motions in the US, but also a number of seismic events around the world are included in their data bank. PEER database is an interactive web-based application, which is widely accepted and used by many scholars and research organizations (e.g. see NEHRP 2011). The PEER Ground Motion Database (2013) allows users to select ground motion acceleration time series in terms of earthquake magnitude, source-to-site distance, fault rupture type, and other general characteristics (PEER 2010b) and (PEER 2011). Also, the user has a choice to select unscaled or scaled data. To scale the selected records, several criteria including ASCE 7-05 rules are provided which can imply a good fits to the standard target response spectrum (Ibid.), such as elastic response spectra generated based on the selected seismic zone per ASCE 7 requirements. ASCE 7-05 (2005), ASCE 7-10 (2010), and ASCE 41-06 (2007a), all stipulate that the elastic response spectra should be defined as 5% damped spectrum, and should consist pairs of horizontal records. The ASCE standard requirements are considered and achieved by application of PEER (2013) web record library.

The concept of spectrum matching, which is the basis of PEER scaling approach, is specifically attractive in the Central, Eastern, and North Eastern parts of the US. In general, spectrum matching not only allows users to apply the real recorded events from active zones, but also enable users to consider and apply higher frequencies. High frequency contents are essential for the above-mentioned zones, and these frequencies would be appeared in the scaled records by matching spectrum approach (NEHRP 2011).

Ground motions in the Central, Eastern, and North Eastern United States are basically different from seismic events in the West of the US. The major difference is a shift towards higher frequency content, i.e. higher energy content (Kunnath et al. 1995a) and (NEHRP 2011), such as 1895 Charleston earthquake in Missouri. For these seismic zones, one of the major challenges is an appropriate record selection,

which, in turn, would be correlated to the magnitude/distance range. The complexity arises from relatively limited available records for the Central, Eastern, and North Eastern parts of the US. Owing to low seismicity rates, lack of moderate to high-recorded ground motions, and sparse instrumentation in these areas (NEHRP 2011), selection of appropriate sets and directly associate records are almost impossible.

It is noteworthy that magnitude, which is related to the ground acceleration of an event, is one of the most important factors in any record selection process. For an appropriate data selection, PEER database library (PEER 2011) requires that user picks a magnitude range. Technically, magnitudes and distances depend on the site seismicity, probability level and the frequency bound of interest. As a general guide for the afore-mentioned regions, the high frequency hazard event for moderate probabilities, namely event with less than  $10^{-4}$  per annum, may be represent by magnitude of  $M \leq 6$  at distances less than 50 km. On the other hand, the low-frequency hazard events may be subjected by large rare events with magnitude of  $M \geq 7$  for farther distances (NEHRP 2011). Thus, these wide ranges of magnitudes should be considered for time history selection in the Central, Eastern, and North Eastern parts of the US. To cover all of them, the magnitude ranges, including for unscaled and scaled record sets, are considered between 5.5 and 7.0.

Corresponding to ASCE 7-05 (2005), there are a few factors that have influence on scaled ground motion set selection and should be defined prior to the scaling process. Besides the magnitude, the most important factors are: shear wave velocity and seismicity in accordance with elastic response spectrum. Moreover, there are some other factors that may help to refine more concise scaled data sets, such as: Fault rupture type, Period range and Factor limit. Among all of the preceding factors, seismicity (which classified site hazard condition) typically plays the dominant role.

Refer to section 2.1, many regions in the North and North Eastern parts of the US can be classified as SDC C in accordance with ASCE 7, but the lower SDC B is selected to represent low seismicity condition. Low to moderate seismicity, reflected as SDC B, probably provides a more acceptable and meaningful assumption to many people and even professional engineers. The selected structures are assumed residential or office buildings (see Chapter 3), so corresponding to the occupancy of

buildings, the allocated Risk Category would be group II (ASCE 7-05). Tables 11.6-1 and 11.6-2 of ASCE 7-05 (2005) are used to determine the  $S_{DS}$  and  $S_{D1}$  respectively. For SDC B classification, ASCE 7-05 (2005) indicates that the range of  $S_{DS}$  and  $S_{D1}$  should be  $0.167 \leq S_{DS} < 0.33$  and  $0.067 \leq S_{D1} < 0.133$ . To have a reasonable arbitrary assumption, the mean value of lower bound and upper bound of  $S_{DS}$  and  $S_{D1}$  are presumed. Therefore, the selected  $S_{DS}$  and  $S_{D1}$  would be equal to 0.249 and 0.1 correspondingly. Figure 4-1 shows the ASCE 7-05 (2005) Code Specification Spectrum, 5% damping, created by the PEER web application data (2013). Figure 4-1 also illustrates three important points and their corresponding accelerations (rounding up to two tenth) on the chart,  $T_0 = 0.2$  ( $S_{D1}/S_{DS}$ ),  $T_s = S_{D1}/S_{DS}$ , and  $T_1 = 1.0$  (Unit: Second) which are based on the ACSE 7-05 chapter 11 definition.

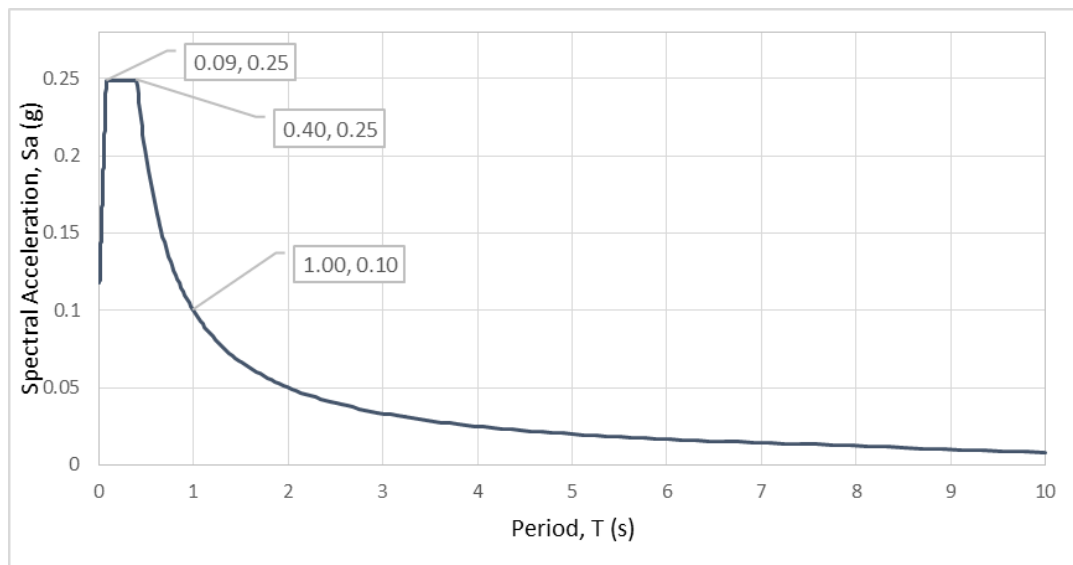


Figure 4-1, Code-specified design response spectrum in accordance with ASCE/SEI 7-05 (PEER web application library 2013, at: [http://peer.berkeley.edu/peer\\_ground\\_motion\\_database/spectras](http://peer.berkeley.edu/peer_ground_motion_database/spectras))

Shear wave velocity,  $V_{s30}$ , is related to the soil type, depth and shear strength. Shear wave velocity is another factor for soil site class classification per ACSE 7-05 and ASCE 41-06. Very stiff and rock type, class A per ASCE 7-05, is observed in many part of the Eastern and North Eastern parts of the US (Nikolous et al. 2012),

which means  $V_{s30}$  to be more than 750 meter per second or 2500 foot per second. USGS web site (2014), (<http://earthquake.usgs.gov/hazards/apps/vs30/predefined.php>), also shows that site class of these areas can mostly be classified as type B or C (figure 4-2), except areas near Atlantic Ocean which are mostly categorized as site class D (including Washington DC metropolitan zone). This information shows that the Eastern and North Eastern parts of the US virtually have a wide range of the shear velocity data. To reach a reasonable data range for selection and scaling of the ground motions, the  $360 < V_{s30} < 620$  are considered in this study. On the USGS aforementioned data map, 360 m/s is the upper bound of the soil type D and 620 m/s is the lower bound of the soil type C, respectively (Figure 4-2). In line with default site class definition in ASCE 41-06 (2007a), ASCE 7-10 (2010) and 7-05 (2005), Site class D is the selected category whenever is needed through this research. Another part of the PEER data bank record selection is Fault Type selection (PEER 2010b) and (PEER 2011). Although technically these parts of the US are typically in the stable condition in term of seismic tectonic zone classification, the Reverse Slip fault is also common in some particular areas and has caused few past seismic activities such as Virginia 2011 earthquake (Horton and Williams 2012). Therefore, in view of PEER web application options and input availability parameters (PEER 2010b) and (PEER 2011), the Normal plus Reverse is the selected fault type.

Long-Period transition period,  $T_L$ , is assumed equal to 8 seconds per chapter 22 of ASCE 7-05 (2005). This  $T_L$  has been selected to present site location near Washington DC metropolitan area, though the  $T_L$  is principally dominant for some special structural system with low frequency such as skyscrapers and base-isolated structures.

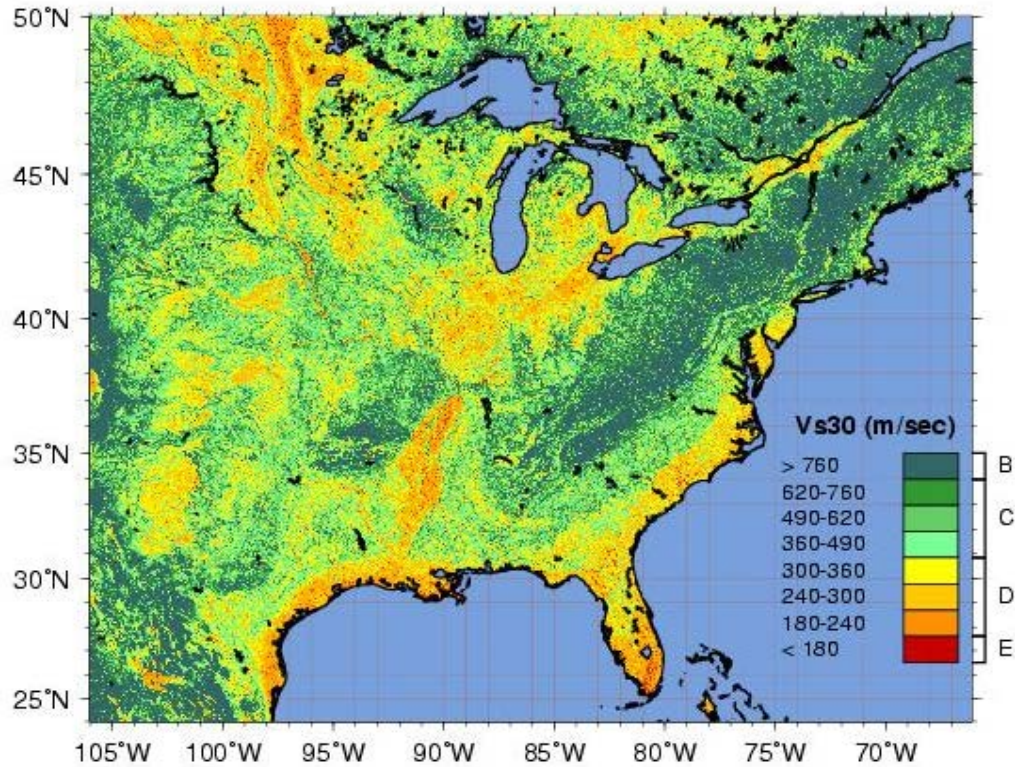


Figure 4-2, Shear Wave Velocity in the Eastern parts of the US (USGS website, <http://earthquake.usgs.gov/hazards>)

An additional parameter which may impact on scaling procedure, i.e. target spectrum method, is the period range or period interval. The recommended interval is  $0.2T_{\min}$  (minimum) and  $3.0T_{\max}$  (maximum) for moment frame buildings where  $T_{\min}$  (or  $T_{\max}$ ) denotes the lesser (or greater) of the first mode translational periods along the two main horizontal axes of the structure (NEHRP 2011). Strictly speaking, the period range, in reality, may show shorter than the fundamental structure period because of higher-mode effects, or periods longer than the fundamental structure period because of structure softening during inelastic response (PEER 2010b). The ASCE 7-05 (2005) stipulates that the period range shall be between  $0.2T$  and  $1.5T$ . In this study, different types of structures with different periods (Table 3-3) are generated. Some recent researches on moderate seismic zones imply that to select a suitable record set, the widest range of structural periods should be considered to account for uncertainty related to ground-motion intensity (Hines et al. 2011). As the

scaling procedures are not part of the current study, the period range was selected based on the four-story basic model, 4B12, on Table 3-3. Per the NEHRP method of period range for moment frames, the lower bound would be  $0.2 \times 1.74s = 0.348s$ . The upper bound would be  $3 \times 1.79s = 5.37s$ . The  $[0.348s, 5.37s]$  interval covers all periods on Table 3-3 which is reasonable within the scope of this study, and has a suitable wide range of periods.

Besides all above assumptions and definitions, one should consider that the impact of the seismo-tectonics on the structural response is still unclear and there are many unknown factors. Therefore, in an area such as the North Eastern part of the US with lack of appropriate seismic records, more refinement may be ineffective, and it is out of the current study scope.

#### **4.2.2. Selected Ground Motion Records**

The above-mentioned criteria were considered and applied to PEER data base web application (2013) in scaled mode condition. Based on the previous limitations and specifications, PEER database (2013) indicated several ground motions (30 records) which basically satisfied the applied norms. Then, amid the suggested data, three pairs of records were chosen, which are Whittier Narrows (WNA), Loma Prieta (LPR), and Northridge (NOR). To filter these records among all suggested records, two other points are considered, first, the selected ground motion should be occurred within the main geographical land of the US, and more importantly, the applied scale factor should be less than five. Harris and co-workers (2013) mentioned that the validity of a record with large scale factor could be imprecise, especially when the source mechanism is different or inconsistent. Table 4-1 shows the major information regarding the selected ground motions.

Figure 4-3 shows the scaled spectral acceleration of the selected records against the target spectrum (Figure 4-1) based on the PEER Ground Motion Database web application (2013). The geometric mean (GM) spectrum of ground motions are illustrated in Figure 4-3. In reality, GM is the base method of PEER web application for scaling pair records, which are depicted in Figure 4-3.

Table 4-1: Summary of Properties of Selected Scaled Horizontal Records\*

Event Name	Year	Station	Magnitude	Scale Factor	PGA (g) (GM)**
Loma Prieta	1989	Fremont - Mission San Jose	6.93	0.9363	0.1311
Whittier Narrows	1987	Huntington Beach - Lake St	5.99	4.0467	0.1668
Northridge	1994	LB - Rancho Los Cerritos	6.69	1.3771	0.2993

\*: Results from PEER Ground Motion Database Search Criteria

\*\* : GM: Geometric Mean, Used by PEER web application to scale records and display spectra

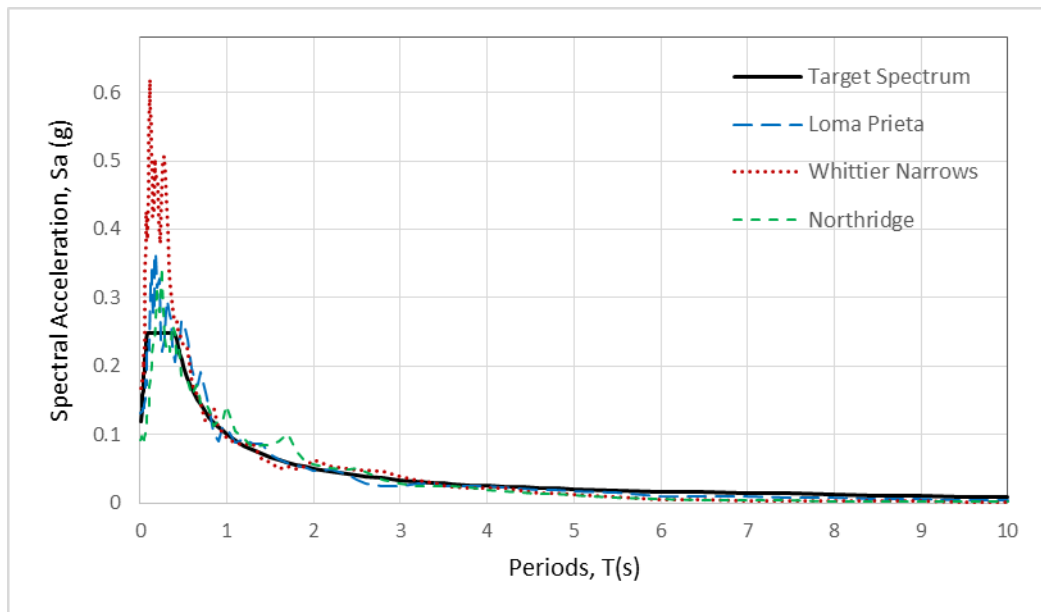


Figure 4-3, Target response spectrum against the scaled selected ground motions spectrum

Figures 4-4, 4-5, and 4-6 show acceleration against time series for LPR, WNA, and NOR pair record sets, respectively. Figures 4-4 thru 4-6 are divided into two parts, Fault Normal and Fault Parallel that represent two perpendicular wave directions. Furthermore, each figure shows both scaled and unscaled records which may delineate the scaled effect.

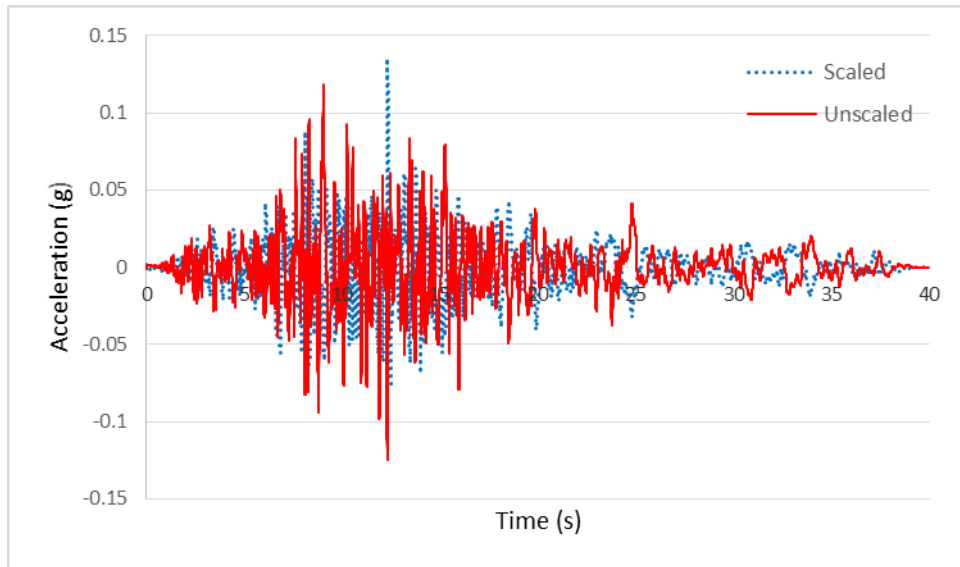


Figure 4-4a, LPR time series for Fault Normal direction

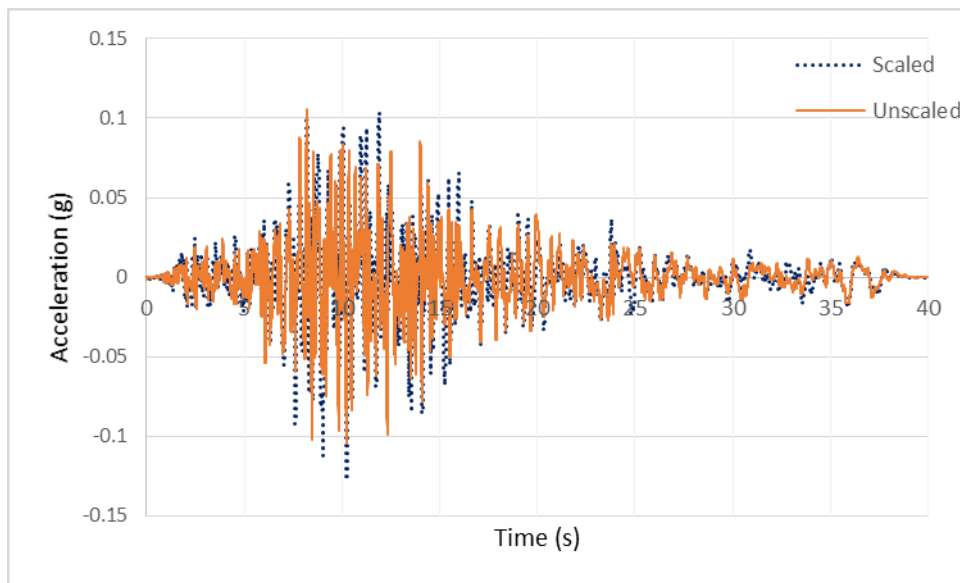


Figure 4-4b, LPR time series for Fault Parallel direction

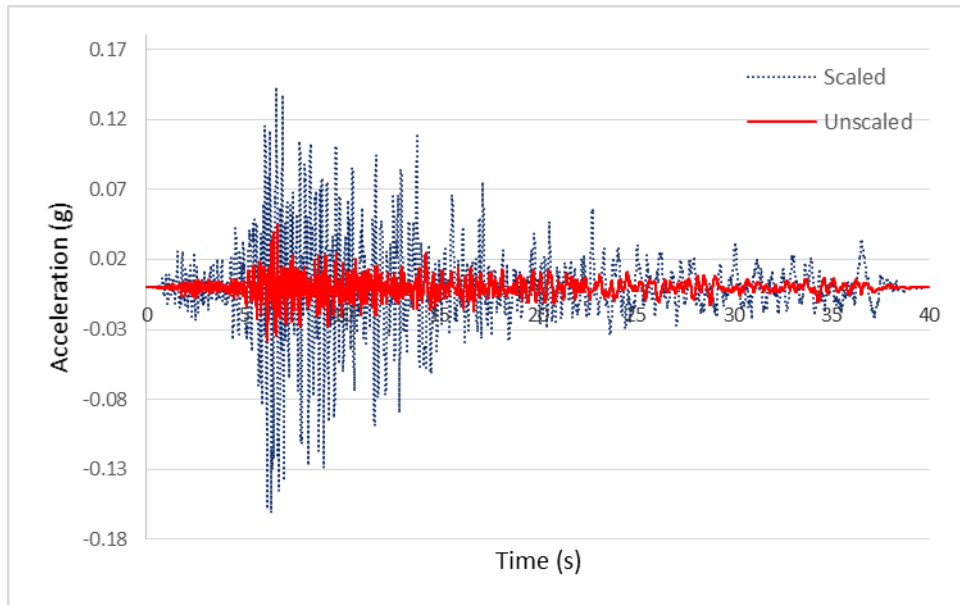


Figure 4-5a, WNA time series for Fault Normal direction

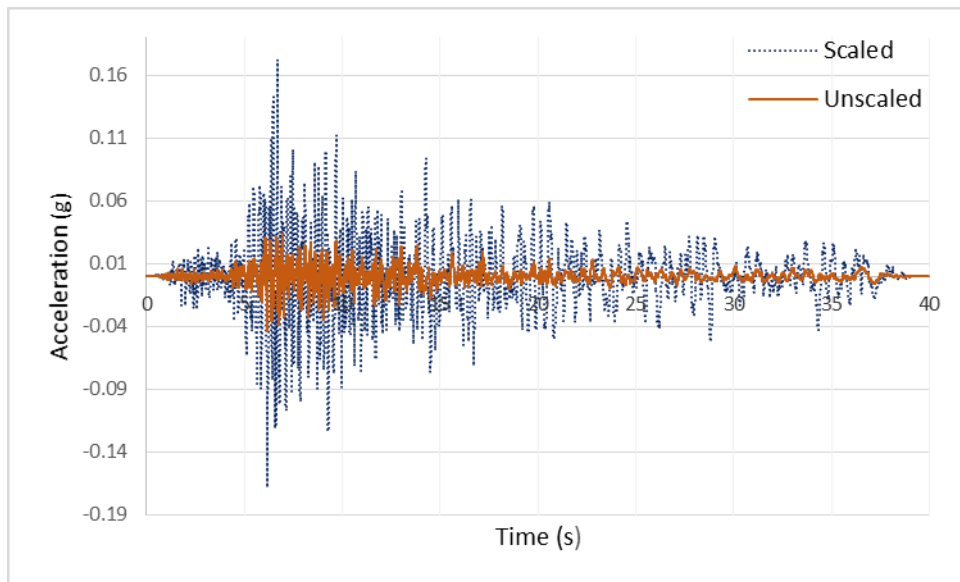


Figure 4-5b, WNA time series for Fault Parallel direction

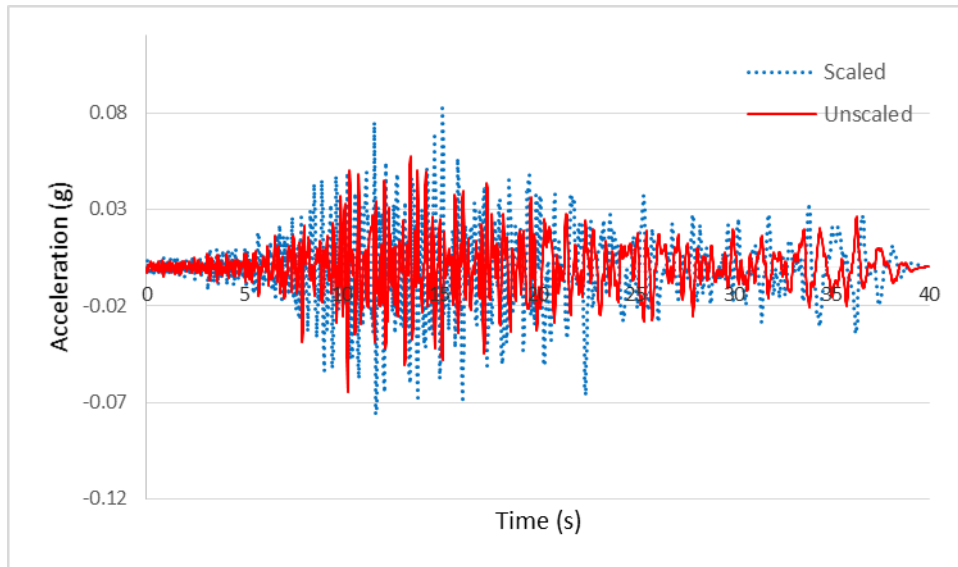


Figure 4-6a, NOR time series for Fault Normal direction

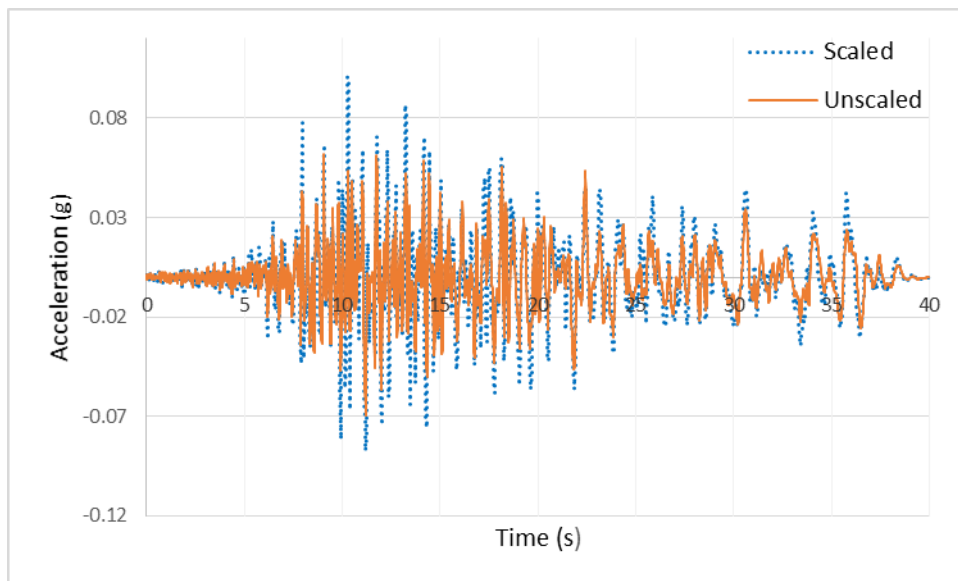


Figure 4-6b, NOR time series for Fault Parallel direction

The last record was selected from the unscaled database of PEER web site (2013). To select the last record set, an earthquake with higher energy content is considered. As mentioned by Kunath and co-workers (1995a), bearing in mind the lack of seismic data for the Eastern and North Eastern parts of the US, the possibility of a stronger seismic event cannot be ignored. Incidentally, the selected event should intrinsically satisfy the Eastern region seismic condition as much as possible.

The 1985 Nahanni (NAH) earthquake, which occurred in the Northwestern Canada, is one of the suggestions for typical event of an East Coast earthquake (Kunnath et al. 1995a). As mentioned in section 2-1, an actual occurred earthquake in the Northern part of America Continent, which can be classified as "typical" especially to the Northern US, can help to verify the assumption that existing Lightly Reinforced Concrete (LRC) structures may suffer serious damage from moderate seismic events. The major information acquired from the PEER database regarding the NAH earthquake is illustrated in table 4-2. Furthermore, it is worth to mention that the distinctive spectral shape of ground motions for a group of buildings with different dynamic response would be arbitrary as shown in the previous section. The reason is difficulties in selecting and scaling a different set of records for a group of structures with a various ranges of first mode periods, which was cited by Haselton and co-workers (2011). Thus, the NAH earthquake is not scaled with spectral matching method to cover more possible similar hazard condition.

Table 4-2: Summary of Properties of Selected Unscaled Horizontal Record\*

Event Name	Year	Station	Magnitude	Maximum Scaled PGA (g)	PGA (g) (GM) **
Nahanni	1985	Site 1	6.76	0.33***	1.0029

\*: Results from PEER Ground Motion Database Search Criteria

\*\* : GM: Geometric Mean, Used by PEER web application to scale records and display spectra

\*\*\*: Applied as direct linear scale factor

For this study, the direct scale method is applied to the Nahanni earthquake. The direct scaling method is one the two principal procedures for ground motion modifications (PEER 2010a). With this technique, a constant scale factor may be applied to the selected ground motion to decrease or increase the amplitude of a record set, which is usually applied to the acceleration data set (Ibid.). According to the PEER database (2013), the NAH earthquake shows  $V_{s30}$  equal to 659.6 meter per second with acceleration of 0.8537g and 1.178g for Fault Normal and Fault Parallel records, respectively. Although the  $V_{s30}$  is under the acceptable coverage bound

(Figure 4-2), the accelerations seem higher than the assumed limit for SDC B (see 4.2.1).

To lower down the acceleration, the upper bound of  $S_{DS}$  in section 4.2.1, i.e. equal to 0.33, would be considered as the maximum accepted acceleration. Therefore, for the nonlinear time history analysis purpose, the whole NAH acceleration record set is directly scaled with an appropriate linear constant to show maximum peak ground acceleration (PGA) equal to 0.33g accordingly. The NAH unscaled time series for both Fault Normal and Fault Parallel directions are illustrated in Figure 4-7.

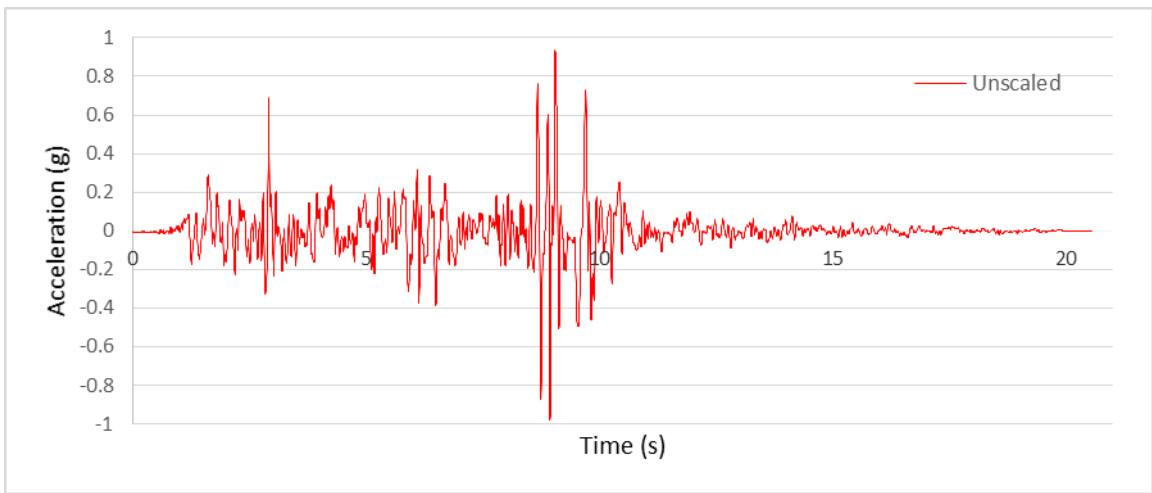


Figure 4-7a, NAH time series for Fault Normal direction

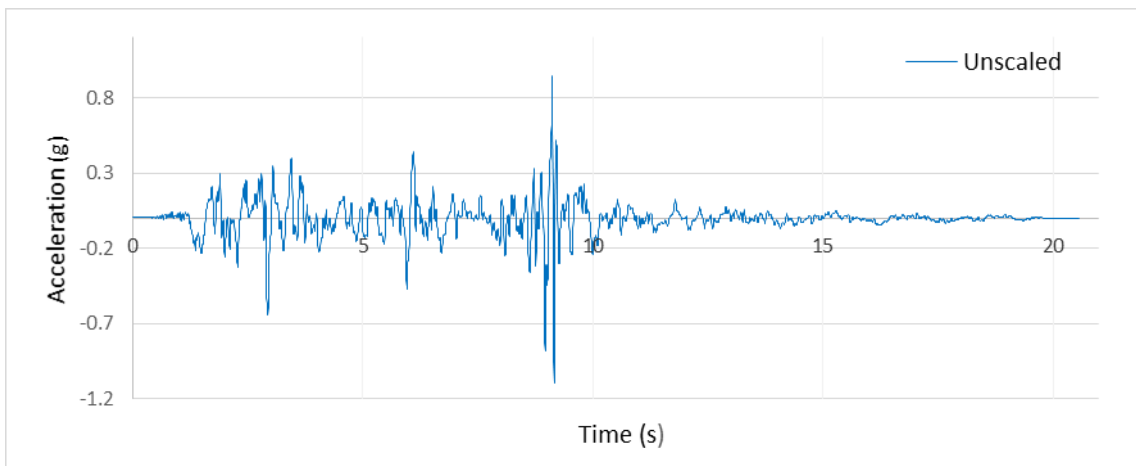


Figure 4-7b, NAH time series for Fault Parallel direction

### **4.3. Plastic Hinge Definition and Allocation to the Models**

#### **4.3.1. Introduction to Lump Plastic Hinge Behavior and Definition**

Generally speaking, seismic design is not a forced-based design, owing to the fact that mainly the deformation causes failure or weakness of a structural system. In fact, collapse of buildings is not due to seismic forces, rather lateral displacements cause structural collapse during the seismic event (Fardis 2009). As deformation capacity of structural members play a significant rule for any seismic nonlinear analysis, the fundamental step would be nonlinear modeling of main structural properties. Nonlinear models are commonly distinguished by two distinct characteristics: fundamental (physical) which is defined in terms of basic material properties, versus phenomenological (behavioral) which is based on the overall component response (PEER/ATC 72-1 2010). There are three major methods which are used to model nonlinear behavior of structural elements: continuum finite element model (implicit model), distributed inelasticity (or fiber model), and concentrated hinges (explicit models). Concentrated hinge plasticity is broadly used to model frame beams and columns (Naeim 2010). In the latter model, the nonlinear behavior is expected to be formed at predetermined structural sections and assumed to be concentrated at specific locations. Commonly lumped plasticity is assigned at both ends of the beams and columns. Also in some situations in which plastic hinge formation may be expected anywhere else through the element length, additional plastic hinges would be assigned at the desired locations. There are several parameters which are important to plastic hinge definitions and properties. For instance, hinge length and transverse reinforcement spacing are some of the foremost effective plastic hinge parameters.

As mentioned before, lumped plastic hinge method is considered in this study. Continuum finite element (FE) model has its own limitations, very difficult to model effectively, and most importantly, they are inappropriate for 3D modeling of multi-stories structures even by using the current advanced software. Although more sophisticated and advanced methods seem better for modeling certain type of behavior, simplified models can provide the response of structure more effectively

with the same or even lower level of approximation (NEHRP 2010b). Widely speaking, lumped plasticity (hinge) models may not perform the same precision of fiber models, but they can be calibrated, which will be briefly addressed in this Section later on, to provide a very well acceptable response. Fiber model is appropriate in nonlinear modeling of flexural walls (Aydinoglu and Önem 2010), and their calibration is not achievable efficiently. While either FE or fiber model can be performed for nonlinear analysis, it is recommended focus on global force-deformation response parameters for concentrated hinge models of frame components (PEER/ATC 72-1 2010).

Providing enough or even ample ductility in structures is one of the most important part of seismic design. Ductility can be defined as ability of structural element to dissipate induced energy by inelastic deformation during severe earthquakes (Chandrasekaran et al. 2010). Ductility in frame structures is mostly achieved through the moment-curvature relationship at critical sections. As mentioned earlier in this section, critical regions are those prone areas which the plastic hinges are expected or imposed to be formed during seismic events. It has been emphasized that result accuracy of any THA or NSA are strongly influenced by basic assumptions and inputs for the mathematical structural model (Ibid.). Major realm of ductility can be classified as: (1) - stress-strain relationship of structural materials; (2) - moment-axial (PMM) yield interaction; (3) - moment rotation capacity of members (Chandrasekaran et al. 2010).

Once a ductile part of structural element passes in the yield field, it can undergo large inelastic deformations with very minor or even no additional resistance. In concrete structures, pure flexure without axial load and flexural deformations (curvatures, chord rotations, etc.) are typical characteristics of this behavior (Fardis 2009). When any structural part enters this zone, the affected zone resembles the behavior of a real hinge connection in which hinge allows limitless rotation under zero moment. In addition, because all of the inelastic nonlinear activities are assumed to a limit of a typical zero length, this type of hinge model may also refer to lumped hinge. Thus, any portions of structural elements which exhibit plastification after its yielding deformation capacity are termed as “lumped plastic hinges”. They are finite

length zones of prismatic members such as beams, columns, slender walls (Fardis 2009). In concrete structures, almost all nonlinear phenomena and ultimate conditions are assumed to be concentrated at plastic hinges. Nonlinear behavior such as wide cracking, spalling of concrete, and yielding and buckling of longitudinal bars can be concentrated and modelled at plastic hinges. Most concrete fractures such as fracture of longitudinal bars or disintegration of concrete can also be accompanied at plastic hinges (Ibid.).

An ideal lumped plastic hinge (hereafter: plastic hinge) is assumed to locate at the center of a specific region of a member which is called plastic hinge length (Aydınoglu and Önem 2010). Plastic hinge can be modeled with strain hardening or, depending on assumptions or limitations may be defined without any strain hardening. Structural element between the predetermined plastic hinge sections is assumed to have linear behavior. Additionally, cyclic hysteretic behavior of plastic hinge should be defined for any Nonlinear Time History Analysis (THA). There are several methods to model hinge hysteretic behavior, such as standard Bilinear model with parallel loading and unloading branches, peak-oriented model with or without pinching, and Takeda hysteresis models (Aydınoglu and Önem 2010). Bilinear self-centering model, also known as S-model, is the simplest model and without any residual displacement when unloaded to zero, and the post yield stiffness is defined as the fraction of the initial stiffness (Lestuzzi et al. 2007). Bilinear self-centering model with energy dissipation has different unloading stiffness and four parameters are involved to specify the models, the initial stiffness, the yield displacement, the post-yield stiffness, and the unloading stiffness. Elastoplastic model, or Bilinear model, mostly is suitable for elastoplastic material such as steel, and three parameters which need to be defined are initial stiffness, the yield displacement, and the post-yield stiffness which is expressed as a portion of the initial stiffness (Lestuzzi et al. 2007). Takeda and Modified Takeda models provide better simulation of materials, such as reinforced concrete. Degradation of stiffness due to increasing damage is taken into account in this model, but strength degradation cannot be considered. Modified Takeda model is specified through five parameters: the initial stiffness, the yield displacement, the post yield stiffness, a parameter relating the stiffness degradation

( $\alpha$ ), and a parameter ( $\beta$ ) specifying the target for the reloading curve (Lestuzzi et al. 2007). Modified Takeda models are defined in several improved models. One of these methods (Pivot model) is used in this study for beam hysteretic behavior modeling. The applied hysteresis behavior to the assigned plastic hinges will be discussed in the next section.

As pointed out previously, plastic hinges should be defined based on the structural behavior and response of material for frame sections (here: RC sections) under dynamic loads. To define and model nonlinear behavior of a plastic hinge for a structural component, a specific curve should be allocated to each frame section. These types of curves are mostly derived from the hysteresis behavior of material (Figure 4-8a), and they should represent three key factors: stiffness parameters, strength parameters, and deformation parameters. The derived curves are usually called backbone curve in most technical literatures, and they may show several specialty code characteristics terms and definitions which are used in FEMA 356 (2000) or similar guidelines. In fact, historically backbone curve has been referred to several structural terms and definition for nonlinear analysis (FEMA 440 2005). For instance, they are used to describe limitations on the force-deformation behavior of structural components. Other nonlinear seismic design expressions, such as damage level, ductility, post yield capacity, elastic property, and deformation limitations, are some of these terms. Namely, backbone curves envelope the force-displacement response of structural components under both cyclic testing and/or under monotonic testing (FEMA 440 2005). NEHRP (2010b) defines the backbone curve as “Relationship between the generalized force and deformation (or generalized stress and strain) of a structural component or assembly that is used to characterize response in a nonlinear analysis model”. Most of the time, backbone curves cannot be directly use in analysis, and a simplified form of backbone curve is performed for nonlinear analysis purpose (Figure 4-8b).

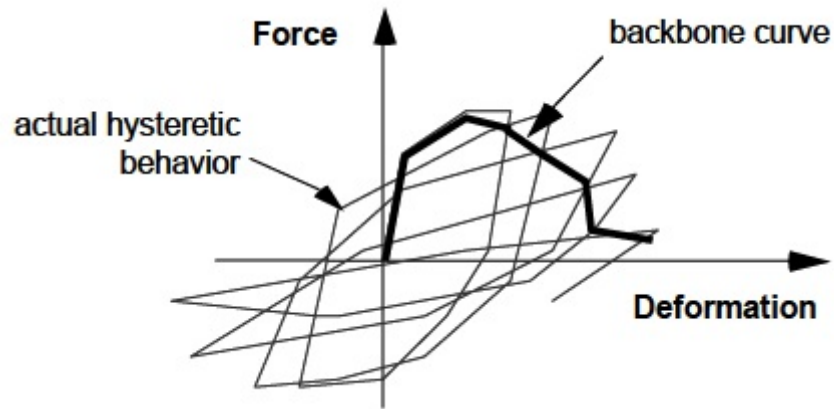


Figure 4-8a, Typical backbone curve derives from hysteretic behavior (Source: FEMA 440 2005)

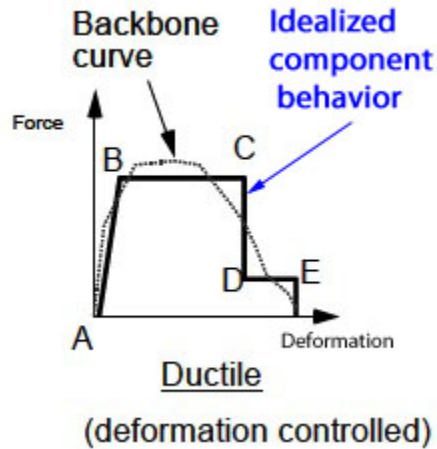


Figure 4-8b, Typical idealized curve derived from backbone curve- Ductile components (Source: FEMA 440 2005)

The idealized component behavior is achieved based on the original backbone curve which reflects the overall expected response of a structural member under dynamic cyclic loads (i.e. seismic load in this study). The strength and stiffness properties from original hysteresis behavior are commonly classified in three major different categories: ductile, semi-ductile, and brittle (FEMA 440 2005). The idealized property, which is used for analysis of structural models, is basically reflected in the primary force-deformation behavior of a structural section through a calibrate-able curve.

In general, seismic design standards, such as ASCE 41 (2007a and 2007b) and Eurocode 8 (part 3), define their own acceptance criteria for plastic hinge response which are mostly defined in terms of plastic rotation capacity. However, different types of concrete members may behave in a very broad range, which means from entirely brittle to complete ductility can be covered by RC concrete members (Fardis 2009). FEMA 356 (2000) and ASCE 41-06 (2007a) and its supplement (ASCE 41-06 2007b) have imposed some limitations to plastic hinges in general for code-wise safety factor manner, and in particular for certain response conditions. The applied limitations prevent unrealistic moment capacity (ductility) of the plastic hinges. For instance, lack of enough hoops or insufficient stirrups compel higher level of brittleness, which is not desired in plastic hinges and ultimately decline the ductility. Therefore, lower level of capacity is enforced in this condition and other similar situations.

Important points on backbone curve (A, B, C, D, E in Figures 4-8b and 4-9) depict key thresholds of component behavior and they are tabulated in advanced seismic provisions such as ASCE 41-06 (2007a and 2007b) and FEMA 356 (2000). Point A is the origin, point B is the yielding point, and there is not any deformation in the hinge up to this point. Point C represents the ultimate capacity of the hinge, and from this point to point D is the hinge residual strength. Point E is the total failure and after this point, the hinge capacity will drop to zero (CSI Analysis Reference Manual 2013). Up to point B, all deformation is elastic. Beyond this point, deformation is comprised of two parts, elastic deformation in the element prior to point B, and plastic deformation after this point.

$Q$  denotes the generalized force, and “a”, “b”, and “c” refers the capacity levels in FEMA 356 under the typical tables with the title of: “Modeling Parameters and Acceptance Criteria for Nonlinear Procedures” (FEMA 356 2000). Incidentally, acceptance criteria for performance design method are defined based on the condition of plastic hinge under the desire design level (dynamic or pushover case) pro rata to the threshold points. Figure 4-9 illustrates the typical idealized curve and threshold definitions from FEMA 356 (2000), which is basically used for this study. Furthermore, three major damage criteria, which are used in performance-based

design method approaches, are shown in Figure 4-9, as Immediate Occupancy (IO), Life Safety (LS), and Collapse Prevention (CP). These latter criteria are typically presented in SAP2000 software (2012). The software calculates and complies the same FEMA356 criteria (CSI Analysis Reference Manual 2013). The damage levels do not change or affect any structural behavior, and they just use for damage classification.

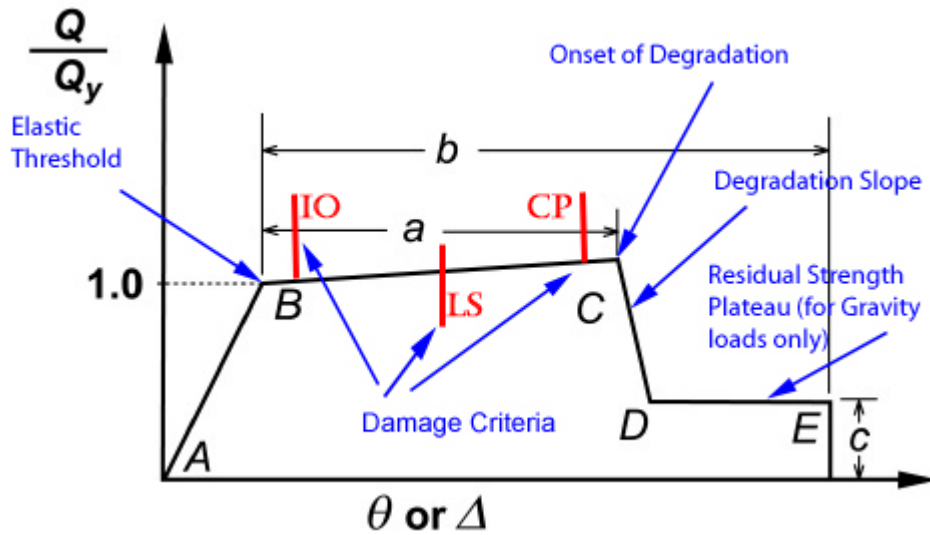


Figure 4-9, Idealized curve and threshold points (Source: FEMA 440 2005)

It is worth to mention that Figures 4-8b and 4-9 only depict the idealized curve in quadrant zone 1 of planar Cartesian system ( $0^\circ$  to  $90^\circ$ ). Applied plastic hinges are covered in both quadrant zone 1 and zone 3 ( $180^\circ$  to  $270^\circ$ ) to replicate the plastic hinge response in sweeping between two zones due to the nature of cyclic loads (Figure 4-10). Also, although usually in both zones 1 and 3 the idealized curve illustrates a similar shape and format, the amount of threshold points, such as maximum loads, are not necessarily symmetric. Despite the fact that the amount of reinforcements at the top or bottom of a RC section may not be the same, some other conditions, such as extra stiffness due to the concrete slab, may affect the response. The idealized curve in Figure 4-10 with proper thresholds is suitable for older RC and LRC structures (FEMA P-440A 2009). Moreover, there are other typical deficiencies which LRC structures may be encountered, such as inadequate joint reinforcements or

concrete confinement. The idealized curve can also covers the latter type of deficiencies. It is clear from Figure 4-10 that for LRC structures the amount of “a”, which directly replicates ductility of a structure member, is low. While zone 1 of the idealized curve would be enough for NSA models, Figure 4-10 shows a suitable general example of boundaries which is applicable to any model of nonlinear analysis with plastic hinge, such as THA analysis. In current study, all plastic hinges in archetype structures are modelled and applied per FEMA 356 (2000) and followed by ASCE 41-06 supplement No.1 (ASCE 41-06 2007b) guidelines to cover LRC deficiencies by performing appropriate idealized boundaries. The applied thresholds and damage criteria will be discussed later in section 4.3.2.

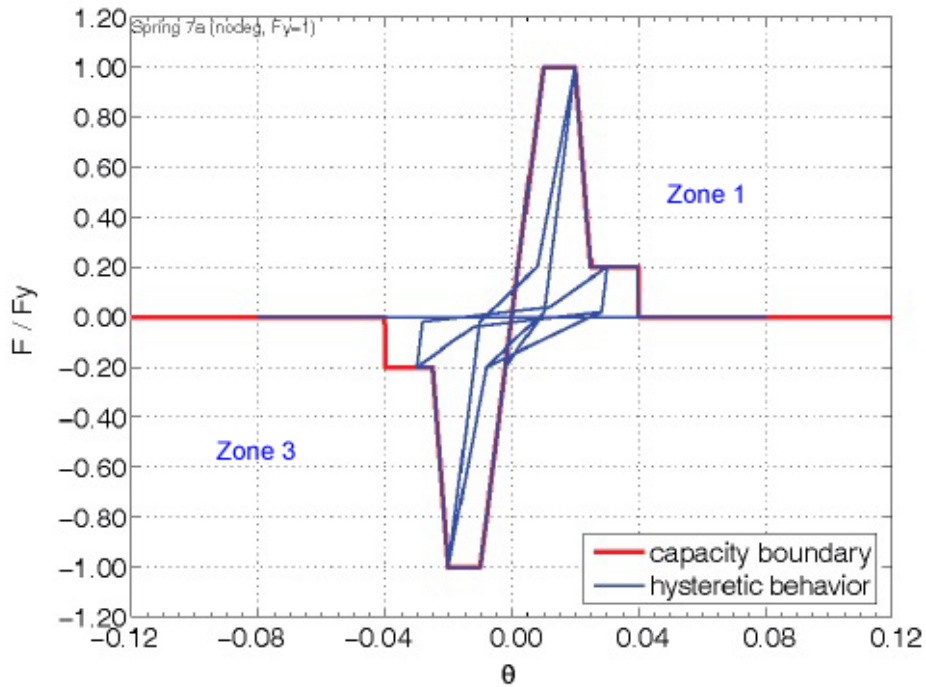


Figure 4-10, Example of suitable idealized curve for LRC structures under cyclic deformation (Source: FEMA P-440A 2009)

#### 4.3.2. Characteristics of the Assigned Plastic Hinges

As mentioned in section 4.3.1, in this study the lumped plastic hinge modelling is used for the RC members where phenomenological hysteresis laws are considered to reflect the behavior of each hinge. In brief, for three major reasons the

plastic hinge model is the best choice within the frame work of this study: (1) - large number of analyses required for the THA and NSA performance of the selected frames; (2) - relatively decent results in the previous studies by different researches, and overall and widely acceptance by popular retrofitting guidelines and codes; (3) - build-in code design criteria in SAP2000 software (2012) with ability to modify and apply user-defined norms for plastic hinges. Shear failure and consequent loss of gravity load bearing capacity is not explicitly included in the analysis models, but it is incorporated through performed hinge failure modes and limitations per FEMA 356 (2000) modeling parameters and acceptance criteria. Indeed, as a result of post-processing problems and considering available technologies and test data, shear-induced axial failure of columns is very difficult to simulate directly into a nonlinear structural model (FEMA P695 2009). In plastic hinge allocations and their associated definitions to members, reinforcement yielding, concrete crushing, and the strength and stiffness degradation can be assigned fairly accurately (Ibid.). On the other hand, buckling and fracture of longitudinal reinforcements and stirrup fracture can be modeled with lower level of accuracy. Although the less precise response of ties and stirrups incorporated in modeling may seem to come out with possible inaccurate results, one should note that on the whole the shear limitations are implied by FEMA 356 (2000) through reduction of ductility portion of plastic hinges (e.g. see Figure 4-10). In fact, the lateral reinforcement in plastic hinge regions of RC components has three main rules to provide (Derecho and Kianoush 2001): (1) - confinement of the concrete core; (2) - supporting of longitudinal compressive reinforcements against inelastic buckling; (3) - resistance against transverse shear (in combination with the confined concrete). All three aforementioned rules can be achieved through the FEMA 356 ductility limitation method. Incidentally, some researchers (Inel and Ozmen 2006) observed that plastic hinge length and transverse reinforcement spacing have not influence on the base shear capacity, while these parameters may have considerable effects on the displacement capacity of the frames. They mentioned that an increase in the amount of transverse reinforcement enhances the displacement capacity of structures, which is not a case of interest in the current study. It should be noted that for moment frames with regular spans, similar to the selected archetypes

models, shear mechanism is not dominant. In fact, overall dynamic analyses of this type of buildings demonstrate flexural response to seismic excitation which can be found in seismic and dynamic analysis reference books (e.g. Chopra 2000).

Assigned plastic hinges have been located with some distance in from the ends of beams or columns, which are typically corresponding to the size of elements at interaction points or end offsets. The end offset effect is briefly discussed in section 3.2.1. By providing some prior adjustments and definitions, the software package considers interaction point and end offset automatically. All plastic deformation, rotation or displacement, technically must be occurred within a discrete plastic hinge. Thus, there should be a length for plastic hinge over which plastic hinge strain or curvature is acquired (CSI Analysis Reference Manual 2013). Plastic hinge length is performed based on the software built-in *Relative Length* (SAP2000 2012). The hinge length is considered as a relative length which is a fraction from near zero to one of the clear length of the object, i.e., the length of the concrete element minus the length of end offsets (Ibid.). The applied automatic plastic hinge length is usually assigned by software following some FEMA 356 (2000) basic recommendations, e.g. equal to average 0.5 times the flexural depth of the RC component.

Generally, acceptance criteria and nonlinear modeling of RC beams and columns should be defined to reflect all modes of deformation and possible deterioration in RC elements. As mentioned before regarding brittle modes, shear failure and beam-column joint failure are not directly considered in the analysis. While the sudden strength loss usually related to the nonlinear modeling of a brittle failure, it may lead to computationally difficult and create convergence problems (Lepage et al. 2010). As rigid diaphragm action and extreme in-plane stiffness of concrete slab, there is not any moment in beams in the weak direction. Therefore, flexural hinging of beams is computed through allocation of plastic hinges to the beams in their strong directions. Software program defines this type of the plastic hinges as type M3. Flexural hinging of columns is assigned under the combined effects of bending in both directions and axial loads, and in SAP2000 terminology, they are known as PM2M3 hinges. All applied terms and limitations for type M3 and PM2M3 hinges are illustrated in tables 4-3 and 4-4, respectively. All addressed items

on tables 4-3 and 4-4 are depicted in Figure 4-9, and verification example for M3 and PM2M3 capacity are provided in Appendix B. For all beams and columns hinges, the post yield over-strength after the yield point (B in Figure 4-9) is applied equal to 10% of the yield strength. Thus, point C in Figure 4-9 is corresponded to  $Q/Q_y = 1.10$  for all allocated hinges. Per FEMA 356 (2000) procedure, it is permitted to interpolate between value of acceptance criteria and modeling parameters, which is considered by the software automatically. In table 4-3,  $\rho$ ,  $\rho'$ , and  $\rho_{bal}$  stand for tension, compression, and balance reinforcement ratio, respectively. From designed and applied longitudinal reinforcements to the selected model beams (see Chapter 3), the previous ratios have been calculated and considered by software automatically.  $V$  denotes the shear force in the section;  $b_w$  and  $d$  represent RC beam width and effective depth, respectively. On table 4-4,  $P$  indicates axial force and  $A_g$  is the gross area of RC column. Other terms are similar to table 4-3.

Table 4-3: Modeling Parameters and Numerical Acceptance Criteria of RC Beams Controlled by Flexure – Nonlinear Procedure\*

Conditions			Modeling Parameters**			Acceptance Criteria**- Performance Level per Plastic Rotation Angle***		
			Plastic Rotation Angle***		Residual Strength Ratio			
$(\rho - \rho')/\rho_{bal}$	Transverse Reinforcement	$V/(b_w d \sqrt{f'_c})$	a	b	c	IO	LS	CP
$\leq 0.0$	NC	$\leq 3$	0.02	0.03	0.2	0.005	0.01	0.02
$\leq 0.0$	NC	$\geq 6$	0.01	0.015	0.2	0.0015	0.005	0.01
$\geq 0.5$	NC	$\leq 3$	0.01	0.015	0.2	0.005	0.01	0.01
$\geq 0.5$	NC	$\geq 6$	0.005	0.01	0.2	0.0015	0.005	0.005

\*: Partially adopted from FEMA 356 (2000)

\*\* : Per FEMA 356, linear interpolation between values listed in Table 4-3 is permitted

\*\*\*: Plastic angle unit: radians

Table 4-4: Modeling Parameters and Numerical Acceptance Criteria of RC Columns  
Controlled by Flexure – Nonlinear Procedure\*

Conditions			Modeling Parameters**			Acceptance Criteria**- Performance Level per Plastic Rotation Angle***		
			Plastic Rotation Angle***		Residual Strength Ratio			
$P/A_g f'_c$	Transverse Reinforcement	$V/(b_w d \sqrt{f'_c})$	a	b	c	IO	LS	CP
≤0.1	NC	≤3	0.006	0.015	0.2	0.005	0.005	0.006
≤0.1	NC	≥6	0.005	0.012	0.2	0.005	0.004	0.005
≥0.4	NC	≤3	0.003	0.01	0.2	0.002	0.002	0.003
≥0.4	NC	≥6	0.002	0.008	0.2	0.002	0.002	0.002

\*: Partially adopted from FEMA 356 (2000)

\*\* : Per FEMA 356, linear interpolation between values listed in Table 4-4 is permitted

\*\*\*: Plastic angle unit: radians

Flexural and axial capacities are calculated and performed automatically by the software (also see Appendix B) based on the defined and assigned reinforcements to the RC sections in chapter 3. Designed reinforcements for all beams are allocated individually at the top and bottom of each section, and also at the start and end of each beam per defined and designed reinforcement in chapter 3. It can be seen from tables 4-3 and 4-4 that for all plastic hinges, and for all beams and columns, the transverse reinforcement are assigned as “NC”. In ASCE 41-06 Supplement No.1 (2007b) and FEMA 356 (2000) within nonlinear analysis abbreviation section, NC denotes the nonconforming transverse reinforcement. According to the conforming definition: “A component is conforming if, within the flexural plastic hinge region, hoops are spaced at  $\leq d/3$ , and if, for components of moderate and high ductility demand, the strength provided by the hoops ( $V_s$ ) is at least three-fourths of the design shear” (Ibid.). As previously mentioned in chapter 2 for LRC structures, usually the conforming condition has not been complied for ties and stirrups. Thus, all assigned plastic hinges (M3 and PM2M3) are considered with NC in the selected models to

meet one of the implied terms regarding low to moderate seismic regions construction styles.

Plastic hinge type M3 are assigned to the start and end of the beams for all tagged models, i.e. Base, Symmetric, and Asymmetric (see section 3.2), and the end offset effect is implied to M3 types as well (see previous page for plastic hinge length). Also all typical B4 beams (located at the first story of asymmetric types structures, A models, see section 3.4) have an extra M3 plastic hinge at their center. B4 typical beams are carrying the discontinued columns loads from upper stories, thus, the intersection of discontinued column and beam in axis B can be a possible plastic hinge point where extra plastic hinge is allocated. PM2M3 plastic hinges for columns are applied at the start and end of every column elements at all stories to cover all possible plastic hinge formations.

Applied effective stiffness values are implied to comply with FEMA 356 (2000) guidelines which are followed for most nonlinear part of this study. Flexural rigidity of all beams are performed equal to  $E_c I_{cr} = 0.5 E_c I_g$ , where  $I_{cr}$  and  $I_g$  stand for the cracked and gross moment of inertia of a member, respectively, and  $E_c$  is the concrete modulus of elasticity. Besides, the reduced stiffness for all beams is considered for their strong directions, i.e. “I<sub>3</sub>”.  $I_3$  has been modified for beams’ stiffness reduction. For this study most of the columns are carried gravity compression loads in average more than  $0.5 A_g f'_c$ , in which  $A_g$  denotes gross area of a column’s section. Therefore,  $E_c I_{cr} = 0.7 E_c I_g$  have been applied to all columns per FEMA 356 (2000) standard. Due to the fact that the selected models will be analyzed in two different directions (under either NSA or THA procedure), reduction of stiffness for moment of inertia are implied at both major directions of each column section.

For all selected models at geometric center of each story plan, a master point (joint) is defined. Accordingly, the master point coordination locates along axis B, and with 27 feet distance above axis “1” for all type of models. Thus, for all Asymmetric, Symmetric, and Base models, with different first story height (NH, MH, and EH, see Chapter 3) the master point is assigned at the geometric center of each story level. To create a uniform format, the master point identification number (ID) is

named based on the corresponding story number. For instance, the master point ID for 5<sup>th</sup> story of either 8A18, or 8S15, or 8B12 are called as Master Point No. 5. Also all assigned master points are allocated to their corresponding rigid diaphragm systems. Therefore, master point at each story level has the same constrain condition as the other points have. Master points are used to compare results and also for monitoring NSA and THA story responses.

#### **4.3.3. Hysteresis Models for Beams and Columns**

Plastic hinge formations and energy dissipation under dynamic loads in general and seismic excitation in particular, are very sensitive to hysteresis definition. Inel and Ozmen (2006) compared and studied SAP2000 (2012) built-in and user-define hinging. They indicated that both models with default built-in hinges and the user-defined hinges estimate plastic hinge formation at the yielding level relatively well. Nonetheless, they also mentioned that there are significant differences in the hinging patterns at the ultimate state. Per their study, hinge locations appear to be consistent with their models, but the model with default built-in hinges showed a ductile beam mechanism in which columns were performed stronger than beams, and damage or failure occurs on beams (Inel and Ozmen 2006).

Furthermore, the capacity of energy absorption in elastic range for moment frame systems is affected mostly by beams than columns, and beams dissipate more energy than columns in the elastic stage of structural response. For moment frame type structures, elastic dissipate energy is related to the stiffness of vertical and horizontal elements. To show the dominant effect of beams, a simple one story (story height:  $H$ ) and one span (span length:  $L$ ) frame is assumed (Figure 4-11), which can be simply expanded to any multi-stories and multi-spans structure (Chopra 2000). From structural analysis, it is accepted to consider only flexural stiffness of structural members, i.e. shear deformation of a moment frame system can be ignored. In Figure 4-11,  $E$  denotes modulus of elasticity of frame elements;  $I_b$  and  $I_c$  stand for beam and column stiffness, respectively. Applied load is  $f$  and corresponding displacement is shown by  $d$ .

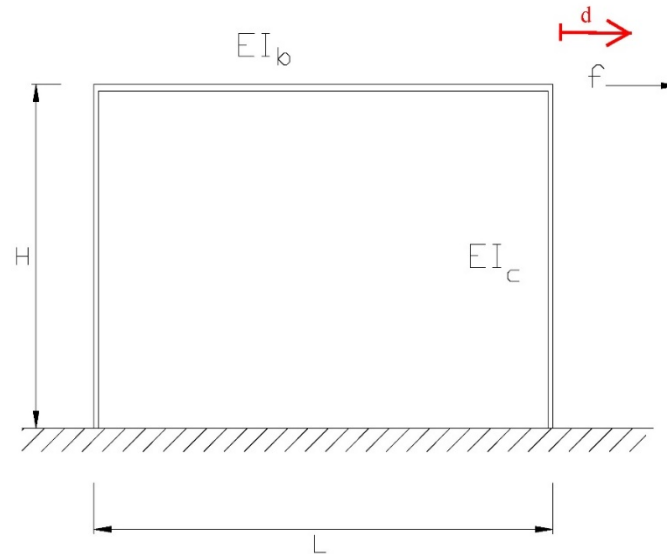


Figure 4-11, One story- one span moment frame (Partially adopted from: Chopra 2000)

In case of a rigid beam or  $EI_b = \infty$ , the frame stiffness can be calculated as (Chopra 2000):

$$k = \sum_{\text{Col.}} \frac{12EI_c}{h^3} = 24EI_c/h^3 \quad [4-2]$$

On the other hand, in case of zero stiffness for the beam or  $EI_b = 0$ , the frame stiffness change into:

$$k = \sum_{\text{Col.}} \frac{3EI_c}{h^3} = 6EI_c/h^3 \quad [4-3]$$

For a general condition between the two above-mentioned ultimates the frame stiffness is calculated as:

$$k = \sum_{\text{Col.}} \frac{24EI_c}{h^3} \times (3I_b + I_c)/(3I_b + 4I_c) \quad [4-4]$$

From the previous equations, it is clear that the frame stiffness is independent from the beam span (L), and drastically affects by beam stiffness. For instance, in

case of  $EI_b = 1/2 EI_c$ ,  $EI_b = EI_c$ , and  $EI_b = 2 EI_c$ , the frame stiffness ratio would be 0.454, 0.571, 0.70, respectively. These ratios show the dominant effect of beam stiffness in frame total stiffness and ultimately to the elastic energy absorption of a frame.

As a consequence, from the elastic stage response of a frame, beams cumulate more energy than columns which is almost constant and unchangeable. In the plastic phase, any extra energy absorption may crucially change the whole response of a moment frame system in case of seismic excitation. Consequently, beam hysteresis model should be defined more precisely, and additional extra induce dissipation capacity to beams will possibly lead to the unrealistic formation of plastic hinge in the beams instead of columns, which may create doubtful or even wrong analysis results. As mentioned earlier by Inel and Ozmen (2006) some built-in hinges of SAP2000 software may not be appropriate for a precise analysis.

For RC columns in selected models, the default software hysteresis model, Elastic-Perfectly Plastic (Elasto-plastic) model, has been performed. Per SAP2000 software (2012) Help menu, Elastic-Perfectly Plastic model is suitable for an independent axial load-deformation relationship. This type of hysteresis behavior is actually built based on the maximum and minimum axial yield values from the interaction surface (SAP2000 2012). Yavari and his co-workers (2009) compared result of frame dynamic response under seismic excitation by using shaking table test and nonlinear analytical modeling. The tested RC moment frame consisted of columns which were designed only for gravity loads. They mentioned that using an elastic-perfectly-plastic model for column plastic hinge performed a good estimate of the displacement demands in case that strength degradation was not significant. Although this type of model may bring few concerns regarding lack of proper degradation modeling, the overall response of columns under seismic action is reasonable. In fact, lower effect of energy dissipation in RC columns than RC beams and overall damping energy absorption of whole structure (see THA section) drastically decrease the negative side of Elastic-Perfectly Plastic models. Parenthetically, considering conservatism approach for column response in term of seismic energy absorption, it is preferred to have inherent higher level of energy

absorption of Elastic-Perfectly Plastic hysteresis models (FEMA P-440A 2009) in column hinges. In fact, hysteresis model corresponding to PM2M3 interaction curve and backbone limitation always uses isotropic energy dissipation, which dissipates more energy than the other models such as Takeda or kinematic hysteresis models (CSI Knowledge Base, see Kalny 2011). It should also be mentioned that the overall backbone curve shape of the column hysteresis models comply the defined curve (see Figures 4-9 and 4-10, and also see Appendix B). Therefore, the global limitations, over-strength, and boundary zones are under the overall defined hinge cap, and the differences between two hysteresis models are related to the loading-unloading path, pinching effect, and degradation format.

On the other hand, RC beam hysteresis modeling needs a more refined hysteretic behavior. For this purpose Pivot hysteresis model, introduced and developed by Dowell and his coworkers (1998), is used. Pivot model is primarily established through similar modified Takeda model and for RC bridge columns. As shown in Figure 4-12, basically, the experimental observations of RC members under cyclic or dynamic loads were determined that majority of unloading paths are generally conducted toward a single point in a typical force-displacement (or moment-rotation) plane, which is called Pivot point (Ibid.). The unloading paths from any displacement level are carried out on the idealized stiffness lines. The first conducted point is named primary pivot point which crosses the elastic loading line (Figure 4-12). In fact, the model is fundamentally defines by parameter  $\alpha$  which is the control unloading stiffness, and  $\beta$  which indicates the pinching pivot point (Figure 4-13).

As mentioned before, original pivot model has been established based on bridge RC columns and circular section (Dowell et al. 1998). Also in the original study, there are limitations regarding axial load and longitudinal reinforcement, and the transverse reinforcement effect has not been considered (Sharma et al. 2013). To model LRC components, Pivot model has several advantages. Some of the pivot model pinpoints are pinching effect, degradation, hysteretic behavior verification through experimental observations, applicability to perform unsymmetrical sections, and simplicity. However, due to the previously mentioned limitations, the original

pivot model may not be completely suitable for frame buildings. Therefore, in this study, the applied pivot hysteretic model to the beams' plastic hinges is calculated and allocated by some adjustments. Sharma and his coworkers (2013) propose refined parameters for pivot model. They provided some suggestions to the Pivot parameters without any change in the main parameters to cover building type structures with rectangular sections.

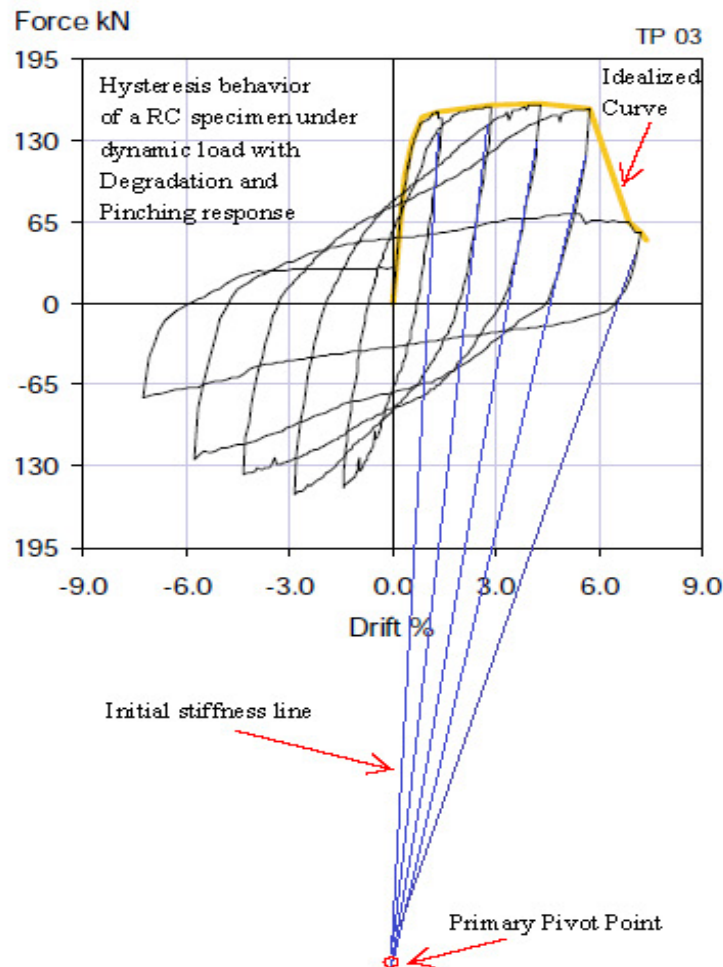


Figure 4-12, Example of an experimental and idealized hysteresis behavior of a RC component (Partially adopted from: FEMA P-440A 2009)

SAP2000 (2012) allows the users to define and assign pivot hysteresis behavior to the plastic hinges by modifying user-defined hinge option. Since the performed software does not have any automatic hinge modification application, all

the M3 hinges (beam hinge type) for all archetype models have been adjusted one by one. Although very time consuming, this procedure amends dynamic response of the beam plastic hinges to reflect behavior that is more realistic. To model pivot behavior, several scalar terms must be allocated to the plastic hinge hysteresis model which is shown in Figure 4-13. Per Dowell and his coworkers (1998) study, the scalar terms are defined as (CSI Analysis Reference Manual 2013):

- $\alpha_1$  indicates the pivot point for unloading to zero from positive force;
- $\alpha_2$  indicates the pivot point for unloading to zero from negative force;
- $\beta_1$  indicates the pivot point for reverse loading from zero to positive force;
- $\beta_2$  indicates the pivot point for reverse loading from zero to negative force;
- $\eta$  determines the amount of degradation of the elastic slopes after plastic deformation.
- Points P1 to P4 are pivot primary points with softening effects, and PP2 and PP4 represent the pinching pivot points.

Taking everything into account, pivot parameters to the selected models M3 hinges are assigned by considering several factors including: the total number of plastic hinges, RC section properties, assigned longitudinal and transverse reinforcements, and rigid diaphragm action (zero axial force in beams). To reduce unnecessary extra input data and simplify modelling, a general average value for each individual case was allocated to the total applied parameters. To do this, mathematical calculations, engineering judgment, original pivot study (Dowell et al. 1998), suggestions and modification by Sharma and his coworkers (2013), and result of a study by Lepage and his coworkers (2010) all are considered. Thus,  $\alpha_1$  and  $\alpha_2$  are performed equal to 2.0,  $\beta_1$  and  $\beta_2$  are assumed equal to 0.3, and  $\eta$  is applied equal to 1.0

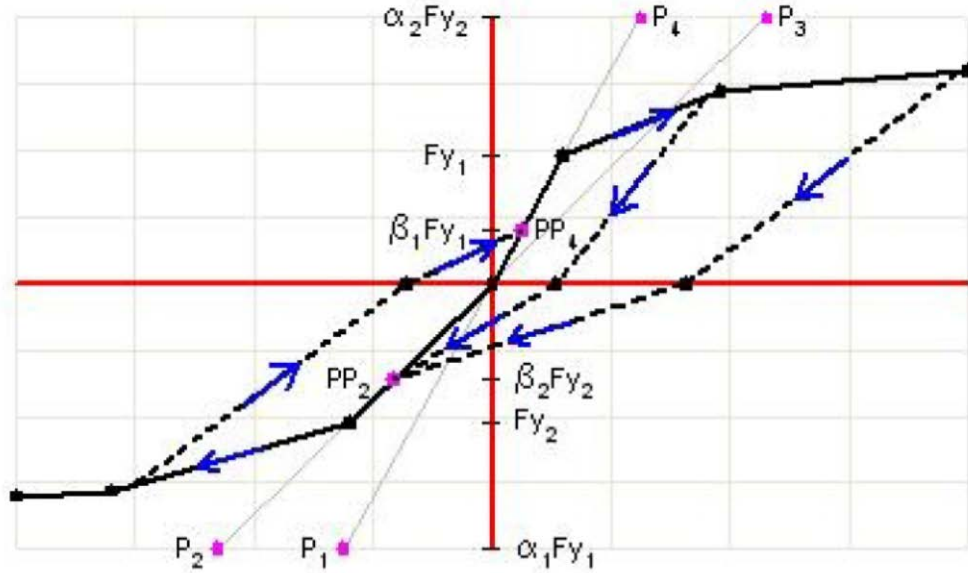


Figure 4-13, Typical Pivot hysteresis parameters (Source: CSI Analysis Reference Manual 2013)

## 4.4. Damping Model Development

### 4.4.1. Introduction to Rayleigh Damping Ratio and Assigned Damping to Selected Models

Damping ratio in structural analysis consists of two parts, elastic damping and hysteretic damping. Elastic damping is usually related to the secant or tangent stiffness of a structure in linear or nonlinear analysis (Smyrou et al. 2011). Regardless of secant or tangent stiffness, in the post-elastic response phase the hysteresis damping starts absorbing of input energy (Ibid.) considerably. In fact, the elastic damping is reduced following of any structural member entering to the post-elastic phase (after point B in Figure 4-9). In the THA analysis method, hysteresis damping is implied through cyclic response of the plastic hinges and technically cyclic performance of plastic hinges dissipates the input energy. Thus, via allocation of the plastic hinges to the beams and columns, hysteresis behavior of those elements

inherently absorbs some part of the applied dynamic energy (i.e. seismic ground motion energy). Basically, some portion of building damping is originated from soil flexibility and radiation, hysteresis response of non-structural components, and relative movement between non-structural components and the structural members (Smyrou et al. 2011) and (Otani 2004). Furthermore, in many nonlinear dynamic analyses there may be several structural members which they do not fall into the post yield range. Therefore, in the initial elastic stage and before the hysteretic damping being triggered a level of elastic damping is required (Smyrou et al. 2011). Because of energy dissipation during dynamic analysis within nonlinear yielded plastic regions, the damping should be reduced to prevent double counting of energy dissipation (CSI Knowledge Base, see Kalny 2011). The over damping effect concern will be discussed later on in this section. However, as mentioned earlier, the load-case damping is still required to cover energy dissipation which occurs outside of the plastic hinges (Ibid.). Hereafter in this section, discussion will be continued for allocation of appropriate damping ratio to the selected models, as the plastic hinge discussion has been included in the previous section.

In theory, damping forces are associated to the relative velocities at story levels to the points in which the translational DOFs are allocated (Lepage et al. 2010). In classical structural dynamic, damping matrix is proportional to the mass and stiffness as shown in Equation 4-5. Although there is no obligation to use classical damping matrix in direct integration, damping matrix is considered as classical in most THA methods. By definition of a system with classical damping, the damping matrix ( $C$ ) is viscous and turns into diagonal when transformed to undamped modal coordinates (Charney 2008). SAP2000 implies classical damping for nonlinear dynamic analysis (CSI Analysis Reference Manual 2013), accordingly in current study the damping matrix is classical. The mass-stiffness damping is very common in the nonlinear analysis of structures. This type of damping is usually referred to as Rayleigh damping (Zareian and Medina 2010). Numerical models of Rayleigh damping almost always define as the linear viscous damping in structural models (Hall 2006). Practically, the stiffness portion of the damping matrix is changed when an element cracks or yields, nevertheless the mass portion remains unchanged

throughout the analysis. Moreover, stiffness portion of Rayleigh damping may increase for higher vibration frequencies of a structure, whereas mass-proportional damping may reduce for higher modes of a structure (Lepage et al. 2010). The mass proportional damping acts as if external supported dampers attached to the structure. Therefore, in reality, they do not physically exist for a typical structure system (CSI Technical Papers, see Wilson 2014).

A classical viscous damping matrix,  $C$ , comprises of linear summation of mass matrix,  $M$ , and stiffness matrix,  $K$  as shown in Equation 4-5:

$$C = \eta M + \delta K \quad [4-5]$$

In which  $\eta$  is the mass-proportional damping coefficient and  $\delta$  stands for the stiffness-proportional damping coefficient with units of  $s^{-1}$  and  $s$ , respectively.

In classical dynamic analysis, the modal equations have orthogonal conditions which allow to re-write Equation 4-5 as (CSI Analysis Reference Manual 2013):

$$\xi_n = \frac{1}{2 \omega_n} \eta + \frac{\omega_n}{2} \delta \quad [4-6]$$

Where:  $\xi_n$  stands for the critical-damping ratio, and  $\omega_n$  is the natural frequency (rad/s).

From Equation 4-6, it is clear that the critical damping ratio varies with natural frequency. To calculate the Rayleigh damping factors ( $\eta$  and  $\delta$ ) in Equation 4-6, two damping ratios,  $\xi_i$  and  $\xi_j$ , must be known or shall be allocated in advance. By using two associated natural frequencies of  $\omega_i$  and  $\omega_j$ , then the mass-proportional damping coefficient and the stiffness-proportional coefficient can be computed. To mathematically determine those coefficients, simply a pair of simultaneous equations (Equation 4-7) must be solved (CSI Knowledge Base, see Kalny 2011):

$$\begin{bmatrix} \xi_i \\ \xi_j \end{bmatrix} = \frac{1}{2} \begin{bmatrix} \frac{1}{\omega_i} & \omega_i \\ \frac{1}{\omega_j} & \omega_j \end{bmatrix} \begin{bmatrix} \eta \\ \delta \end{bmatrix} \quad [4-7]$$

For nonlinear dynamic analysis, damping can be assigned to SAP2000 either by specifying coefficients  $\eta$  and  $\delta$  directly, or by allocation of the critical damping ratio. For the latter one, the damping ratio may be allocated separately for two different sets of either frequencies or periods (CSI Analysis Reference Manual 2013). In this study, Rayleigh damping ratio coefficients are calculated based on the method which is mentioned by Hall (2006). The procedure and computed amounts will be illustrated in next section (4.4.2).

As noted earlier in this section, effective damping may affect response of a structure when yielding occurs in areas of concentrated inelasticity (Hall 2006). Several researchers stated that in such cases, there is possibility of inducing artificial viscous damping forces in plastic hinges (Hall 2006), (Charney 2008), and (Zareian and Medina 2010). The artificial viscous damping may induce significant forces which may lead to invalid analysis results, and such artificial damping forces are not easily detectable (Ibid.). In consequence, overestimation of damping ratio may create noteworthy errors in calculation of maximum nonlinear displacement of structures which have intermediate to long period range. On the other hand, underestimation of the damping value may lead to overrate of displacement for shorter period range, namely, less than 0.4 seconds (Dwairi et al. 2007). However, by reviewing the result of their study (Ibid.), which is basically based on THA analyses, it seems that the low ductile structures (such as LRC) illustrate lower scatter in damping amount comparable with the higher ductile models.

Moreover, for nonlinear dynamic analysis, and particularly for THA, a distinctive damping ratio has not been properly realized yet, and there are ambiguities regarding appropriate modeling procedures (Charney 2008), (Hall 2006), and (Zareian and Medina 2010). Widely held damping ratio equal to 5% for concrete buildings may cause unrealistic responses (Ibid.), and damping is one of the main uncertainties in dynamic design and analysis process (Smyrou et al., 2011) which there still are many issues and conflict among the suggested methods (PEER/ATC 72-1 2010). On the other hand, it was found that for structural systems with less than 10% of inherent damping, corresponding error due to use of viscous damping might be insignificant (Charney 2008). Some studies show that for low/mid-rise RC

buildings, namely, maximum 30 stories, the maximum critical damping ratio can be up to 8% (PEER/ATC 72-1 2010). These studies have been done in the US and Japan which results were gathered through vibration tests of real buildings under mechanical force vibrations, wind induced vibrations, earthquakes (in Japan) , and analyzing of recorded strong ground motions for 85 buildings (in the US) (Ibid.).

Conversely, many proposed corrected Rayleigh damping methods need significant calculations and modeling process just for the damping implication which is not part of this study. Due to lack of experimental data and rare seismic events in low- to moderate- seismic zones in the Eastern and North Eastern parts of the US, appropriate damping allocation to any structural model brings more difficulties to the nonlinear mechanism. As cited by Hall (2006), field data illustrate that modal damping ratios are fairly constant for a given structure. Therefore, within the limit of this study, for each of the selected models just one damping ratio has been allocated to cover all frequencies, which is practical and common among dynamic and seismic studies (e.g. see NEHRP 2010b and 2010c).

As mentioned earlier, 5% critical damping is very popular among seismic studies of RC moment frame structures (NEHRP 2010c). To calculate viscous damping ratio used in nonlinear analysis of typical buildings, a very simple equation is recommended by PEER/ATC joint venture program (PEER/ATC 72-1 2010). For low/mid-rise buildings with less than 30 stories, the maximum percent of critical damping ( $\xi$ ) is defined as (Ibid.):

$$\xi = \alpha / 30 \quad [4-8]$$

In which  $\alpha$  is a coefficient between 60 and 120. RC structures would be likely closer to the upper bound of  $\alpha$  coefficient (PEER/ATC 72-1 2010). To reach a reasonable damping ratio in this study,  $\alpha$  coefficient is assumed equal to 105. Therefore, the damping ratio per Equation 4-8 would be equal to 3.5%. By considering  $\alpha$  equal to 105, the selected damping is close to the condensed area of diagrams which demonstrate damping ratios in Figures 2-24, 2-25(b), and 2-28 of PEER/ATC report (2010). This damping percentage shows a suitable amount among

the presented studies in aforementioned references. Hence, all Base (2B12 through 8B12 models) and Symmetric plan models (2S15 through 8S18) are assumed to have 3.5% critical damping ratio. Experimental results from a LRC asymmetric plan structure showed that 2% critical damping might be reasonable (Bhatt and Bento 2011) for this type of structures. Thus, to reach a reasonable result, and to acquire a suitable damping ratio for low-to moderate- seismic zones with irregular plan, 2% damping ratio is applied for Asymmetric models (2A12 through 8A18 models).

#### 4.4.2. Allocated Rayleigh Damping Coefficients to Selected Models

Table 3-3 shows three first periods of each selected model. These three modes comprise the majority of participated modal masses for the selected models. To calculate linear viscous damping factors in Equation 4-6, the procedure presented by Hall (2006) would be followed. Calculation of  $R$  factor is the first step.  $R$  represents the ratio of natural frequencies (rad/s) of important modes which are the first three modes in this study. The next step is calculating  $\Delta$  (Equation 4-9) which determines bounds on the damping ratios within the specific frequency range (Ibid.).

$$\Delta = \xi \frac{1+R-2\sqrt{R}}{1+R+2\sqrt{R}} \quad [4-9]$$

As mentioned earlier,  $\xi$  is equal to 2% for selected models type A, and 3.5% for the rest models. Hall (2006) cited that if the bound factor, i.e.  $\Delta$ , is considerably low (relative to  $\xi$ ), then  $\eta$  and  $\delta$  can be found from:

$$\eta = 2\xi\omega \frac{2R}{1+R+2\sqrt{R}} \quad [4-10]$$

$$\delta = 2\xi\left(\frac{1}{\omega}\right)\left(\frac{2}{1+R+2\sqrt{R}}\right) \quad [4-11]$$

In Equations 4-10 and 4-11,  $\omega$  denotes the first mode of vibration (rad/s), other terms have been defined previously.

The results for all selected models are illustrated in table 4-5.  $R_i$  is the ratio of the third natural frequency to the first natural frequency for each selected model ( $i= 2, 4, 8$ ). From table 4-5, it is clear that the bound factor ( $\Delta_i$ ) may be considered as zero. Thus, the viscous factors,  $\eta_i$  and  $\delta_i$  for each selected model are calculated and presented based on Equations 4-10 and 4-11. These factors will be applied to each associated model for nonlinear time history analysis.

Table 4-5: Viscous Damping Coefficients for Selected Models

<b>8 Stories Selected Models</b>						
Model Name	<b>8A12</b>	<b>8A15</b>	<b>8A18</b>	<b>8B12</b>	<b>8S15</b>	<b>8S18</b>
R <sub>8</sub>	1.1494	1.1762	1.1847	1.0775	1.0746	1.0726
$\Delta_8$	0.0000	0.0000	0.0000	0.0000	0.0000	0.0000
$\eta_8$ (s <sup>-1</sup> )	0.0486	0.0474	0.0463	0.0745	0.0719	0.0700
$\delta_8$ (s)	0.0082	0.0084	0.0086	0.0164	0.0170	0.0175
<b>4 Stories Selected Models</b>						
Model Name	<b>4A12</b>	<b>4A15</b>	<b>4A18</b>	<b>4B12</b>	<b>4S15</b>	<b>4S18</b>
R <sub>4</sub>	1.1858	1.2328	1.2727	1.0529	1.0489	1.0435
$\Delta_4$	0.0000	0.0001	0.0001	0.0000	0.0000	0.0000
$\eta_4$ (s <sup>-1</sup> )	0.1019	0.0973	0.0917	0.1260	0.1166	0.1039
$\delta_4$ (s)	0.0039	0.0041	0.0043	0.0097	0.0105	0.0118
<b>2 Stories Selected Models</b>						
Model Name	<b>2A12</b>	<b>2A15</b>	<b>2A18</b>	<b>2B12</b>	<b>2S15</b>	<b>2S18</b>
R <sub>2</sub>	1.2209	1.2182	1.2455	1.0360	1.0236	1.0192
$\Delta_2$	0.0000	0.0000	0.0001	0.0000	0.0000	0.0000
$\eta_2$ (s <sup>-1</sup> )	0.1318	0.1032	0.1020	0.1945	0.1711	0.1396
$\delta_2$ (s)	0.0030	0.0039	0.0039	0.0063	0.0072	0.0088

## Chapter 5: Nonlinear Analysis and Modeling

### **5.1. Nonlinear Dynamic Approach and Current Approaches**

#### **5.1.1. Introduction**

In brief, time history analysis in seismic design is a linear or nonlinear advanced method to calculate the response of a structure to a specific earthquake ground motion or an artificial record through numerical integration of the equation of motion. The records are mostly in form of time domain against acceleration, velocity or displacement.

Nonlinear time history analysis (THA) is a very powerful tool, the most natural and intuitive approach to analysis structure against earthquake (Pinho 2007). Nevertheless, the analysis is inherently complex and usually very time consuming. Significant effort is needed to define appropriate approximations and proper modelling assumptions to establish the numerical approach part. The THA procedure is also sensitive to the integration time step, the integration strategy, and the nonlinear incremental iterative method (Elnashai and Di Sarno 2008), (Pinho 2007), and (Powell 2004). All the complexities and time dependent process may be drastically escalated whenever the number of DOFs and involving members increase. The nonlinear THA procedure subjected to seismic loads requires continuously changing and resolving of equations due to the fact that stiffness and vibration characteristics are changing during the analysis process (Elnashai and Di Sarno 2008). Due to the chaotic character of seismic events, it is possible for a specific structure that analysis results predict collapse under a certain ground motion, whereas the same structure subjected to a given stronger record stay survived without collapse. In fact, both analyses may be correct, but the responses are different (FEMA P-750 2009).

Sophistication levels of the nonlinear models are governed by the required accuracy, the available computational resources, and, for most practical cases, the project budget. While refined nonlinear finite element (FE) models may be appropriate for the detailed study of small parts of the structure (e.g. beam to column connections, see chapter four), frame models are currently the only economical or even possible nonlinear solution to analyze structures with several hundred members (Pinho 2007).

#### **Nonlinear Dynamic Analysis Features**

As previously mentioned, nonlinear dynamic analysis can predict the nonlinear inelastic response of a structure subjected to dynamic loading. Earthquake loading may be implied by ground motion excitation. To do dynamic analysis, mass and damping must be defined to the model (Pinho 2007).

Dynamic analyses consist of direct integration of equations of motion and nonlinearity of the analysis leads to use of an incremental iterative solution procedure. In consequence, loads should be applied in predefined increments and equilibrated through an iterative algorithm (Pinho 2007). The fundamental method of iteration loop application in nonlinear dynamic analysis is to compute the internal forces and the corresponding displacement increments until either convergence is attained, or the maximum number of iteration is reached. At the end of each incremental step, the stiffness matrix is refined to reflect nonlinear changes in structural stiffness (Ibid.). For most frame analysis software, this iteration algorithm usually consists of a combination of the Newton-Raphson and/or the modified Newton-Raphson procedures.

There are two main integration methods, explicit and implicit. Basically, the explicit direct integration methods use the differential equation at a specific time,  $t$ , to predict a solution at time  $t+\Delta t$  (Wilson 2002). Whereas, the implicit methods try to solve the differential equation at time  $t$  after the solution at time  $t-\Delta t$  has been achieved (Ibid.). One of the major differences between these two methods is associated to the numerical stability. All explicit methods can be defined as conditionally stable in comparison to implicit methods which can be both conditionally or unconditionally stable (Ibid.). Conditional stability of the former

method is directly correlated with the size of time step. Although several more accurate, higher-order, and multi-step methods have been developed to solve dynamic equation, those procedures presume that the solution is a smooth function resulting from higher continuous derivatives (Ibid.). The solution of almost all nonlinear time history seismic analysis related to the accelerations as the input. Accelerations are the second derivative of the displacements, and they are not smooth functions in these cases (Ibid.). So per Wilson (2002) recommendation, implicit, unconditional stable, and single step methods can be classified as the most suitable method for seismic analysis of structures. For nonlinear analysis, during each time increment  $\Delta t$ , it is assumed that the structure is elastic and linear. Between time intervals, the geometry and/or material of the stiffness matrix are adjusted to reflect the current deformation condition (Elnashai and Di Sarno 2008).

There are different convergence check methods which typically imply three distinct criteria: displacement/rotation, force/moment, and energy based (Pinho 2007). The convergence check mostly employs at the end of each iteration. The latter two criteria are normally checked for typical advanced frame analysis software including SAP2000. The displacement/rotation criterion shows a direct local control of convergence and usually provides overall accuracy. The force/moment criterion is useful when the displacement convergence cannot show that the internal forces of the elements are adequately balanced. The highest level of accuracy and solution control is achieved by combining both displacement and force convergence criteria (Pinho 2007). For any of the abovementioned methods, convergence tolerances must be well-defined and applied before beginning of analysis procedure.

### **5.1.2. Direct-integration Time-history Nonlinear Analysis**

Basically, direct-integration method comprises solving of equation of motion under a series of time steps. Time steps are relatively small in comparison with loading duration. The nonlinearity of response directly depends on the defined properties, the loading magnitude, and the specified analytical parameters, and would be indirectly related to the duration and frequencies of the applied records. Generally speaking, the stiffness, damping, and loads may be governed by displacements,

velocities, and time. Thus, THA analysis requires to be done in an iterative manner for solving of the equations of motion. Equation 5-1 (CSI Analysis Reference Manual 2013) is shown the classical dynamic equation:

$$Ku(t) + C\dot{u}(t) + M\ddot{u}(t) = r(t) \quad [5-1]$$

In which  $K$  stands for the stiffness matrix,  $C$  is the damping matrix, and  $M$  indicates diagonal mass matrix.  $u$ ,  $\dot{u}$ , and  $\ddot{u}$  are the time dependent displacements, velocities, and accelerations of the structure respectively. Finally  $r$  is the applied load function in which for seismic analysis usually demonstrates the input ground motion. SAP2000 solves Equation 5-1 iteratively in each time step which involves re-forming and re-solving of the stiffness and damping matrices until reaching the convergence (CSI Analysis Reference Manual 2013). In cases that convergence cannot be achieved, SAP2000 divides the steps into smaller sub-steps to meet the possible converging solution (Ibid.).

In a time history analysis, the applied load may be represented as an arbitrary function of time and space. It can be generalized as (Ibid.):

$$r(t) = \sum_i f_i(t) p_i \quad [5-2]$$

Indeed, for the analytical purpose, any applied time history case can be defined in a finite sum of spatial load vector,  $p_i$ , multiplied by time function,  $f_i(t)$ . SAP2000 considers the applied accelerations to represent the spatial load vectors (CSI Analysis Reference Manual 2013), and the time function is simply consistent to the record time steps.

In current study, the dynamic input data has been devoted to the models as ground acceleration time histories which were performed at all the points of the base of the models. For each of the selected model, four (4) pairs of the scaled records, defined in section 4-2, have been applied, i.e. LPR, NAH, NOR, and WNA. As mentioned in section 4-2, the selected records from PEER seismic database (PEER Ground Motion Database, 2013) represent two orthogonal directions for each pair of

data. Every selected record has different data values for each orthogonal directions which are defined as FN and FP. Each pair of scaled record has been applied in two separate load cases, FP and FN for every single selected model to specify the input direction in the analysis. FN data series applied to the East-West direction of the models, and FP data series applied to the North-South direction of the models. These records specify the spatial load vector in Equation 5-2. Therefore, for each archetype symmetric plan model, from 2B12 to 8S18, total eight (4 x 2) different THAs have been performed. For the asymmetric plan models, 2A12 to 8A18, the models are unsymmetrical in the North-South direction. To cover this situation, an extra case of FP with negative direction for each structure model type *A* is considered as well. The original discrete time steps of the selected scaled records must be applied without any change to keep the frequency content of the records the same as of the applied record. The time steps for all the selected records were 0.005s, except for NOR data which was 0.02s. All acquired scaled records from PEER database (Ibid.) have been sorted to be in an acceptable SAP2000 (2012) input data format.

#### **Selected Integration Method**

To solve Equation 5-1, SAP2000 provides several options. The numerical integration method is one of the most important part of any time history analysis which may drastically affect the reliability and convergence of the responses. Among the available methods in SAP2000 (2012), two methods were selected: 1) Newmark method, which is cited in many references and textbooks, e.g. (Chopra 2000) and (Wilson 2002). Newmark method is powerful, almost fast, and in many cases provides a reliable and stable analysis and response results. This method has been considered as the first choice of solver in this study; 2) Hilber-Hughes-Taylor (HHT) is the default method of software (CSI Analysis Reference Manual 2013). In case of instability and numerical issues, HHT method was applied.

Newmark method is essentially a single-step integration which performs Taylor series to solve Equation 5-1 by assuming that the acceleration is linear within the time step. To be applicable for nonlinear dynamic analysis, extra iterations are needed at each time step. These extra iterations are necessary to satisfy equilibrium in

nonlinear analysis, and they impose ample and longer execution time. The Newmark base formula would be illustrated through the following equations (Wilson 2002):

$$u(t) = u_{t-\Delta t} + \Delta t \dot{u}_{t-\Delta t} + \left(\frac{1}{2} - \beta\right) \Delta t^2 \ddot{u}_{t-\Delta t} + \beta \Delta t^2 \ddot{u}_t \quad [5-3a]$$

$$\dot{u}(t) = \dot{u}_{t-\Delta t} + (1 - \gamma) \Delta t \ddot{u}_{t-\Delta t} + \gamma \Delta t \ddot{u}_t \quad [5-3b]$$

The Newmark method with gamma ( $\gamma$ ) equal to 0.5 and beta ( $\beta$ ) equal to 0.25 has been used. Indeed, the previously mentioned gamma and beta coefficient values can be defined as the same average acceleration method with trapezoidal rule (CSI Analysis Reference Manual 2013) and it may satisfy the unconditional stability requirement of the Newmark method. The stability requirement is illustrated in Equation 5-4 (Wilson 2002).

$$2\beta \geq \gamma \geq 1/2 \quad [5-4]$$

HHT method (also known as  $\alpha$  method) is essentially the modified Newmark technique (Wilson 2002). In this method, the revised equation of motion (Equation 5-1) has been introduced as:

$$M\ddot{u}_t + (1 + \alpha)C\dot{u}_t + (1 + \alpha)Ku_t = (1 + \alpha)F_t - \alpha F_t + \alpha C\dot{u}_{t-\Delta t} + \alpha Ku_{t-\Delta t} \quad [5-5]$$

All terms are similar to Equation 5-1, except  $F_t$ , which is the discrete applied load, and the parameter of  $\alpha$ , which controls the amount of numerical dissipation. In Equation 5-5, parameter  $\alpha$  can be correlated to the Newmark method through (Elnashai and Di Sarno 2008):

$$\gamma = \frac{(1-2\alpha)}{2} \quad [5-6a]$$

$$\beta = \left(\frac{1-\alpha}{2}\right)^2 \quad [5-6b]$$

HHT method generates numerical energy dissipation in the higher modes (Wilson 2002). In this method, only one parameter ( $\alpha$ ) must be defined which should be in the domain of  $-1/3 \leq \alpha \leq 0$ . Likewise, the HHT method with  $\alpha = 0$  is changed into the Newmark method when the former cited gamma and beta (0.5 and 0.25, respectively) are applied (CSI Analysis Reference Manual 2013).

### 5.1.3. Analytical Stability Conditions and Output Accuracy

To reach and conduct a stable response, as mentioned in the previous section, the Newmark method or HHT method must show analytical convergence. Per SAP2000 manual (CSI Analysis Reference Manual 2013),  $\beta = 1/4$  is recommended and applied. As mentioned earlier,  $\beta = 1/4$  means the constant acceleration in Newmark method (Ibid.). In case of zero damping, the conditional stability of the Newmark method can be defined by Equation 5-7 (Wilson 2002):

$$\frac{\Delta t}{T_{min}} \leq \frac{1}{2\pi \sqrt{\frac{\gamma}{2} - \beta}} \quad [5-7]$$

In Equation 5-7,  $T_{min}$  represent the lowest period of a structure, and  $\Delta t$  stands for time step. Structural models with larger number of DOFs usually contain some small periods that may be smaller than the selected time step (i.e. 0.1s or 0.05s and will be discussed later on). Although the above equation is defined for the zero damping models, the low value of the applied damping to the selected models in this study (Chapter 4) may create some numerical problems with the Newmark method. Incidentally, three (3) major periods of the archetype structures are considered for the selection of time step, but the selected models inherently have more than three natural periods which are also smaller than the three first major periods. Both the former and latter conditions may generate instability and convergence issues in some models. For those reasons, in cases which convergence did not meet, the second method of direct integration, HHT, was considered in this study as well.

HHT with a non-zero  $\alpha$  value often damps out responses by eliminating spurious higher modes (Elnashai and Di Sarno 2008). HHT methods are implemented

by several advanced FE and analytical programs (Ibid.). Although equal to zero demonstrates the most accurate response for HHT method, it may show excessive vibrations, unstable conditions, and disturbance in the higher frequency modes (Wilson 2002). The upper bound (zero) yields to the constant acceleration again, but to get a stable response, the lower amount of  $\alpha$  can be used. The lower bound value (i.e.  $-1/3$ ) tends to remove noise from the response up to about 10 times the selected time steps. CSI advises users to start with relatively low negative value  $-1/24$  or  $-1/48$  (Kalny 2011). In the current study, the same procedure was followed. It means for any THA case which showed poor convergence, the Newmark integration method was shifted to HHT procedure with  $\alpha = -1/48$ . In case the response was not converged again,  $\alpha$  value gradually increased to reach a stable response with the minimum applicable and possible  $\alpha$  value.

To solve the convergence issue, as mentioned earlier, the software can subdivide the time steps. Per the software recommendation, maximum and minimum substep sizes, tolerance, and maximum iterations per steps are kept as the default values, except for cases with numerical issues. For those conditions, different scenarios in term of the substep maximum, minimum, and iterations have been tried to meet convergence.

Sufficient output time steps are very important to acquire accurate response. Although the lowest time increment may technically lead to the most accurate output, in reality the analytical process would be very long and practically impossible without any computational efficiency. Often, for most structural models, the higher mode of vibrations are associated with very low effective mass, so they do not show a significant change in overall response of the whole structure. This means that it is not necessary to choose integration time increment based on the highest mode of vibration (Elnashai and Di Sarno 2008). Per CSI recommendation (CSI Analysis Reference Manual 2013) the selected time increment of one-tenth of the shortest interested time period may show precise analytical response. Table 3-3 shows the most dominant periods of the selected models in which the lowest period is about 1.1 second. Thus, the selected time step is 0.10 second for most of the THAs. The selected 0.1s for output time step provides balance between accuracy and execution

time. To capture better results for few models, a lower time increment equal to 0.05 second was applied. It should be noted that for selecting the abovementioned time steps, it is usually advised to choose the output time steps that evenly divided by the input time steps (CSI Analysis Reference Manual 2013), i.e. 0.005s or 0.02s, which has been fulfilled as well.

Another aspect of output data which must be monitored is the free vibration response. From the dynamic analysis standpoint, the structure response to seismic load is not limited to the total ground motion record time. The total vibration time of a structure under seismic excitation may continue much longer than the actual seismic duration time until completely damped out. This effect is called free vibration part of response in structural dynamic terminology, and sometimes the free vibration response might be very dominant, particularly for some cases such as low damping structures. Another example is the possible effect of resonance in case that one of the structure vibration period falls into a close range with the dominant frequency content of the applied seismic record. To consider the possible free vibration effect, for all THA cases, minimum 5.0s has been added to the output time duration of each applied seismic record to acquire free vibration response. Furthermore, the base shear and/or top displacement response under each seismic record has been reviewed in term of maximum response amplitude. If the approximate last pike of the response in the end of 5.0s extra duration time was less than 20% of the maximum amplitude, the free vibration extra 5.0s time has been considered sufficient. Otherwise, the total output analysis time has been increased up to the point that the response damped up or the ratio of the approximate last vibration pike to the maximum pike amount reached to less than 20%. As an example, Figure 5-1 is shown the base shear of 4A18 model in E-W direction under FN component of LPR record. The total analytical time duration has been increased up to 15s to reach a complete damped response.

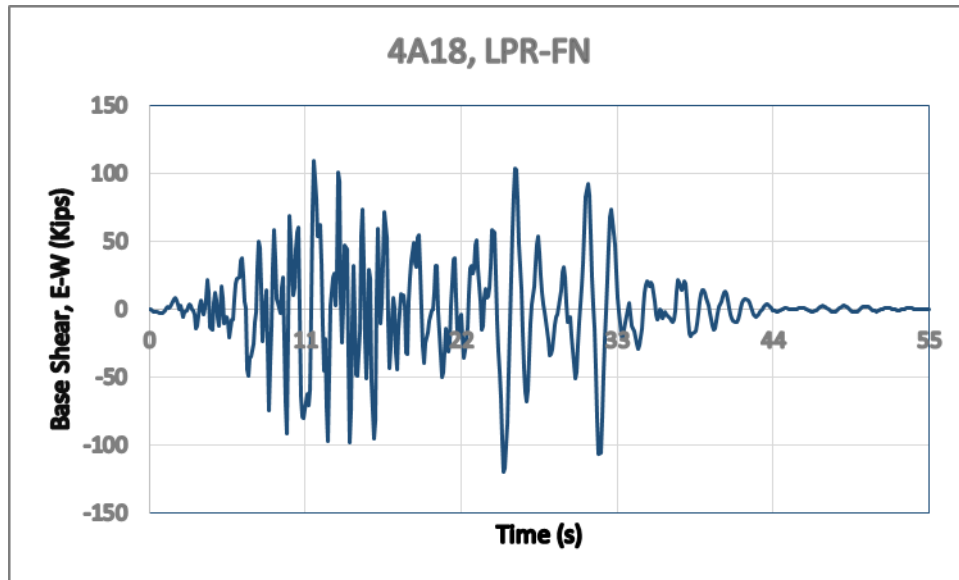


Figure 5-1, Example of extended analysis time duration up to damped free vibration

## 5.2. Nonlinear Static Approach on Regular/Irregular Structures

### 5.2.1. Introduction

By definition, Nonlinear Static Analysis (NSA) is a simplified analysis procedure to estimate earthquake demands on structures (Moehle 2006). The loading procedure consists of two major steps. The first step is applying gravity loads. The next step is monotonically increasing lateral forces in a constant or time-varying profile over the height of the structure (Moehle 2006). The entire building pushes in the same direction of an applied lateral load. The incremental lateral load distribution represents the inertia forces during expected earthquake and should reflect response at the floor levels (NEHRP 2010b). The lateral load distribution is usually proportional to the floor masses and the fundamental mode of vibration. Although other lateral force distributions are applicable, several studies have illustrated that those methods have little effect on the accuracy of NSA procedure (NEHRP 2010b). The lateral load is applied step by step until the imposed displacements reach the pre-defined target displacement. The target displacement shows the demand for the structural component which may be compared with the corresponding acceptance criteria for

the desired performance level (e.g. Figure 4-9). Overall demand parameters, such as story drifts and base shears, may also be checked (Ibid.).

All methods of nonlinear static analysis fundamentally perform a series of sequential elastic analysis which are superimposed to build an approximate force-displacement curve. The reduced resistance of yielding element is comprised by adjustment of the mathematical model. Pushover curves illustrate approximately the structure behavior after exceeding the elastic limit (Poluraju and Nageswara Rao 2011). This diagram shows the overall capacity of a structure (Figure 5-2). The basic approach for all of these methods is almost the same, and the most important differences rely on the determination of displacement demand. The foremost pertinent methods are namely: 1) FEMA 273 which further developed in FEMA 356 and NEHRP provisions as Displacement Coefficient Method; 2) ATC 40 which is based on spectrum method as Capacity Spectrum Method; 3) N2 procedure which is relevant in the Eurocode; and 4) Modal Pushover Analysis (MPA); (Fajfar 2002), (Chopra and Goel 2004), and (Fragiadakis et al. 2011). Mathematically, pushover analysis may not guarantee a unique solution (CSI Analysis Reference Manual 2013), particularly in unstable conditions, such as loss of strength or in cases where the geometric nonlinearity is dominant. Due to the nature of pushover analysis, the overall displacement shape of a model would be dissimilar for different lateral load patterns, although the target displacement might be the same for all the applied patterns (Ibid.)

#### **Nonlinear Static versus Nonlinear Dynamic Analyses:**

Nonlinear dynamic analysis methods usually provide more accurate structural response to ground motion (NEHRP 2010b). In fact, THA yields to more reliable assessment of earthquake performance in comparison with NSA. However, NSA procedure provides a convenient and fairly reliable method for structures which have the first vibration mode dominant (Ibid.). Comparing the deformed geometry from a pushover analysis and the elastic first-mode vibration shape is a simple way to check the overall accuracy of NSA procedure. In general, NSA methods are mostly suitable for low-rise structures with less than about five stories and symmetrical regular configurations (NEHRP 2010b). Slight torsional irregularities may be allowed in case

the three (3) dimensional structural model is used (Aydinoglu and Önem 2010). However, there is no doubt that application of NSA (particularly single-mode pushover) to high-rise buildings, irregular structures, and irregular bridges comprising three-dimensional response would lead to incorrect and unreliable results (Ibid.). Predominantly, for the structures that their first mode is the dominant vibrations mode nonlinear static analysis provides good estimates of local inelastic deformations and global deformations. It has been mostly recognized that the pushover methods, in any form, cannot capture the response of irregular structures, vertically or horizontally, with an acceptable accurate range. Even the modal pushover analysis, which has been developed for irregular structures, cannot provide a reasonable estimate of structure response where a soft first story exists (NEHRP 2010c). In case of a concentrated strength irregularity in a single story structure, NSA is expected to provide good estimates of drift and force demand parameters (NEHRP 2010c). In comparison, THA has no limitation for any type of irregularity or higher mode shape effect, and nonlinear static analysis can be used to just globally identify some possible soft story mechanisms or bad configuration of structures in design (Marsh and Browning 2002).

The limitations of NSA methods are related to their theoretical assumptions. The base of NSA procedure relies on assumption in which the response of a multi-degree of freedom system is directly related to the response of an equivalent single-degree of freedom (SDOF) system as shown in Figure 5-2 (Fragiadakis et al. 2011). As mentioned before, often this assumption is not accurate enough as higher modes may contribute considerably to some element demands. The accuracy of pushover analysis is usually evaluated relative to the results of nonlinear dynamic analyses (Ibid.). Similar to THA methods, pushover analysis is sensitive to the type of inelastic mechanism and to the modeling of the structural components. NSA methods are generally unable to develop multiple inelastic mechanisms. In contrast, THA methods are capable to provide variety of modal interactions and variability in time-response function produce response traction in the nonlinear time history analyses. Incidentally, NSA methods mostly tend to overestimate deformation demands where the defined mechanisms are pre-determined to occur (Fragiadakis et al. 2011).

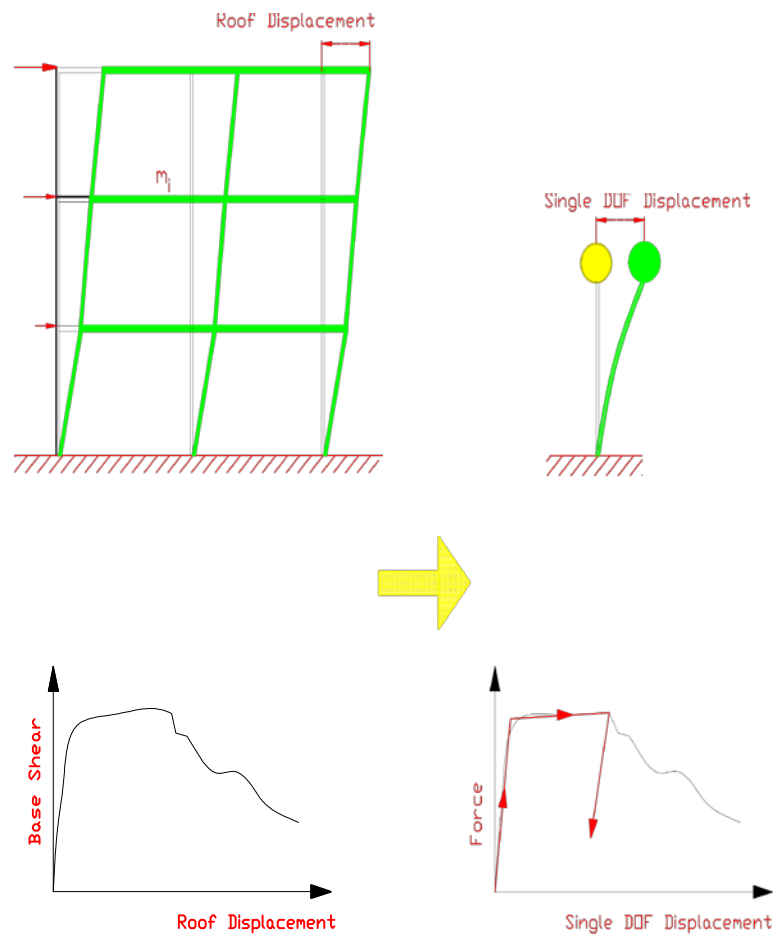


Figure 5-2, Pushover analysis approach: conversion of a system response (left) to equivalent SDOF system (right) (Adopted from Moehle 2006)

Nonlinear dynamic analysis has ability to reduce uncertainty in demand predictions (NEHRP 2010b). On the other hand, in nonlinear or linear static analyses the uncertainties are considered by simplified analysis assumptions. It should be mentioned that even with nonlinear dynamic analyses it is practically impossible to determine precisely all the variability in demand parameters (Ibid.). In comparison, selection of a suitable set of ground motion records remains a difficult controlling variable to predict accurately. NSA can eliminate the selection of the earthquake record set conveniently. Nonlinear static analysis may simplify analysis and design methods to evaluate maximum drift, story drift ratio, rotational response and demands, and element shear (Marsh and Browning 2002).

Based on the results of a vast study, FEMA 440 summarized the practical implications of NSA as (FEMA 440 2005):

- NSA methods generally provide reliable estimates of maximum floor and roof displacements;
- NSA methods are not able to predict accurate maximum story drifts, which are mostly seen within flexible structures;
- NSA methods are very poor to predict story forces such as shears and overturning moments;
- The first mode load vector has been assumed due to the relatively good displacement estimates;
- Multi-mode pushover analysis, i.e. multiple load vectors proportional to the structure mode shapes, statistically shows better estimates in inter-story drifts over the heights of the structures;
- When higher modes are significant, the FEMA 356 methods may not be reliable;
- Explicit limitations to show when NSA methods produce reliable results are elusive.

Based on the result of aforementioned study, FEMA 440 (2005) cites that in many cases, a single time history analysis of a MDOF model may present better indications of drifts and story forces than any of the approximate SDOF estimates.

It should be noted that up to now, there is not any simple method which provides a reliable and applicable approach for multistory buildings. Thus, THA still remains the most powerful method for seismic performance evaluation (Fragiadakis et al. 2011). As a general rule, NSA is very useful and should be part of the inelastic structural evaluation process. NEHRP (2010c) provides the following list for situations where nonlinear static analysis is valuable:

- 1) Checking and debugging a nonlinear analysis model;
- 2) Overall evaluating of modeling assumptions;
- 3) Improvement in understanding of yielding mechanisms and deformation demands;
- 4) Examination of load path adequacy;
- 5) Alternative design parameters and the effect of variations in the component properties on nonlinear and inelastic response can be reviewed;

- 6) Behavior of structure in close to collapse condition can be studied;
- 7) Estimation of the lateral strength of the structure;
- 8) Structural over-strength associated with seismic design can be estimated;
- 9) As a general role: “Providing information to help establish a force-displacement capacity boundary of a structure in order to estimate global response characteristics such as roof displacement using an equivalent single-degree-of-freedom system”;
- 10) An overall understanding of base shear versus roof displacement response. Besides, it may help to estimate post-yield stiffness and related displacement at which the tangent stiffness becomes clearly negative;
- 11) Approximate determination of excessive deformation locations. Those locations may need more detailed study;
- 12) Problems associate with overloading components with inadequate ductility can be discovered;
- 13) Potential problems caused by story-based strength and stiffness discontinuities can be traced;
- 14) Possible problems caused by P- $\Delta$  effects and strength weakening can be found.

#### **Fundamental of NSA Formulation**

Pushover solution is basically derived from static analysis by utilizing an incremental-iterative solution of the static equilibrium equation. In each step the behavior is assumed linear and for a small amount of load increment ( $\Delta F$ ) equilibrium can be expressed as (Elnashai and Di Sarno 2008):

$$K \Delta x = \Delta F \quad [5-8a]$$

Considering load increment Equation 5-8a may be rewritten as:

$$K_t \Delta x + R_t = F \quad [5-8b]$$

In which  $K$  is the stiffness,  $\Delta x$  is the increment, and  $K_t$  denotes the tangent stiffness for the current load increment.  $R_t$  represents the restoring forces at the beginning of the load increment (Ibid.), and it may present as:

$$R_t = \sum_{k=1}^{j-1} K_{t,k} \Delta u_k \quad [5-9]$$

Where  $j$  is the incremental step and  $\Delta u_k$  is the local deformation at each corresponding step. For each increment, the resistance of the structure is re-evaluated from the internal equilibrium. The tangent stiffness matrix may require to be updated as well. Then the out-of-balance forces evaluate and re-apply to satisfy convergence criteria. When convergence is achieved, the tangent stiffness matrix is updated and another increment displacement is performed (Elnashai and Di Sarno 2008).

For any pushover method, some important parameters must be defined in order to analyze the system and provide numerical solution. Distribution pattern along the structure height (e.g. uniform or triangular), magnitude, target displacement, the number of applied load steps, iterative strategy, and convergence criteria are the most significant parameters (Ibid.).

### **5.2.2. Estimation of the Displacement Demand per FEMA 356 NSA Procedure**

FEMA 356 (2000) NSA requires to accomplish three (3) basic procedure: 1)- develop the pushover curve; 2)- estimate the target displacement; and 3)- check acceptability criteria (Goel and Chopra 2004). Nearly all FEMA 356 NSA concepts and requirements are accepted in ASCE 41-06 (2007a) as well. Per FEMA 356 (2000) the control node shall be located at the center of mass at the roof of a building. FEMA 356 NSA requires to establish a pushover curve which basically shows the relationship between the base shear and lateral displacement of a control node (FEMA 356 2000). As mentioned before, to develop the pushover curve, at first step the gravity loads should be considered. After that, a specified height-wise distributed lateral forces must be monotonically applied to the model. Then, the behavior of the structure is categorized by a capacity curve that illustrates the base shear force versus the displacement of the roof (Figure 5-2) (Inel and Ozmen 2006). This is the central concept of NSA in FEMA 356. Furthermore, this curve can be used to determine some important points for the target displacement calculation, such as effective lateral stiffness of the structure ( $K_e$ ) or yield strength ( $V_y$ ) (FEMA 356 2000). The

acceptability criteria and evaluation of the performance level will be briefly discussed in the next chapter.

### **Target Displacement**

Target displacement is the key element of NSA procedure. The FEMA 356 NSA target displacement formula is presented in Equation 5-10, which is basically a coefficient procedure. The coefficient method, which is commonly use for both research and practice (NEHRP 2010c), is the most often used pushover method in practice and several software platforms, such as SAP2000. The target displacement is computed by multiplying the elastic deformation of an SDOF system by four (4) coefficients, namely:  $C_0$ ,  $C_1$ ,  $C_2$ , and  $C_3$  (Goel and Chopra 2004). Indeed, in order to estimate the inelastic displacements, these modifier factors should apply to the spectral displacement of a system (NEHRP 2010c).

$$\delta_t = C_0 C_1 C_2 C_3 S_a (T_e^2 / 4\pi^2) g \quad [5-10]$$

In which  $C_0$  accounts for the modification factor to relate spectral displacement of an equivalent SDOF system to the roof displacement of the building at the control node;  $C_1$  stands for the modification factor which applies to relate anticipated maximum inelastic displacements to displacements calculated for linear elastic response;  $C_2$  represents effects of pinching, stiffness degradation, and strength deterioration in hysteresis curve on maximum displacement response; and  $C_3$  accounts for the increased displacements due to P- $\Delta$  effects (FEMA 356 2000) and (Goel and Chopra 2004).  $T_e$  is the effective fundamental period of the building in the direction of push (unit: second).  $S_a$  denotes the response spectrum acceleration at the effective fundamental period. This item depends on the site seismicity and damping ratio of the building in the direction of push. Finally  $g$  is the acceleration of gravity (FEMA 356 2000).

Each of the afore-said modification factors has its own definitions and limitations. They are also function of some other factors. In FEMA 356 (2000), there are some recommended and prescribed values and/or calculation procedure to compute these coefficients. SAP2000 has built-in FEMA 356 target displacement

criteria (SAP2000 2012), which is considered in pushover analysis of the selected models. Within the framework of this study, the pushover method is the supplementary procedure. Thus, for the sake of brevity, the more detail of equation 5-10 coefficients are not presented here. For verification, one of the software calculated target displacement has been ratified in Appendix C. Tables 5-1a and b show the calculated target displacements and the corresponding base shears for the archetype symmetric and unsymmetric plan models, respectively, per FEMA 356 (2000).

Table 5-1a: NSA results for the symmetric plan models

<b>Model tag</b>	<b>2B12</b>		<b>2S15</b>		<b>2S18</b>	
Pushover direction	E-W	N-S	E-W	N-S	E-W	N-S
Target displacement (ft)	0.21	0.20	0.24	0.23	0.29	0.28
Base Shear (kips)	88.41	92.70	69.62	76.26	65.22	51.83

<b>Model tag</b>	<b>4B12</b>		<b>4S15</b>		<b>4S18</b>	
Pushover direction	E-W	N-S	E-W	N-S	E-W	N-S
Target displacement (ft)	0.34	0.32	0.37	0.34	0.41	0.39
Base Shear (kips)	107.48	114.37	103.66	110.23	92.52	98.63

<b>Model tag</b>	<b>8B12</b>		<b>8S15</b>		<b>8S18</b>	
Pushover direction	E-W	N-S	E-W	N-S	E-W	N-S
Target displacement (ft)	0.62	0.57	0.65	0.60	0.67	0.62
Base Shear (kips)	117.99	123.01	117.53	125.07	117.26	125.08

Table 5-1b: NSA results for the asymmetric plan models

Model tag	2A12			2A15			2A18		
Pushover direction	E-W	N-S	N-SN	E-W	N-S	N-SN	E-W	N-S	N-SN
Target displacement (ft)	0.19	0.19	0.20	0.23	0.24	0.25	0.24	0.44	0.25
Base Shear (kips)	115.43	126.20	105.31	86.76	97.97	81.15	95.43	147.23	91.47

Model tag	4A12			4A15			4A18		
Pushover direction	E-W	N-S	N-SN	E-W	N-S	N-SN	E-W	N-S	N-SN
Target displacement (ft)	0.22	0.24	0.24	0.24	0.26	0.26	0.26	0.29	0.29
Base Shear (kips)	149.94	165.26	129.49	152.11	165.77	129.51	151.39	168.16	131.21

Model tag	8A12			8A15			8A18		
Pushover direction	E-W	N-S	N-SN	E-W	N-S	N-SN	E-W	N-S	N-SN
Target displacement (ft)	0.47	0.53	0.54	0.49	0.56	0.56	0.50	0.58	0.58
Base Shear (kips)	140.77	163.86	117.76	140.86	160.43	115.41	140.52	162.23	113.04

### 5.2.3. Analysis Assumptions and Approach

The majority of basic assumptions for nonlinear method, described in Chapter 4, are the same for NSA procedure. For instance, the damping equal to 5% and the same plastic hinge assumptions are kept the same. In current study, the displacement coefficient method defined by FEMA 356 (2000) has been carried out, which is explained in the previous section. SAP2000 (2012) has few built-in target displacement methods and FEMA 356 coefficient is one of them. For the first estimate, the maximum monitored displacement is defined as 2% of the height for the associated DOF. For example, for 8S18 model, the maximum monitor displacement with 102 feet total height would be equal to 2.04 feet. Per FEMA 356 (2000), the push shall be continued after the target point. The increment percentage is usually

assumed minimum 150% (FEMA 356 2000). Thus, the computed target displacement by software has been compared with 2% pre-defined value. In very few cases that the 2% value was less than 150% of the calculated target displacement by software, the maximum monitored displacement was increased to cover FEMA 356 criteria. For all pushover cases, a specific joint (master point at plan geometric center explained in chapter 3) at the roof level has been allocated for the maximum monitoring response. It should be mentioned that the maximum monitored displacement is different from the FEMA 356 (2000) target displacement. The former just relates to the structure height, but FEMA 356 target displacement corresponds to several factors which were explained before. Despite the fact that 2% maximum monitored displacement can be usually reached for well seismically designed structures, the selected models were pushed monotonically in order to reach the FEMA 356 target displacement or lost equilibrium otherwise. In case a model reached the FEMA 356 target displacement, the pushover continued beyond that point up to the defined maximum monitored displacement or failure case whichever occurred first.

For each archetype symmetric plan model, from 2B12 to 8S18, two (2) different NSAs have been performed, i.e. in North-South and East-West directions. For the asymmetric plan models, 2A12 to 8A18, an extra pushover case with negative action in North-South direction for each A model is considered as well (N-SN case in table 5-1b). Also, the same nonlinear load orders in THA analyses are applied for NSA procedure. It means nonlinear P- $\Delta$  is the first nonlinear case. The nonlinear dead load and live load (defined load combination in chapter 4) has been considered at second stage of each analysis which has been performed at the end of the previous case. Then the pushover case has been continued from state at the end of nonlinear dead-live load case.

#### **Load and Displacement Controls**

The applied nonlinear cases for pushover normally are divided by Load control and Displacement control. Per CSI manual (CSI Analysis Reference Manual 2013) the load control applied to the cases in which the magnitude of the load is known. So the gravity load cases (Dead load and Live load) are considered as Load control cases in this study. The same situation also is applied for P- $\Delta$  case. On the

other hand, the displacement control would be applied to the cases in which the desired or acceptable displacement of a structure is predictable, but the required load to get the target displacement is unknown. The structural elements which may lose the load carrying capacity or the whole model may become unstable during the course of analysis under the displacement case (Ibid.). All the lateral displacement cases in current study are covered under the displacement control conditions.

Displacement should be similar or close to the actual possible displacement due to earthquake. A force-displacement pattern equivalent to the expected distribution of the inertial force (mass) may reflect the closest condition. Therefore, the load pattern was applied based on the seismic load force distribution which almost always reflects mass contribution in a frame type structure. SAP2000 has a built-in auto lateral load pattern which covers several codes (SAP2000 2012). IBC (2006) linear seismic force code application was selected for the applied displacement pattern. Per FEMA 356 (2000) at least two force distributions must be considered. It is shown that the use of multiple load patterns may not necessarily provide more benefits and improvement between NSA and THA results (NEHRP 2010c). Based on this finding, the use of a single load pattern was suggested as well (Ibid.). Thus, due to the fact that the NSA is the supplementary method in this study and it is found that the more load patterns may not lead to more accurate result, the load pattern based on IBC 2006 seismic load distribution is considered enough as far as this study is concerned.

#### **Solution Control**

SAP2000 solves the nonlinear equations iteratively in each load or displacement step and incrementally for the whole procedure (CSI Analysis Reference Manual 2013) to achieve convergence. To accomplish the pushover analysis, the program re-forms and re-solves the stiffness matrix in each step. Similar for the output control, for the models without any major convergence issues, the program default maximum total steps, null steps, maximum iteration per steps, and iteration tolerance have been used. In several cases, through application of the default values, the models did not reach the target displacement. Thus, these steps have been revised or increased accordingly. Per software recommendation (CSI Analysis

Reference Manual 2013), Null steps occur during the pushover analysis due to: 1)- a frame hinge unloading; 2)- a significant event (e.g. yielding) triggering another event; 3)- iteration cannot be converged and therefore a smaller step size is tried. For the iteration, the logic of program is basically established to apply constant-stiffness to solve for equilibrium. If convergence has not been completed, Newton-Raphson iteration would be applied at next trial. If both previous methods fail, the program reduces the step size and repeats the process for that step (Ibid.). For the models which may show numerical or geometrical instabilities, smaller tolerance values, higher number of iteration for the whole analysis, and increasing of the null steps, individually or combined with each other, were used to solve the issues.

Hinge unloading is another important portion in SAP2000 pushover computation process with frame hinge properties models. Technically, for case of ultimately yield hinge, the program removes the loads which were carrying by the hinges to redistribute them to the rest of the model (CSI Analysis Reference Manual 2013). Indeed, hinge unloading would be carried out by the software whenever the stress-strain curve illustrates a drop in capacity, such as from point C to D (Figure 4-9). Specifically, unloading along a negative slope may create instability for pushover analysis and can be one of the reasons not to reach a unique mathematical solution (CSI Analysis Reference Manual 2013). The program provides three (3) different unloading methods for NSA: 1)- Unload Entire Structure which is the default case of the program and has been used as the first option during analysis process of the selected models. This method usually needs a moderate number of null steps, and it may fail if two hinges start unloading almost at the same time (CSI Analysis Reference Manual 2013). Specifically, when one hinge requires reducing the load while the other hinge needs to increase the load simultaneously the response may not be converged. 2)- Apply Local Redistribution is the second unload method which has been used for very few NSA cases in this study. Instead of unloading of the entire model, only the elements which are involving with hinge process will be unloaded. In this method, basically, SAP2000 applies a temporary and localized internal load to reverse the strains and transferring the removed loads to adjacent elements (Ibid.). 3)- The last method is called Restart Using Secant Stiffness. This method is mentioned as

the least efficient method and provides the lowest likelihood of failure among three unloading techniques. Failure in this method may occur when gravity load implies large enough stress in a hinge to make secant negative (Ibid.). The latter method, which is developed in FEMA 440 (2005) was performed for most of the analytical models in this study.

For output proposition, the software default maximum and minimum numbers of saved steps have been accepted in most cases. In some conditions with convergence issues, the number of maximum steps was increased. These steps are only useful for output review and they do not change the response of the structures.

## Chapter 6: Parametric Study

### 6.1. Evaluation Overview

Inherent Capacity (IC) is the lateral capacity of a structural system to resist against earthquakes by using structural capacity of the gravity or wind design alone, provided that seismic resistance requirements are not considered in the original design. In this chapter, effect and resistance of the selected models due to their IC and under the different irregularity configurations were compared. There is ongoing debate regarding impact of seismic uncertainties (PEER/ATC 72-1 2010). Due to significant uncertainties associated with seismic activity, it was suggested that modeling uncertainties should be ignored (PEER/ATC 72-1 2010) which is followed in this study. In fact, a more refined and complex computer analysis may exceed the accuracy of its input. It can be understood by considering the uncertainties about soil behavior, its inherent lack of homogeneity, and rare seismic event in low to moderate active zones.

Usually, yielding due to compression and bending at the base of columns, i.e. at top of foundation or basement podium, is acceptable (Naeim 2010), but simultaneous top and bottom yielding at the first story cause story mechanism is unacceptable which is common in soft story action (Chapter 2). The story mechanism occurrence will be reviewed in selected models where plastic hinges form at both ends of any vertical member in the analytical system. Although it is possible for the central columns to have slightly higher stiffness, due to increase in axial load (Priestley 1995), it is assumed that all the columns at each level with same section have same stiffness. Actually, when different response under variable load application is performed, it would be impossible to assign different stiffness to columns (Priestley 1995). Therefore, all the results are presented with accepting the previous assumption.

### **Acceptability Criteria**

The basis in FEMA 356 (2000) to assess the acceptance criteria relies on the performance of structural elements, which play a critical role on the overall performance of the structure (Kunnath 2005). As a result, acceptance criteria are quantified at the component level. The deformation (or force demands) in each structural component is calculated at the end of the applied THA input time duration or at the end of the target displacement for NSA method. Then, the response would be compared against acceptability criteria set forth in the FEMA 356 (Goel and Chopra 2004). The acceptability criteria depend on several factors: material (e.g. concrete or steel), type of member (e.g. beam, column), importance of the member in a system (e.g. primary or secondary), and the performance level (e.g. immediate occupancy, life safety, or collapse prevention) (Goel and Chopra 2004). Tables 4-3 and 4-4 show the criteria in accordance with the performance level. FEMA 356 (2000) and ASCE 41-06 (2007a and 2007b) define performance level which is briefly illustrated in table 6-1 with regard to the main elements of concrete frame structures.

SAP2000 follows the same FEMA 356 acceptance criteria (SAP2000 2012). Depending on the level of plastic hinge formation, the software shows the possible damage stage in a hinge. The overall concept for damage level is shown in Figure 4-9, and the program illustrate seven (7) different levels associated with the response stages, namely B, IO, LS, CP, C, D, and E.

### **Global Failure Criteria**

The possibility of global failure in each story of the selected models was checked. As mentioned above, acceptability criteria in each member is considered to cover the local damage consideration. One key factor that determines the global failure was assumed to coincide with story drift by preventive inter-story drift limit per FEMA 356 (2000) rehabilitation requirements. Structural performance levels and damage for vertical elements is presented in table C1-3 of FEMA 356 (2000). This table for concrete frames states that maximum acceptable drift for Collapse Prevention is 4%, Life Safety 2%, and 1% is the acceptable range for Immediate Occupancy. Notwithstanding of mechanism formation or hinge damage level, a

structure was considered to have collapsed in case the drift exceeded 4% which is in agreement with other irregularity research studies such as by Athanassiadou (2008).

Table 6-1: Performance levels\*

Acceptance level	Collapse prevention (CP)	Life safety (LS)	Immediate occupancy (IO)	Operational (elastic response)
Structure Damage				
Overall damage	Severe	Moderate	Light	Very light
General condition	Low residual stiffness and strength. Columns still bear loads. Considerable permanent drifts. Structure is near collapse	Strength and stiffness decrease significantly in all stories. Gravity-load-bearing elements still work. Some permanent drift. Structure may be beyond economical repair.	No permanent drift. Structure holds original strength and stiffness. Minor cracking of structural elements. Structure is in repairable condition.	No permanent Drift. Structure substantively keeps original strength and stiffness. Minor cracking of structural component. Very minor structural repair may require.

\*Partially adopted from (Poluraju and Nageswara Rao 2011)

### Plastic Hinge Mechanism

Plastic hinge formation has been obtained at different displacement levels for each direction under every single applied record set or pushover case. The number of hinge formations have been counted and presented in Appendix D for all selected models. The acquired and counted hinge formation levels are summarized in the subsequent section (section 6-2). The illustrated graphs in section 6-2 are presented based on the damage stages which previously defined through statistics results in Appendix D. Graphs are consist of two major parts, the first story results and the average of all stories which are also divided into beam and column hinge formations (in case of occurrence). As briefly explained in chapter 4, arithmetic average of nonlinear results is a routine procedure in the seismic codes. Parenthetically, the main

objectives of this study are to develop and investigate irregularity effect on the first story. Therefore, the number of hinge formations in the first level is considered.

As mentioned in chapters 4 and 5, the asymmetric archetype models (*A* types) have been considered in the N-S direction with two different directions of seismic excitation or pushover cases. Both of these cases are exactly the same except the direction of application which has 180 degree difference. For the symmetric models (i.e. *B* and *S* models), the direction of excitation would not change the result, whereas for *A* type structures the difference of stiffness may lead to dissimilar response in the unsymmetrical direction. From Appendix D, it can be seen that reversing of applied record or pushover direction may increase or decrease the response. Although opposite direction has affected the results, the effect of implied excitation itself on the response of asymmetric models is beyond the scope of this study. In order to cover the worst possible case for *A* type models, the damage stages are comprised of the arithmetic mean of each individual condition. Thus, for *A* type models at the first step, the average of both N-S directions was calculated, then the computed average was used to acquire the average of whole stories of the system or the first story hinge response. In case the average number shows both integer and fraction digits, the fraction part has been rounded up to the next integer digit. For instance, in table D-1 of appendix D for 2A12 model, under N-S direction (FP), the first story hinge formation for columns is displayed that the total eight (8) type B hinges have been formed due to LPR excitation. For the same condition but with reverse excitation, the total number of formed hinges is equal to 11 which is shown in the prentices. The average number for this case is considered equal to 10.

## **6.2. Hinge Formation Results**

Graphs 6-1a to 6-1f show the hinge formation results for the two stories models. In the same way, graphs 6-2a to 6-2f and 6-3a to 6-3f illustrate the hinge formation results for the four (4) and eight (8) stories models, respectively. Numbers in the 1<sup>st</sup> story bar represent the arithmetic means of results for all seismic cases for the first level (i.e. averages of hinge formation for LPR, NAH, NOR, and WNA). For

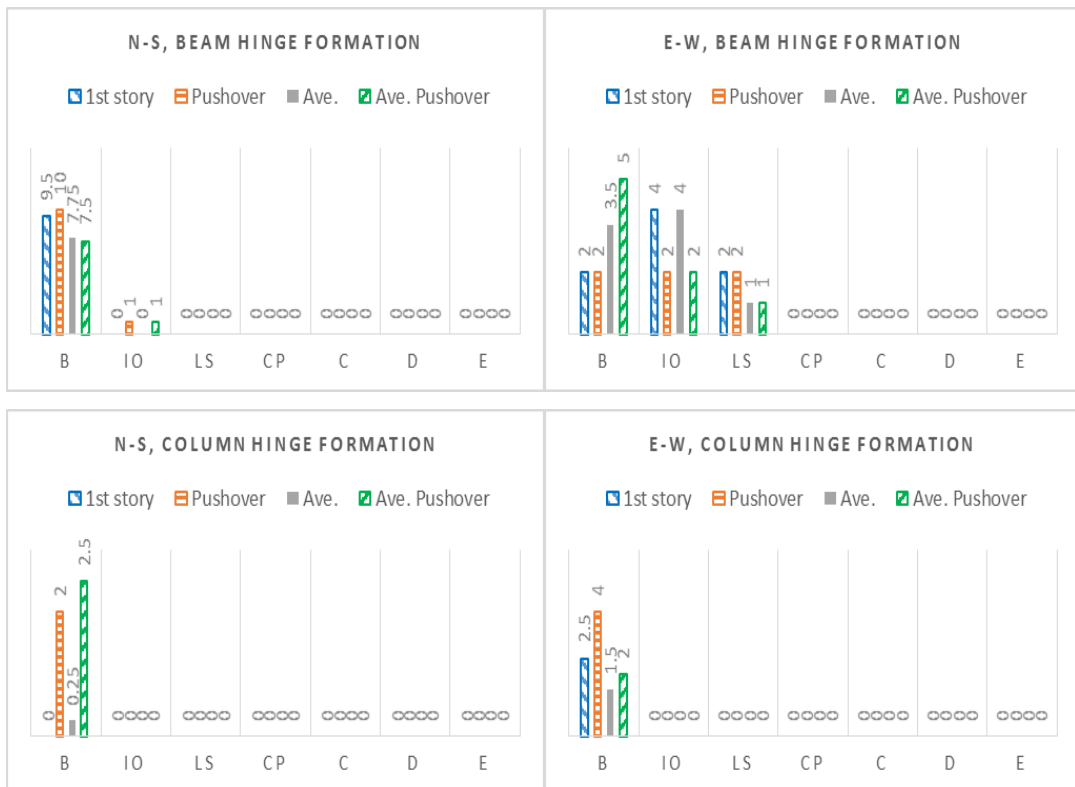
the same level, the number of hinge formation under pushover case represents in the adjacent bar. Averages of hinge formations for all four seismic excitations and pushover procedure, for whole structural defined elements, are presented under Ave. and Ave. Pushover bars, respectively. As previously mentioned, results have been classified under the direction of analysis and type of element (i.e. beams or columns). In these cases, the numbers are rounded up to maximum three decimal points, and nil number is used for each condition that the selected models under all cases did not reach the corresponding level of hinge formation.



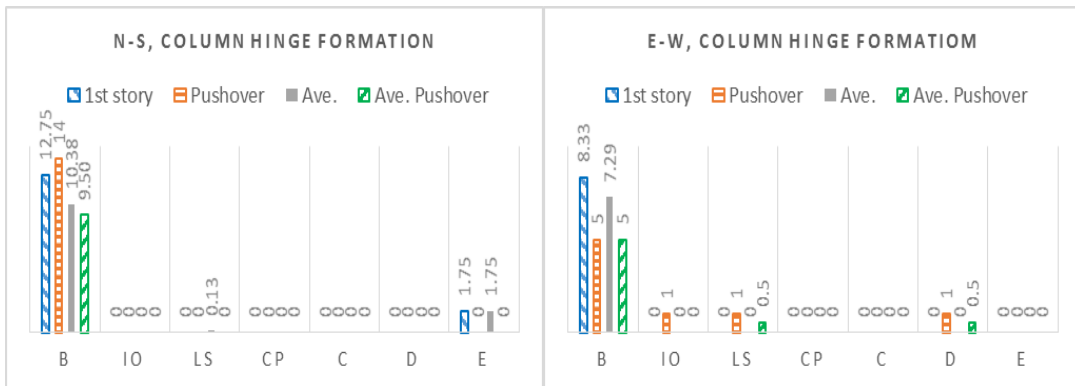
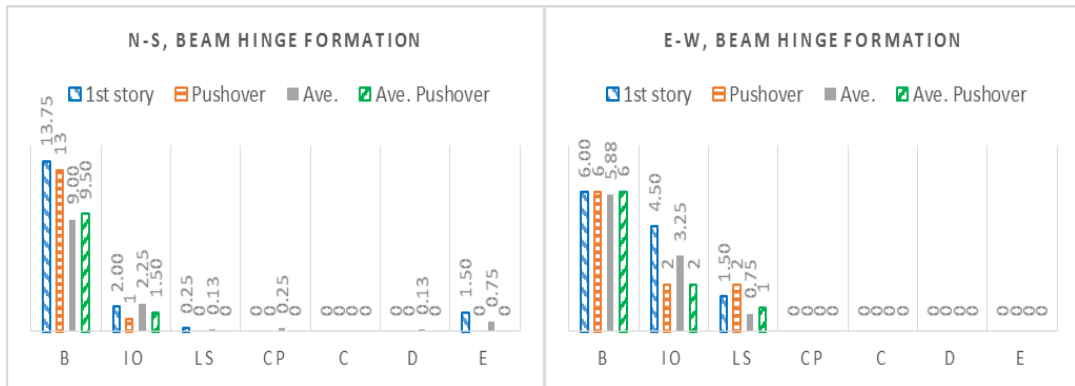
Graph 6-1a, Hinge formation results for selected model 2B12



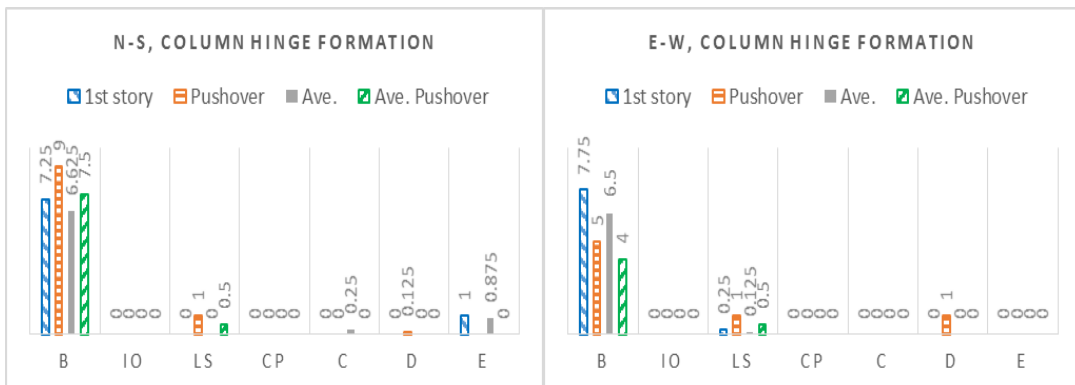
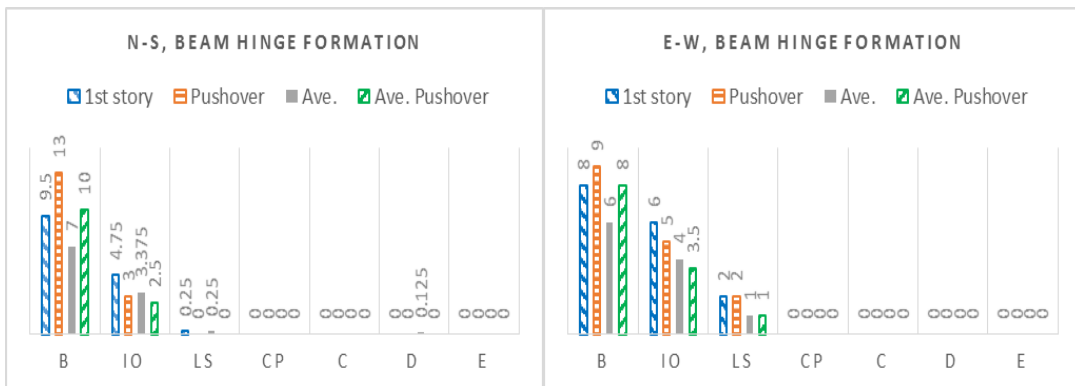
Graph 6-1b, Hinge formation results for selected model 2S15



Graph 6-1c, Hinge formation results for selected model 2S18



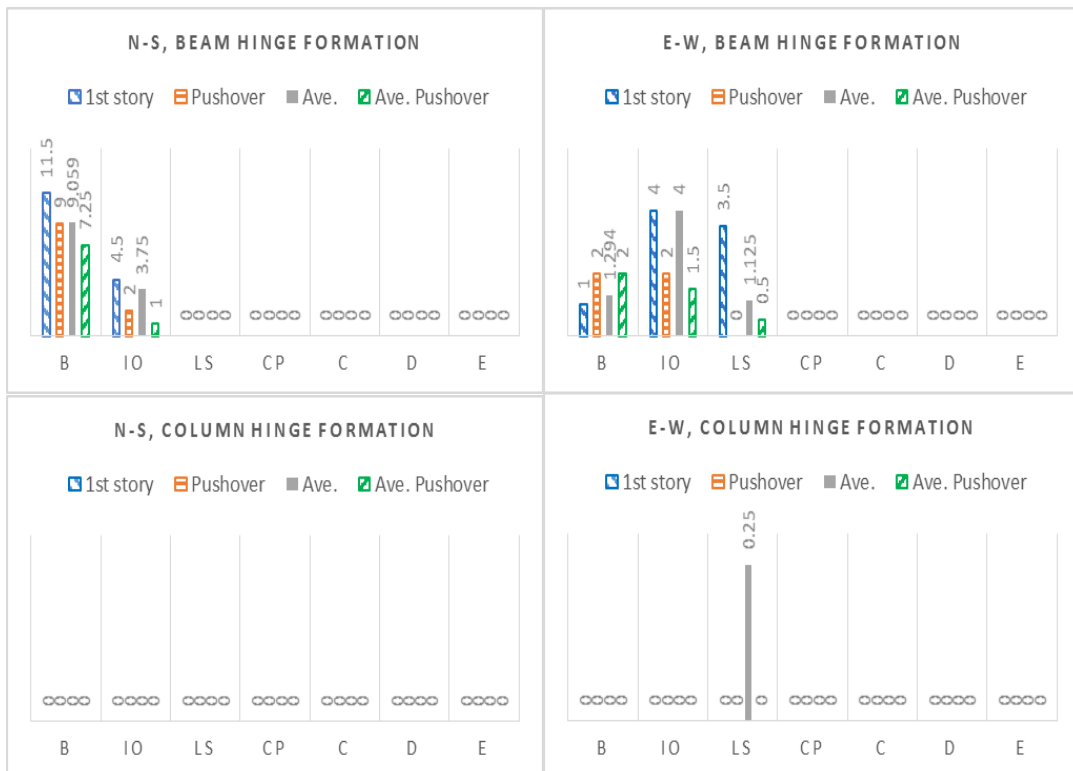
Graph 6-1d, Hinge formation results for selected model 2A12



Graph 6-1e, Hinge formation results for selected model 2A15



Graph 6-1f, Hinge formation results for selected model 2A18



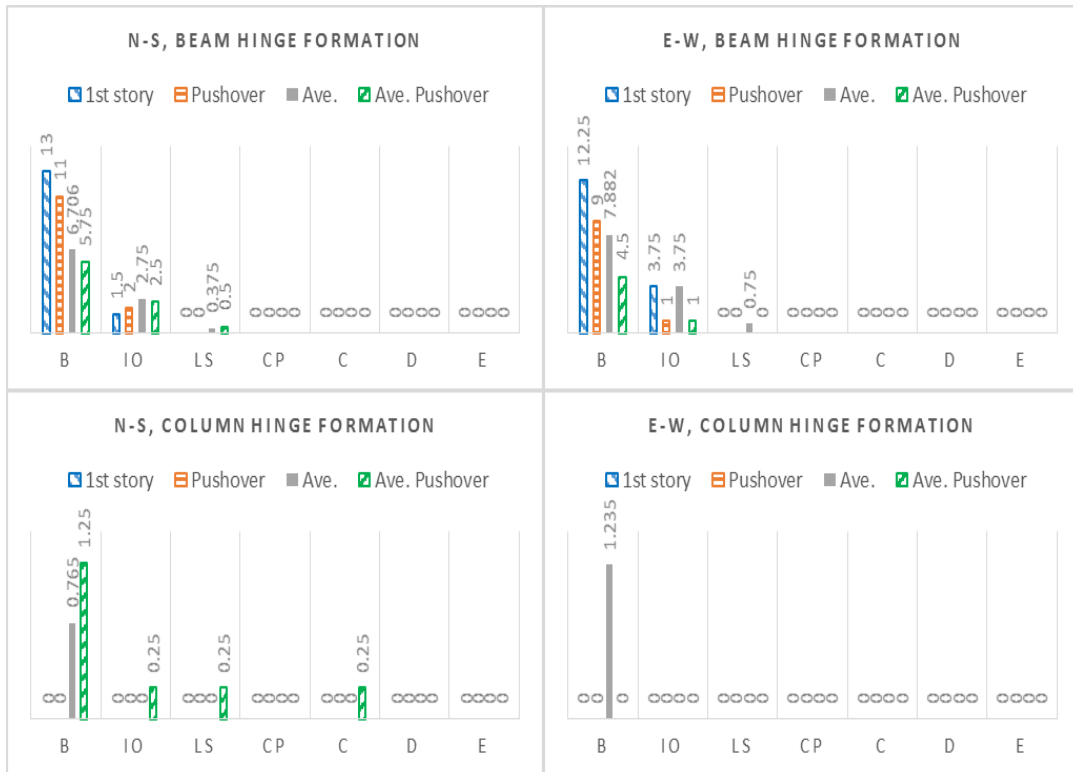
Graph 6-2a, Hinge formation results for selected model 4B12



Graph 6-2b, Hinge formation results for selected model 4S15



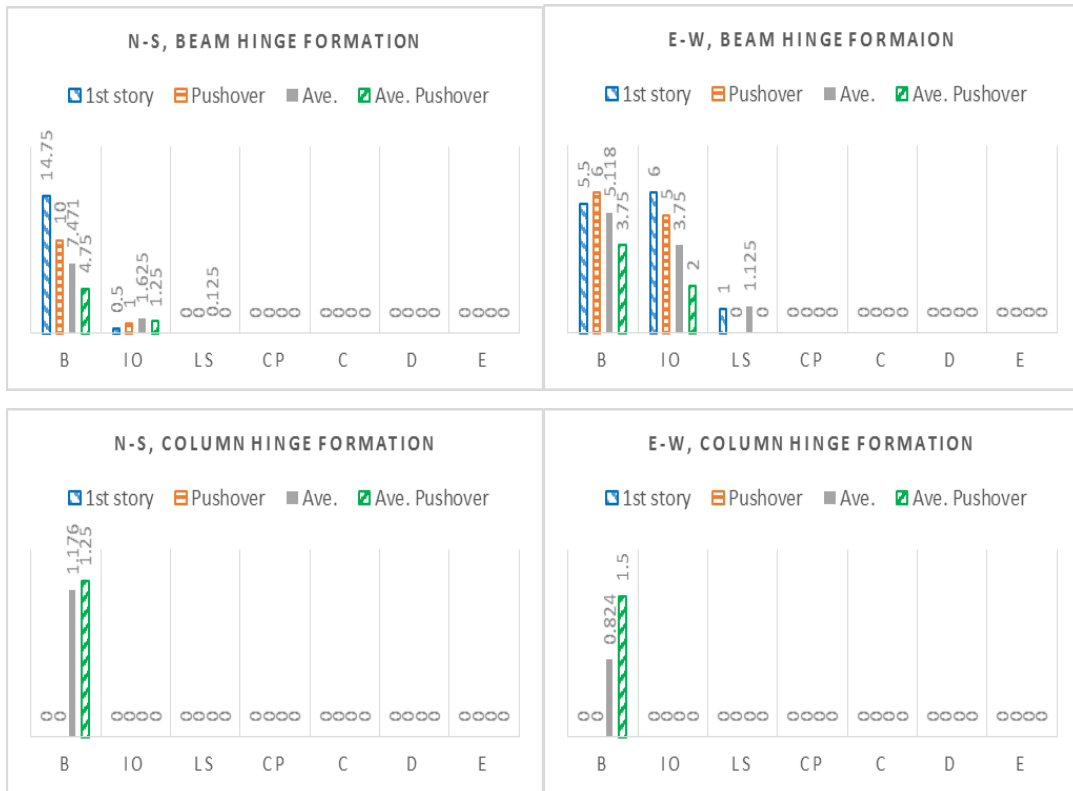
Graph 6-2c, Hinge formation results for selected model 4S18



Graph 6-2d, Hinge formation results for selected model 4A12



Graph 6-2e, Hinge formation results for selected model 4A15



Graph 6-2f, Hinge formation results for selected model 4A18



Graph 6-3a, Hinge formation results for selected model 8B12



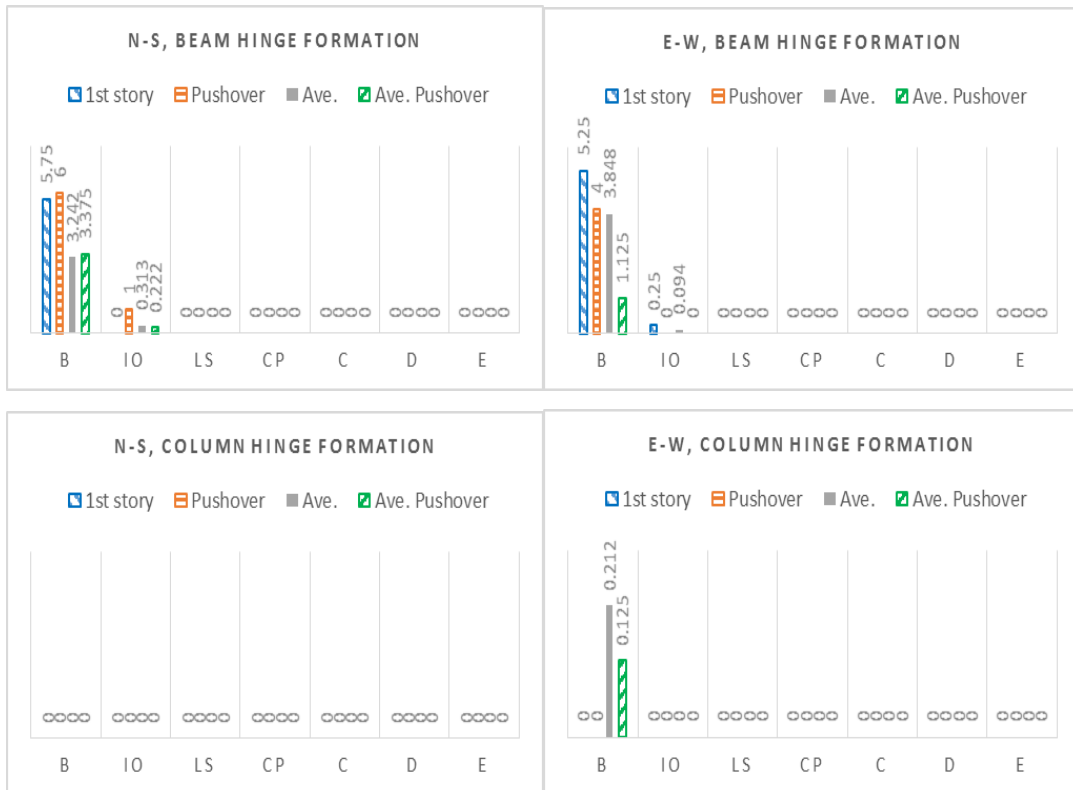
Graph 6-3b, Hinge formation results for selected model 8S15



Graph 6-3c, Hinge formation results for selected model 8S18



Graph 6-3d, Hinge formation results for selected model 8A12



Graph 6-3e, Hinge formation results for selected model 8A15



Graph 6-3f, Hinge formation results for selected model 8A18

### 6.2.1. Overall Hinge Formation Trend

In general, as it can be seen from the above graphs, total numbers of hinges are decreased with increase of the number of stories in archetype models. The total hinge numbers show a slight difference between two (2) and four (4) stories models, although the severity of formed hinges in terms of damage levels are higher for two (2) stories models. The eight (8) stories models in terms of level of damages and total number of hinge formations illustrate significant reduction. Moreover, for almost all cases, the number of hinge formations is more considerable in beams than the columns. This latter condition is desirable in seismic design which is almost satisfied successfully for all the selected models. The reduction of total number of formed hinges and the damage level severity from two (2) stories models to eight (8) stories can be justified with higher IC of larger structures. The margin level of safety in taller and bigger structures is usually higher than the smaller one. These effects are probably due to accumulation of overall factor of safety used for design of each

individual member in corresponding codes (particularly for columns). As an example, applied live loads are intentionally higher for the lower columns in practice.

Furthermore, review of the graphs reveals that in the E-W direction the total formed hinges, in terms of number and intensity of hinges, are more than N-S direction. This trend is observed for both beams and columns. Specifically, this effect is more recognizable for two (2) and four (4) story selected models. Comparison of total formed hinges and damage severity for the 1<sup>st</sup> story, average of stories, and pushover cases demonstrate that the previously mentioned trend is constant and weighting toward E-W direction. The maximum and overall average applied PGA in both FP and FN directions (chapter 4) for each pair of records are very similar. Thus, the simplest, but the most dominant reason, can be explained with the number of involved frames in the direction of applied ground motions. A very simple frame stiffness calculation shows that the E-W direction of the selected models, particularly for Base (*B* group models) and Symmetric type models (*S* groups), encompasses more stiffness than the N-S direction. For example, by using the primary mathematical model 2S15, performed for linear static analysis and design in chapter 3, the stiffness in each orthogonal main direction has been calculated. The stiffness in the N-S direction is achieved equal to  $\approx 360$  kips/ft, while for the same model but under the E-W direction the computed stiffness is  $\approx 400$  kips/ft. Therefore, providing that not any other influence situation is prevailing, such as resonance in response, absorption of induce forces would be more along the stiffer direction under similar ground motion acceleration and equal gravity load.

### **6.2.2. Hinge Formation Comparison-Two (2) Story Models**

Review of graphs 6-1a to 6-1f reveals the following results for the two (2) stories selected models:

- 1) Increment of the first story height from 12ft to 18ft shows a slight reverse hinge formation in beams for the 1<sup>st</sup> story of models 2B12, 2S15, and 2S18 in both directions.

- 2) Average formed hinges in terms of damage severity and total numbers are more in model 2S15 than 2B12 and 2S18 for all beams and in both N-S and E-W directions.
- 3) Pushover method for both 1<sup>st</sup> and average condition predicts formed hinges in beams conservatively for B damage level, whilst for the same condition the upper level damages are mostly predicted in unconservative manner by NSA method.
- 4) The 1<sup>st</sup> story and average formed hinge for columns of 2B12, 2S15, and 2S18 models do not show any specific trend in both directions for THA method.
- 5) NSA method shows conservative results for the 1<sup>st</sup> and average hinge formed in columns compared with THA method. Also, the level of conservatism is observed significantly more for column hinge results of NSA method in 2B12 model.
- 6) One to one comparison between asymmetric and the corresponding symmetric models (e.g. 2B12 to 2A12) reveals that the average formed hinges and damage levels for A type models are more than the corresponding regular plan model. The differences are seen regardless of type of member, i.e. beam or column, direction of excitation, and also for both THA and NSA methods.
- 7) For the asymmetric models, by increasing of the first story height, difference between THA and NSA results become more considerable. The result difference is more scattered for the columns than the beams.
- 8) The damage level and the hinge formed at the first story columns show reduction from 2A12 model to 2A18 in THA procedure.
- 9) The 1<sup>st</sup> story and average column hinge formations illustrate closer differences for model 2A12 and 2A15 in both directions under THA procedure. However, columns' hinges for model 2A18 suffer noticeable lower hinged formation particularly in N-S direction.
- 10) The severity of formed hinges in beams and in E-W direction of asymmetric models is higher than the N-S direction.

- 11) Among the two stories A type models, model 2A15 shows higher damage level of formed hinges than the other two models.

### **6.2.3. Hinge Formation Comparison-Four (4) Story Models**

Review of graphs 6-2a to 6-2f reveals the following results for the four (4) stories selected models:

- 1) In comparison with THA method, fluctuation of NSA responses is increased by increasing of the first story height and/or involving of plan irregularity.
- 2) In general, the 1<sup>st</sup> story and average hinge formations and damage level in columns are very low. Also, the overall minimum columns hinge formations are observed for models 4B12 and 4A12.
- 3) In the N-S direction and among models 4B12, 4S15, and 4S18, the former one shows higher amount of IO damage level for beams in THA method. In contrast, among those models and under the same direction, model 4S15 shows the maximum amount of formed hinges in B damage level.
- 4) For models 4B12, 4S15, and 4S18, again in THA method, for beams, and under the E-W direction, the overall 1<sup>st</sup> story and average formed hinges for all three previously mentioned models show a very similar trend.
- 5) Except for columns in 4S18 model and the beam at 1<sup>st</sup> story for model 4S15 (only at the N-S direction), overall pushover results illustrate an acceptable difference with THA method in 4B12, 4S15 and 4S18 models.
- 6) For both directions, column hinge formation in term of severity and numbers show increase from model 4B12 to 4S18 although the differences are very low.
- 7) Similar to the two (2) stories model, one to one comparison between asymmetric and the corresponding symmetric models (e.g. 4S15 to 4A15) display that the 1<sup>st</sup> story and average formed hinges and damage

levels for A type models are more than symmetric plan models. These differences are observed regardless of type of member, i.e. beam or column, direction of excitation, and also for both THA and NSA methods.

- 8) For the asymmetric models, in general, differences between THA and NSA results are not very high. Also overall results in the E-W direction are more than the N-S direction.
- 9) All three asymmetric models illustrate similar damage level in terms of number of formed hinges and hinge severity level.
- 10) Comparison between asymmetric and symmetric plan models show that beams in symmetric plan models and in the E-W direction suffer LS level of damage, mostly at the 1st story under THA method, while in asymmetric plan models the same damage levels have not been seen.

#### **6.2.4. Hinge Formation Comparison-Eight Story Models**

Review of graphs 6-3a to 6-3f reveals the following results for the eight (8) stories selected models:

- 1) For symmetric plan models, i.e. 8B12, 8S15, and 8S18, the 1<sup>st</sup> story and average plastic hinge formations at beams are observed in the N-S direction under THA procedure. The E-W direction for the same condition almost shows zero formed hinges.
- 2) The above-mentioned frames do not show any plastic hinge formation in columns under both THA and NSA procedures.
- 3) Under THA procedure, model 8B12 shows more formed hinges in terms of numbers and severity than 8S15 and 8S18. As mentioned, for all symmetric models the damage level is observed as low as B stage. The only exception is the beams under the N-S excitation for model 8B12 which shows damage level IO.

- 4) NSA method presents a close to reasonable approximation for both directions and for beams and columns, except for formed hinges at beams of the 1<sup>st</sup> story of model 8S18.
- 5) Very similar to two (2) and four (4) stories models, one to one comparison of eight (8) stories symmetric and asymmetric plan models illustrate that A type models have more number of hinged formation in beams under THA procedure for the N-S direction. However, the severity of results remains mostly in low damage condition (B stage) and increase in IO damage level are observed low.
- 6) Contrary to eight (8) story symmetric plan models, asymmetric eight (8) story models display formed hinges in the E-W direction. In this case, the severity and number of hinge formations also are observed very similar to the N-S direction for each asymmetric plan under THA method and for beams.
- 7) There are few formed hinges in columns of asymmetric plan (eight stories). These hinges are formed at upper stories and no formed hinge is observed in columns at the 1<sup>st</sup> story level for both THA and NSA methods. Moreover, difference between hinge formation in columns under THA and NSA procedure shows good agreement in terms of severity and numbers.
- 8) The formed hinge in column of A type models almost occurs at the E-W direction with almost zero occurrence in the N-S direction.
- 9) For asymmetric plan models, NSA method shows a reasonable difference with THA method.
- 10) In general, for symmetric models increasing of the 1<sup>st</sup> story height from 12ft to 18ft show that the number of formed hinges is reduced. On the other hand, for asymmetric plan models the increase of the first story height shows growth of formed hinges (in terms of numbers and severity).

### **6.2.5. Brief Review of Few Similar Observed Hinge Formation Behaviors in Models**

In axis 4 of Asymmetric models and at both sides of column B4 for about 30 analysis cases (under THA and NSA) plastic hinges are formed. Regardless of the first story height, these plastic hinges are observed for two (2), four (4), and eight (8) stories A type models (Figure 6-1). The most detected hinges are developed and observed at the first story (Figure 6-2), where discontinued columns are located. For some four (4) or eight (8) stories models the hinges (in beams to column located at B4) are progressed in the upper stories as well (Figure 6-1). In addition, these hinges are usually shown higher damage level in comparison with other formed hinges in the same story level and for the same structure (Figure 6-2). The afore-mentioned nonlinear formed hinge can be justified due to the unsymmetrical plan of these types of selected models. The center of rigidity of the typical A archetype models is set toward axis 4. The frame in axis 4 of the first level has more stiffness than the other side of these models (e.g. axis 1), which reflects the effect of additional number of columns in axis 4. As a matter of fact, simple static analysis of asymmetric frames, particularly under the gravity loads, is not able to show the problem of uneven stiffness in a structure (chapter 3). The hinge formation in both sides of column B4 is seen and occurred under all four (4) applied records. Thus, it can be said that technically the characteristics of the applied records may not drastically amplify or pacify the observed formed hinges in axis 4. Bearing in mind that the intensities of the applied ground motions are low and the hinge formations at stiff part of the models are observed under both excitation directions (i.e. the E-W and N-S), considerable damages is possible to form in the stiff part of LRC structures, even under low to medium intense seismic event in unsymmetrical structures.



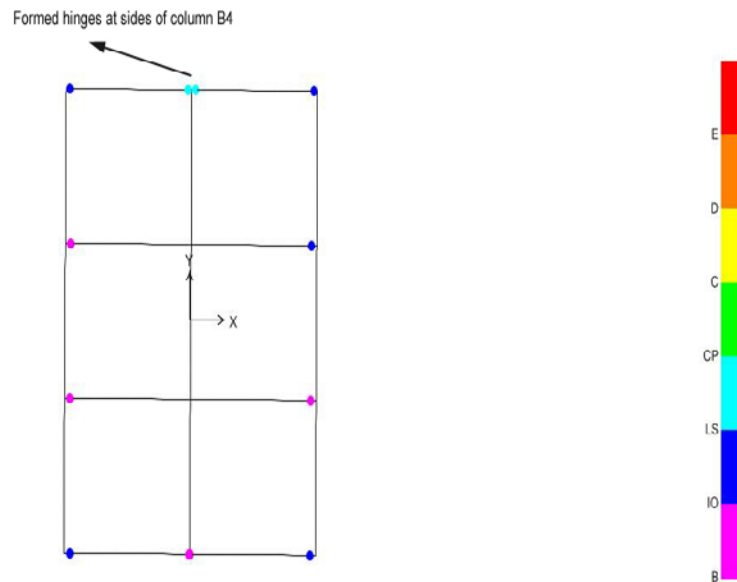


Figure 6-2, Hinges at 1<sup>st</sup> level (plan) of model 4A18 under NAH N-S excitation at time 35s, overall increase in total of hinges and more severe damage level for hinges at axis 4 around column B4

The hinging pattern is plotted at axis 1 in Figures 6-3 for models 4A12 and 8A18 under NAH excitation. Plastic hinge formation in columns starts with column ends at interior middle columns (axis B) of top story for four (4) story models then spread to the bottom of the same interior column at the same story for some seismic cases. Next, the hinge formation propagates to axis A and/or C in the same story level, i.e. column end at the top-level story. The afore-mentioned pattern mostly occurs at axis 1, then for some cases, they extend to axis 2 and 3 as well. This type of hinge formation is observed for 4A12 and 4A15 models in one seismic case and 4A18 in two cases. For eight (8) story models, the plastic hinge formations at the end of the uppermost columns start at axis A or C of frame in axis 1, and then for few cases spread to frames at axis 2 or 3 or both of them. Similar to four (4) story models, 8A12 and 8A15 frames show one case of this pattern each, whereas three similar cases are detected for model 8A18. The afore-mentioned trend is only observed for asymmetric frames in the E-W direction. Similar to the previous overall observation, static analysis is not able to trace this damage. Per static analysis and under the typical dead

and live loads, the girders which support the discontinued columns are strong enough to carry static loads. Under dynamic analysis, and even without any vertical seismic excitation, the middle girders in axes 1, 2, and 3 would be deformed excessively. The vertical deformation, as it can be seen from figure 6-3, induces more moment at side columns at top level. Generally speaking, the middle column seems hang from the two sides. The outermost axis from the end, axis 1, suffers the maximum vertical deflection at the girder to column connection point (i.e. B1). Indeed, the column line B4 acts as a support for whole axis B. For instance, in model 4A12, connection point B4 at the first level shows just -0.042 inch deflection under NAH excitation in the E-W direction at time step 26s. However, for the same condition and at the same level, but at points B3, B2, and B1, deflections are equal to -1.322, -1.476, and -1.584 inch, respectively. Negative sign illustrates the downward deflection.

As mentioned before, three seismic cases for each of 8A18 and 4A18 models show the top-level column hinge formation. The number of involved cases for the first story height equal to 18 feet can be explained through extra-induced deformation at the first story due to vertical irregularity exacerbation. For example, the node A1 or C1 at the first story level (axis 1) for 8A12 model under NAH excitation in the E-W direction show 0.047 inch vertical downward deflection. On the contrary, for the same nodes at the same seismic action, 0.071 inch deflection is observed for model 8A18.

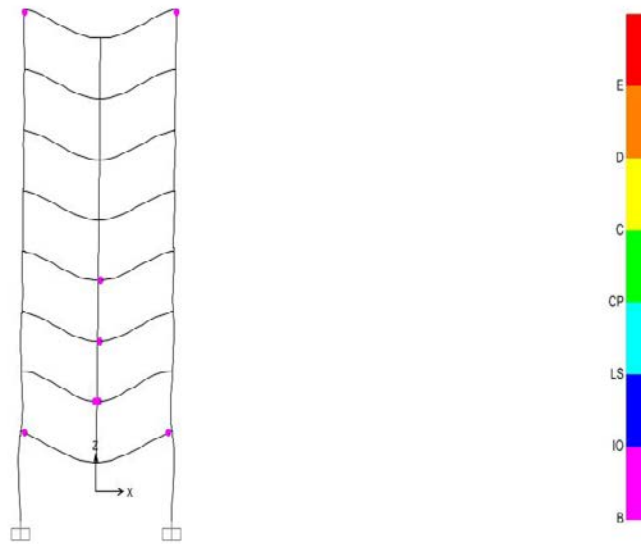
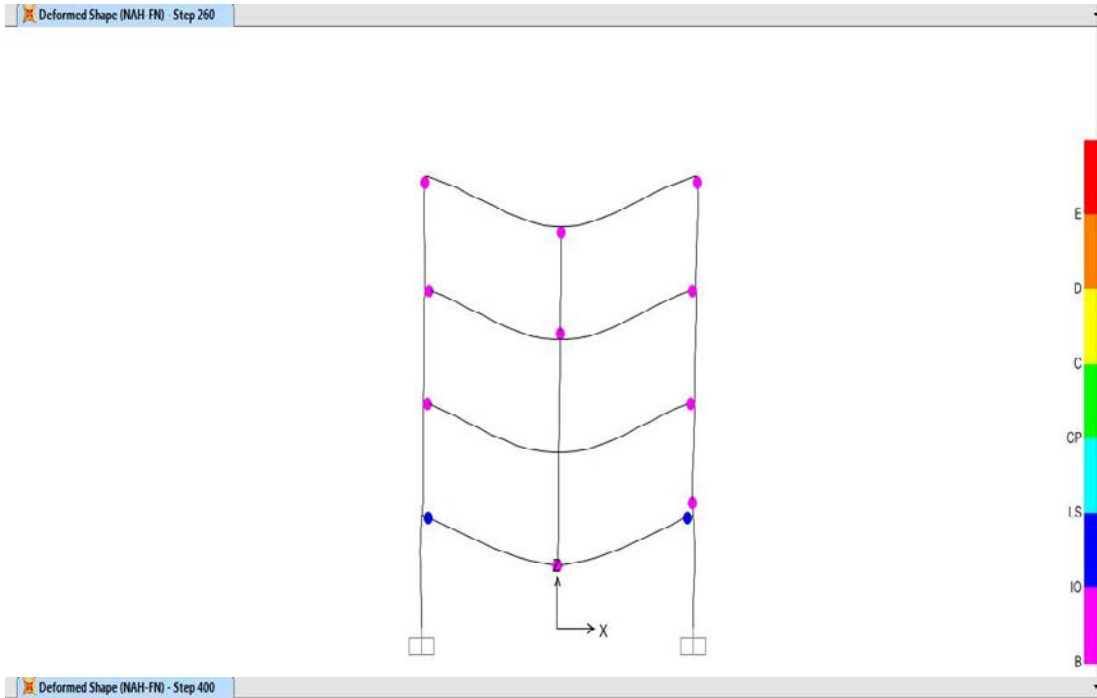


Figure 6-3, Top: Hinges at axis 1 (elevation) of model 4A12 under NAH E-W excitation at time 26s; Bottom: Hinges at axis 1 (elevation) of model 8A18 under NAH E-W excitation at time 40s

The hinge formation at the connection of column to the base is observed mostly for the two (2) stories model. Basically, in this case the damage level remains

at B stage with few cases with one higher damage level, i.e. IO level. However, for models 2A15, 2S15, and 2A12 plastic hinges at support locations in axes A and C and for frame lines 1, 2, or even 3 have suffered collapse damage stage (i.e. hinge level E). The collapse hinge formation is caused when the NOR seismic applied in the N-S direction for both models 2A15 and 2S15. The collapse hinge formation of model 2A12 occurs when LPR seismic is applied in the same direction of N-S. Model 2A18 shows only one collapse stage hinge at base location which is observed at column B4 support location. The middle column support hinge formation in this case happens under NAH excitation and for the E-W direction of analysis. For four (4) stories models, the archetype models 4S15 and 4S18 show the column to the base hinge formations under the NOR seismic action in the N-S direction which are observed in low damage level (i.e. B stage) as shown in Figure 6-4. The observed hinge formation at support location for other four (4) story models is very few and sporadic. There is not any hinge formation at support location for eight (8) stories models. The observed story mechanism will be discussed in section 6-3.

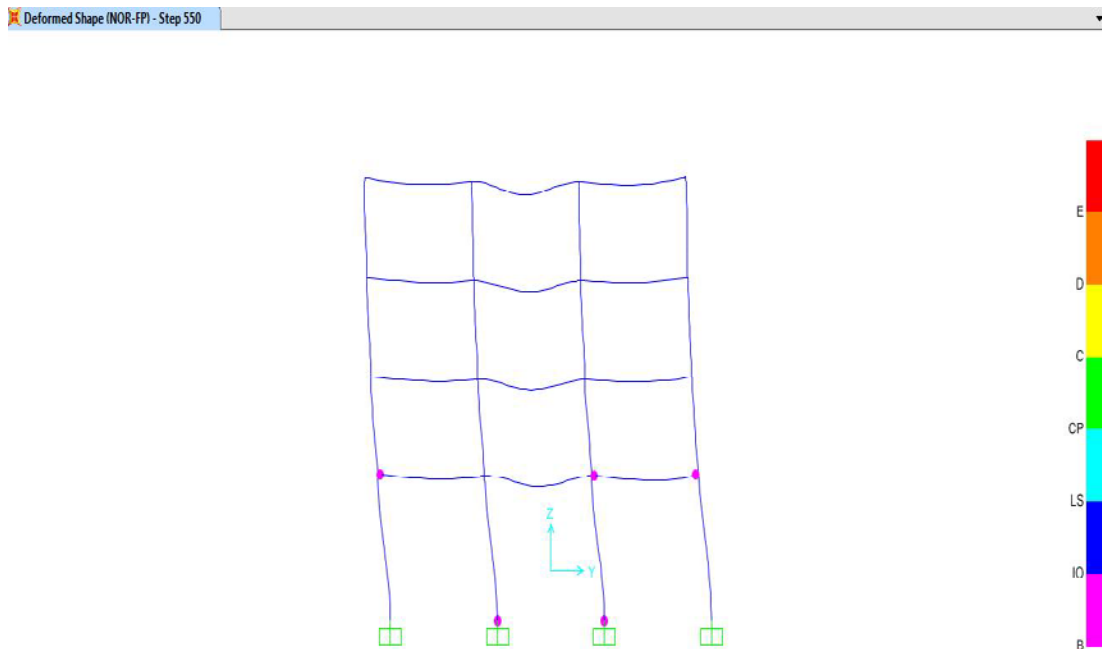


Figure 6-4, Hinges at axis 2 (elevation) of model 4S18 under NOR N-S excitation at time 55s

### **6.3. Story Mechanism**

Two severe story mechanisms are observed under THA procedure. The first one is occurred in model 2S15 for applied ground motion NOR under N-S direction. All columns in axis B at base enter collapse damage level (E type of hinge formation) while ends of those columns at top of the first story elevation suffer type B hinge formation damage. However, the worst level of damage is observed for model 2A12 under LPR in N-S direction. Axis 1 of the model shows total story collapse at the second story level and the structure is very close to the total story mechanism in the first story level (Figure 6-5a). Moving from axis 1 toward 4, the level of damages is decreased although the numbers of hinges designated with damage level E are still high, i.e. minimum four E type hinge damages for each frame. The columns display higher severe damage level than the beams. The negative and positive directions of LPR excitation show similar response that correspondingly represents a significant seismic risk for a structure in a low seismic zone. Model 2A15 shows hinge formation at top and bottom of columns in axis 1 under the same execution time for LPR earthquake in N-S direction, but the damage level is much less and remains within the B damage category (Figure 6-5b). Interestingly, the level of damage for 2A18 model at the same condition and frame axis does not show any column mechanism and no high level of damage is observed for this model (Figure 6-5c). The salient feature of the soft story mechanism definitions is basically established according to story height (chapters 2 and 3). The acquired results in this case are actually against those basic assumptions. The execution time and the excitation intensity for all three (3) models are the same. The applied damping in table 4-5 shows that the mass proportional damping ratio for model 2A12 is about 21.7% more in comparison with model 2A15. On the other hand, the difference between the same damping for models 2A15 and 2A18 is about 1.2%. However, the stiffness proportional damping for model 2A12 is about 30.5% less than model 2A15, with zero difference between models 2A15 and 2A18 for the same condition. In fact, damping levels for all three afore-mentioned models are typically low. Although per classic dynamic of analysis, e.g. Chopra (2000), it is proved that low damping ratio has a significant effect on amplifying of

response, these damping factors may not be the reason of higher level of damage for model 2A12. Parenthetically, the other applied seismic records (NAH, NOR, and WNA) are performed with the same base amount of damping for the aforementioned models, but they do not show similar response.

To review this issue, first the corresponding modes on N-S direction are presented in table 6-2. The service case period is actually the same period as in table 3-3 which is under elastic condition. The second row is the cracked concrete period, which can approximately be considered for pre-full yield point. This period is basically calculated same as the method that has been explained in Appendix C. The third row shows  $T_i$  which is calculated by SAP2000 per FEMA 356 (2000) guideline for pushover method (section 5-2). It should be mentioned that due to the unsymmetrical plan of these models, the N-S vibration mode actually contains torsional response as well. The torsional participating effective mass ratio for this mode is about 12%. Also for the most dominant torsional mode, the third mode of vibration of model 2A12 in elastic phase, the mode period is 0.86s (table 3-3). The same mode in the approximate cracked method (Appendix C) is about 1.06 second. The torsional participating effective mass ratio for the third mode of model 2A12 is about 80%.

Table 6-2: Period in the N-S direction

<b>Model tag</b>	<b>2A12</b>	<b>2A15</b>	<b>2A18</b>
<b>Modal case/ Period</b>			
Service case	1.05 (s)	1.34 (s)	1.37 (s)
Cracked concrete	1.40 (s)	1.54 (s)	1.80 (s)
Pushover	1.30 (s)	1.77 (s)	1.74 (s)

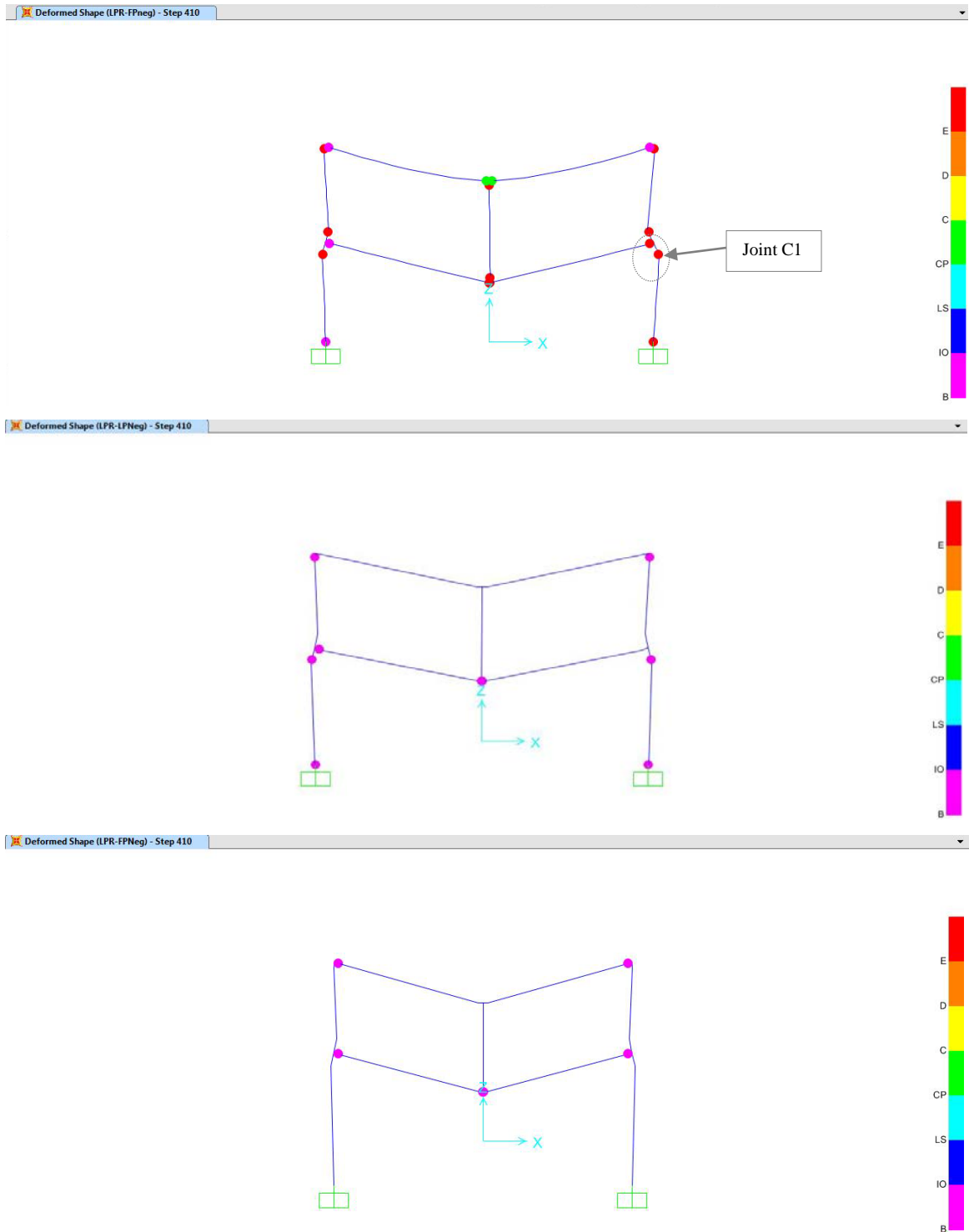


Figure 6-5, Damage level under LPR N-S excitation at time 41.0s for axis 1(Elevation view): a) top, story mechanism for model 2A12, b) middle, low damage level for model 2A15, c) bottom, model 2A18 without story mechanism damage level

To investigate the story mechanism of model 2A12 under LPR event, the input ground motion is changed to the frequency domain. Fast Fourier Transform (FFT) method is implied to bring the data from time domain to frequency domain. The result is presented in figure 6-6. To make the result more comparable, the abscissa shows the period in logarithmic scale. As it explained before, the 2<sup>nd</sup> and 3<sup>rd</sup> modes of vibration for model 2A12 are predominantly involved on the total response. The forth mode of response is about 0.39s for the elastic phase and 0.48s in approximate for the cracked phase. Bearing in mind that through nonlinear and inelastic analyses where the stiffness of the model is rectified in each step (chapter 5), all periods of the models would be soften and elongated from the elastic to the plastic mode. The lower and upper bounds of all these periods for 2A12 model, i.e. 0.39s to 1.40s, are within the maximum amplitude part of LPR N-S ground motion. The boundary of period for model 2A12 including 1<sup>st</sup>, 2<sup>nd</sup>, 3<sup>rd</sup>, and 4<sup>th</sup> modes of vibration are within the drawn box in figure 6-6. This box clearly displays that the effective modes of vibration from elastic to the approximate cracked conditions are overlapped by the maximum portion of LPR component. On the other hand, from table 6-2 it can be realized that the relative dominant vibration modes with considerable effective mass ratio for selected models 2A15 and 2A18 are far from the spikes in figure 6-6. In addition, as model 2A18 has longer period than model 2A15, the excitation part for this model would be located farther at the right side of figure 6-6. This may justify severe reduction of response for model 2A18 in comparison with model 2A15 as shown in figures 6-5c and 6-5b, respectively.

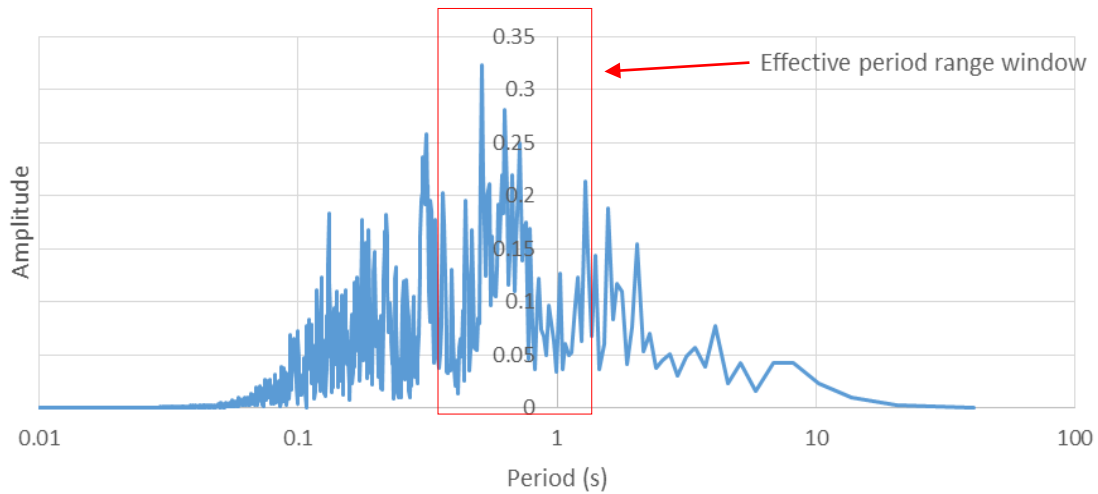


Figure 6-6, FFT of LPR record in N-S direction and period range for model 2A12

To get a better idea, frequency domain of acceleration response for the joint C1 located at the first story, intersection of axis C with axis 1 (Figure 6-5a), is presented in figure 6-7. The abscissa and ordinate axis unit is selected similar to figure 6-6. Figure 6-7 shows some important features of the response. The effect of lower amount of damping leads to drastic change in amplitude response. The acceleration amplitude of response intensifies considerably in comparison with the input acceleration amplitude. As it is displayed in figure 6-7, the climax of response occurs at period time about 1.35s. This period is very similar to the dominant approximate cracked period in table 6-2, i.e. 1.4s. Indeed the resonance of response can be realized from the maximum response coincidence from these periods.

Another important point is the other climax point in the left side of figure 6-7. This high amplitude response is happened at period time of around 0.45s. This period is very close by the 4<sup>th</sup> mode of vibration. As it is clear from left side of figure's vertical axis, the resonance effect for the 4<sup>th</sup> mode is considerable. The effective modal mass of model shows that the forth vibration mode is mostly corresponded to the rotation mode around axis Y of selected model 2A12 (in N-S direction). This mode also contains vertical modal component in some degree. Similar trend is observed for models 2A15 and 2A18. The forth mode of vibration for all the three aforementioned models are very close to each other, and this vibration mode is within

the time period of resonance phenomena for the applied record (LPR). Thus, the plan irregularity and resonance affect both lead to intensify the response. It should be mentioned that in this case, the participate effective modal mass for the 4<sup>th</sup> mode of vibration is low. Therefore, although the 4<sup>th</sup> mode amplitude is high, the overall 4<sup>th</sup> mode resonance effect in total response is lower in comparison to the first three modes.

For the same joint, i.e. column-beam intersection at C1, the acceleration against time for the applied LPR (FP) is illustrated at figure 6-8a through 6-8c for models 2A12, 2A15, and 2A18, respectively.

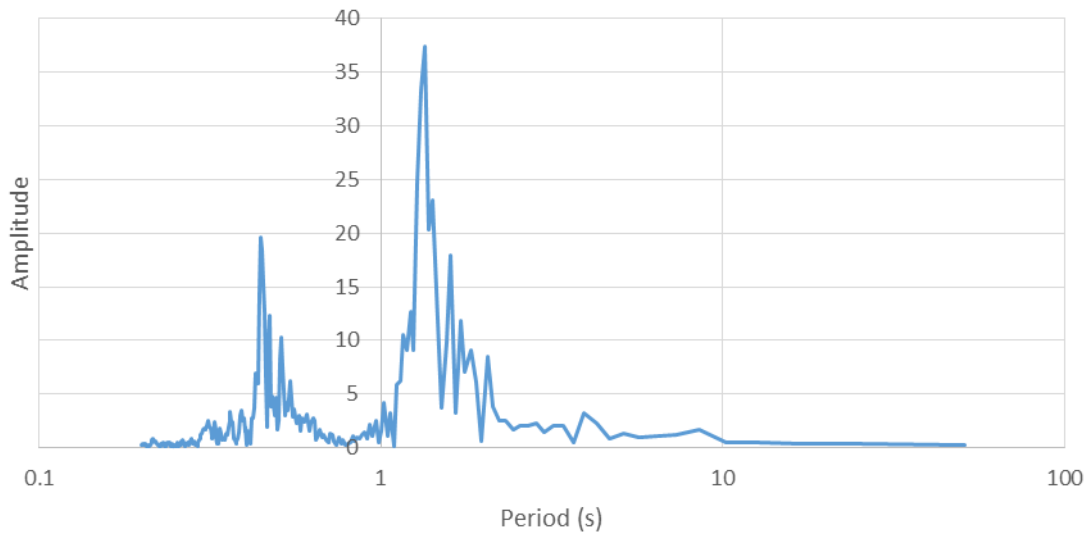


Figure 6-7, FFT of Acceleration response at joint C1 under LPR record in N-S direction for model 2A12

Figure 6-8 demonstrates few other points. As it can be expected from the previous explanation, the maximum response occurs at frame line 1 of model 2A12. The acceleration for the selected joint for this model is almost 25% more than that for model 2A15, and about 36% more than that for model 2A18. The above-mentioned response chronicle also depicts on figure 6-5 regarding hinge formation damage level. A further result from figure 6-8 can be interpreted in associate with damping. The first part of the response begins to reduce up to some point around time 30s which is similar for all three (3) models. After about time step 300 (30 second), the response

enters the free vibration phase. For model 2A12, the plastic hinge formations are developed up to the ultimate levels, therefore the response is damped out very quickly. As it can be seen from figures 6-5b and c, the number and level of hinge formation for models 2A15 and 2A18 are much less. For these latter models, the formed hinges are in the B damage level and consequently mostly only the overall effective viscous damping (section 4.4) is governed. The afore-said damping is low, thus, the impulse in response is taken place in free vibration phase. In addition, model 2A18 shows approximately 10% more acceleration response than that for model 2A15 through comparison of figures 6-8b and c. Although it might be possible that the taller first story of model 2A18 magnifies the free phase response, most probably the lower response of model 2A15 in free vibration phase can be justified with its higher number of entered joints in plastic phase.

It should be mentioned that NSA method neither shows any higher damage plastic hinge formation for model 2A12 nor illustrates similar to THA-LPR hinge formation for any of those models in N-S or E-W directions. On the other hand, FEMA 356 (2000) method that is applied to calculate  $T_i$  period (section 5.2), shows good agreement with the acquired dominant period through THA result from LPR record and for all three models, i.e. 2A12, 2A15, and 2A18. For instance, figure 6-9 depicts frequency response (using FFT) of acceleration at master point (chapter 3) of model 2A18 at roof level. This joint (point) is technically considered for computing of  $T_i$  in NSA procedure. The climax of period is about 1.71s, which is very close to 1.74s, calculated by software for NSA method, presented in table 6-2. This response may demonstrate that the FEMA 356 (2000) period calculation in NSA technique is accurate enough to use for low to mid-rise concrete frame structures with plan and/or elevation irregularities.

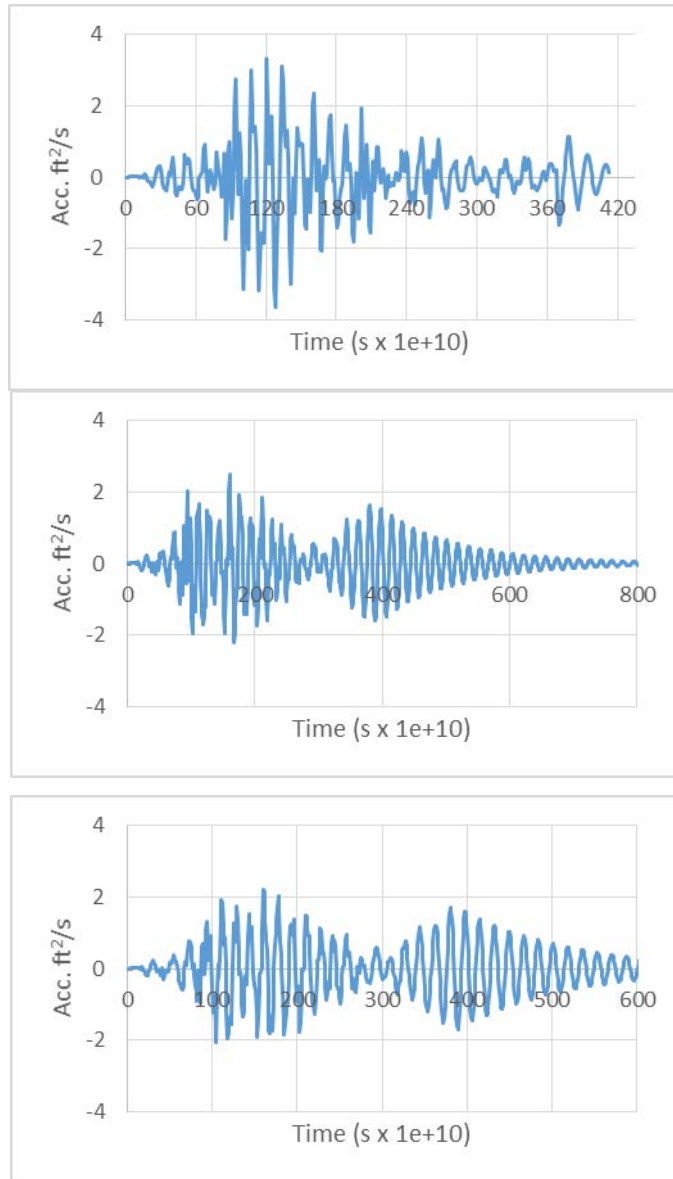


Figure 6-8, Acceleration vs. time for Joint C1 at the first story under LPR record in N-S direction response at joint C1 under LPR record in N-S direction, a) Top: model 2A12, b) Middle: model 2A15, c) Bottom: Model 2A18

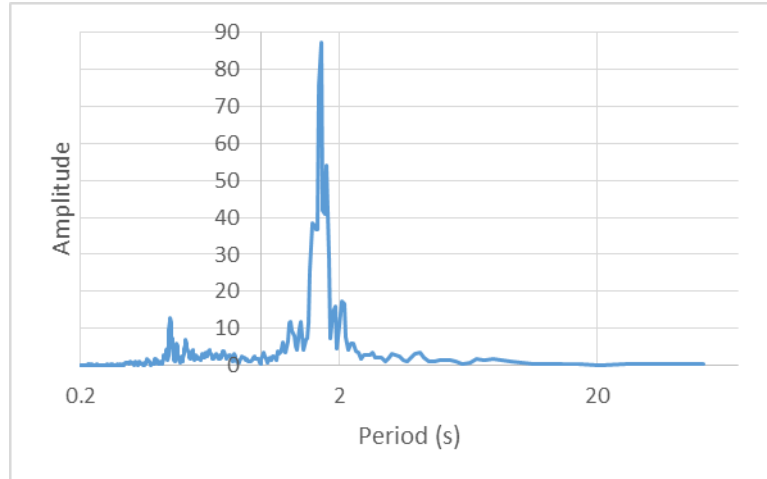


Figure 6-9, FFT of Acceleration response at master point of roof level under LPR record in N-S direction for model 2A18

#### 6.4. Drift Comparison

Story drift (also known as Relative Displacement) is one of the most practical and relevant measurements in the seismic design and studies of structures. Several codes, such as ASCE 41-06 (2007a), just simply use “drift” instead of “story drift” or “relative drift”, which is followed hereafter. ASCE 41-06 (2007a) defines drift as “Horizontal deflection at the top of the story relative to the bottom of the story.” In this chapter, under the global failure criteria (section 6-1), acceptable structural performance levels and damages regarding drift is mentioned. These criteria are according to FEMA 356 (2000) and ASCE 41-06 (2007a) for the vertical elements of concrete frames.

Strictly speaking, maximum (max.) drift may not only lead to structural damages, but also create several problems interrelated to the serviceability of buildings. For instance, breakage of pipes and utility lines, severe damages to architectural and ornamental members, and failure of nonstructural elements are some of maximum drift issues. This is highly undesirable and traditional seismic code methods have shown that transit drift in a seismic event may cause catastrophic impairment damages. For instance, FEMA E-74 (2012) provides information on nonstructural earthquake damages due to drift. Despite this fact, only the structural

response is measured and reviewed in this section, and effects on nonstructural elements are beyond of this study.

### **Maximum Drift**

Table 6-3 illustrates the maximum absolute drift ( $d_i$ ) for the selected models. Generally speaking, the maximum drift is directly comparative to the maximum forces developed in the structure (Wilson 2002). The absolute value of drift in the geometrical center of every story level (master point/joint) is acquired. Maximum drift is presented for each separate direction. The two, four, and eight stories models are classified into groups 1, 2, and 3, respectively. Basically, the drift value associates with the maximum drift response among the four applied records for each model. Regardless of the story level, the presented drifts are categorized only corresponding to the excitation direction, i.e. E-W or N-S. Expectedly, the maximum absolute drift for each direction is related to the same direction of applied seismic records. For example, the E-W (FN) component of the excitations causes the maximum absolute drift in the E-W direction of each model. From table 6-3, the following results can be perceived:

- 1) It can be seen that the maximum absolute drift for group 1 or group 2 is not related to the applied excitation record. Nevertheless, the maximum drift for group 3 in each direction may depend on a specific applied seismic record and its component. Independency of maximum absolute drift to the input records for two and four story models can also be seen for both symmetric and asymmetric plan models. On the other hand, the maximum absolute drift for eight story models in each direction and for both symmetric and asymmetric plan models may be subject to a specific input record.
- 2) The maximum amount of drift is observed for 2A12 and 2A15 models in the N-S direction. 4S18 model has the most vulnerable condition in both N-S and E-W directions.
- 3) Overall, the eight story models show less maximum absolute drift in comparison with the other groups.

- 4) In the E-W direction, maximum absolute drift of group 2 and group 3 is mostly concentrated at the higher story levels while in the N-S direction reverse condition is observed.
- 5) For group 1, increase in the first story height indicates low effect on maximum absolute drift response of regular plan models. For A type models of this group, the increase of the first story height may even lead to the reduction of  $d_i$ . This response is corresponded to the hinge formation (section 6-3)
- 6) For group 2, A type models are unaffected by the first story height alteration, but the first story height increment is induced higher value of maximum story drift in the symmetric plan models. For the latter models, the maximum story drift is almost concentrated on the first story as well.
- 7) Comparison of group 3 results reveals that there is not any specific pattern for both asymmetric and symmetric plan models of this group.

By looking at table 6-3, it is clear that none of the models exceed FEMA 356 (2000) LS performance criterion, although the number of models which suffer over IO drift damage level are considerable. Graph 6-4 provides statistics data from the former table to examine the performance level criterion. Maximum absolute drift ( $d_i$ ) for each group are counted and divided into three (3) categories: 1)-  $d_i$  less than 0.95% which shows acceptable drift response and can be considered as operational level (table 6-1); 2)- within 0.95% to 1.05% which means IO condition with 5%± margin; and 3)- more than 1.05% which may lead to more structural permanent damages.

Graph 6-4 reveals that there is not any sizable difference between asymmetric plan and symmetric plan models in each group in term of  $d_i$ . In addition, this graph shows that eight (8) story models suffer less severe drift and their maximum drifts remain mostly within or less than the 1% criterion associate with IO damage level. Numbers of upper bound and lower bound of maximum drift for both group 1 and group 2, with no difference between the plan type, are very similar and almost the

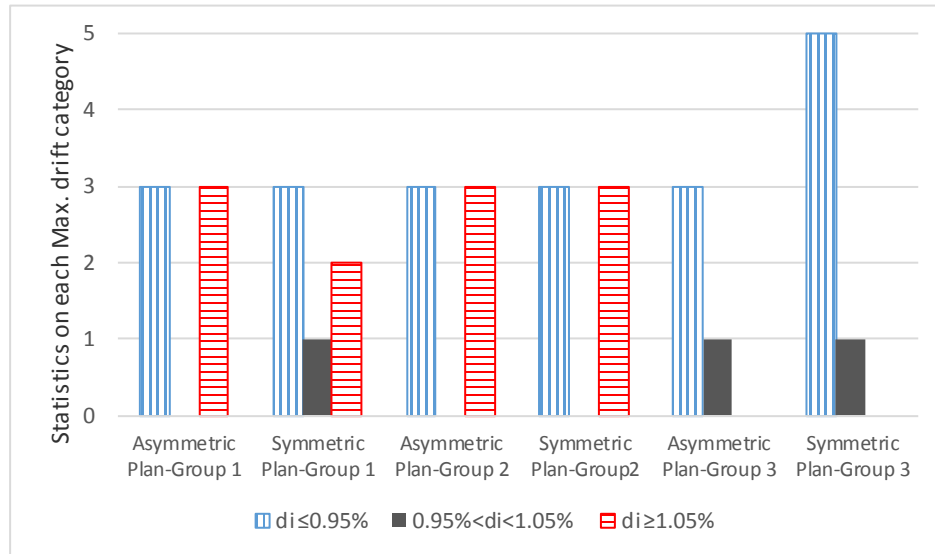
same. For these groups, per FEMA 356 (2000) drift criteria, each of these models under the applied records may encounter higher than IO level of damage.

Table 6-3: Maximum absolute drift ( $d_i$ )

Model Name	Max. Drift, E-W	Corresponding Story level	Associate Record regarding Max. E-W drift	Max. Drift, N-S	Corresponding Story level	Associate Record regarding Max. N-S drift
<b>Group 1: Two story models</b>						
2A12	0.0086	1	WNA-FN	0.0151	2	LPR-FP
2A15	0.0110	1	NOR-FN	0.0138	1	NOR-FP
2A18	0.0093	1	NAH-FN	0.0085	1	LPR-FP
2B12	0.0090	1	NAH-FN	0.0089	1	LPR-FP
2S15	0.0098	1	NOR-FN	0.0106	1	NOR-FP
2S18	0.0125	1	WNA-FN	0.0089	1	LPR-FP
<b>Group 2: Four story models</b>						
4A12	0.0068	3	NAH-FN	0.0106	3	NOR-FP
4A15	0.0069	3	NAH-FN	0.0112	2	NOR-FP
4A18	0.0066	3	NOR-FN	0.0108	2	NOR-FP
4B12	0.0093	2	NOR-FN	0.0069	1	LPR-FP
4S15	0.0106	2	LPR-FN	0.0082	1	NAH-FP
4S18	0.0128	1	WNA-FN	0.0115	1	NOR-FP
<b>Group 3: Eight story models</b>						
8A12	0.0077	5	WNA-FN	0.0075	3	NOR-FP
8A15	0.0071	3	WNA-FN	0.0095	3	NAH-FP
8A18	0.0085	5	WNA-FN	0.0096	3	NAH-FP
8B12	0.0099	5	LPR-FN	0.0067	2	NAH-FP
8S15	0.0091	5	LPR-FN	0.0070	2	NAH-FP
8S18	0.0088	5	LPR-FN	0.0066	2	NAH-FP

Within maximum drift results and outcomes of the selected models, it is clear that low intense seismic events may create a degree of noticeable damages in LRC structures. The level of damage is greater for low-rise structures in comparison with the taller models. Furthermore, the first story height is just invoked to build up the worst case mostly for group 1 models and the symmetric plan models of N-S direction for group 2. Per seismic design regulations in most building codes, e.g. ASCE 7-05 (2005), it is expected to see higher damage level for asymmetric plan

structures. The unsymmetrical plan models indicate almost similar drift performance in comparison with the symmetrical plan models regarding maximum drift criterion.



Graph 6-4, Number of maximum absolute drift ( $d_i$ )- classified as group number and plan type

### Average Drift

Although maximum absolute drift may at least be attributed to LRC deficits, it cannot reflect the commensurate drift change of all stories. Exclusively, irregularity influence on drift formation may be unclear. Despite the maximum absolute drift trend, in seismic rehabilitation of LRC structures, drift response of all involving stories encompasses the overall behavior of the system as a whole, not the behavior of a single story. To compare and review the drift response of all selected models, the maximum drift result of each story level is acquired. To do so, the N-S and E-W directions are extracted separately. This procedure is done for all the applied records (i.e. LPR, NAH, NOR, and WNA). For the maximum drift condition, the absolute of the drift was presented. Here, in agreement with the selected Cartesian system (geometrical center of story level as the Cartesian center of the system), the drift response is collected with negative sign and positive sign for each direction of applied record. Indeed, the applied seismic excitation oscillates the models and any movement toward up or right side of the geometric center is gathered as drift with

positive sign and vice versa as negative sign. Then, the arithmetic mean of results (e.i. average of maximum drift of each story level under all applied records) for all seismic cases is calculated for negative and positive directions. To do so, for every story level two cases regarding FN or FP component of the records (N-S or E-W) is computed independently.

The first set of results is illustrated in figures 6-10 to 6-15. To study the effect of first story height on drift response, each figure consists of results for asymmetric or symmetric plan models separately. Moreover, they are classified based on the number of stories (i.e. two, four, or eight story models), and both direction of seismic excitation (E-W or N-S) are depicted in independent diagram. Average drift in both directions of oscillation (negative or positive) comprises the horizontal axis and the story level is the vertical axis of the diagrams.

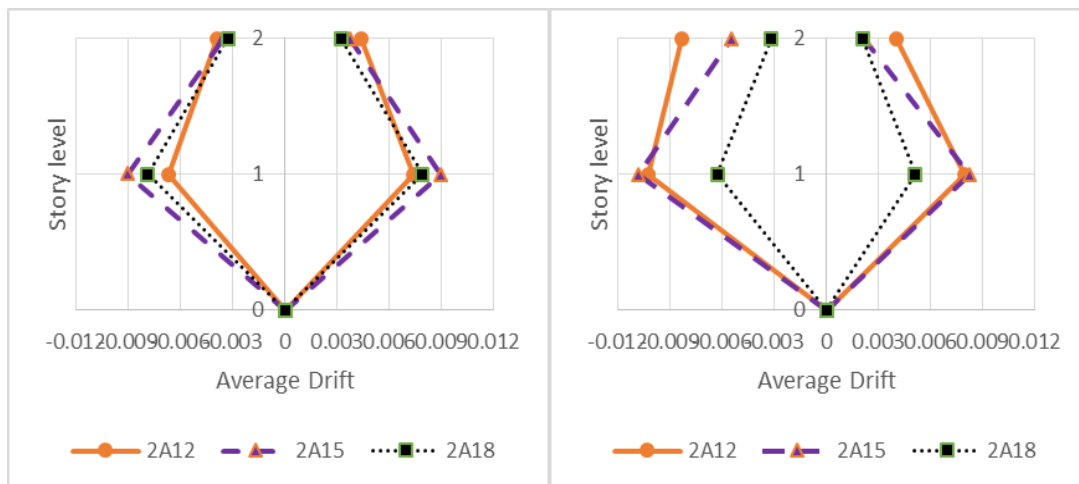


Figure 6-10, Group 1, asymmetric plan models, average drift response for E-W direction (left) and N-S direction (right)

Overall, responses in figures 6-10 to 6-15 are in agreement with the maximum absolute drift in table 6-3. In other words, the inherent and specific characteristics of the applied earthquakes may have lesser effect on the displacement response in comparison with the structural dynamics behavior of the models.

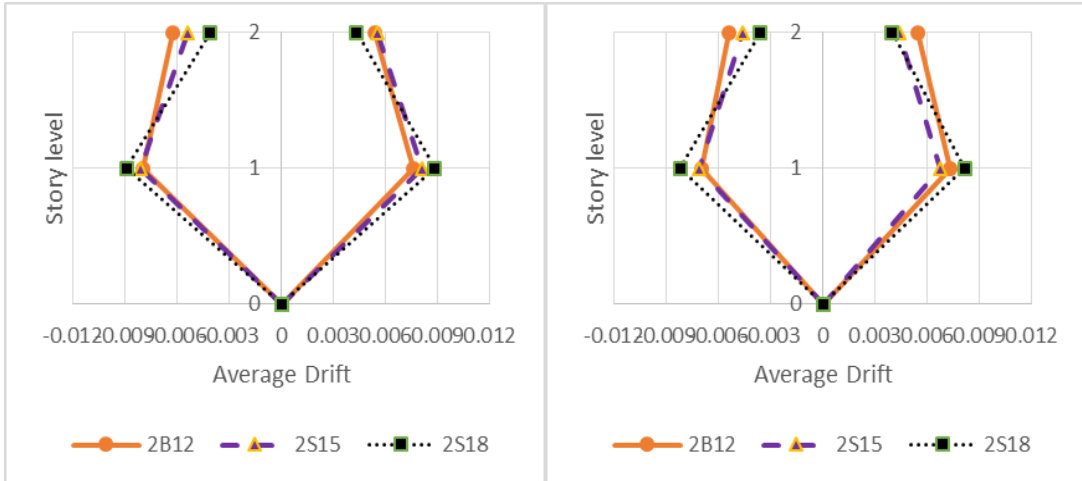


Figure 6-11, Group 1, symmetric plan models, average drift response for E-W direction (left) and N-S direction (right)

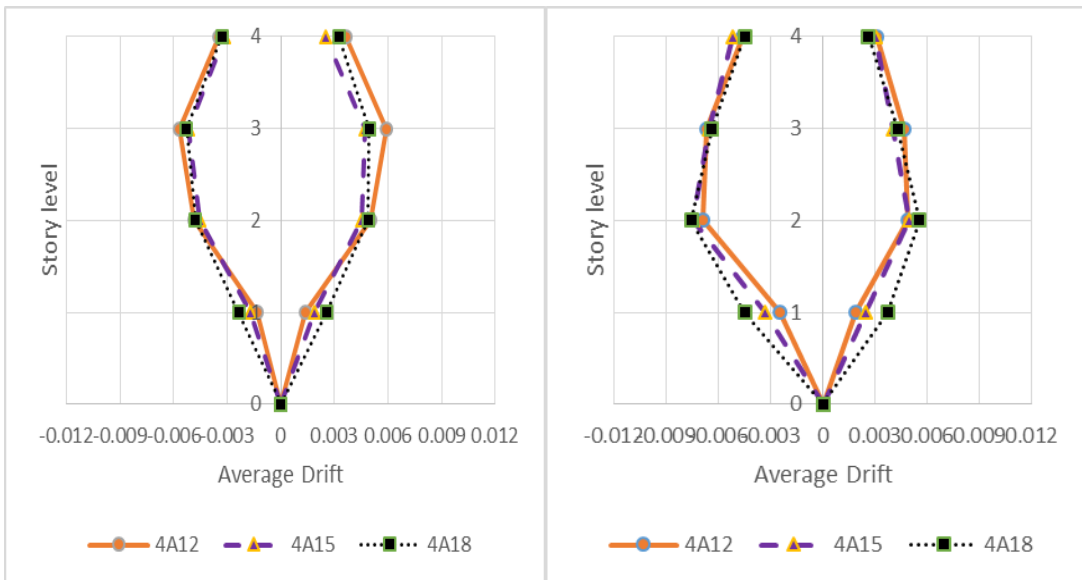


Figure 6-12, Group 2, asymmetric plan models, average drift response for E-W direction (left) and N-S direction (right)

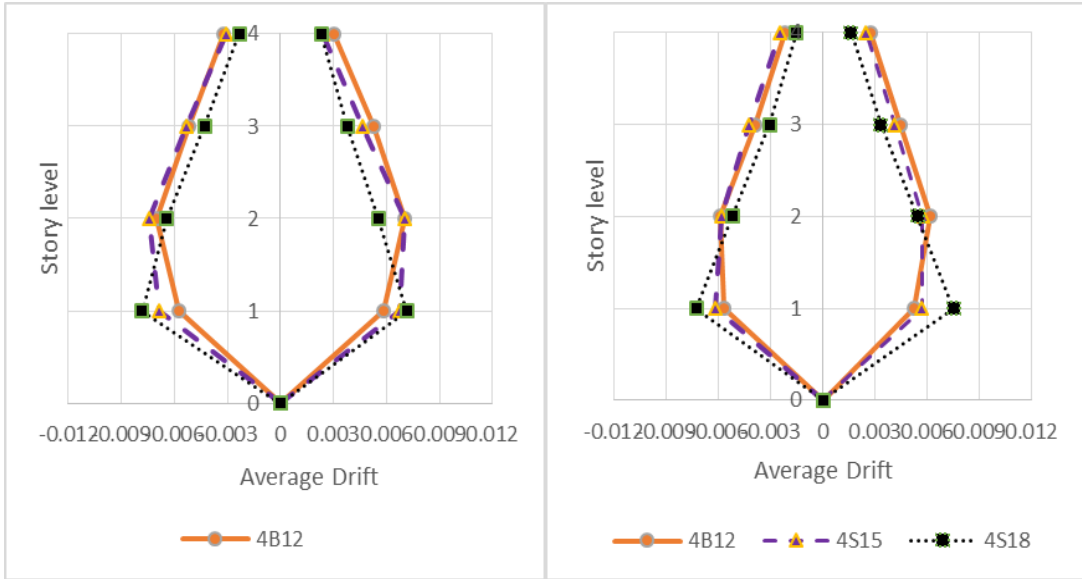


Figure 6-13, Group 2, symmetric plan models, average drift response for E-W direction (left) and N-S direction (right)

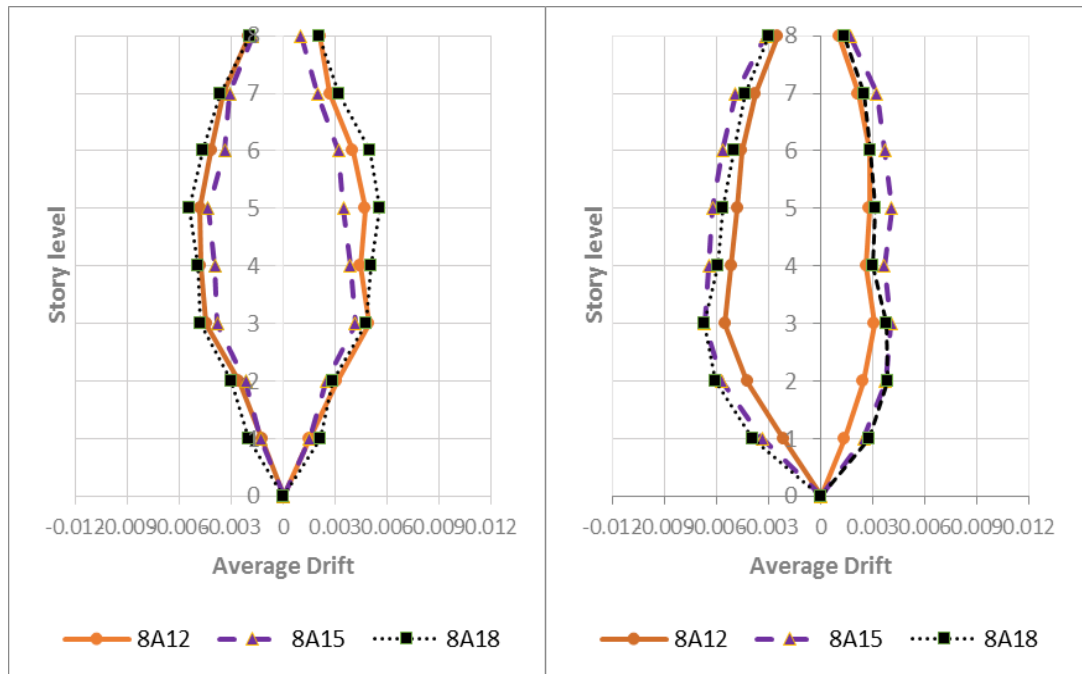


Figure 6-14, Group 3, asymmetric plan models, average drift response for E-W direction (left) and N-S direction (right)

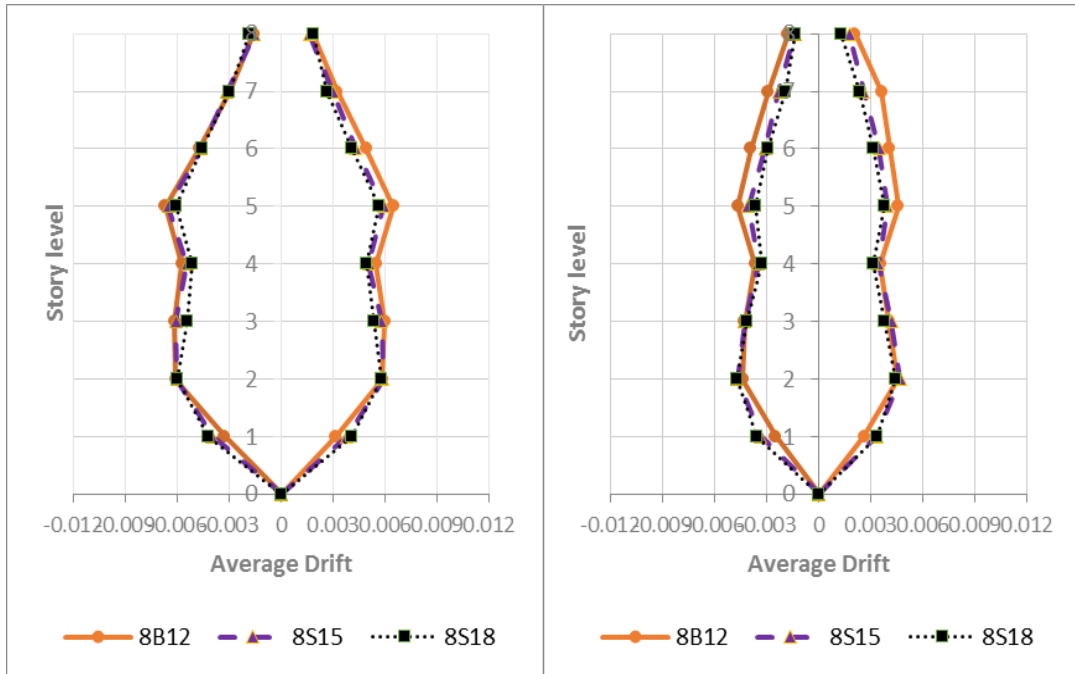


Figure 6-15, Group 3, symmetric plan models, average drift response for E-W direction (left) and N-S direction (right)

Figures 6-14 and 6-15 reveal that the average drift responses of eight story models are less than the other models. This trend is observed for plastic hinge formation in section 6-2 as well.

Regardless of the first story height, the N-S direction of asymmetric plan models show more average first story drift compared to the E-W direction. Lack of central columns in the first story at axis B (Frames 1 to 3, section 3-4) is the most probable reason for this behavior. Archetype models 2A12 and 2A15 in the N-S direction suffer more than 1% average drift. Over IO drift level criterion is occurred only in the N-S direction at the first story level of the abovementioned models. Owing primarily to the higher level of hinge formations (up to story mechanism in model 2A12, section 6-3), these models suffer more lateral deformation. None of other selected models goes beyond the FEMA 356 (2000) IO damage level although light sparse of results is observable among the latter models.

Four (4) story asymmetric plan models have the same column section for their first story level. This is also the case for the eight (8) story asymmetric plan models, which are obtained through traditional linear static analysis and design approach

(chapter 3). The average drift response of the first story of these models shows a typical sequence. It means by increasing of the first story height for each group of models with taller first stories have more drift value. As mentioned, the column sections are the same, and the previous sequence is occurred for both E-W and N-S directions. Thus, these can only be understood by considering soft story possibility, although in this case the acquired drift is far less than story mechanism level. Furthermore, difference between the E-W responses for all of these models is less in contrast with the N-S direction (Figures 6-12 and 6-14). This shows the effect of central column elimination on the average drift response. For the aforementioned models, the response of upper stories do not show any specific trend and more drift is observed for all those models in upper stories than the first story. Due to the facts that the input of excitations for all of these cases are the same, similarity of the material and structural sections for all of the abovementioned models, and despite the inherent similar dynamic analysis approach, this complex phenomena in upper levels may only be associated with the irregular format of these models.

The previous trend is attributed to symmetric plan models; i.e. model with taller first story show more first story drift. However, the first story column section is not similar for this group of models. In fact, 4S15 and 4S18 models have similar first story column section while model 4B12 has a smaller section. Additionally, model 8B12 and 8S15 have similar first story section while column section of model 8S18 is different in this case. The similarity of the first story average drift between the symmetric and asymmetric plan model show that the vertical irregularity may involve more in the erratic upper stories response than the plan irregularity. In agreement with the above statement, figure 6-13 is addressed. In this figure, which is for group 2 models with symmetric plan, both principal directions of model 4S18 response depict more drift concentration on the first story. This case is a classical condition of susceptible soft story response. 4B12 model is more regular while 4S15 model behaves between 4S18 and 4B12 models with bias toward 4B12 drift response than 4S18. Though the vertical irregularity effect in particular and overall drifts response in general is less dominant for the eight story models, this is also the case for eight story models with regular plan (figure 6-15).

Figures 6-10 to 6-15 are categorized based on the similarity in both of the number of stories and the first story plan type. To get a better view from the preceding results and to review the effect of number of stories on the response, the same average drift results are presented according to story height similarity. In this time, figures 6-16 to 6-18 are provided to show the average drift for models with the first story height equal to 12, 15, and 18 feet respectively. These figures may also be uses to compare the plan irregularity effect on the response of the models.

Unequivocally, the same result regarding lesser average drift for eight story models in comparison with four story models is observable in the following figures. The same trend is clear for comparison of four story models with the two story models.

Review of eight story models response shows another aspect of the results. As mentioned in section 6-2, the eight story models mostly remain in the elastic phase. Their response is attributed to the elastic stiffness. In addition, the archetype models are originally designed for dead and live load effects (dominant load combinations). The structural members for A type models are heavier than the symmetric plan models, specifically in the first two stories. The stiffer lower story levels of model 8A12 in the E-W direction (figure 6-16, top) have less average drift in comparison with the 8B12 model in its lower stories. Their response gets closer in the upper stories.

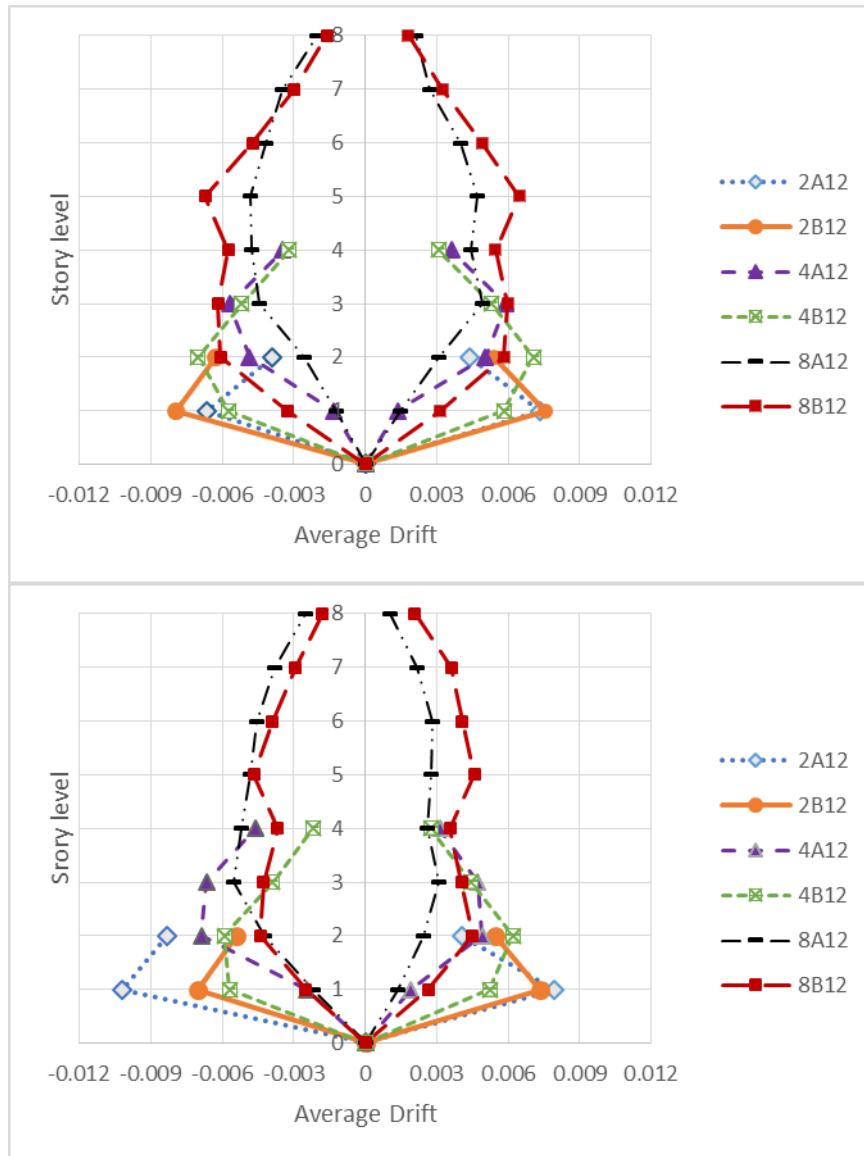


Figure 6-16, Average drift response for models with the first story height equal to twelve feet, E-W direction (top) and N-S direction (bottom)

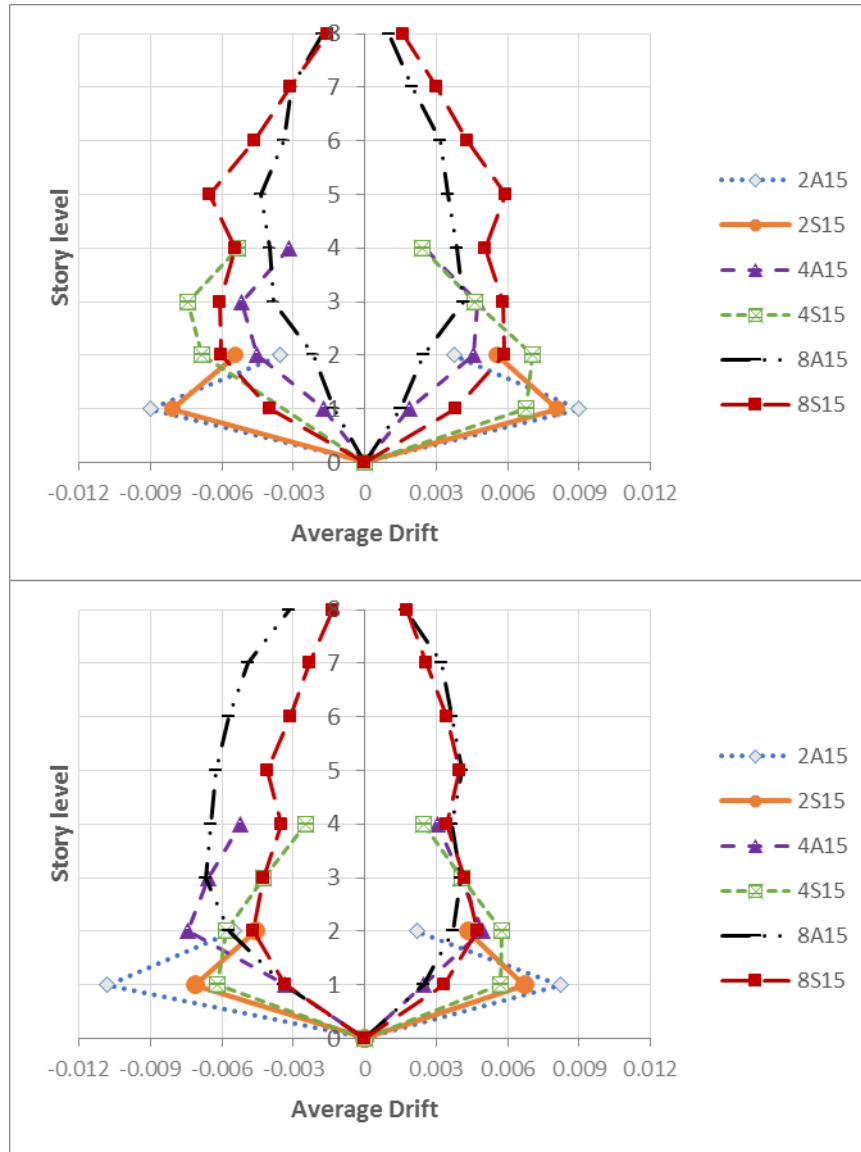


Figure 6-17, Average drift response for models with the first story height equal to fifteen feet, E-W direction (top) and N-S direction (bottom)

Another similar trend is observed for 8A15 and 8S15 models (figure 6-17). 8A18 model also has less average drift at its first story than 8S18 while the difference between 8A18 and 8S18 becomes mostly closer in lower levels. Again, the possible soft story phenomenon may be prominent in this case. Models with 18 feet first story height illustrate higher level of erratic response than 15 feet first story height models.

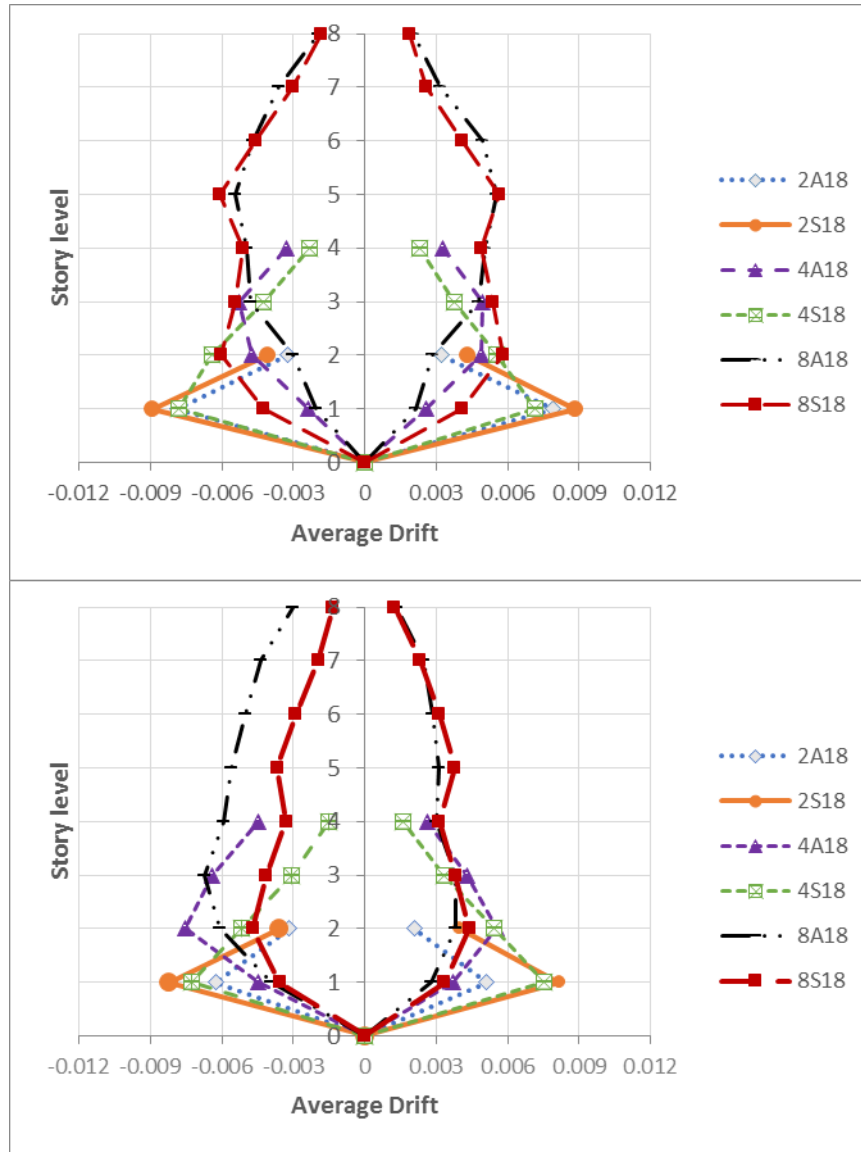


Figure 6-18, Average drift response for models with the first story height equal to eighteen feet, E-W direction (top) and N-S direction (bottom)

For the abovementioned models, the response of models 8A18 to 8S18 is very close for the positive part of the N-S direction (figure 6-18, bottom). It is the case for the models 8A15 and 8S15 in figure 6-17 (bottom). The possible reason for this behavior is the presence of strong frame in axis 4 of asymmetric plan models, which help to absorb the seismic energy (movement) elastically. In the negative direction of applied seismic, the less stiff part of the frame system (lack of middle column line for axes 1 to 3) leads to increase in the overall response of models 8A18 and 8A15 in

contrast with the 8S18 and 8S15 models. The difference between average drift for models 8A12 and 8B12 becomes much less in the negative part of N-S direction. It means the weak part of stiffness irregularity (in plan) causes more drift in its side (which may be achievable in elastic analysis as well), but the elevation irregularity can exacerbate the drift response considerably.

To do the same analogy, overall response in the E-W direction and N-S direction of four (4) story models are very similar to the former response of eight story models. In this case, the difference between responses is sharper than eight story models. Almost all asymmetric four story models have less drift in their first story than the symmetric plan models. The results get closer or reverse for higher levels. The reason relies on two factors. First, the lower columns and beams in asymmetric four story models are stronger than corresponding symmetric models (figure 3-3). As mentioned in the beginning of this section, the induced force is directly corresponded to the drift, and the induced forces are related to the strength of members. However, all four story selected models have similar column section at levels above the first level. Thus, the response becomes closer toward upper levels. Another reason for response difference between four story regular plans with irregular plans is related to entering the plastic phase mode in different performance stages. Formation of plastic hinges, no matter at which stage, influences the displacement result drastically and usually increases the drift value. The effect of first story height does not illustrate any specific trend for this group of models.

The former discussion about strength and plastic hinge applies to two (2) story models as well. In average, these models show more plastic hinge regarding both total formed hinge number and damage level (section 6-2). Thus, two story models have more drift while their response is more sporadic in comparison with other models. Although 2A12, 2A15, and 2A18 models have stronger beams and columns at their first story level than 2B12, 2S15, and 2S18, respectively, the effect of plastic hinge formation is obvious here. Refer to sections 6-2 and 6-3, models 2A12 and 2A15 which suffer the heaviest damage level. At the same time, figures 6-16 and 6-17 show that 2A12 and 2A15 models have more or at least very close average drift corresponding to their symmetric plan models. On the other hand, model 2A18,

which suffers less plastic hinge, demonstrates less drift than 2S18 model. Therefore, in case of plastic hinge formation (in terms of both level and numbers), the story drift is observed more among the selected models. Otherwise, the first story height more than plan irregularity affects the drift response.

While there is a general agreement on hazardous effect of plan irregularity corresponding to drift response in high seismic zones (chapter 2), figure 6-10 to 6-18 show that there might be considerable disagreement in this case regarding selected models of this study. These figures illustrate that the taller models suffer less drift, and asymmetric plan in the first story does not change the overall response significantly. Indeed, for several conditions, the plan irregular models illustrate lower amount for average drift. However, consequence of the first story height still affects the drift response of the selected models.

## Chapter 7: Summary, Conclusions, and Recommendations

Prior to summarizing the current study, it should be mentioned that the acquired results are applicable to the building models used here. These LRC models contain several approximations and assumptions although the models are designed based on the realistic approaches as practically as possible. The results and conclusions basically associate with low to mid-rise frame structures, holding vertical and/or plan irregularity, which are located in low seismic zones.

### **7.1. Summary**

Building damage level in low seismic zones has been underestimated, at least for the irregular RC structures. Performance levels of LRC structures under appropriate low intensity ground shaking have to be examined to find the proper demand parameters and applicable acceptance criteria. The traditional engineering approach entails the application of linear static analysis for seismic design, if any, for low seismic zones. In case of seismic consideration, the linear approach has been performing for low seismic zone mostly regardless of irregularity computation. The current seismic standards in the US are drafted according to high seismic zone criteria. These standards have led to questions concerning the ability of these code provisions to predict appropriate performance of LRC structures in low seismic zones. In fact, the applicability of irregular prescriptive code provisions to LRC structural systems is obscure. The other concern is lack of universal set of standard ground motions, even for high seismic areas. In some instances, there is not any sufficient information and thus, proper assumption is required to supply the low seismic activity missing data. This is also the case for estimate of capacity associated with LRC structures, particularly frame structures in this study. Failure modes, effect of irregularities, and design provisions should be involved of nonlinear states.

The salient features of this study focus on the tall ground (first) story for soft story mechanism analysis, which may contain the central column elimination at the same story level to reflect the torsional irregularity. Seismicity of the Northern and North Eastern parts of the US is considered as a sample for low seismic risk region. To the best author's knowledge, there has not been any effort in the literatures to consider both vertical and plan irregularity effects in the low seismic regions for LRC structures. The linear static design procedure, according to the standard concrete design code (ACI 318), and under dead, lives, and wind loads are accomplished. They cover the common US design practice, especially the construction method of previous decades. The statically designed models are analyzed under THA and NSA methods. FEMA 356 (2000) regulation is applied for basic plastic hinge definition and acceptance criteria. The results are attained in terms of plastic hinge formation and drift ratio to provide an insight into the real behavior of LRC frame structures in low seismic zone regions. The result can be used to alert researchers and code writers about possible potential paucities of current seismic code provisions and design standards for existing LRC building, or even newly designed RC structures, regarding vertical or plan irregularities.

Within the framework of this study, result has shown that although IC of LRC structures may provide some level of seismic resistance, the asymmetric plan structures may suffer higher level of damage up to even severe collapse stage for the low-rise models. The first story vertical irregularity and soft story mechanism under the THA procedure for selected models do not occur. It is important to be mentioned that taller than the first story height based on the severe ASCE 7-05 (2005) code requirement is considered. Depending on the number of involved frames, direction of seismic excitation may affect response of the structures. Desirable seismic response associated with weak beam/strong column response is observed for almost all the models, regardless of the number of story. Pushover method based on seismic distribution load pattern, according to FEMA 356 procedure, shows a good agreement with the results from the THA method for the vertical irregular structures. The least agreement between THA and NSA methods is observed for the extreme irregular structure, i.e. 2A18, with both plan and vertical irregularities. By increasing the

number of stories from two (2) to four (4), and from four (4) to eight (8), it is understood that the number of plastic hinges and their damage level decrease considerably. However, for almost all models some level of damage is observed. The same procedure is observed for drift ratio of the selected models. It is illustrated that the frequency content of the applied seismic record, even for a low intensity motion, may significantly affect the response and may cause total collapse.

Overall, although most of the seismic analyses and record selections of this study reflect the Eastern and North Eastern parts of the US, the damage level of the selected two story LRC inventory indicates possible considerable damage for similar structures in low seismic zones. On the other hand, the level of damage and drift ratio for the tallest models (eight story models) are low, and negligible for the regular models of this group. The four story models suffer drift and damage level between the two aforementioned eight and two story models. It is also unlikely that soft story mechanism occurs for the vertical irregular structures under current US seismic code requirements. The irregular plan models perform poorly. In fact, more severe damages to the main structural elements of LRC structures may be expected for irregular plan structures. Even under a possible low seismic event, the vulnerability stage will be significant for the low-rise two story selected models, while the taller models, specifically eight story models, may suffer less damage.

## **7.2. Overview of the Findings and Conclusion**

### **7.2.1. Overview of Important Findings**

Employing THA and NSA procedures, primary facts on the prediction of the nonlinear behavior of the selected models are listed below:

- The severity of formed hinges, in terms of damage levels, is higher for two (2) stories models than the other models.
- On the other hand, the symmetric plan eight (8) story models show zero up to little damage levels. The damage level of four story selected

models is roughly stood between levels of two story and eight story models.

- Regardless of the first story height, the plastic hinges are observed for two (2), four (4), and eight (8) stories asymmetric plan models. The hinge formations at the stiff part of the models are seen under both excitation directions (i.e. the E-W and N-S). It is noticed that considerable damages are possible to form in the stiff part of LRC structures, even under low to medium intense seismic events in unsymmetrical structures.
- Review of results shows that in the E-W direction, the total formed hinges, in terms of number and intensity state of hinges, are more than in the N-S direction. This trend is observed for using both THA and NSA methods. The reason can be justified due to more involved frames in the E-S direction.
- For asymmetric models, by increasing of the first story height, difference between THA and NSA results becomes more noticeable. The result difference is more scattered for the columns than for the beams.
- NSA method illustrates reasonable similarity with THA method for symmetric models. The higher level of conservatism is observed for columns of *B* type models in NSA method in associate with THA results. Indeed, NSA method shows some formed hinges which have not been seen in THA method for the same *B* type models. In comparison with THA method, the variation of NSA response is increased by raising the first story height and/or involving of plan irregularity for all the selected models.
- The severe story mechanism is observed for model 2A12 under LPR seismic action with collapse damage level. Frequency domain analysis of the result reveals the resonance between the input ground motion (LPR) and the frequency of the model is the reason for the observed collapse stage damage level.

- Except for few models, the eight story models show less maximum absolute drift in comparison with the other models.
- THA analysis shows that the maximum absolute drift for all eight story models are within IO damage level per FEMA 356 (2000) criteria. Four and two story models may suffer more drift, although their maximum drift does not reach LS level. For the latter models, low intense seismic event may impose noticeable damage state in LRC structures.
- Regardless of symmetric or asymmetric plan configuration, the maximum absolute drift is independent to the input records for two and four story models, versus eight story models in which input record is the dominant parameter for the acquired maximum absolute drift.
- The maximum absolute drifts for both plan and/or vertical irregular structures of this study do not show considerable difference. This result is in disagreement with most design code interpretations and assumptions regarding higher expected drift value for a structure with both plan and height irregularities.
- Maximum average drift reveals that the structural dynamic behavior may affect response more than the inherent characteristics of applied ground motions.
- Lack of the first story middle row column for asymmetric plan model causes more drift in the N-S directions comparing to the E-W direction of the same models.
- Irregularities of the models affect the models' drift response in their higher story levels. Models with more irregularity (i.e. both plan and vertical irregularities) illustrate more erratic drift response in their upper levels than models with one irregular condition.
- The structural member size in lower stories has considerable effect in the maximum average drift response in the lower stories; differences between models get closer in the upper stories.

- For asymmetric plan models, the direction of excitation (in the N-S axis) affects the maximum average drift response.
- Despite the overall poor response prediction of NSA models for asymmetric plan structures, the effective mass in the first mode of the symmetric selected models (*B* and *S* models) are approximately more than 60%. Therefore, it may be expected that the NSA will yield accurate results for these cases. On the other hand, the tall first story effect combined with column elimination may drastically change the result accuracy. Unsymmetrical stiffness and more involvement of the effective mass associated with torsional response may cause the NSA unpredictable behavior and results.

### **7.2.2. Conclusion**

The major conclusions identified in this study are drawn below:

- Total numbers of formed hinges are decreased with increase of the number of stories in the archetype models.
- For almost all cases, the number of hinges is formed more in beams than columns.
- Increase of the first story height does not perceptibly change the hinge formation damage level and number of formed hinges for symmetric plan models.
- One to one comparison between asymmetric and the corresponding symmetric models reveals that the average formed hinges and damage levels for *A* type models are more than for their corresponding regular plan model. This trend occurs in both THA and NSA methods.
- Plastic hinge formation in columns is very limited for the eight story selected models. It seems that regardless of irregularities, non-seismic designed frame buildings per requirements of ASCE 7 and ACI 318 are conservative. On the other hand, the two story models may suffer higher level of damages. The four story models undergo damages between two models.

- Increase of the first story height has minor effect to maximum absolute drift of the symmetric plan models. However, the maximum average drift values for eight and four story models are increased through increment of the first story height. Possible soft story effect can be explained in those cases.
- Increase of the first story height shows negligible and even reverse effect to the maximum absolute drift for most asymmetric plan models. Similar to symmetric plan models, the maximum average drift values for eight and four story models are increased through increment of the first story height. Additionally, similar to the previous paragraph, the same possible soft story influence on the maximum average response is recognizable for these cases as well.
- Drift ratios of irregular models remain quite low. As far as this study alone concerned, combination of this fact with the limited plastic hinge formation in columns eliminates the possibility of collapse mechanism for most cases.
- Design of structural members per early edition of design codes, without any seismic consideration, seems to be sufficient to withstand the applied ground motions regarding drift requirements. However, due to lack of enough ductility, the low imposed drift may not guaranty the collapse prevention, as it has been seen for one of the cases.
- Failures do not seem to occur for structural members with vertical irregularities, while extreme vertical irregularity is applied for selection of the first story height. It seems like that the more strict requirements of ASCE 7-05 (2005) or 7-10 (2010) with regard to vertical irregularities is more dominant for high seismic zones.
- The NSA method is approximate in nature and is based on static loading. It is found out that this method may exaggerate some response, while some other response might be ignored. However, this study indicates that pushover analyses are rationally effective in

capturing the hinge locations and damage level for the selected LRC structures, except most of asymmetric plan models. Nonetheless, the THA method illustrates more plastic hinge formation in the upper levels for the irregular cases, which is not estimated adequately by NSA method.

- This study shows that the code provisions for LRC frame systems may provide an acceptable level of safety for mid to high-rise structures within SDC B seismic level. However, particularly for asymmetric plan models, the higher damage level and drift ratio may be expected for low-rise LRC models in these regions under the low intense ground motions.

### **7.3. Suggestions for Future Research**

Some of the future research needs related to the assessment of seismic vulnerability of LRC frame structures in the low seismic zones are listed below:

- One of the extension for further work would be the examination of different other geometrical formations. Addition and/or alteration of story height, plans, bay length, number of stories, number of spans, and member dimensions may expose a deeper insight into the response of LRC structures in low seismic zones.
- The acquired results should be verified by additional parametric studies utilizing different types of ground motions, soil types, and ultimately different record scale procedures.
- The NSA method is conducted in association with one lateral load pattern. Other type of lateral load vectors, or other method of NSA procedure, such as Modal pushover, might be useful to study LRC irregular response.

- Different parameters may be assigned to investigate the influence of current design standard criteria. For instance, fiber hinge method, beam-column joint rotation, and the bond-slip effect are some of them.
- The shear reinforcement has not been explicitly considered. The shear action aspect is applied through the limitation in hinge capacity per FEMA 356 (2000) guideline. In fact, the Bernoulli beam assumption regarding deformation is adopted here. This method is unable to adopt shear deformation properly. In order to achieve a more comprehensive approach, a better beam hinge feature with the incorporation of direct shear model would be recommended.
- Obviously, experimental methods, which involving real time seismic excitations, e.g. shaking table test, are very useful to examine the response of LRC structures with vertical and/or plan irregularities.

## Appendices

### **Appendix A: Abbreviations and Acronyms List**

ACI: American Concrete Institute  
ASCE: American Society of Civil Engineering  
ATC: Applied Technology Council  
CQC: Complete Quadratic Combination  
CP: Collapse Prevention  
CTBUH: Council on Tall Buildings and Urban Habitat  
DCR: Demand Capacity Ratio  
DOF: Degree Of Freedom  
EH: Extra Height  
E-W: East-West  
FE: Finite Element  
FEMA: Federal Emergency Management Agency  
FFT: Fast Fourier Transform  
FN: Fault Normal  
FP: Fault Parallel  
GM: Geometric Mean  
HHT: Hilber-Hughes-Taylor  
IBC: International Building Code  
IC: Inherent Capacity  
IMF: Intermediate Moment Frame  
IO: Immediate Occupancy  
LATBSDC: Los Angeles Tall Buildings Structural Design Council  
LPR: Loma Prieta (earthquake)  
LRC: Lightly Reinforced Concrete  
LS: Life Safety  
MCE: Maximum Considered (or Credible) Earthquake

MDOF: Multi Degree Of Freedom  
MH: Medium Height  
NAH: Nahanni (earthquake)  
NC: Nonconforming  
NEHRP: National Earthquake Hazards Reduction Program  
NH: Normal Height  
NIST: National Institute of Standards and Technology  
N-S: North-South  
NOR: Northridge (earthquake)  
NSA: Nonlinear Static Analysis (or: Pushover)  
OMF: Ordinary Moment Frame  
PEER: Pacific Earthquake Engineering Research Center  
PGA: Peak Ground Acceleration  
RC: Reinforced Concrete  
SDC: Seismic Design Category  
SDOF: Single Degree Of Freedom  
SEAOC: Structural Engineers Association of California  
SMF: Special Moment Frame  
SRSS: Square Root of the Sum of the Squares  
THA: Time History Analysis (or: Nonlinear Dynamic Response History  
Analysis)  
UBC: Uniform Building Code  
USA: the United States of America  
USGS: United States Geological Survey  
US: the United States (of America)  
WNA: Whittier Narrows (earthquake)

## Appendix B: Software Plastic Hinge Verification

### B.1. Verification Example for Assigned Beam Yield Moment

Plastic hinge capacity plays a significant role in all nonlinear static and time history analyses of reinforced concrete structures with lumped plasticity modeling, which are used in this study (see Chapters 4 and 5). The post-yielding capacity of the members, curvature, and degradation are typically depending on the first yield moment,  $M_y$ . SAP2000 (2012) automatically calculates and applies the amount of  $M_y$  to each concrete member at the defined hinge position based on the assigned material properties, allocated reinforcements, and member dimensions. All these basic information are defined in Chapter 3 of this thesis.

To verify the allocated automatic yield moment to the hinges, several software assigned yield moments has been checked. The variety of beam size and sections in different stories are randomly selected and the allocated plastic hinge capacity has been checked. The automatic assigned moment and hand-calculated results provide very good conformation and negligible deviation. As an example, one of those calculations is presented here to show the procedure and level of compromising between the software and hand-calculated results.

The current example shows the plastic hinge yield moment comparison for the selected structure model of 4B12, beam type B1, located at the first story between axis A and B. As mentioned in Chapter 4, plastic hinges are allocated to the start and end of every beam member, including B1. The designed reinforcements in Chapter 3 are used for all automatic and hand calculations. Based on Chapter 3, the assigned dimensions and properties for the selected B1 beam at the first hinge location (left side of beam at Axis A) are:

$H = 12.0$  inch (height),  $B = 8.0$  inch (width);

$A_s = 1.08$  square inch (top reinforcement);

$A'_s = 0.88$  square inch (bottom reinforcement);

$d = 9.5$  inch (effective depth of tension steel),  $d' = 2.5$  inch (centroid of compression steel to the extreme compression edge), and also:

$f_y = 60.0$  ksi,  $E_s = 29000$  ksi,

$$f'_c = 4.0 \text{ ksi}, \quad E_c = 3605 \text{ ksi (per ACI 318-08 clause 8.5.1)}$$

The software assigned name to the hinge is 324H1, and Figure B-1 shows the capacity, elastic, plastic, post plastic, plus yield moment at top and bottom of the hinge. The negative and positive scaled points are B<sup>-</sup> and B, respectively. The magnitudes of moments are shown based on Kips-inch units.

Verification procedure for only the negative yield moment is presented here and the positive yield moment may be obtained in a similar manner. From figure B-1, the negative yield moment, calculated by the software is equal to 538.4118 kips.in ( $\approx 44.88$  kips.ft).

Based on provided reinforcements and section dimensions, the steel ratio may be calculated as:

$$\rho^- = \rho = A_s / bd = 1.08 / (8'' \times 9.5'') = 0.0142$$

$$\rho^+ = \rho' = A'_s / bd = 0.88 / (8'' \times 9.5'') = 0.0116$$

$$\therefore n = E_s / E_c = 8.044;$$

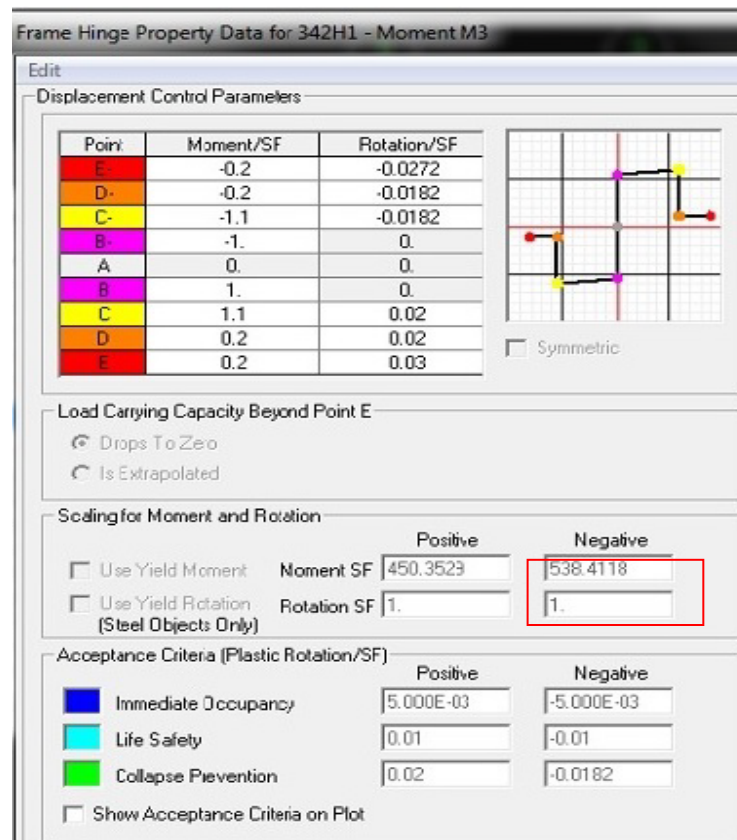


Figure B-1: Example of Software Allocated Hinge Parameters-Moment M3

Park and Paulay (1975) mentioned that stress-strain curve for reinforced concrete sections can be approximately assumed linear, up to even concrete maximum stress, i.e. stress equal to  $f'_c$ . This assumption is only valid provided that the concrete stress does not exceed its maximum when the steel stress reaches its yield strength. Thus, the depth to the neutral axis,  $k$ , can be derived by using a straight-line formula, presented by equation B-1 (Ibid.):

$$k = [(\rho + \rho')^2 n^2 + 2(\rho + \frac{\rho' d'}{a})n]^{1/2} - (\rho + \rho')n \quad [B-1]$$

The yield moment may be obtained by equation B-2 (Ibid.):

$$M_y = A_s f_y j d \quad [B-2]$$

In which  $jd$  stands for the distance from the centroid of compressive forces in the steel and concrete to the centroid of the tension force.

By substitution of terms in equation B-1,  $k$  would be equal to 0.3588, and then:

$$kd = 0.3588 \times 9.5'' = 3.3086 \text{ inch}$$

Steel yield strain can be calculated as:

$$\varepsilon_s = f_y / E_s = \frac{60}{29000} \approx 0.0021 \quad [B-3]$$

Considering linear stress-strain diagram, the concrete strain is:

$$\varepsilon_c = \varepsilon_s \times \frac{kd}{d - kd} = 0.0011 \quad [B-4]$$

The concrete stress can be derived as:

$$f_c = \varepsilon_c E_c = 3.9655 \text{ ksi} \quad [B-5]$$

Because  $f_c \leq f'_c$ , the triangular stress block is an acceptable stress-strain assumption and can be used with a linear equation.

For the compression steel (bottom reinforcement), the corresponding strain can be calculated as:

$$\varepsilon'_s = \varepsilon_c \times \frac{kd-d'}{kd} \approx 0.0003 \quad [\text{B-6}]$$

Therefore, the steel compression stress is:

$$\therefore f'_s = \varepsilon'_s \times E_s = 8.7 \text{ ksi} \quad [\text{B-7}]$$

Then the concrete and steel compression forces would be:

$$C_c = \frac{1}{2} \times f'_c bkd = 52.481 \text{ kips} \quad [\text{B-8}]$$

$$C_s = A'_s f'_s = 7.656 \text{ kips} \quad [\text{B-9}]$$

The total compression force is:

$$\therefore C_t = C_s + C_c = 60.137 \text{ kips}$$

The total compression force is implied  $\bar{y}$  at where:

$$\bar{y} = [(d' \times C_s) + (C_c \times kd/3)] / C_t = 1.281 \text{ inch} \quad [\text{B-10}]$$

$$\therefore jd = d - \bar{y} = 8.219 \text{ inch}$$

Finally, by substituting all the terms into equation B-2, the yield moment would be:

$$M_y = 1.08 \times 60 \times 8.219 = 532.5912 \text{ kips.inch}$$

Comparing the abovementioned calculated yield moment and the allocated yield moment by software in Figure B-1 shows a very minor difference so the software automatic allocation is validated.

## **B.2. Verification Example for Assigned Column Axial Force-Moment**

### **Interaction Curve**

Similar to the beam yield moment, SAP2000 (2012) automatically allocates Axial Force-Biaxial Moment interaction curves to each column member based on the defined-assigned section properties. At the beginning and the end of each column member PM2M3 hinge is assigned (see Chapter 4). The result is an almost elliptical shape curve, in which every boundary points on the 3D surface show their corresponding maximum capacities of the referred hinge including axial force, and moments in two different major directions for each section.

To verify the software calculated PM2M3 curve, several curves for different models in different stories have been checked randomly. The automatic assigned PM2M3 curves and hand-calculated results exhibit very close conformation. One of the PM2M3 capacity calculation is presented to show the general procedure and level of similarity between the software assigned curve and hand-calculated results.

The current example is an interaction curve for column line B2 located at the first story of 4S15 model (C1414-8#7). The selected PM2M3 plastic hinge is placed at the start point of the column B2 close to the base support. The designated reinforcements in Chapter 3 are used in all automatic allocation, and consequently they are considered for hand calculations as well. Based on Chapter 3, the assigned dimensions and properties for the selected column are:

Square section 14.0 inch by 14.0 inch;

Longitudinal Reinforcement: 8#7, 3 rebar at each side;

Steel cover to stirrups: 1.5 inch, and  $f_y$ ,  $E_s$ ,  $f'_c$ , and  $E_c$  are the same as those for section B-1.

The software assigned PM2M3 with hinge name of 294H1 to the column, and Figure B-2 shows the interaction curve of the selected hinge. For convenience, the

interaction curve is illustrated for maximum M2 condition (curve surface 1), but results can be viewed for any other combination and angle of interaction. The maximum capacity of axial force and moments are calculated (left side of Figure B-2) and all other corresponding axial force and moment are scaled based on the maximum amounts accordingly. Due to symmetry of the selected section, the maximum moment capacities in both main directions are equal.

The overall PMM interaction calculation is a typical and classical reinforced concrete design procedure, which is mentioned in many references and textbooks. Using the same reference for the plastic moment calculation by Park and Paulay (1975), verification procedure for the maximum axial compression force capacity is presented here. Then the validation for maximum moment capacity and its corresponding axial force is demonstrated.

Due to the traditional method of calculation and accessibility in many references, detail computation is not shown here. It is worth to mention that the interaction curve plays a groundwork rule for the nonlinear capacity definition, but in-depth hand calculation for any PM2M3 plastic hinge would be very cumbersome. There are two main modes of failures for this type of plastic hinge, namely steel yielding or concrete crush (Chandrasekaran et al. 2010), and consequently there would be several complex combinations of these two modes in different zones of an interaction curve. In this study, besides the hand calculation, few PM2M3 hinges have been checked by the graphs provided by the previous reference, i.e. (Chandrasekaran et al. 2010). The allocated hinges by software and the graph results showed a very reasonable conformation.

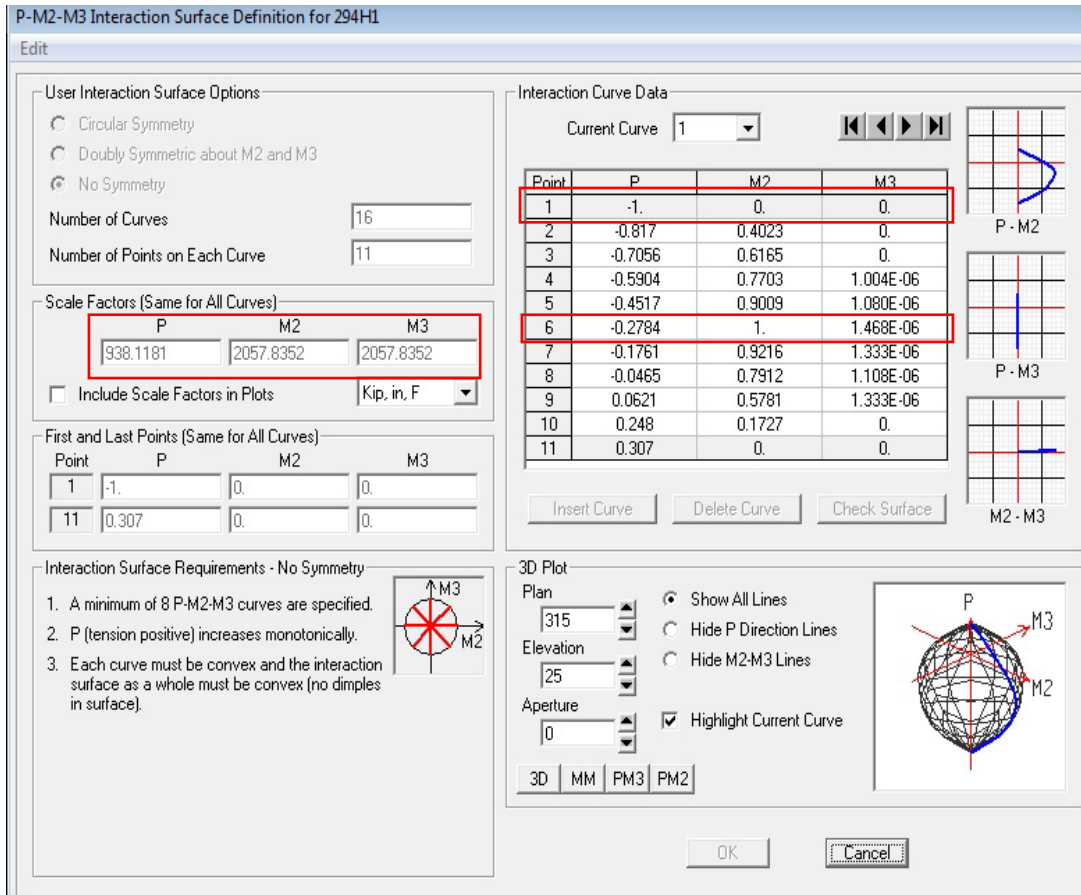


Figure B-2: Example of Software Allocated Hinge Parameters-PM2M3 Type

The maximum axial capacity can be driven from Equation 10-2 of ACI 318-08 (2008), except that for nonlinear capacity computation there is not any cap limit due to the strength reduction factor:

$$P_n = 0.85f'_c (A_g - A_s) + f_y A_s \quad [B-11]$$

Substituting all the terms in equation B-3:

$$P_n = 0.85 \times 4 \times (142 - 8 \times 0.6) + 60 \times 8 \times 0.6 = 938.08 \text{ kips}$$

Expectedly, the maximum compression force by hand calculation and software allocated are equal as can be seen from Figure B-2 and calculated  $P_n$ .

Maximum M2 (surface with M3 = 0) and its corresponding P (axial force) mean the balanced failure on the interaction curve, or simply  $f_s$  would be equal to  $f_y$ . Considering 1.5 inch concrete cover (same as applied cover to square column section), and #4 ties (see chapter 3),  $d$  and  $d'$  would be equal to 11.56 inch and 2.44 inch, respectively. Therefore, from similar triangles the depth to the neutral axis is:

$$c = \varepsilon_c \times \frac{d}{(\varepsilon_c + \varepsilon_s)} = 6.8 \text{ inch} \quad [\text{B-12}]$$

In which  $\varepsilon_c$  is equal to 0.003 per ACI 318-08 (2008) clause 10.3, and  $\varepsilon_s$  is defined in equation B-3. Strain in compression steel is:

$$\varepsilon'_s = \varepsilon_c \times \frac{c-d'}{c} \approx 0.0019 \quad [\text{B-13}]$$

Using Equation B-7, the compression steel stress is:  $f'_s = 55.1$  ksi. Considering section 10.2.7 of ACI 318-08 (2008),  $\beta_1$  is equal to 0.85, and the depth of the equivalent rectangular stress block, i.e.  $a$ , is computed as 5.78 inch. Thus, the concrete force may be calculated as:

$$C_c = 0.85f'_c ab = 275.13 \text{ kips} \quad [\text{B-14}]$$

3#7 reinforcements are on the tension side, and 3#7 on the compression side, with 2#7 at neutral axis (middle of the section), so the tensile force (by ignoring the middle reinforcements) is:

$$F_s = f_y \times A_{st} = 108 \text{ kips (tension)} \quad [\text{B-15}]$$

And steel compression force would be:

$$C_s = (f'_s - 0.85f'_c) A_{sc} = 93.06 \text{ kips} \quad [\text{B-16}]$$

The resultant force would be:

$$\therefore C_t = C_s + C_c - F_s = 260.19 \text{ kips}$$

By comparison with Figure B-2, the scaled axial force corresponding to the maximum moment is:

$$P = 0.2784 \times 938.1181 = 261.17 \text{ kips, which shows a very negligible difference.}$$

By allowing for sign of the loads, the maximum moment would be calculated as:

$$M_n = C_c (h/2 - a/2) + F_s (h/2 - d) + C_s (h/2 - d') = 2047.62 \text{ kips.inch} \quad [\text{B-17}]$$

Again, comparing the calculated  $M_n$  and the maximum  $M_2$  in Figure B-2 exhibits a very minor difference between those two moments, which is actually less than 0.5% difference.

## Appendix C: Verification of Software Computed Target

### Displacement

SAP2000 (2012) can automatically calculate FEMA 356 target displacement. As mentioned in chapter 5, target displacement is the key element of FEMA 356 (2000) pushover method. To verify the software assigned target displacement, hand-calculated verification was accomplished. The results provide very good agreement between the software and hand-calculated values. Following is one example to illustrate the procedure and level of compromising between the software and hand-calculated outcomes.

The current example shows the target displacement for selected structure model of 2A15, in the East-West push direction (X coordinate in SAP2000). As previously cited, FEMA 356 (2000) pushover basically follows Coefficient Method. The program applies equation 5-10 to calculate the target displacement which is here computed equal to 0.232 ft. Figure C-1 shows the computed coefficients per FEMA356 method by the software.

To verify the software calculation, coefficients in Equation 5-10 were computed in accordance with FEMA 356 target displacement method through application of FEMA 356 (2000) recommendations. Also, to calculate the effective fundamental period of the building ( $T_e$ ) an approximate method has been performed. Equation 5-1 is repeated here, and all terms and definitions have been explained in section 5-2 of the main text.

$$\delta_t = C_0 C_1 C_2 C_3 S_a (T_e^2 / 4\pi^2) g \quad \text{[Repetitive 5-10]}$$

$C_0$  is a coefficient which accounts for the difference between the roof displacement of an MDOF structure and the equivalent SDOF system (FEMA 356 2000). The software applies the accurate method per FEMA 356 technique by using of actual deflected shape vector. For verification procedure, the accurate method would be very cumbersome. Instead, the corresponding simplified value tabulated in FEMA 356 has been used. In the simplified method, a straight-line vector with equal

masses at each floor level is assumed (Ibid.), which shows a close agreement with the selected model. Based on Table 3-2 of FEMA 356 (2000), for a two-story model this factor can be assumed equal to 1.20.

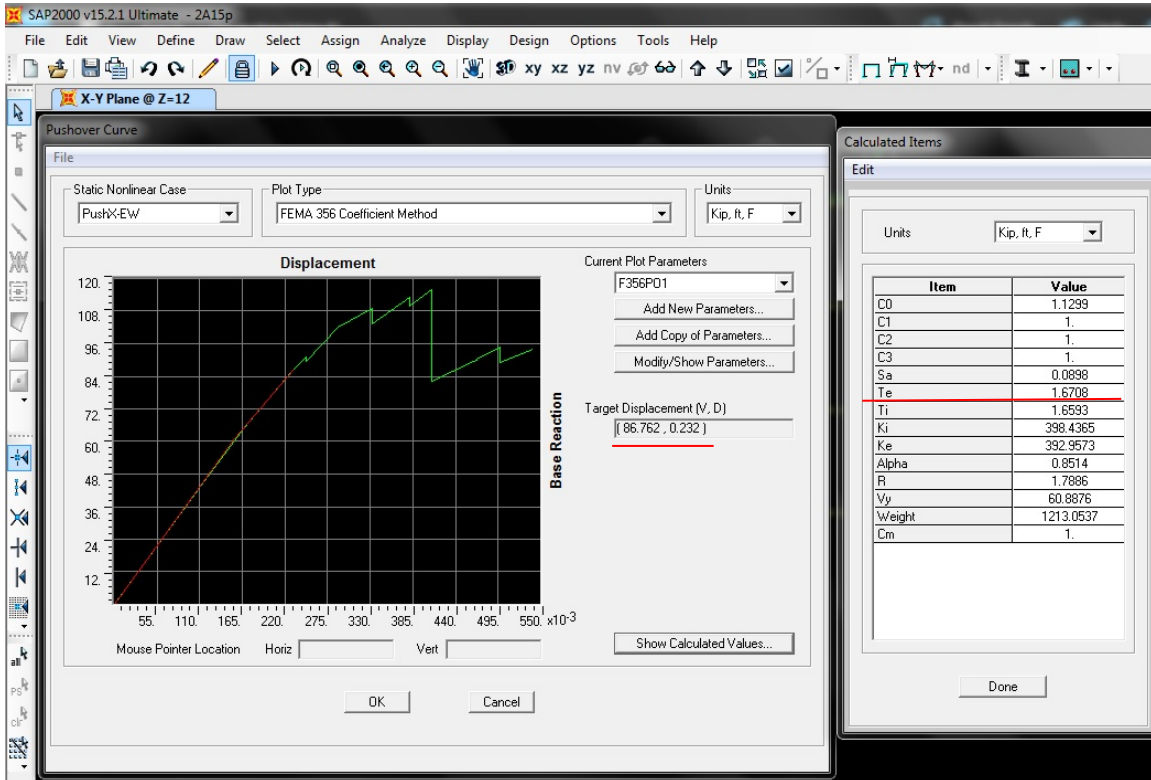


Figure C-1: Software computed target displacement and related coefficient for model 2A15 (East-West direction)

Per FEMA 356 (2000), if  $T_e \geq T_s$ , then  $C_1$  would be equal to one (1.0).  $T_s$  is defined in chapter 4. From Figure 4-1, it can be seen that  $T_s$  is equal to 0.40 s. Later on it will be illustrated that  $T_e$  is much higher than 0.40 s, so  $C_1$  is assumed equal to 1.0.

$C_2$  represents the effect of stiffness degradation and hysteretic shape. Per FEMA 356, for nonlinear analysis and due to fact that these effects have been modelled in plastic hinges allocation (chapter 4),  $C_2$  can be considered equal to one (1.0).

$C_3$  accounts for dynamic P- $\Delta$  effect. The effect of second order displacement has been performed through one of the nonlinear cases (chapters 4 and 5). Thus, this factor can be assumed equal to 1.0.

$S_a$  is the response spectrum acceleration. Per FEMA 356 (2000), for  $T > T_s$ :

$$S_a = S_{X1} / (B_1 T) \quad [C-1]$$

$$S_{X1} = F_v S_1 \quad [C-2]$$

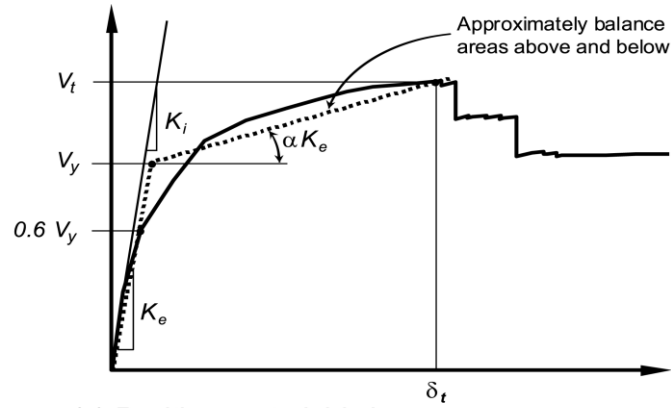
In which  $T$  is the period of the structure,  $S_{X1}$  is the spectral response acceleration parameter at one-second, which is similar to  $S_{M1}$  in ASCE 7-05 (2005) and IBC (2012).  $B_1$  is the function of effective damping. 5% damping ratio is assumed for the selected models (chapter 4). Per FEMA 356 (2000) for 5% damping ratio this factor is equal to 1.0.  $F_v$  is the long-period site coefficient at 1.0 second period, which is equal to 2.4 for the selected site class D (FEMA 356 2000; ASCE 7-05 2005).  $S_{D1}$  is defined in chapter 4, which is equal to 0.1s in this study. Per IBC (2012) and/or ASCE 7-05 (2005)  $S_{D1}$  can be defined as:

$$S_{D1} = (2/3) S_{X1} \quad [C-3]$$

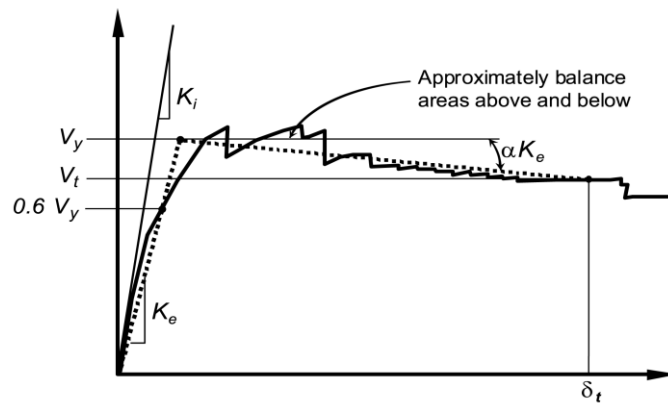
Hence, from equations C-2 and C-3,  $S_1$  and  $S_{X1}$  would be equal to 0.0625 and 0.15, respectively.

The effective fundamental period of the structure ( $T_e$ ) in the direction of pushover is another involved factor. This period should be based on the idealized force-displacement curve (FEMA 356 2000). Figure C-2 shows description of elastic lateral stiffness ( $K_i$ ) and effective lateral stiffness ( $K_e$ ) in FEMA 356 (2000).  $T_e$  should be calculated in accordance with Equation C-4:

$$T_e = T_i \sqrt{\frac{K_i}{K_e}} \quad [C-4]$$



(a) Positive post-yield slope



(b) Negative post-yield slope

Figure C-2: Definition for idealized force-displacement curves for two different post yield cases (Source: FEMA 356 2000)

To compute  $T_e$ , force-displacement curve must be known. SAP2000 (2012) creates the curve and calculates all terms in equation C-4 successively. Instead of using the software curve to calculate the effective period, another approximate approach has been implied. As it can be seen from Figure C-2,  $K_e$  and  $T_e$  are related to the  $0.6 V_y$ , in which  $V_y$  stands for the effective yield strength. At this level of load and deformation, concrete would be cracked. Then, the cracked concrete component stiffnesses are applied to the model 2A15. The cracked condition is assumed according to the effective stiffness value in ASCE 41-06 (2007b), in which for the beams:  $I_{cr} = 0.3I_g$  and  $A_{cr} = 0.4A_w$ . Considering the level of stress,  $I_{cr} = 0.7I_g$  and  $A_{cr} = 0.4A_w$  have been applied for the columns as well. For the slabs  $I_{cr} = I_g/3$  has been

devoted.  $I_{cr}$  and  $I_g$  stand for the section cracked and gross moments of inertia, respectively.  $A_{cr}$  and  $A_w$  denote the cracked and gross shear area correspondingly. Thus, the effective fundamental period of structure can be obtained through the effective cracked assumption. Bearing in mind that the pushover method in general, and idealized force-displacement curve method in particular, are both approximate procedures by their nature, the effective stiffness method may represent enough accuracy for the purpose of validation. The former cracked sections led to the effective period equal to 1.54 s in the direction of push. Consequently,  $S_a$  in equation C-1 is computed equal to 0.097.

All the above-mentioned assumptions and calculated terms are applied to equation 5-10 to calculate the corresponding target displacement:

$$\delta_{t-2A15} = 1.2 \times 1.0 \times 1.0 \times 1.0 \times 0.097 (1.54^2 / 4\pi^2) \times 32.147 = 0.225 \text{ ft.}$$

From figure C-1, the program target displacement is shown equal to 0.232 ft, which unequivocally has shown very close approximate to the hand-calculated value with less than 0.1 inch difference.

## **Appendix D: Table of Hinge Formation Results for the Selected**

### **Models**

For all selected models under the applied seismic excitations and pushover cases total number of hinge formations at different inelastic cases is counted and presented. The results are illustrated for each load direction, the North-South (N-S) and East-West (E-W), for each story level, and for column and beam separately. The hinge formation sequences are classified per FEMA 356 (2000) and SAP2000 (2012), which are based on the acceptance criteria and damage stages previously defined in chapter 4. The level of damages is distinct in the backbone curves which are defined in chapter 4. Hinge formation in B stage means the entry level of deformation after elastic phase, and the ultimately E stage means total failure of a hinge. Blank cells mean no entry data and the models have not suffered any hinge formation for that case under the associate action.

In following tables, LPR, NAH, NOR, and WNA denote the applied seismic cases and FN and FP are related to the excitation directions which are all defined in chapter 4. The corresponding hinge formations for each case are attained through THA results at the end response including the total record excitation and free vibration time phase defined in chapter 5. Moreover, the results due to NSA procedure are illustrated under PUSH case which means pushover analysis results. NSA total hinge formations are presented at the target displacement at the final stage of PUSH case for both N-S and E-W directions. The total numbers are classified per story level and for the beams and columns individually. Plastic hinge locations are explained in chapter 4. Thus, the results are corresponding to the same hinge locations.

For Asymmetric (2A12 up to 8A18) models, hinge formation may show two different numbers in each case on a common cell for both THA and/or NSA procedures. The presented number in prentices denotes the related hinge formation under the same action and for the same story level and component, except that the direction of excitation or pushover case is reversed. To consider the effect of direction for asymmetric plan models, two exact similar excitations or PUSH cases are applied

to A models. The only difference between two cases is the direction and it was explained in chapters 4 and 5.

Table D-1: Number of Hinge Formation for Selected Model 2A12

Hinge condition at different damage levels											
Structure State					Number of Hinge formation at each stage						
Model Type	Direction	Story	Action	Component	B	IO	LS	CP	C	D	E
2A12	N-S (FP)	1st	LPR	Beam	11 (12)	0 (6)	1				6 (6)
				Column	8 (11)					8 (5)	
			NAH	Beam	16 (14)	0 (2)					
				Column	15 (14)						
			NOR	Beam	14 (14)	2 (2)					
				Column	11 (12)						
		WNA	Beam	14 (14)	2 (2)						
			Column	14 (14)							
		PUSH	Beam	12 (14)	0 (2)						
			Column	16 (11)							
		2nd	LPR	Beam	6 (4)	2(6)		1 (2)		1	
				Column	11 (8)		0 (2)			7 (6)	
			NAH	Beam	4 (4)	2 (2)					
				Column	7 (7)						
			NOR	Beam	4 (4)	2 (2)					
				Column	7 (7)						
			WNA	Beam	4 (4)	2 (2)					
				Column	7 (9)						
	PUSH		Beam	4 (8)	2						
			Column	6 (4)							
	E-W (FN)	1st	LPR	Beam	6	4	2				
				Column	5						
			NAH	Beam	5	5	2				
				Column	11						
			NOR	Beam	7	5					
				Column							
			WNA	Beam	6	4	2				
				Column	9						
			PUSH	Beam	6	3	2				
				Column	4		1			1	
2nd		LPR	Beam	6	2						
			Column	6							
		NAH	Beam	6	2						
			Column	9							
		NOR	Beam	5	2						
			Column	6							
		WNA	Beam	6	2						
			Column	5							
PUSH	Beam	6	1								
	Column	6									

Table D-2: Number of Hinge Formation for Selected Model 2A15

Hinge condition at different damage levels											
Structure State					Number of Hinge formation at each stage						
Model Type	Direction	Story	Action	Component	B	IO	LS	CP	C	D	E
2A15	N-S (FP)	1st	LPR	Beam	9 (11)	3 (4)					
				Column	8 (8)						
			NAH	Beam	7 (7)	4 (4)					
				Column	2 (4)						
			NOR	Beam	12 (11)	6 (8)	0 (1)				
				Column	14 (13)					4 (4)	
		WNA	Beam	9 (9)	4 (4)						
			Column	4 (4)							
		PUSH	Beam	14 (11)	2 (4)						
			Column	11 (6)		4			1		
		2nd	LPR	Beam	4 (4)	2 (2)					
				Column	6 (6)						
			NAH	Beam	4 (4)	2 (2)					
				Column	5 (5)						
			NOR	Beam	6 (5)	2 (2)	0 (1)				
				Column	6 (8)				3 (1)	3 (3)	
		WNA	Beam	4 (4)	2 (2)						
			Column	6 (5)							
	PUSH	Beam	6 (8)	2 (2)							
		Column	7 (4)								
	E-W (FN)	1st	LPR	Beam	8	6	2				
				Column	2						
			NAH	Beam	8	6	2				
				Column	12						
			NOR	Beam	8	6	2				
				Column	13		1				
		WNA	Beam	8	6	2					
			Column	4							
		PUSH	Beam	9	5	2					
			Column	5		1					
2nd		LPR	Beam	4	2						
			Column	4							
		NAH	Beam	4	2						
			Column	6							
		NOR	Beam	4	2						
			Column	6							
WNA		Beam	4	2							
		Column	5								
PUSH	Beam	7	2								
	Column	3									

Table D-3: Number of Hinge Formation for Selected Model 2A18

Hinge condition at different damage levels											
Structure State					Number of Hinge formation at each stage						
Model Type	Direction	Story	Action	Component	B	IO	LS	CP	C	D	E
2A18	N-S (FP)	1st	LPR	Beam	12 (10)	2	2				
				Column	0 (1)						
			NAH	Beam	12 (12)						
				Column							
			NOR	Beam	8 (8)						
				Column							
		WNA	Beam	12 (10)	0 (2)						
			Column								
		PUSH	Beam	8 (10)	4 (2)						
			Column	13 (7)		2			2	1	
		2nd	LPR	Beam	6 (8)	2 (2)					
				Column							
	NAH		Beam	8 (8)	2 (2)						
			Column								
	NOR		Beam	6 (6)	2 (2)						
			Column								
	WNA	Beam	8 (8)	2 (0)							
		Column									
	PUSH	Beam	6 (10)	6 (2)							
		Column	10 (11)								
	E-W (FN)	1st	LPR	Beam	12	2	2				
				Column							
			NAH	Beam	12	4	2				
				Column	9					1	
NOR			Beam	10	4	2					
			Column	10							
WNA		Beam	12	4							
		Column									
PUSH		Beam	5	3	2						
		Column									
2nd		LPR	Beam	6	2						
			Column								
	NAH	Beam	9	2							
		Column	3					1			
	NOR	Beam	6	2							
		Column									
WNA	Beam	6	2								
	Column										
PUSH	Beam	6	2								
	Column										

Table D-4: Number of Hinge Formation for Selected Model 2B12

Hinge condition at different damage levels											
Structure State					Number of Hinge formation at each stage						
Model Type	Direction	Story	Action	Component	B	IO	LS	CP	C	D	E
2B12	N-S (FP)	1st	LPR	Beam	14						
				Column	4						
			NAH	Beam	10						
				Column							
			NOR	Beam	12						
				Column	2						
		WNA	Beam	10							
			Column								
		PUSH	Beam	8							
			Column	10							
		2nd	LPR	Beam	8	2					
				Column	4						
	NAH		Beam	2	2						
			Column								
	NOR		Beam	2	2						
			Column	4							
	WNA	Beam	2	2							
		Column									
	PUSH	Beam	4	2							
		Column	2								
	E-W (FN)	1st	LPR	Beam	5	2					
				Column							
			NAH	Beam	4	2	2				
				Column	7						
NOR			Beam	4	2	2					
			Column	3							
WNA		Beam	2	4							
		Column									
PUSH		Beam	2	2							
		Column	6								
2nd		LPR	Beam	6	2						
			Column	1							
	NAH	Beam	6	2							
		Column	2								
	NOR	Beam	5	3							
		Column	4								
WNA	Beam	6	2								
	Column										
PUSH	Beam	1	3								
	Column	2									

Table D-5: Number of Hinge Formation for Selected Model 2S15

Hinge condition at different damage levels											
Structure State					Number of Hinge formation at each stage						
Model Type	Direction	Story	Action	Component	B	IO	LS	CP	C	D	E
2S15	N-S (FP)	1st	LPR	Beam	10	2					
				Column							
			NAH	Beam	8						
				Column							
			NOR	Beam	13	6					
				Column	12						4
		WNA	Beam	8							
			Column								
		PUSH	Beam	10							
			Column	3							
		2nd	LPR	Beam	8						
				Column	2						
	NAH		Beam	8							
			Column								
	NOR		Beam	10	4						
			Column	2							
	WNA	Beam	8								
		Column									
	PUSH	Beam	8								
		Column	2								
	E-W (FN)	1st	LPR	Beam	6	4					
				Column							
			NAH	Beam	2	4	4				
				Column	4						
			NOR	Beam	2	4	4				
				Column	4						
		WNA	Beam	6	4						
			Column								
		PUSH	Beam	8							
			Column	3							
2nd		LPR	Beam	8	4						
			Column								
	NAH	Beam	8	4							
		Column	4								
	NOR	Beam	8	4							
		Column	4								
WNA	Beam	8	4								
	Column										
PUSH	Beam	8									
	Column	7									

Table D-6: Number of Hinge Formation for Selected Model 2S18

Hinge condition at different damage levels											
Structure State					Number of Hinge formation at each stage						
Model Type	Direction	Story	Action	Component	B	IO	LS	CP	C	D	E
2S18	N-S (FP)	1st	LPR	Beam	10						
				Column							
			NAH	Beam	8						
				Column							
			NOR	Beam	10						
				Column							
		WNA	Beam	10							
			Column								
		PUSH	Beam	10	1						
			Column	2							
		2nd	LPR	Beam	6						
				Column	2						
			NAH	Beam	6						
				Column							
			NOR	Beam	6						
	Column										
	WNA		Beam	6							
			Column								
	PUSH		Beam	5	1						
		Column	3								
	E-W (FN)	1st	LPR	Beam	4	4					
				Column							
			NAH	Beam	4	4					
				Column							
			NOR	Beam		4	4				
				Column	4						
			WNA	Beam		4	4				
				Column	6						
			PUSH	Beam	2	2	2				
		Column		4							
2nd		LPR	Beam	6	4						
			Column								
		NAH	Beam	2	4						
			Column								
		NOR	Beam	6	4						
	Column										
WNA	Beam	6	4								
	Column	2									
PUSH	Beam	5	2								
	Column	2									

Table D-7: Number of Hinge Formation for Selected Model 4A12

Hinge condition at different damage levels											
Structure State					Number of Hinge formation at each stage						
Model Type	Direction	Story	Action	Component	B	IO	LS	CP	C	D	E
4A12	N-S (FP)	1st	LPR	Beam	14 (14)	2					
				Column							
			NAH	Beam	12 (12)						
				Column							
			NOR	Beam	12 (12)	4 (4)					
				Column							
		WNA	Beam	14 (14)							
			Column								
		PUSH	Beam	8 (14)	2						
			Column								
		2nd	LPR	Beam	4 (6)	6 (6)					
				Column							
			NAH	Beam	6 (6)	2 (2)					
				Column							
			NOR	Beam	7 (8)	2 (1)	6 (6)				
				Column	4 (1)						
		WNA	Beam	4 (4)	6 (6)						
			Column								
		PUSH	Beam	4 (3)	4 (6)	2					
			Column	1	1						
		3rd	LPR	Beam	4 (4)	6 (6)					
				Column							
			NAH	Beam	8 (8)						
				Column							
			NOR	Beam	9 (9)	6 (6)					
				Column	4 (4)						
		WNA	Beam	4 (4)	4 (4)						
			Column								
		PUSH	Beam	5 (6)	4 (2)						
			Column	2		1		1			
4th	LPR	Beam	4 (4)								
		Column	1 (2)								
	NAH	Beam	4 (4)								
		Column									
	NOR	Beam	0 (3)	4 (2)							
		Column	2 (3)								
WNA	Beam	4 (4)									
	Column	0 (1)									
PUSH	Beam	2 (2)									
	Column	2									

Table D-7 (continue): Number of Hinge Formation for Selected Model 4A12

Hinge condition at different damage levels											
Structure State					Number of Hinge formation at each stage						
Model Type	Direction	Story	Action	Component	B	IO	LS	CP	C	D	E
4A12	E-W (FN)	1st	LPR	Beam	14	2					
				Column							
			NAH	Beam	10	6					
				Column							
			NOR	Beam	12	4					
				Column							
		WNA	Beam	13	3						
			Column								
		PUSH	Beam	9	1						
			Column								
		2nd	LPR	Beam	8	3	1				
				Column							
			NAH	Beam	12	6	2				
				Column	6						
			NOR	Beam	4	4	2				
				Column	2						
		WNA	Beam	8	2	2					
			Column								
		PUSH	Beam	5	2						
			Column								
		3rd	LPR	Beam	8	4					
				Column							
			NAH	Beam	10	2	2				
				Column	2						
			NOR	Beam	8	2	2				
				Column	2						
		WNA	Beam	8	3	1					
			Column								
		PUSH	Beam	3	1						
			Column								
		4th	LPR	Beam	5						
				Column							
			NAH	Beam	6						
				Column	9						
			NOR	Beam	4						
				Column							
		WNA	Beam	4							
			Column								
		PUSH	Beam	1							
			Column								

Table D-8: Number of Hinge Formation for Selected Model 4A15

Hinge condition at different damage levels											
Structure State				Number of Hinge formation at each stage							
Model Type	Direction	Story	Action	Component	B	IO	LS	CP	C	D	E
4A15	N-S (FP)	1st	LPR	Beam	12 (12)	4 (4)					
				Column							
			NAH	Beam	16 (16)						
				Column							
			NOR	Beam	12 (12)	6 (6)					
				Column							
		WNA	Beam	16 (16)							
			Column								
		PUSH	Beam	10 (12)	2 (2)						
			Column								
		2nd	LPR	Beam	6 (6)	6 (6)					
				Column							
			NAH	Beam	6 (6)	4 (4)					
				Column							
			NOR	Beam	9 (8)	3 (4)	6 (6)				
				Column	4 (5)						
		WNA	Beam	10 (10)							
			Column								
		PUSH	Beam	4 (5)	4 (6)						
			Column								
		3rd	LPR	Beam	6 (8)	6 (4)					
				Column							
			NAH	Beam	5 (4)	4 (6)					
				Column							
			NOR	Beam	12 (12)	6 (6)					
				Column	4 (4)						
		WNA	Beam	10 (10)							
			Column								
		PUSH	Beam	8 (5)	0 (5)						
			Column	2							
		4th	LPR	Beam	6 (6)						
				Column	1 (1)						
			NAH	Beam	6 (6)						
				Column	2 (2)						
			NOR	Beam	5 (5)	1 (2)					
				Column	2 (3)						
WNA	Beam	5 (5)									
	Column	1 (1)									
PUSH	Beam	3 (4)									
	Column										

Table D-8 (continue): Number of Hinge Formation for Selected Model 4A15

Hinge condition at different damage levels											
Structure State					Number of Hinge formation at each stage						
Model Type	Direction	Story	Action	Component	B	IO	LS	CP	C	D	E
4A15	E-W (FN)	1st	LPR	Beam	10	6					
				Column							
			NAH	Beam	8	6	4				
				Column							
			NOR	Beam	13	3					
				Column							
		WNA	Beam	12	4						
			Column								
		PUSH	Beam	7	4						
			Column								
		2nd	LPR	Beam	11	3	2				
				Column							
			NAH	Beam	9	6	4				
				Column	6						
			NOR	Beam	10	5					
				Column							
		WNA	Beam	10	4						
			Column								
		PUSH	Beam	9	1	1					
			Column	2							
		3rd	LPR	Beam	10	5					
				Column							
			NAH	Beam	9	5	2				
				Column	2						
			NOR	Beam	11	4					
				Column							
		WNA	Beam	10	5						
			Column								
		PUSH	Beam	6	1						
			Column	2							
		4th	LPR	Beam	10						
				Column							
			NAH	Beam	11	1					
				Column	6						
			NOR	Beam	8						
				Column							
		WNA	Beam	9							
			Column								
		PUSH	Beam	3							
			Column	1							

Table D-9: Number of Hinge Formation for Selected Model 4A18

Hinge condition at different damage levels											
Structure State					Number of Hinge formation at each stage						
Model Type	Direction	Story	Action	Component	B	IO	LS	CP	C	D	E
4A18	N-S (FP)	1st	LPR	Beam	14 (14)						
				Column							
			NAH	Beam	14 (14)						
				Column							
			NOR	Beam	17 (16)	0 (4)					
				Column							
		WNA	Beam	14 (14)							
			Column								
		PUSH	Beam	10 (10)	0 (2)						
			Column								
		2nd	LPR	Beam	9 (9)	2 (2)					
				Column							
			NAH	Beam	11 (9)	0 (2)					
				Column							
			NOR	Beam	9 (6)	4 (7)	2 (2)				
				Column	4 (4)						
		WNA	Beam	9 (9)	2 (2)						
			Column								
		PUSH	Beam	6 (4)	2 (4)						
			Column	2							
		3rd	LPR	Beam	6 (6)						
				Column							
			NAH	Beam	9 (8)	0 (2)					
				Column	2						
			NOR	Beam	11 (11)	2 (2)					
				Column	4 (4)						
		WNA	Beam	6 (6)							
			Column								
		PUSH	Beam	4 (4)	0 (2)						
			Column	2							
4th	LPR	Beam									
		Column	0 (2)								
	NAH	Beam									
		Column	1 (1)								
	NOR	Beam									
		Column	2 (2)								
WNA	Beam										
	Column										
PUSH	Beam										
	Column	2									

Table D-9 (continue): Number of Hinge Formation for Selected Model 4A18

Hinge condition at different damage levels											
Structure State					Number of Hinge formation at each stage						
Model Type	Direction	Story	Action	Component	B	IO	LS	CP	C	D	E
4A18	E-W (FN)	1st	LPR	Beam	7	5					
				Column							
			NAH	Beam	5	5	2				
				Column							
			NOR	Beam	4	8	2				
				Column							
		WNA	Beam	6	6						
			Column								
		PUSH	Beam	6	5						
			Column								
		2nd	LPR	Beam	5	4					
				Column							
			NAH	Beam	12		4				
				Column	5						
			NOR	Beam	13		4				
				Column	3						
		WNA	Beam	6	2	2					
			Column								
		PUSH	Beam	6	2						
			Column	2							
		3rd	LPR	Beam	4	4					
				Column							
			NAH	Beam	5	2	2				
				Column							
			NOR	Beam	10	2	2				
				Column	2						
		WNA	Beam	5	4						
			Column								
		PUSH	Beam	3	1						
			Column	2							
		4th	LPR	Beam	1						
				Column							
			NAH	Beam	2						
				Column	6						
			NOR	Beam	2						
				Column	3						
WNA	Beam										
	Column	1									
PUSH	Beam										
	Column	1									

Table D-10: Number of Hinge Formation for Selected Model 4B12

Hinge condition at different damage levels											
Structure State					Number of Hinge formation at each stage						
Model Type	Direction	Story	Action	Component	B	IO	LS	CP	C	D	E
4B12	N-S (FP)	1st	LPR	Beam	10	6					
				Column							
			NAH	Beam	12	4					
				Column							
			NOR	Beam	12	4					
				Column							
		WNA	Beam	12	4						
			Column								
		PUSH	Beam	9	2						
			Column								
		2nd	LPR	Beam	12	4					
				Column							
			NAH	Beam	12	2					
				Column							
			NOR	Beam	12	2					
				Column							
		WNA	Beam	12	4						
			Column								
		PUSH	Beam	8	2						
			Column								
		3rd	LPR	Beam	14	2					
				Column							
			NAH	Beam	10						
				Column							
NOR	Beam		10								
	Column										
WNA	Beam	10									
	Column										
PUSH	Beam	10									
	Column										
4th	LPR	Beam	4								
		Column									
	NAH	Beam	4								
		Column									
	NOR	Beam	4								
		Column									
WNA	Beam	4									
	Column										
PUSH	Beam	2									
	Column										

Table D-10 (continue): Number of Hinge Formation for Selected Model 4B12

Hinge condition at different damage levels											
Structure State					Number of Hinge formation at each stage						
Model Type	Direction	Story	Action	Component	B	IO	LS	CP	C	D	E
4B12	E-W (FN)	1st	LPR	Beam		8					
				Column							
			NAH	Beam	4	4					
				Column							
			NOR	Beam			8				
				Column							
		WNA	Beam		4	4					
			Column								
		PUSH	Beam	2	2	2					
			Column								
		2nd	LPR	Beam		8					
				Column							
			NAH	Beam	4	4					
				Column							
			NOR	Beam		4	4				
				Column		4	4				
		WNA	Beam								
			Column								
		PUSH	Beam	2	2	2					
			Column								
		3rd	LPR	Beam	4	4					
				Column							
			NAH	Beam	4	4					
				Column							
NOR	Beam		4	4							
	Column										
WNA	Beam	2	6								
	Column										
PUSH	Beam	4	2								
	Column										
4th	LPR	Beam									
		Column									
	NAH	Beam									
		Column									
	NOR	Beam									
		Column									
WNA	Beam										
	Column										
PUSH	Beam										
	Column										

Table D-11: Number of Hinge Formation for Selected Model 4S15

Hinge condition at different damage levels											
Structure State					Number of Hinge formation at each stage						
Model Type	Direction	Story	Action	Component	B	IO	LS	CP	C	D	E
4S15	N-S (FP)	1st	LPR	Beam	14						
				Column							
			NAH	Beam	14	2					
				Column							
			NOR	Beam	14						
				Column							
		WNA	Beam	16							
			Column								
		PUSH	Beam	7	4						
			Column	2							
		2nd	LPR	Beam	16						
				Column							
			NAH	Beam	16						
				Column							
			NOR	Beam	16						
				Column							
		WNA	Beam	14							
			Column								
		PUSH	Beam	8	2						
			Column	4							
		3rd	LPR	Beam	14						
				Column							
			NAH	Beam	10						
				Column							
			NOR	Beam	8						
				Column							
		WNA	Beam	8							
			Column								
PUSH	Beam	10									
	Column										
4th	LPR	Beam									
		Column									
	NAH	Beam									
		Column									
	NOR	Beam									
		Column									
WNA	Beam										
	Column										
PUSH	Beam										
	Column										

Table D-11 (continue): Number of Hinge Formation for Selected Model 4S15

Hinge condition at different damage levels											
Structure State					Number of Hinge formation at each stage						
Model Type	Direction	Story	Action	Component	B	IO	LS	CP	C	D	E
4S15	E-W (FN)	1st	LPR	Beam	4		8				
				Column	2						
			NAH	Beam	4	4					
				Column							
			NOR	Beam		4	4				
				Column							
		WNA	Beam		4	4					
			Column								
		PUSH	Beam	2	2	2					
			Column								
		2nd	LPR	Beam		4	4				
				Column	2						
			NAH	Beam	4	4					
				Column							
			NOR	Beam		6	2				
				Column							
		WNA	Beam		8						
			Column								
		PUSH	Beam	2	2	2					
			Column	2							
		3rd	LPR	Beam		8					
				Column							
			NAH	Beam	4	4					
				Column							
NOR	Beam		4	4							
	Column										
WNA	Beam	4	4								
	Column										
PUSH	Beam	4	2								
	Column										
4th	LPR	Beam									
		Column									
	NAH	Beam									
		Column									
	NOR	Beam									
		Column									
WNA	Beam										
	Column										
PUSH	Beam										
	Column										

Table D-12: Number of Hinge Formation for Selected Model 4S18

Hinge condition at different damage levels											
Structure State					Number of Hinge formation at each stage						
Model Type	Direction	Story	Action	Component	B	IO	LS	CP	C	D	E
4S18	N-S (FP)	1st	LPR	Beam	10						
				Column							
			NAH	Beam	16						
				Column							
			NOR	Beam	11	8					
				Column	2						
		WNA	Beam	12							
			Column								
		PUSH	Beam	10	2	2					
			Column	6			2				
		2nd	LPR	Beam	10						
				Column							
			NAH	Beam	12						
				Column							
			NOR	Beam	12	4					
				Column							
		WNA	Beam	10							
			Column								
		PUSH	Beam	8	4						
			Column	4							
		3rd	LPR	Beam	8						
				Column							
			NAH	Beam	10						
				Column							
			NOR	Beam	12						
				Column							
		WNA	Beam	10							
			Column								
		PUSH	Beam	8							
			Column								
		4th	LPR	Beam	4						
				Column							
			NAH	Beam	4						
				Column							
			NOR	Beam	4						
				Column							
		WNA	Beam	4							
			Column								
		PUSH	Beam	2							
			Column								

Table D-12 (continue): Number of Hinge Formation for Selected Model 4S18

Hinge condition at different damage levels												
Structure State					Number of Hinge formation at each stage							
Model Type	Direction	Story	Action	Component	B	IO	LS	CP	C	D	E	
4S18	E-W (FN)	1st	LPR	Beam		8						
				Column								
			NAH	Beam	4	4						
				Column								
			NOR	Beam		6	2					
				Column								
			WNA	Beam	4		8					
				Column	4							
			PUSH	Beam	4	2	2					
				Column	6				2			
			2nd	LPR	Beam	4	4					
					Column							
		NAH		Beam	4	4						
				Column								
		NOR		Beam	4	4						
				Column								
		WNA		Beam		4	4					
				Column								
		PUSH		Beam	4	4						
				Column	4							
		3rd		LPR	Beam	8						
					Column							
			NAH	Beam	4	4						
				Column								
			NOR	Beam	6	2						
				Column								
			WNA	Beam	2	6						
				Column								
			PUSH	Beam	4	2						
				Column								
			4th	LPR	Beam							
					Column							
		NAH		Beam								
				Column								
		NOR		Beam								
				Column								
		WNA		Beam								
				Column								
		PUSH		Beam								
				Column								

Table D-13: Number of Hinge Formation for Selected Model 8A12

Hinge condition at different damage levels											
Structure State					Number of Hinge formation at each stage						
Model Type	Direction	Story	Action	Component	B	IO	LS	CP	C	D	E
8A12	N-S (FP)	1st	LPR	Beam	3 (3)						
				Column							
			NAH	Beam	2 (2)						
				Column							
			NOR	Beam	5 (5)						
				Column							
		WNA	Beam	4 (7)							
			Column								
		PUSH	Beam	4 (3)							
			Column								
		2nd	LPR	Beam							
				Column							
			NAH	Beam							
				Column							
			NOR	Beam	0 (6)						
				Column							
		WNA	Beam	0 (2)							
			Column								
		PUSH	Beam								
			Column								
		3rd	LPR	Beam							
				Column							
			NAH	Beam							
				Column							
NOR	Beam		6 (6)								
	Column										
WNA	Beam	6 (6)									
	Column										
PUSH	Beam	4 (3)									
	Column										
4th	LPR	Beam	2								
		Column									
	NAH	Beam									
		Column									
	NOR	Beam	6 (6)								
		Column									
WNA	Beam	4 (6)									
	Column										
PUSH	Beam	4 (2)									
	Column										

Table D-13 (continue): Number of Hinge Formation for Selected Model 8A12

Hinge condition at different damage levels												
Structure State					Number of Hinge formation at each stage							
Model Type	Direction	Story	Action	Component	B	IO	LS	CP	C	D	E	
8A12	N-S (FP), continue	5th	LPR	Beam								
				Column								
			NAH	Beam								
				Column								
			NOR	Beam	10 (10)							
				Column								
		WNA	Beam	4 (4)								
			Column									
		PUSH	Beam	1 (1)								
			Column									
		6th	LPR	Beam								
				Column								
			NAH	Beam								
				Column								
			NOR	Beam	10 (6)							
				Column								
		WNA	Beam	4 (4)								
			Column									
		PUSH	Beam	1								
			Column									
		7th	LPR	Beam								
				Column								
			NAH	Beam								
				Column								
			NOR	Beam	0 (2)							
				Column								
		WNA	Beam	4 (4)								
			Column									
		PUSH	Beam									
			Column									
8th	LPR	Beam										
		Column										
	NAH	Beam										
		Column										
	NOR	Beam										
		Column	1									
WNA	Beam	4 (4)										
	Column											
PUSH	Beam											
	Column											

Table D-13 (continue): Number of Hinge Formation for Selected Model 8A12

Hinge condition at different damage levels											
Structure State					Number of Hinge formation at each stage						
Model Type	Direction	Story	Action	Component	B	IO	LS	CP	C	D	E
8A12	E-W (FN)	1st	LPR	Beam	3						
				Column							
			NAH	Beam	6						
				Column							
			NOR	Beam	3						
				Column							
		WNA	Beam	7	1						
			Column								
		PUSH	Beam	3							
			Column								
		2nd	LPR	Beam							
				Column							
			NAH	Beam	2						
				Column							
			NOR	Beam							
				Column							
		WNA	Beam	9							
			Column								
		PUSH	Beam	7							
			Column								
		3rd	LPR	Beam	1						
				Column							
			NAH	Beam	2						
				Column							
			NOR	Beam							
				Column							
		WNA	Beam	20							
			Column								
		PUSH	Beam	4	1						
			Column								
		4th	LPR	Beam	1						
				Column							
			NAH	Beam							
				Column							
			NOR	Beam	1						
				Column							
		WNA	Beam	16	1						
			Column								
		PUSH	Beam	5	1						
			Column	2							

Table D-13 (continue): Number of Hinge Formation for Selected Model 8A12

Hinge condition at different damage levels												
Structure State					Number of Hinge formation at each stage							
Model Type	Direction	Story	Action	Component	B	IO	LS	CP	C	D	E	
8A12	E-W (FN) continue	5th	LPR	Beam								
				Column								
			NAH	Beam	1							
				Column								
			NOR	Beam	1							
				Column								
		WNA	Beam	8								
			Column									
		PUSH	Beam	5	1							
			Column	2								
		6th	LPR	Beam								
				Column								
			NAH	Beam								
				Column								
			NOR	Beam								
				Column								
		WNA	Beam	6								
			Column									
		PUSH	Beam	2								
			Column	2								
		7th	LPR	Beam								
				Column								
			NAH	Beam								
				Column								
			NOR	Beam								
				Column								
		WNA	Beam	5								
			Column									
		PUSH	Beam	1								
			Column									
8th	LPR	Beam										
		Column										
	NAH	Beam										
		Column	5									
	NOR	Beam										
		Column										
WNA	Beam	4										
	Column	3										
PUSH	Beam											
	Column	2										

Table D-14: Number of Hinge Formation for Selected Model 8A15

Hinge condition at different damage levels											
Structure State					Number of Hinge formation at each stage						
Model Type	Direction	Story	Action	Component	B	IO	LS	CP	C	D	E
8A15	N-S (FP)	1st	LPR	Beam	5 (4)						
				Column							
			NAH	Beam	2 (2)						
				Column							
			NOR	Beam	10 (10)						
				Column							
		WNA	Beam	4 (7)							
			Column								
		PUSH	Beam	6 (6)	1						
			Column								
		2nd	LPR	Beam							
				Column							
			NAH	Beam							
				Column							
			NOR	Beam	4 (5)						
				Column							
		WNA	Beam	0 (2)							
			Column								
		PUSH	Beam	3 (5)							
			Column								
		3rd	LPR	Beam	2 (2)						
				Column							
			NAH	Beam							
				Column							
			NOR	Beam	6 (6)						
				Column							
		WNA	Beam	6 (6)							
			Column								
		PUSH	Beam	3 (5)							
			Column								
		4th	LPR	Beam	4 (4)						
				Column							
			NAH	Beam							
				Column							
			NOR	Beam	8 (8)						
				Column							
		WNA	Beam	4 (6)							
			Column								
		PUSH	Beam	2 (4)							
			Column								

Table D-14 (continue): Number of Hinge Formation for Selected Model 8A15

Hinge condition at different damage levels												
Structure State					Number of Hinge formation at each stage							
Model Type	Direction	Story	Action	Component	B	IO	LS	CP	C	D	E	
8A15	N-S (FP) continue	5th	LPR	Beam	4 (4)							
				Column								
			NAH	Beam								
				Column								
			NOR	Beam	4 (4)	4 (4)						
				Column								
		WNA	Beam	4 (4)								
			Column									
		PUSH	Beam	2 (4)	0 (2)							
			Column									
		6th	LPR	Beam	4 (4)							
				Column								
			NAH	Beam								
				Column								
			NOR	Beam	4 (4)	4 (4)						
				Column								
		WNA	Beam	4 (4)								
			Column									
		PUSH	Beam	2 (4)								
			Column									
		7th	LPR	Beam	4 (4)							
				Column								
			NAH	Beam								
				Column								
			NOR	Beam	2 (4)	2						
				Column								
		WNA	Beam	4 (4)								
			Column									
		PUSH	Beam	2 (2)								
			Column									
8th	LPR	Beam	4 (4)									
		Column										
	NAH	Beam										
		Column										
	NOR	Beam	4 (4)									
		Column										
WNA	Beam	4 (4)										
	Column											
PUSH	Beam	2 (2)										
	Column											

Table D-14 (continue): Number of Hinge Formation for Selected Model 8A15

Hinge condition at different damage levels											
Structure State					Number of Hinge formation at each stage						
Model Type	Direction	Story	Action	Component	B	IO	LS	CP	C	D	E
8A15	E-W (FN)	1st	LPR	Beam	6						
				Column							
			NAH	Beam	6						
				Column							
			NOR	Beam	3						
				Column							
		WNA	Beam	6	1						
			Column								
		PUSH	Beam	4							
			Column								
		2nd	LPR	Beam	3						
				Column							
			NAH	Beam	2						
				Column							
			NOR	Beam	2						
				Column							
		WNA	Beam	9							
			Column								
		PUSH	Beam	2							
			Column								
		3rd	LPR	Beam							
				Column							
			NAH	Beam	2						
				Column							
			NOR	Beam							
				Column							
		WNA	Beam	20							
			Column								
		PUSH	Beam	2							
			Column								
		4th	LPR	Beam							
				Column							
			NAH	Beam	1						
				Column							
			NOR	Beam	2						
				Column							
		WNA	Beam	16	2						
			Column								
		PUSH	Beam	1							
			Column	1							

Table D-14 (continue): Number of Hinge Formation for Selected Model 8A15

Hinge condition at different damage levels											
Structure State					Number of Hinge formation at each stage						
Model Type	Direction	Story	Action	Component	B	IO	LS	CP	C	D	E
8A15	E-W (FN) continue	5th	LPR	Beam							
				Column							
			NAH	Beam	1						
				Column							
			NOR	Beam	1						
				Column							
		WNA	Beam	8							
			Column								
		PUSH	Beam								
			Column								
		6th	LPR	Beam	4						
				Column							
			NAH	Beam							
				Column							
			NOR	Beam	4						
				Column							
		WNA	Beam	6							
			Column								
		PUSH	Beam								
			Column								
		7th	LPR	Beam	4						
				Column							
			NAH	Beam							
				Column							
NOR	Beam		4								
	Column										
WNA	Beam	5									
	Column										
PUSH	Beam										
	Column										
8th	LPR	Beam	4								
		Column									
	NAH	Beam									
		Column	5								
	NOR	Beam	4								
		Column									
WNA	Beam	4									
	Column	2									
PUSH	Beam										
	Column										

Table D-15: Number of Hinge Formation for Selected Model 8A18

Hinge condition at different damage levels													
Structure State					Number of Hinge formation at each stage								
Model Type	Direction	Story	Action	Component	B	IO	LS	CP	C	D	E		
8A18	N-S (FP)	1st	LPR	Beam	3 (3)								
				Column									
			NAH	Beam	8 (8)	5 (5)							
				Column									
			NOR	Beam	9 (9)	1 (1)							
				Column									
			WNA	Beam	7 (5)								
				Column									
			PUSH	Beam	6 (7)	1							
				Column									
			2nd	LPR	Beam								
					Column								
		NAH		Beam	7 (7)	4 (4)							
				Column									
		NOR		Beam	8 (8)								
				Column									
		WNA		Beam	2 (2)								
				Column									
		PUSH		Beam	3 (5)								
				Column									
		3rd		LPR	Beam	2							
					Column								
			NAH	Beam	5 (5)	4 (4)							
				Column									
			NOR	Beam	8 (8)								
				Column									
			WNA	Beam	4 (4)								
				Column									
			PUSH	Beam	2 (5)								
				Column									
			4th	LPR	Beam	4 (4)							
					Column								
		NAH		Beam	4 (7)	4 (4)							
				Column									
		NOR		Beam	6 (6)	2 (2)							
				Column									
		WNA		Beam	4 (4)								
				Column									
		PUSH		Beam	2 (4)	0 (1)							
				Column									

Table D-15 (continue): Number of Hinge Formation for Selected Model 8A18

Hinge condition at different damage levels											
Structure State					Number of Hinge formation at each stage						
Model Type	Direction	Story	Action	Component	B	IO	LS	CP	C	D	E
8A18	N-S (FP) continue	5th	LPR	Beam	4 (4)						
				Column							
			NAH	Beam	6 (6)	4 (4)					
				Column							
			NOR	Beam	6 (4)	4 (4)					
				Column							
		WNA	Beam	4 (4)							
			Column								
		PUSH	Beam	3 (4)	2 (2)						
			Column								
		6th	LPR	Beam	4 (4)						
				Column							
			NAH	Beam	6 (6)	4 (4)					
				Column							
			NOR	Beam	4 (4)	4 (4)					
				Column							
		WNA	Beam	4 (4)							
			Column								
		PUSH	Beam	1 (2)	2 (2)						
			Column								
		7th	LPR	Beam	4 (4)						
				Column							
			NAH	Beam	4	4 (4)					
				Column							
			NOR	Beam		4 (4)					
				Column							
		WNA	Beam	4 (4)							
			Column								
		PUSH	Beam	2 (2)							
			Column								
		8th	LPR	Beam	4 (4)						
				Column							
			NAH	Beam	4 (4)						
				Column	1 (1)						
			NOR	Beam	4 (4)						
				Column							
WNA	Beam	4 (4)									
	Column										
PUSH	Beam	2 (4)									
	Column										

Table D-15 (continue): Number of Hinge Formation for Selected Model 8A18

Hinge condition at different damage levels											
Structure State					Number of Hinge formation at each stage						
Model Type	Direction	Story	Action	Component	B	IO	LS	CP	C	D	E
8A18	E-W (FN)	1st	LPR	Beam	6						
				Column							
			NAH	Beam	6						
				Column							
			NOR	Beam	6						
				Column							
		WNA	Beam	7	2						
			Column								
		PUSH	Beam	3	1						
			Column								
		2nd	LPR	Beam	6						
				Column							
			NAH	Beam	6						
				Column							
			NOR	Beam	3						
				Column							
		WNA	Beam	8							
			Column								
		PUSH	Beam	3							
			Column								
		3rd	LPR	Beam							
				Column							
			NAH	Beam	7						
				Column							
			NOR	Beam							
				Column							
		WNA	Beam	18							
			Column								
		PUSH	Beam	4							
			Column								
4th	LPR	Beam									
		Column									
	NAH	Beam	9								
		Column									
	NOR	Beam	1								
		Column									
WNA	Beam	18									
	Column										
PUSH	Beam	3									
	Column										

Table D-15 (continue): Number of Hinge Formation for Selected Model 8A18

Hinge condition at different damage levels											
Structure State					Number of Hinge formation at each stage						
Model Type	Direction	Story	Action	Component	B	IO	LS	CP	C	D	E
8A18	E-W (FN) continue	5th	LPR	Beam	2						
				Column							
			NAH	Beam	7						
				Column							
			NOR	Beam	2						
				Column							
		WNA	Beam	13							
			Column								
		PUSH	Beam	1							
			Column								
		6th	LPR	Beam	4						
				Column							
			NAH	Beam	4						
				Column							
			NOR	Beam	4						
				Column							
		WNA	Beam	4	2						
			Column								
		PUSH	Beam	1							
			Column								
		7th	LPR	Beam	4						
				Column							
			NAH	Beam	4						
				Column							
NOR	Beam		4								
	Column										
WNA	Beam	6									
	Column										
PUSH	Beam										
	Column										
8th	LPR	Beam	4								
		Column	2								
	NAH	Beam	4								
		Column	3								
	NOR	Beam	4								
		Column									
WNA	Beam	4									
	Column	4									
PUSH	Beam	2									
	Column	1									

Table D-16: Number of Hinge Formation for Selected Model 8B12

Hinge condition at different damage levels											
Structure State					Number of Hinge formation at each stage						
Model Type	Direction	Story	Action	Component	B	IO	LS	CP	C	D	E
8B12	N-S (FP)	1st	LPR	Beam	4						
				Column							
			NAH	Beam	1	4					
				Column							
			NOR	Beam	4						
				Column							
		WNA	Beam	4							
			Column								
		PUSH	Beam	1	2						
			Column								
		2nd	LPR	Beam	4						
				Column							
			NAH	Beam	10	4					
				Column							
			NOR	Beam		4					
				Column							
		WNA	Beam	4							
			Column								
		PUSH	Beam	1	2						
			Column								
		3rd	LPR	Beam	4						
				Column							
			NAH	Beam	1	4					
				Column							
			NOR	Beam	2	2					
				Column							
		WNA	Beam	4							
			Column								
		PUSH	Beam	1	2						
			Column								
		4th	LPR	Beam	4						
				Column							
			NAH	Beam		4					
				Column							
			NOR	Beam		4					
				Column							
		WNA	Beam	4							
			Column								
		PUSH	Beam		2						
			Column								

Table D-16 (continue): Number of Hinge Formation for Selected Model 8B12

Hinge condition at different damage levels											
Structure State					Number of Hinge formation at each stage						
Model Type	Direction	Story	Action	Component	B	IO	LS	CP	C	D	E
8B12	N-S (FP) continue	5th	LPR	Beam	4						
				Column							
			NAH	Beam	2	4					
				Column							
			NOR	Beam		4					
				Column							
		WNA	Beam	4							
			Column								
		PUSH	Beam		2						
			Column								
		6th	LPR	Beam	4						
				Column							
			NAH	Beam		4					
				Column							
			NOR	Beam	2	2					
				Column							
		WNA	Beam	4							
			Column								
		PUSH	Beam	2							
			Column								
		7th	LPR	Beam	4						
				Column							
			NAH	Beam	4						
				Column							
NOR	Beam		4								
	Column										
WNA	Beam	4									
	Column										
PUSH	Beam	2									
	Column										
8th	LPR	Beam	4								
		Column									
	NAH	Beam	4								
		Column									
	NOR	Beam	4								
		Column									
WNA	Beam	4									
	Column										
PUSH	Beam	2									
	Column										

Table D-16 (continue): Number of Hinge Formation for Selected Model 8B12

Hinge condition at different damage levels												
Structure State					Number of Hinge formation at each stage							
Model Type	Direction	Story	Action	Component	B	IO	LS	CP	C	D	E	
8B12	E-W (FN)	1st	LPR	Beam								
				Column								
			NAH	Beam								
				Column								
			NOR	Beam								
				Column								
		WNA	Beam									
			Column									
		PUSH	Beam									
			Column									
		2nd	LPR	Beam	2							
				Column								
			NAH	Beam								
				Column								
			NOR	Beam								
				Column								
		WNA	Beam									
			Column									
		PUSH	Beam	2								
			Column									
		3rd	LPR	Beam								
				Column								
			NAH	Beam								
				Column								
NOR	Beam											
	Column											
WNA	Beam											
	Column											
PUSH	Beam											
	Column											
4th	LPR	Beam										
		Column										
	NAH	Beam										
		Column										
	NOR	Beam										
		Column										
WNA	Beam											
	Column											
PUSH	Beam											
	Column											

Table D-16 (continue): Number of Hinge Formation for Selected Model 8B12

Hinge condition at different damage levels												
Structure State					Number of Hinge formation at each stage							
Model Type	Direction	Story	Action	Component	B	IO	LS	CP	C	D	E	
8B12	E-W (FN) continue	5th	LPR	Beam								
				Column								
			NAH	Beam								
				Column								
			NOR	Beam								
				Column								
		WNA	Beam									
			Column									
		PUSH	Beam									
			Column									
		6th	LPR	Beam								
				Column								
			NAH	Beam								
				Column								
			NOR	Beam								
				Column								
		WNA	Beam									
			Column									
		PUSH	Beam									
			Column									
		7th	LPR	Beam								
				Column								
			NAH	Beam								
				Column								
NOR	Beam											
	Column											
WNA	Beam											
	Column											
PUSH	Beam											
	Column											
8th	LPR	Beam										
		Column										
	NAH	Beam										
		Column										
	NOR	Beam										
		Column										
WNA	Beam											
	Column											
PUSH	Beam											
	Column											

Table D-17: Number of Hinge Formation for Selected Model 8S15

Hinge condition at different damage levels												
Structure State					Number of Hinge formation at each stage							
Model Type	Direction	Story	Action	Component	B	IO	LS	CP	C	D	E	
8S15	N-S (FP)	1st	LPR	Beam								
				Column								
			NAH	Beam	8							
				Column								
			NOR	Beam	2							
				Column								
		WNA	Beam									
			Column									
		PUSH	Beam	2								
			Column									
		2nd	LPR	Beam								
				Column								
			NAH	Beam	12							
				Column								
			NOR	Beam	4							
				Column								
		WNA	Beam									
			Column									
		PUSH	Beam	6								
			Column									
		3rd	LPR	Beam								
				Column								
			NAH	Beam	6							
				Column								
			NOR	Beam	4							
				Column								
		WNA	Beam									
			Column									
		PUSH	Beam	4								
			Column									
		4th	LPR	Beam								
				Column								
			NAH	Beam	4							
				Column								
			NOR	Beam	4							
				Column								
		WNA	Beam									
			Column									
		PUSH	Beam	3								
			Column									

Table D-17 (continue): Number of Hinge Formation for Selected Model 8S15

Hinge condition at different damage levels											
Structure State					Number of Hinge formation at each stage						
Model Type	Direction	Story	Action	Component	B	IO	LS	CP	C	D	E
8S15	N-S (FP) continue	5th	LPR	Beam	4						
				Column							
			NAH	Beam	4						
				Column							
			NOR	Beam	4						
				Column							
		WNA	Beam	4							
			Column								
		PUSH	Beam	2							
			Column								
		6th	LPR	Beam	4						
				Column							
			NAH	Beam	4						
				Column							
			NOR	Beam	4						
				Column							
		WNA	Beam	4							
			Column								
		PUSH	Beam	2							
			Column								
		7th	LPR	Beam	4						
				Column							
			NAH	Beam	4						
				Column							
NOR	Beam		4								
	Column										
WNA	Beam	4									
	Column										
PUSH	Beam	2									
	Column										
8th	LPR	Beam	4								
		Column									
	NAH	Beam	4								
		Column									
	NOR	Beam	4								
		Column									
WNA	Beam	4									
	Column										
PUSH	Beam	2									
	Column										

Table D-17 (continue): Number of Hinge Formation for Selected Model 8S15

Hinge condition at different damage levels												
Structure State					Number of Hinge formation at each stage							
Model Type	Direction	Story	Action	Component	B	IO	LS	CP	C	D	E	
8S15	E-W (FN)	1st	LPR	Beam								
				Column								
			NAH	Beam								
				Column								
			NOR	Beam								
				Column								
		WNA	Beam									
			Column									
		PUSH	Beam									
			Column									
		2nd	LPR	Beam								
				Column								
			NAH	Beam								
				Column								
			NOR	Beam								
				Column								
		WNA	Beam									
			Column									
		PUSH	Beam	2								
			Column									
		3rd	LPR	Beam								
				Column								
			NAH	Beam								
				Column								
NOR	Beam											
	Column											
WNA	Beam											
	Column											
PUSH	Beam											
	Column											
4th	LPR	Beam										
		Column										
	NAH	Beam										
		Column										
	NOR	Beam										
		Column										
WNA	Beam											
	Column											
PUSH	Beam											
	Column											

Table D-17 (continue): Number of Hinge Formation for Selected Model 8S15

Hinge condition at different damage levels											
Structure State					Number of Hinge formation at each stage						
Model Type	Direction	Story	Action	Component	B	IO	LS	CP	C	D	E
8S15	E-W (FN) continue	5th	LPR	Beam							
				Column							
			NAH	Beam							
				Column							
			NOR	Beam							
				Column							
		WNA	Beam								
			Column								
		PUSH	Beam								
			Column								
		6th	LPR	Beam							
				Column							
			NAH	Beam							
				Column							
			NOR	Beam							
				Column							
		WNA	Beam								
			Column								
		PUSH	Beam								
			Column								
		7th	LPR	Beam							
				Column							
			NAH	Beam							
				Column							
NOR	Beam										
	Column										
WNA	Beam										
	Column										
PUSH	Beam										
	Column										
8th	LPR	Beam									
		Column									
	NAH	Beam									
		Column									
	NOR	Beam									
		Column									
WNA	Beam										
	Column										
PUSH	Beam										
	Column										

Table D-18: Number of Hinge Formation for Selected Model 8S18

Hinge condition at different damage levels												
Structure State					Number of Hinge formation at each stage							
Model Type	Direction	Story	Action	Component	B	IO	LS	CP	C	D	E	
8S18	N-S (FP)	1st	LPR	Beam								
				Column								
			NAH	Beam	6							
				Column								
			NOR	Beam								
				Column								
		WNA	Beam									
			Column									
		PUSH	Beam	6								
			Column									
		2nd	LPR	Beam								
				Column								
			NAH	Beam	6							
				Column								
			NOR	Beam								
				Column								
		WNA	Beam									
			Column									
		PUSH	Beam	6								
			Column									
		3rd	LPR	Beam								
				Column								
			NAH	Beam	4							
				Column								
NOR	Beam		2									
	Column											
WNA	Beam											
	Column											
PUSH	Beam	6										
	Column											
4th	LPR	Beam										
		Column										
	NAH	Beam	4									
		Column										
	NOR	Beam	4									
		Column										
WNA	Beam											
	Column											
PUSH	Beam	2										
	Column											

Table D-18 (continue): Number of Hinge Formation for Selected Model 8S18

Hinge condition at different damage levels											
Structure State					Number of Hinge formation at each stage						
Model Type	Direction	Story	Action	Component	B	IO	LS	CP	C	D	E
8S18	N-S (FP) continue	5th	LPR	Beam	4						
				Column							
			NAH	Beam	4						
				Column							
			NOR	Beam	4						
				Column							
		WNA	Beam	4							
			Column								
		PUSH	Beam	2							
			Column								
		6th	LPR	Beam	4						
				Column							
			NAH	Beam	4						
				Column							
			NOR	Beam	4						
				Column							
		WNA	Beam	4							
			Column								
		PUSH	Beam	2							
			Column								
		7th	LPR	Beam	4						
				Column							
			NAH	Beam	4						
				Column							
			NOR	Beam	4						
				Column							
		WNA	Beam	4							
			Column								
		PUSH	Beam	2							
			Column								
8th	LPR	Beam	4								
		Column									
	NAH	Beam	4								
		Column									
	NOR	Beam	4								
		Column									
WNA	Beam	4									
	Column										
PUSH	Beam	2									
	Column										

Table D-18 (continue): Number of Hinge Formation for Selected Model 8S18

Hinge condition at different damage levels												
Structure State					Number of Hinge formation at each stage							
Model Type	Direction	Story	Action	Component	B	IO	LS	CP	C	D	E	
8S18	E-W (FN)	1st	LPR	Beam								
				Column								
			NAH	Beam								
				Column								
			NOR	Beam								
				Column								
		WNA	Beam									
			Column									
		PUSH	Beam									
			Column									
		2nd	LPR	Beam								
				Column								
			NAH	Beam								
				Column								
			NOR	Beam								
				Column								
		WNA	Beam									
			Column									
		PUSH	Beam	2								
			Column									
		3rd	LPR	Beam								
				Column								
			NAH	Beam								
				Column								
NOR	Beam											
	Column											
WNA	Beam											
	Column											
PUSH	Beam											
	Column											
4th	LPR	Beam										
		Column										
	NAH	Beam										
		Column										
	NOR	Beam										
		Column										
WNA	Beam											
	Column											
PUSH	Beam											
	Column											

Table D-18 (continue): Number of Hinge Formation for Selected Model 8S18

Hinge condition at different damage levels												
Structure State					Number of Hinge formation at each stage							
Model Type	Direction	Story	Action	Component	B	IO	LS	CP	C	D	E	
8S18	E-W (FN) continue	5th	LPR	Beam								
				Column								
			NAH	Beam								
				Column								
			NOR	Beam								
				Column								
		WNA	Beam									
			Column									
		PUSH	Beam									
			Column									
		6th	LPR	Beam								
				Column								
			NAH	Beam								
				Column								
			NOR	Beam								
				Column								
		WNA	Beam									
			Column									
		PUSH	Beam									
			Column									
		7th	LPR	Beam								
				Column								
			NAH	Beam								
				Column								
			NOR	Beam								
				Column								
		WNA	Beam									
			Column									
		PUSH	Beam									
			Column									
8th	LPR	Beam										
		Column										
	NAH	Beam										
		Column										
	NOR	Beam										
		Column										
WNA	Beam											
	Column											
PUSH	Beam											
	Column											

## **Appendix E: Validation of Analysis Procedure through Load-Displacement Response**

To attest nonlinear analysis validation, the overall or local hysteresis behavior is one of the suitable ways. Within the framework of this study, the overall behavior of the selected models must follow an appropriate load-displacement response regarding LRC models. The proper reflection of the load-displacement response curve may provide validation of THA analysis process in associate with the primary assumptions in chapters four (4) and five (5). To verify the structural behavior, the response must be free of any disruption due to applied frame irregularities. Indeed, this procedure helps to track potential errors in the modeling process. Therefore, they should be free from any possible erratic or dispersion of results regarding geometrical form of the archetype models in order to certify response function. Thus, the median of the base (regular) models, i.e. model 4B12, is selected for the load-displacement validation procedure. LPR time history record, for both FP and FN cases (the N-S and E-W directions), is the selected applied ground motion. As both aforementioned cases show very similar response, only FP condition is presented here. In addition, to be comparable with NSA case, the base shear versus displacement response of master point (or master joint, i.e. geometrical plane center) on the 4<sup>th</sup> level is depicted.

Because this procedure is only for verification purpose, the applied LPR accelerations to the model are arbitrary multiplied by factor of 1.5 which is applied directly to LPR scaled ground motion record. The arbitrary scale is done to artificially force the model into nonlinear phase more than the attained results through the principal assumptions of low seismic zones in this study. Hence, in this case a better view of the cyclic behavior of the selected model in accordance with stiffness degradation in nonlinear phase is achievable.

Furthermore, the same model (4B12) under NSA case is analyzed with increasing the target displacement equal to approximate 1.5 times of the FEMA 356 (2000) requirement in chapter 5. The target displacement is intensified intentionally to get the same prospect of THA analysis regarding higher level of nonlinearity. NSA

base-shear against displacement response is drawn to examine the possible divergence between stiffness in THA response with NSA response.

Both THA and NSA base-shear versus displacement responses are illustrated in figure E-1. This figure demonstrates a very good agreement between the primarily nonlinear assumptions and features with the acquired analysis results in term of stiffness and hysteresis behavior. From this figure, it can be understood that:

- a. The overall response of THA method conforms to the expected LRC model case. The hysteresis behavior is almost narrow, which is reflect poor absorb energy of this type of models against seismic excitation, e.g. see Chopra (2000), FEMA P-440A (2009), or NEHRP (2010a) for more information.
- b. The hysteresis behavior, especially for the outer loops of cycle, shows overall proper stiffness degradation which is part of the modeling assumption in chapter 4.
- c. The initial stiffness for THA case is in match with NSA case. It means, both NSA's slope and THA's primary slope are approximately very close. Within the assumption of this study and without extra 1.5 scale factor application, both slopes results are actually fit. Considering the extra 1.5 scale factor, NSA response shows buckling in its response before reach the final extra-imposed target point.
- d. The overall THA response determines a reasonable dispersion among hysteresis cycles which also may reflect the appropriate analysis procedure in terms of dynamic nonlinear solution method and the selected input assumptions.
- e. The proper fitness of stiffness slopes between NSA and THA cases may help to demonstrate the decent array of applied damping coefficients to the model (section 4-4). Bearing in mind that the applied Rayleigh damping for THA model is mostly effective in the linear part of the response, the NSA method shows the same approximate linear stiffness as THA method.

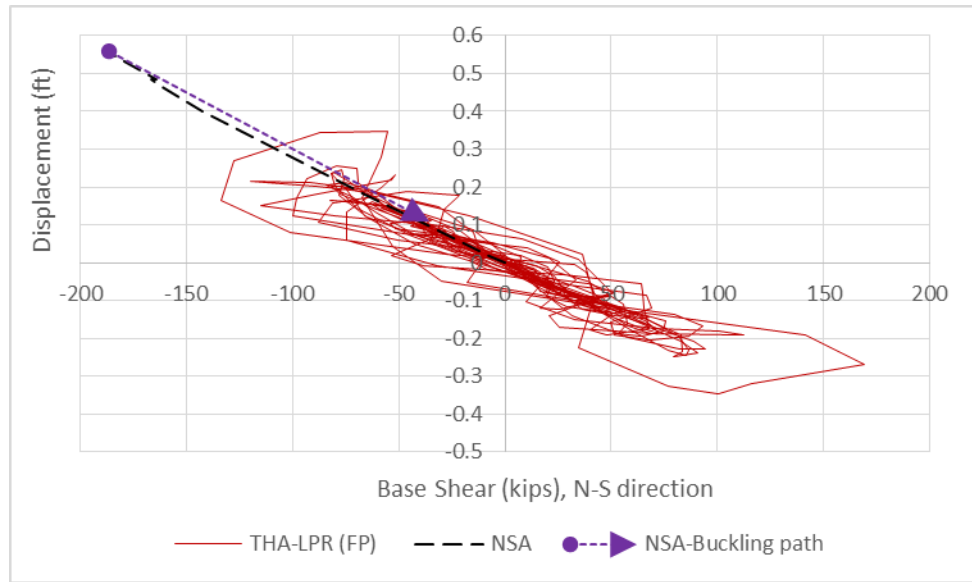


Figure E-1: Base-shear versus displacement response of model 4B12 for intensified LPR and Pushover case

## Bibliography

ACI Committee 318, (2008). “Building Code Requirements for Structural Concrete (ACI 318-08) and Commentary (ACI 318R-08)”, *American Concrete Institute (ACI)*, Farmington Hills, MI.

Akita, T., Kuramoto, H., (2008). “Time History Response Prediction for Multi-Story Buildings. Consisting of Mixed Soft and Rigid Stories under Earthquake Motions”, *The 14<sup>th</sup> World Conference on Earthquake Engineering*, 12-17 October, Beijing, China.

Antonopoulos, T.A., Anagnostopoulos, S.A., (2010). “Optimum Partial Strengthening for Improved Seismic Performance of Old Reinforced Concrete Buildings with Open Ground Story”, *Advances in Performance-Based Earthquake Engineering*, Chapter 37, Geotechnical, Geological, and Earthquake Engineering 13 (GGEE 13), Springer Science+Business Media B.V.

ASCE 7-10, (2010). Minimum Design Loads for Buildings and other Structures, ASCE/SEI, *American Society of Civil Engineers*, Reston, VA.

ASCE 7-05, (2005). Minimum Design Loads for Buildings and other Structures, ASCE/SEI, *American Society of Civil Engineers*, Reston, VA.

ASCE 41-06, (2007a). *Seismic Rehabilitation of Existing Buildings*, ASCE/SEI, American Society of Civil Engineers, Reston, VA.

ASCE 41-06, (2007b). *Seismic Rehabilitation of Existing Buildings – Supplement No. 1*, ASCE/SEI, American Society of Civil Engineers, Reston, VA.

Athanassiadou, C.J., (2008). “Seismic Performance of R/C Plane Frames Irregular in Elevation”, *Engineering Structures*, Vol. 30, Issue 5, pp. 1250–1261.

Aycardi, L.E., Mander, J.B., Reinhorn, A.M., (1994). “Seismic Resistance of Reinforced Concrete Frame Structures Designed Only for Gravity Loads: Experimental Performance of Subassemblages”, *ACI Structural Journal*, Title No. 91-S53, Vol. 91, No. 5.

Aydinoglu, M.N., Önem, G., (2010). “Evaluation of Analysis Procedures for Seismic Assessment and Retrofit Design”, Editors: Garevski, M., Ansal, A., *Earthquake Engineering in Europe*, Chapter 8, Geotechnical, Geological, and Earthquake Engineering 17, Springer Science+Business Media B.V.

Bahmani, P., Van de Lindt, J.W., Pryor S.E., Mochizuki, G.L., Gershfeld, M., Rammer, D., Tian, J., Symans, M.D., (2014). “Performance-Based Seismic Retrofit of Soft-Story Woodframe Buildings”, *Structure Magazine*,

<http://www.structuremag.org/Archives/2014-6/C-StrucPerformance-Bahmani-June14.pdf>, June 2014.

Bento, R., Azevedo, J., (2000). "Behaviour Coefficient Assessment for Soft Storey Structures", *12<sup>th</sup> World Conference on Earthquake Engineering (WCEE)*, Paper No. 0779, 30 January - 4 February, Auckland, New Zealand.

Bertero, V.V., Bertero, R.D., (1995). "Formulation of a Conceptual Seismic Code", *Recent Development in Lateral Force Transfer in Buildings*, ACI, SP 157-12, pp. 255-288.

Bhatt, C., Bento, R., (2011). "Extension of the CSM-FEMA440 to Plan-Asymmetric Real Building Structures", *Earthquake Engineering and Structural Dynamics*, Vol. 40, Issue 11, pp. 1263-1282.

Biskinis, D.E., Roupakias, G.K., Fardis, M.N., (2004). "Degradation of Shear Strength of Reinforced Concrete Members with Inelastic Cyclic Displacements", *ACI Structural Journal*, Title No. 101-S76, Vol. 101, No. 6.

Bournas, D., Triantafillou, T., (2010). "Innovative Seismic Retrofitting of RC Columns Using Advanced Composites", Editor: Fardis, M.N., *Advances in Performance-Based Earthquake Engineering*, Chapter 36, Geotechnical, Geological, and Earthquake Engineering 13, Springer Science+Business Media B.V.

Bracci, J.M., Reinhorn, A.M., Mander, J.B., (1995a). “Seismic Resistance of Reinforced Concrete Frame Structures Designed for Gravity Loads: Performance of Structural System”, *ACI Structural Journal*, Title No. 92-S58, Vol. 92, No. 5, September-October 1995.

Bracci, J.M., Reinhorn, A.M., Mander, J.B., (1995b). “Seismic Retrofit of Reinforced Concrete Buildings Designed for Gravity Loads: Performance of Structural Model”, *ACI Structural Journal*, Title No. 92-S68, Vol. 92, No. 6, November-December 1995.

Briman, V., Ribakov, Y., (2009). “Using Seismic Isolation Columns for Retrofitting Buildings with Soft Stories”, *The Structural Design of Tall and Special Buildings*, Vol. 18, Issue 5.

Calvi, G.M., (2010). “Engineers Understanding of Earthquakes Demand and Structures Response”, Editors: Garevski, M., Ansal, A., *Earthquake Engineering in Europe*, Chapter 10, Geotechnical, Geological, and Earthquake Engineering 17, Springer Science+Business Media B.V.

Chandler, A.M., Lam, N.T.K., (2001). “Performance-Based Design in Earthquake Engineering: A Multidisciplinary Review”, *Engineering Structures*, Vol. 23, Issue 12, pp. 1525-1543.

Chandrasekaran, S., Nunziante, L., Serino, G., Carannante, F., (2010). *Seismic Design Aids for Nonlinear Analysis of Reinforced Concrete Structures*, CRC Press, Taylor & Francis Group.

Charney, A.F., (2008). “Unintended Consequences of Modeling Damping in Structures”, *Journal of Structural Engineering*, Vol. 134, No. 4.

Chesca, A.B., Seki, M., Vacareanu, R., Okada, T., Georgescu, B., Kaminosono, T., Kato, H., (2007). “Seismic Rehabilitation of an Existing Soft and Weak Ground Floor Building. Case Study”, *The JICA Technical Cooperation Project in Romania, International Symposium on Seismic Risk Reduction (ISSRR)*, Paper No. 09, Bucharest, Romania.

Chopra, A., Goel, R., (2004). “Modal Pushover Analysis: Symmetric- and Unsymmetric-Plan Buildings”, Editors: Fajfar, P., Krawinkler, H., *Peer Report 2004/05, Performance-Based Seismic Design Concepts and Implementation*, Proceedings of the International Workshop, 28 June – 1 July, Bled, Slovenia.

Chopra, A.K., (2000). *Dynamics of Structures: Theory and Applications to Earthquake Engineering*, 2<sup>nd</sup> edition, Prentice Hall.

City Manager Report, (2005). Subject: “Potentially Hazardous Soft, Weak, or Open Front Story Buildings”, *City Manager's Office*, City of Berkeley, CA, Action Calendar: 10/18/2005, at: <http://www.ci.berkeley.ca.us/manager>.

CSI Analysis Reference Manual for SAP2000®, ETABS®, SAFE® and CSiBridge®, (2013). *Computers and Structures, Inc.*, Berkeley, California.

CTBUH, (2008). “Recommendations for the Seismic Design of High-rise Buildings”, Prepared by: Willford, M., Whittaker, A., Klemencic, R., Editor: Wood, A., *CTBUH Seismic Design Guide*, Chicago, Illinois.

Deierlein, G., (2012). “Engineering Needs for Existing Buildings Research Perspective”, Presentation on November 19, 2012, *ACEHR Meeting*, NIST- NEHRP.

De-la-Colina, J., Valdes-Gonzalez, J., Gonzalez-Perez, C.A., (2013). “Experiments to Study the Effect of Foundation Rotation on the Seismic Building Torsional, Response of a Reinforced Concrete Space Frame”, *Engineering Structures*, Vol. 56, pp. 1154-1163.

Derecho, A.T., Kianoush, M.R., (2001). “Seismic Design of Reinforced Concrete Structures”, Edited: Naeim, F., Chapter 10, *Seismic Design Handbook*, 2<sup>nd</sup> edition, Kluvier Academic Publisher.

De Stefano, M., Pintucchi, B., (2008). “A Review of Research on Seismic Behaviour of Irregular Building Structures since 2002”, *Bulletin of Earthquake Engineering*, Vol. 6, Issue 2, pp. 285–308.

De Stefano, M., Tanganelli, M., Viti, S., (2013). “On the Variability of Concrete Strength as a Source of Irregularity in Elevation for Existing RC Buildings: A Case Study”, *Bulletin of Earthquake Engineering*, Vol. 11, Issue 5, pp. 1711–1726.

Dimova, S.L., Alashki, I., (2003). “Seismic Design of Symmetric Structures for Accidental Torsion”, *Bulletin of Earthquake Engineering*, Vol. 1, Issue 2, pp. 303–320.

Dooley, K.L., Bracci, J.M., (2001). “Seismic Evaluation of Column-to-Beam Strength Ratios in Reinforced Concrete Frames”, *ACI Structural Journal*, Title No. 98-S80, Vol. 98, No. 6.

Dowell, R.K., Seible, F., Wilson, E.L., (1998). “Pivot Hysteresis Model for Reinforced Concrete Members”, *ACI Structural Journal*, Title no. 95-S55, Vol. 95, No. 5.

Dusicka, P., Davidson, B.J., Ventura, C. E., (2000). “Investigation into the Significance of Strength Characteristics in Inelastic Torsional Seismic Response”,

12<sup>th</sup> World Conference on Earthquake Engineering (WCEE), Paper No. 2850, 30 January - 4 February, Auckland, New Zealand.

Dutta, S.C., (2001). "Effect of Strength Deterioration on Inelastic Seismic Torsional Behaviour of Asymmetric RC Buildings", *Building and Environment*, Vol. 36, Issue 10, pp. 1109-1118.

Dwairi, H.M., Kowalsky, M.J., Nau, J.M., (2007). "Equivalent Damping in Support of Direct Displacement-Based Design", *Journal of Earthquake Engineering*, Vol. 11, Issue 4, pp. 512-530.

El-Attar, A.G., White, R.N., Gergely, P., (1997). "Behavior of Gravity Load Designed Reinforced Concrete Buildings Subjected to Earthquakes", *ACI Structural Journal*, Title No. 94-S14, Vol. 94, No. 2.

El-Howary, H.A., Mehanny, S.S.F., (2011). "Seismic Vulnerability Evaluation of RC Moment Frame Buildings in Moderate Seismic Zones", *Earthquake Engineering and Structural Dynamics*, Vol. 40, Issue 2, pp. 215-235.

Ellingwood, B.R., Celik, C.O., Kinali, K., (2007). "Fragility Assessment of Building Structural Systems in Mid-America", *Earthquake Engineering and Structural Dynamics*, Vol. 36, Issue 13, pp. 1935-1952.

Elnashai, A.S., Di Sarno, L., (2008). *Fundamentals of Earthquake Engineering*, 1<sup>st</sup> edition, *John Wiley & Sons*.

Erduran, E., (2008). “Assessment of Current Nonlinear Static Procedures on the Estimation of Torsional Effects in Low-Rise Frame Buildings”, *Engineering Structures*, Vol. 30, Issue 9, pp. 2548–2558.

Fakhouri, M.Y., Igarashi, A., (2011). “Upgrading The Seismic Performance of Soft First Story Frame Structures by Isolators with Multiple Sliding Surfaces”, Paper No. 134, *Proceedings of the Ninth Pacific Conference on Earthquake Engineering Building an Earthquake-Resilient Society*, Auckland, New Zealand.

Fajfar, P., (2002). “Structural Analysis in Earthquake Engineering- A Breakthrough of Simplified Non-Linear Methods”, *12<sup>th</sup> European Conference on Earthquake Engineering*, Paper Reference 843, 9-13 September, London, UK.

Fardis, M.N., Panagiotakos, T.B., (2001). “Effect of Immediate Occupancy Design on Performance of RC Frames at Collapse Prevention Level”, *Peer Report 2002/02*, The Third U.S.-Japan Workshop on Performance-Based Earthquake Engineering Methodology for Reinforced Concrete Building Structures, 16–18 August, Seattle, Washington.

Fardis, M.N., (2009). “General Principles for the Design of Concrete Buildings for Earthquake Resistance”, *Seismic Design, Assessment and Retrofitting of Concrete Buildings*, Geotechnical, Geological, and Earthquake Engineering 8, Springer Science+Business Media B.V.

FEMA 356, (2000). Prestandard and Commentary for the Seismic Rehabilitation of Buildings, Prepared for the Federal Emergency Management Agency by American Society of Civil Engineers (ASCE), Washington D.C.

FEMA 366, (2008). Estimated Annualized Earthquake Losses for the United States, HAZUS MH, Washington D.C.

FEMA 440, (2005). Improvement of Nonlinear Static Seismic Analysis Procedures, Prepared for FEMA by Applied Technology Council (ATC), Washington, D.C.

FEMA E-74, (2012). Reducing the Risks of Nonstructural Earthquake Damage—A Practical Guide, Washington D.C.

FEMA P-440A, (2009). Effects of Strength and Stiffness Degradation on Seismic Response, Prepared for FEMA by Applied Technology Council (ATC), Washington, D.C.

FEMA P695, (2009). Quantification of Building Seismic Performance Factors, Prepared for FEMA by Applied Technology Council (ATC), Washington, D.C.

FEMA P-750, (2009). NEHRP Recommended Seismic Provisions for New Buildings and Other Structures, Prepared for the Federal Emergency Management Agency of the U.S. Department of Homeland Security by the Building Seismic Safety Council of the National Institute of Building Sciences, Washington, D.C.

FEMA P-752, CD, (2009). 2009 NEHRP Recommended Seismic Provisions: Training and Instructional Materials, Prepared for the Federal Emergency Management Agency of the U.S. Department of Homeland Security by the Building Seismic Safety Council of the National Institute of Building Sciences, Washington, D.C.

Fintel, M., Khan, F.R., (1969). "Shock-Absorbing Soft Story Concept for Multistory Earthquake Structures", *ACI Journal*, Title No. 66-29.

Fragiadakis, M., Vamvatsikos, D., Aschheim, M., (2011). "Static Versus Dynamic Methods of Analysis for Estimating Seismic Performance", Editor: Dolsek, M., *Protection of Built Environment against Earthquakes*, Chapter 6, Springer Science+Business Media B.V.

Ghannoum, W.M., Moehle, J.P., (2012a). “Shake-Table Tests of a Concrete Frame Sustaining Column Axial Failures”, *ACI Structural Journal*, Title No. 109-S34, Vol. 109, No. 3, May-June 2012.

Ghannoum, W.M., Moehle, J.P., (2012b). “Dynamic Collapse Analysis of a Concrete Frame Sustaining Column Axial Failures”, *ACI Structural Journal*, Title No. 109-S35, Vol. 109, No. 3, May-June 2012.

Goel, R.K., Chopra, A.K., (2004). “Evaluation of Modal and FEMA Pushover Analyses: SAC Buildings”, *Earthquake Spectra*, Vol. 20, Issue 1.

Goel, R.K., (2003). “Performance of Buildings during the January 26, 2001 Bhuj Earthquake”, *Internet: ceenve.calpoly.edu/faculty-pages/goel/indian\_eqk/index.htm*.

Guevara-Perez, L.T., (2012). “Soft Story and Weak Story in Earthquake Resistant Design: A Multidisciplinary Approach”, *15<sup>th</sup> World Conference on Earthquake Engineering*, Lisbon, Portugal.

Hall, J.F., (2006). “Problems Encountered from the Use (or Misuse) of Rayleigh Damping”, *Earthquake Engineering and Structural Dynamics*, Vol. 35, Issue 5, pp. 525-545.

Hamburger, R.O., Scawthorn C., (2005). “Seismic Design of Buildings”, Editors: Chen, W.F., Lui, E.M., *Handbook of Structural Engineering*, Chapter 19, 2<sup>nd</sup> edition, CRC Press.

Harris, K.D., Robinson, N.D., Sammarco, E.L., (2013). “Seismic Time Histories, A Practical Approach”, *Structure Magazine*, [www.structuremag.org/Archives/2013-3/C-PracSolutions-Harris-March13.pdf](http://www.structuremag.org/Archives/2013-3/C-PracSolutions-Harris-March13.pdf), March 2013.

Haselton, C.B., Liel, A.B., Deierlein, G.G., Dean, B.S., Chou, J.H., (2011). “Seismic Collapse Safety of Reinforced Concrete Buildings. I: Assessment of Ductile Moment Frames”, *Journal of Structural Engineering*, ASCE, Vol. 137, No. 4.

Hejazi, F., Noorzaei, J., Chieng, C.Y., Jaafar, M.S., Abangali, A.A., (2011). “Effect of Soft Story on Structural Response of High Rise Buildings”, Paper No. 012034, *IOP Conference Series: Materials Science and Engineering*, Vol. 17.

Hines, E.M., Baise, L.G., Swift, S.S., (2011). “Ground-Motion Suite Selection for Eastern North America”, *Journal of Structural Engineering*, ASCE, Vol. 137, No. 3, Special Issue: Earthquake Ground Motion Selection and Modification for Nonlinear Dynamic Analysis of Structures.

Horton, J.W., Williams, R.A., (2012). “The 2011 Virginia Earthquake: What Are Scientists Learning?”, *EOS*, Vol. 93, No. 33, pp. 317-324.

IBC (International Building Code) (2012). *International Code Council*, Falls Church, VA.

IBC (International Building Code) (2006). *International Code Council*, Falls Church, VA.

Ichinose, T., Umeno, T., (2000). “Storey Shear Safety Factor for RC Buildings”, *12<sup>th</sup> World Conference on Earthquake Engineering (WCEE)*, Paper No. 1723, 30 January - 4 February, Auckland, New Zealand.

Inel, M., Ozmen, H.B., (2006). “Effects of Plastic Hinge Properties in Nonlinear Analysis of Reinforced Concrete Buildings”, *Engineering Structures*, Vol. 28, Issue 11, pp. 1494-1502.

Kabeyasawa, T., Tasai, A., Igarashi, S., (2002). “An Economical and Efficient Method of Preventing Old Reinforced Concrete Buildings from Collapse under Major Earthquake”, *7<sup>th</sup> US National Conference on Earthquake Engineering (7NCEE)*, 21-25 July, Boston.

Kalny, O., (2011). *CSI Knowledge Base*, Internet:  
<https://wiki.csiamerica.com/display/kb/Home>.

Karnovsky, I.A., Lebed, O., (2010). “Dynamics of Elastic Systems”, Chapter 14, *Advanced Methods of Structural Analysis*, Springer Science+Business Media, LLC.

Katsanos, E.I., Sextos, A.G., Manolis, G.D., (2010). “Selection of Earthquake Ground Motion Records: A State-Of-The-Art Review from A Structural Engineering Perspective”, *Soil Dynamics and Earthquake Engineering*, Vol. 30, Issue 4, pp. 157-169.

Kim, Y., Kabeyasawa, T., (2004). “Dynamic Test and Analysis of an Eccentric Reinforced Concrete Frame to Collapse”, Paper No. 381, *13<sup>th</sup> World Conference on Earthquake Engineering*, 1-6 August, Vancouver, B.C., Canada.

Kim, Y., Kabeyasawa, T., Igarashi, S., (2012). “Dynamic Collapse Test on Eccentric Reinforced Concrete Structures with and without Seismic Retrofit”, *Engineering Structures*, Vol. 34, pp. 95-110.

Kirac, N., Dogan, M., Ozbasaran, H., (2011). “Failure of Weak-storey during Earthquakes”, *Engineering Failure Analysis*, Vol. 18, Issue 2, pp. 572-581.

Kosmopoulos, A.J., Fardis, M.N., (2007). “Estimation of Inelastic Seismic Deformations in Asymmetric Multistorey RC Buildings”, *Earthquake Engineering and Structural Dynamics*, Vol. 36, Issue 9.

Kunnath, S.K., Hoffmann, G., Reinhorn, A.M., Mander, J.B., (1995a). “Gravity-Load-Designed Reinforced Concrete Buildings Part I: Seismic Evaluation of Existing Construction”, *ACI Structural Journal*, Title No. 92-S33, Vol. 92, No. 3, May-June 1995.

Kunnath, S.K., Hoffmann, G., Reinhorn, A.M., Mander, J.B., (1995b). “Gravity Load-Designed Reinforced Concrete Buildings Part II: Evaluation of Detailing Enhancements”, *ACI Structural Journal*, Title No. 92-S45, Vol. 92, No. 4, July-August 1995.

Kunnath, S.K., (2005). “Performance-Based Seismic Design and Evaluation of Building Structures”, Editors: Chen, W.F., Lui, E.M., *Handbook of Structural Engineering*, Chapter 21, 2<sup>nd</sup> edition, CRC Press.

Kusunoki, K., Kato, H., Fukuta, T., Kumazawa, F., (2001). “Experimental Study on Dynamic Response Characteristics of Frame Structures with Eccentricity”, *PEER Report 2002/02*, The Third U.S.-Japan Workshop on Performance-Based Earthquake Engineering Methodology for Reinforced Concrete Building Structures, 16–18 August, Seattle, Washington.

Lee, H.-S., Ko, D.-W., (2004). “Seismic Response of High-Rise RC Bearing-Wall Structures with Irregularities at Bottom Stories”, Paper No. 148, *13<sup>th</sup> World Conference on Earthquake Engineering*, 1-6 August, Vancouver, B.C., Canada.

Lee, H.-S., Woo, S.-W., (2002). “Seismic Performance of a 3-Story RC Frame in a Low-Seismicity Region”, *Engineering Structures*, Vol. 24, Issue 6, pp. 671-838.

Lepage, A., Hopper, M.W., Delgado, S.A., Dragovich, J.J., (2010). “Best-Fit Models for Nonlinear Seismic Response of Reinforced Concrete Frames”, *Engineering Structures*, Vol. 32, Issue 9, pp. 2931-2939.

Lestuzzi, P., Belmouden, Y., Trueb, M., (2007). “Non-Linear Seismic Behavior of Structures with Limited Hysteretic Energy Dissipation Capacity”, *Bulletin of Earthquake Engineering*, Vol. 5, Issue 4, pp. 549-569.

Liel, A.B., Haselton, C.B., Deierlein, G.G., (2006). “The Effectiveness of Seismic Building Code Provisions on Reducing the Collapse Risk of Reinforced Concrete Moment Frame Buildings”, Paper No. 232, *4<sup>th</sup> International Conference on Earthquake Engineering*, 12-13 October, Taipei, Taiwan.

Liel, A.B., Haselton, C.B., Deierlein, G.G., (2011). “Seismic Collapse Safety of Reinforced Concrete Buildings. II: Comparative Assessment of Nonductile and Ductile Moment Frames”, *Journal of Structural Engineering*, ASCE, Vol. 137, No. 4.

Lu, Y., Tassios, T.P., Zhang, G.-F., Vintzileou, E., (1999). “Seismic Response of Reinforced Concrete Frames with Strength and Stiffness Irregularities”, *ACI Structural Journal*, Title No. 96-S24, Vol. 96, No. 2.

Magliulo, G., Ramasco, R., Realfonzo, R., (2004). “Seismic Vulnerability of R/C Frames with Strength Irregularity in Elevation”, Paper No. 1519, *13<sup>th</sup> World Conference on Earthquake Engineering*, 1-6 August, Vancouver, B.C., Canada.

Mahdi, T., Soltan Gharaie, V., (2011). “Plan Irregular RC Frames: Comparison of Pushover with Nonlinear Dynamic Analysis”, *Asian Journal of Civil Engineering (Building and Housing)*, Vol. 12, No. 6, pp. 679-690.

Marsh, J.N., Browning, J.A., (2002). “Correlating Dynamic and Static Nonlinear Analysis of Frames”, *7<sup>th</sup> US National Conference on Earthquake Engineering (7NCEE)*, 21-25 July, Boston.

Matsumoto, K., Kuramoto H., Kabeyasawa, T., Fukuta, T., (2004). “Sub-Structure Pseudo Dynamic Testing on Reinforced Concrete Buildings with Soft First Story”, Paper No. 2451, *13<sup>th</sup> World Conference on Earthquake Engineering*, 1-6 August, Vancouver, B.C., Canada.

Mezzi, M., Parducci, A., (2005). “Preservation of Existing Soft-First-Story Configurations by Improving the Seismic Performance”, *3<sup>rd</sup> International Conference on the Conceptual Approach to Structural Design*, Singapore.

Miyamoto, H.K., Scholl, R.G., (1996). “Case Study: Seismic Rehabilitation of a Non-Ductile Soft Story Concrete Structure Using Viscous Dampers”, Paper No. 315, *11<sup>th</sup> World Conference on Earthquake Engineering*, Acapulco, Mexico.

Moehle, J.P., (2008). “Earthquake Collapse Risk of Older Concrete Buildings”, *Seminario en Honor del Profesor del Departamento de Ingenieria Civil Ambiental*, Bogota, Colombia.

Moehle, J.P., (2006). “Seismic Analysis, Design, and Review for Tall Buildings”, *The Structural Design of Tall and Special Buildings*, Vol. 15, Issue 5, pp. 495-513.

Moehle, J.P., Ghannoum, W., Bozorgnia, Y., (2006). “Collapse of Lightly Confined Reinforced Concrete Frames during Earthquakes”, pp. 317-332, Editors: Wasti, S.T., Ozcebe, G., *Advances in Earthquake Engineering for Urban Risk Reduction*, IV Earth and Environmental Sciences, Vol. 66, Springer.

Mola, E., Negro, P., Pinto, A.V., (2004). “Evaluation of Current Approaches for the Analysis and Design of Multi-Storey Torsionally Unbalanced Frames”, Paper No. 3304, *13<sup>th</sup> World Conference on Earthquake Engineering*, 1-6 August, Vancouver, B.C., Canada.

Naeim, F., (2010). “Performance Based Seismic Design of Tall Buildings”, Editors: Garevski, M., Ansal, A., *Earthquake Engineering in Europe*, Chapter 7,

Geotechnical, Geological, and Earthquake Engineering 17, Springer Science+Business Media B.V.

Nafday, A.M., (2011). “Defination of Structural irregularity in Seismic Codes”, *Structure Magazine*, <http://www.structuremag.org/article.aspx?articleID=1227>.  
March 2011.

NEHRP Consultants Joint Venture, (2011). “Selecting and Scaling Earthquake Ground Motions for Performing Response-History Analyses”, *NIST GCR 11-917-15*.

NEHRP Consultants Joint Venture, (2010a). “Program Plan for the Development of Collapse Assessment and Mitigation Strategies for Existing Reinforced Concrete Buildings”, *NIST GCR 10-917-7*, August 2010.

NEHRP Seismic Design Technical Brief No. 4, (2010b). “Nonlinear Structural Analysis for Seismic Design”, *NIST GCR 10-917-5*, October 2010.

NEHRP Consultants Joint Venture, (2010c) “Applicability of Nonlinear Multiple-Degree-of-Freedom Modeling for Design”, *NIST GCR 10-917-9*, September 2010.

Nikolaou, S., (2013). “The Eastern United States, We had an Earthquake in Virginia – Now What?” *Structure Magazine*,  
<http://www.structuremag.org/article.aspx?articleID=1615>, March 2013.

Nikolaou, S., Go, J.E., Beyzaei, C.Z., Moss, C., Deming, P.W., (2012). “Geo-Seismic Design in the Eastern United States: State of Practice”, Keynote Lecture, *Geo Congress 2012 (ASCE)*, GSP 226, Editors: Rollins, K., Zekkos, D., 25-29 March, Oakland, CA.

Otani, S., (2004). “Earthquake Resistant Design of Reinforced Concrete Buildings Past and Future”, *Journal of Advanced Concrete Technology*, Vol. 4, No. 1, pp. 3-24.

Panagiotakos, T.B., Fardis, M.N., (2001). “Deformations of Reinforced Concrete Members at Yielding and Ultimate”, *ACI Structural Journal*, Title No. 98-S13, Vol. 98, No. 2.

Pantazopoulou, S.J., Syntzirma, D.V., (2010). “Deformation Capacity of Lightly Reinforced Concrete Members – Comparative Evaluation”, Edited: Fardis, M.N., *Advances in Performance-Based Earthquake Engineering*, Chapter 34, Geotechnical, Geological, and Earthquake Engineering 13 (GGEE 13), Springer Science+Business Media B.V.

Pardalopoulos, S.J., Thermou, G.E., Pantazopoulou, S.J., (2005). “Seismic Assessment of an Irregular Three-Storey Full Scale RC Test Structure with Substandard Details”, *Proceeding of 4<sup>th</sup> European Workshop on the Seismic Behaviour of Irregular and Complex Structure*, Paper No. 45, 26-27 August, Thessaloniki, Greece.

Parducci, A., Comodini, F., Lucarelli, M., (2005). “A Synergic Dissipation Approach to Retrofit Framed Structures with A Soft First Storey”, *9<sup>th</sup> World Seminar on Seismic Isolation, Energy Dissipation and Active Vibration Control of Structures*, 13-16 June Kobe, Japan.

Park, R., Paulay, T., (1975). Reinforced Concrete Structures, 1<sup>st</sup> edition, *John Wiley & Sons*.

Paulay, T., (1996). “Seismic Design for Torsional Response of Ductile Buildings”, *Bulletin of the New Zealand National Society for Earthquake Engineering*, Vol. 29, No. 3.

Paulay, T., (1999). “A Simple Seismic Design Strategy Based on Displacement and Ductility Compatibility”, *Earthquake Engineering and Engineering Seismology*, Vol. 1, No. 1, pp. 51-67.

PEER Ground Motion Database, (2013). *Internet*:  
[http://peer.berkeley.edu/peer\\_ground\\_motion\\_database/site](http://peer.berkeley.edu/peer_ground_motion_database/site).

PEER, (2011). User Manual for the PEER Ground Motion Database Web Application, Beta Version.

PEER, (2010a). “Seismic Design Guidelines for Tall Buildings”, PEER Report 2010/05, Developed by the Pacific Earthquake Engineering Research Center (PEER) as part of the Tall Buildings Initiative, California, November 2010.

PEER, (2010b). Technical Report for the PEER Ground Motion Database Web Application, Beta Version, October 2010.

PEER/ATC 72-1, (2010). Modeling and Acceptance Criteria for Seismic Design and Analysis of Tall Buildings, Prepared for: Pacific Earthquake Engineering Research Center (PEER), California.

Pinarbasi, S., Konstantinidis, D., Kelly, J.M., (2007). “Seismic Isolation for Soft-Story Buildings”, *10<sup>th</sup> World Conference on Seismic Isolation, Energy Dissipation and Active Vibrations Control of Structures*, 28-31 May, Istanbul, Turkey.

Pinho, R., (2007). “Nonlinear Dynamic Analysis of Structures Subjected to Seismic Action”, Edited: Pecker, A., *Advanced Earthquake Engineering Analysis*, CISM No. 494.

Plumier, A., Doneux, C., Stoychev, L., Demarco, T., (2005). “Mitigation of Soft Storey Failures of R.C. Structures under Earthquake by Encased Steel Profiles”, Proceeding of the ICASS’ 05, *4<sup>th</sup> International Conference on Advances in Steel Structures*, Shanghai, China.

Poluraju, P., Nageswara Rao, P.V.S., (2011). “Pushover Analysis of Reinforced Concrete Frame Structure Using SAP 2000”, *International Journal of Earth Sciences and Engineering*, Vol. 4, No. 06 SPL, pp. 684-690.

Powell, G., (2004). “Collapse Analysis Made Easy (More or Less)”, *CSI Technical Knowledge Base*, Internet: <https://wiki.csiamerica.com>, Presented at LATBSDC.

Priestley, M.J.N., (2000). “Performance Based Seismic Design”, *12<sup>th</sup> World Conference on Earthquake Engineering (WCEE)*, Paper No. 2831, 30 January-4 February, Auckland, New Zealand.

Priestley, M.J.N., Benzoni, G., (1996). “Seismic Performance of Circular Columns with Low Longitudinal Reinforcement Ratios”, *ACI Structural Journal*, Title No. 93-S44, Vol. 93, No. 4.

Priestley, M.J.N., (1995). “Myths and Fallacies in Earthquake Engineering - Conflicts between Design and Reality”, *Recent Development in Lateral Force Transfer in Buildings*, ACI, SP 157-11, pp. 231-254.

Rajeev, P., Tesfamariam, S., (2012). “Seismic Fragilities for Reinforced Concrete Buildings with Consideration of Irregularities”, *Structural Safety*, Vol. 39, pp. 1-13.

Ramamoorthy, S.K., Gardoni, P., Bracci, M., (2008). “Seismic Fragility and Confidence Bounds for Gravity Load Designed Reinforced Concrete Frames of Varying Height”, *Journal of Structural Engineering*, ASCE, Vol. 134, No. 4.

Ramdane, K.-E., Kusunoki, K., Teshigawara, M., Kato, H., (2004). “Non-Linear Numerical Analyses to Improve the Seismic Design Method for Soft First Story RC Building”, Paper No. 2224, *13<sup>th</sup> World Conference on Earthquake Engineering*, 1-6 August, Vancouver, B.C., Canada.

Reyes, J.C., Kalkan, E., (2012). “How Many Records Should Be Used in an ASCE/SEI-7 Ground Motion Scaling Procedure?” *Earthquake Spectra*, Volume 28, No. 3, pp. 1223–1242.

Richard, M.J., Albano, L.D., Kelly, D., Liel, A.B., (2010). “Case Study on the Seismic Performance of Reinforced Concrete Intermediate Moment Frames using ACI Design Provisions”, *2010 Structures Congress*, ASCE, 12-15 May, Orlando, Florida.

Rutenberg, A., Tso, W.K.,(2004). “Horizontally Irregular Structures: Some Recent Developments”, Editors: Fajfar, P., Krawinkler, H., *Peer Report 2004/05*, Performance-Based Seismic Design Concepts and Implementation, Proceedings of the International Workshop, 28 June-1 July, Bled, Slovenia.

SAP 2000, (2012). *Integrated Finite Element Analysis and Design of Structures*, Computers and Structures Inc. (CSI), Berkeley, CA.

Sfura, J.F., Hayes, J.R., Foutch, D.A., (2002). “Nonlinear Seismic Response of Asymmetric Systems”, *7<sup>th</sup> US National Conference on Earthquake Engineering (7NCEE)*, 21-25 July, Boston.

Sharma, A., Eligehausen, R., Reddy, G.R., (2013). “Pivot Hysteresis Model Parameters for Reinforced Concrete Columns, Joints, and Structures”, *ACI Structural Journal*, Title No. 110-S19, Vol. 110, No. 2.

Shin, M., Kang, T.H.-K, Grossman, J.S., (2010). “Practical Modelling of High-Rise Dual Systems with Reinforced Concrete Slab-Column Frames”, *The Structural Design of Tall and Special Buildings*, Vol. 19, Issue 7, pp. 728–749.

Stathopoulos, K.G., Anagnostopoulos, S.A., (2000). “Inelastic Earthquake Response of Buildings Subjected to Torsion”, *12<sup>th</sup> World Conference on Earthquake Engineering (WCEE)*, Paper No. 0781, 30 January-4 February, Auckland, New Zealand.

Stathopoulos, K.G., Anagnostopoulos, S.A., (2010). “Accidental Design Eccentricity: Is It Important for the Inelastic Response of Buildings to Strong Earthquakes?”, *Soil Dynamics and Earthquake Engineering*, Vol. 30, Issue 9, pp. 782-797.

Smyrou, E., Priestley, M.J.N., Carr, A.J., (2011). “Modelling of Elastic Damping in Nonlinear Time-History Analyses of Cantilever RC Walls”, *Bulletin of Earthquake Engineering*, Vol. 9, Issue 5, pp. 1559-1578.

Teramoto, N., Obata, A., Kanno, H., Nishida, T., Kobayashi, J., (2012). “Experimental Studies on Side Columns of A RC Frame with Soft 1st Story Designed on the Assumption of Different Failure Modes”, *15<sup>th</sup> World Conference on Earthquake Engineering*, Lisbon, Portugal.

Thuat, D.V., (2011). “Story Strength Demands of Irregular Frame Buildings under Strong Earthquakes”, *The Structural Design of Tall and Special Buildings*, Wiley Online Library (wileyonlinelibrary.com).

Thuat, D.V., Ichinose, T., (2004). “Criterion for Preventing Formation of Story Mechanism in Vertically Irregular Wall Buildings”, *Journal of Advanced Concrete Technology*, Vol. 2, No. 3, pp. 1-10.

Tremblay, R., Poncet, L., (2005). “Seismic Performance of Concentrically Braced Steel Frames in Multistory Buildings with Mass Irregularity”, *Journal of Structural Engineering*, ASCE, Vol. 131, No. 9.

Tsai, K.C., Weng, Y., (2001). “Computing Story Drift Demands for RC Building Structures During the 1999 Chi-Chi Taiwan Earthquake”, *PEER Report 2002/02*, The Third U.S.-Japan Workshop on Performance-Based Earthquake Engineering Methodology for Reinforced Concrete Building Structures, 16–18 August, Seattle, Washington.

UBC 94, (1994). Uniform Building Code, Volume 2, Structural Engineering Design Provisions, *International Council of Building Officials (ICBO)*, Whittier, California.

USGS, (2014). “Seismic Hazard Maps and Data”, *Internet*: <http://earthquake.usgs.gov/hazards/products/>.

USGS, (2010). “Predefined Vs30 Mapping”, *Internet*: <http://earthquake.usgs.gov/hazards/apps/vs30/predefined.php>.

USGS, (2008). “Documentation for the 2008 Update of the United States National Seismic Hazard Maps”, *Open-File Report 2008–1128*, US Geological Survey, Reston, Virginia.

Valente, M., (2013). “Seismic Upgrading Strategies for Non-Ductile Plan-Wise Irregular R/C Structures”, *Procedia Engineering*, Vol. 54, pp. 539-553.

Varadharajan, S., Sehgal, V.K., Saini, B., (2014). “Seismic Response of Multistory Reinforced Concrete Frame with Vertical Mass and Stiffness Irregularities”, *The Structural Design of Tall and Special Buildings*, Vol. 23, Issue 5, pp. 362-389.

White, D.W., (1996). “Comprehensive Performance Assessment of Building Structural Systems: Research to Practice”, *Engineering Structures*, Vol. 18, Issue 10, pp. 778-785.

Wibowo, A., Wilson, J.L., Gad, E.F., Lam, N.T.K., (2011). “Drift Capacity of Lightly Reinforced Soft Storey Structures”, *Proceedings of the Ninth Pacific Conference on Earthquake Engineering Building an Earthquake-Resilient Society*, Paper No. 148, 14-16 April, Auckland, New Zealand.

Wibowo, A., Wilson, J.L., Lam, N.T.K., Gad, E.F., (2010). “Collapse Modelling Analysis of A Precast Soft Storey Building in Australia”, *Engineering Structures*, Vol. 32, Issue 7, pp. 1925-1936.

Wilson, E.L., (2014). “Damping and Energy Dissipation: Linear Viscous Damping is a Property of the Computer Model and is Not a Property of a Real Structure”, CSI (Computers & Structures Inc.), *CSI Technical Papers*, Internet: <http://www.csiberkeley.com/support/technical-papers>.

Wilson, E.L., (2002). Three-Dimensional Static and Dynamic Analysis of Structures (A Physical Approach with Emphasis on Earthquake Engineering), 3<sup>rd</sup> edition, *Computer and Structures, Inc.*

Wilson, J., Lam, N.T.K., Rodsin, K., (2008). “Collapse Modeling of Soft-Storey Buildings”, *Australasian Structural Engineering Conference (ASEC)*, Paper No. 105, 26–27 June, Melbourne Australia.

Wren, J., (2006). “Recent Development in Post-Earthquake Investigations”, *Structure Magazine*, <http://www.structuremag.org/Archives/2006-12/SF-SEISMIC-Dec06-p25-28.pdf>, December 2006.

Yavari, S., Elwood, K. J., Wu, C.-L., Lin, S.-H., Hwang, S.-J. Moehle, J. P., (2013). “Shaking Table Tests on Reinforced Concrete Frames without Seismic Detailing”, *ACI Structural Journal*, Title No. 110-S81, Vol. 110, No. 6.

Yavari, S., Elwood, K. J., Wu, C.-L., (2009). “Collapse of a Nonductile Concrete Frame: Evaluation of Analytical Models”, *Earthquake Engineering and Structural Dynamics*, Vol. 38, Issue 2, pp. 225–241.

Yoshimura, M., (2003). “Control of Seismic Drift Demand for Reinforced Concrete Buildings with Weak First Stories”, *Earthquake Engineering and Engineering Seismology*, Vol. 4, No. 1.

Zareian, F., Medina R.A., (2010). “A Practical Method for Proper Modeling of Structural Damping in Inelastic Plane Structural Systems”, *Computers and Structures*, Vol. 88, Issue 1-2, pp. 45-53.

Zeris, C., Vintzeleou, E., Repapis, C., (2005). “Seismic Performance of Existing Irregular RC Buildings”, *Proceeding of 4<sup>th</sup> European Workshop on the Seismic Behavior of Irregular and Complex Structure*, Paper No. 32, 26-27 August, Thessaloniki, Greece.

Zuccaro, G., Papa, F., Masi, A., Dolce, M., (2002). “Remarks on the Seismic Damage in the Recent Earthquakes in Europe”, *12<sup>th</sup> European Conference on Earthquake Engineering*, Paper Reference 706, 9-13 September, London, UK.

**Notes:**

- *Due to the dynamic nature of the internet, any referred link, website, or domain in this study may have changed and may no longer be available.*
- *Most of the illustrations and photos used for this study were attained from FEMA, NEHRP, USGS and other free educational/governmental sources. These materials are in the public domain and not subject to copyright.*